Approaching Human Performance

The Functionality Driven Awiwi Robot Hand

Markus Grebenstein

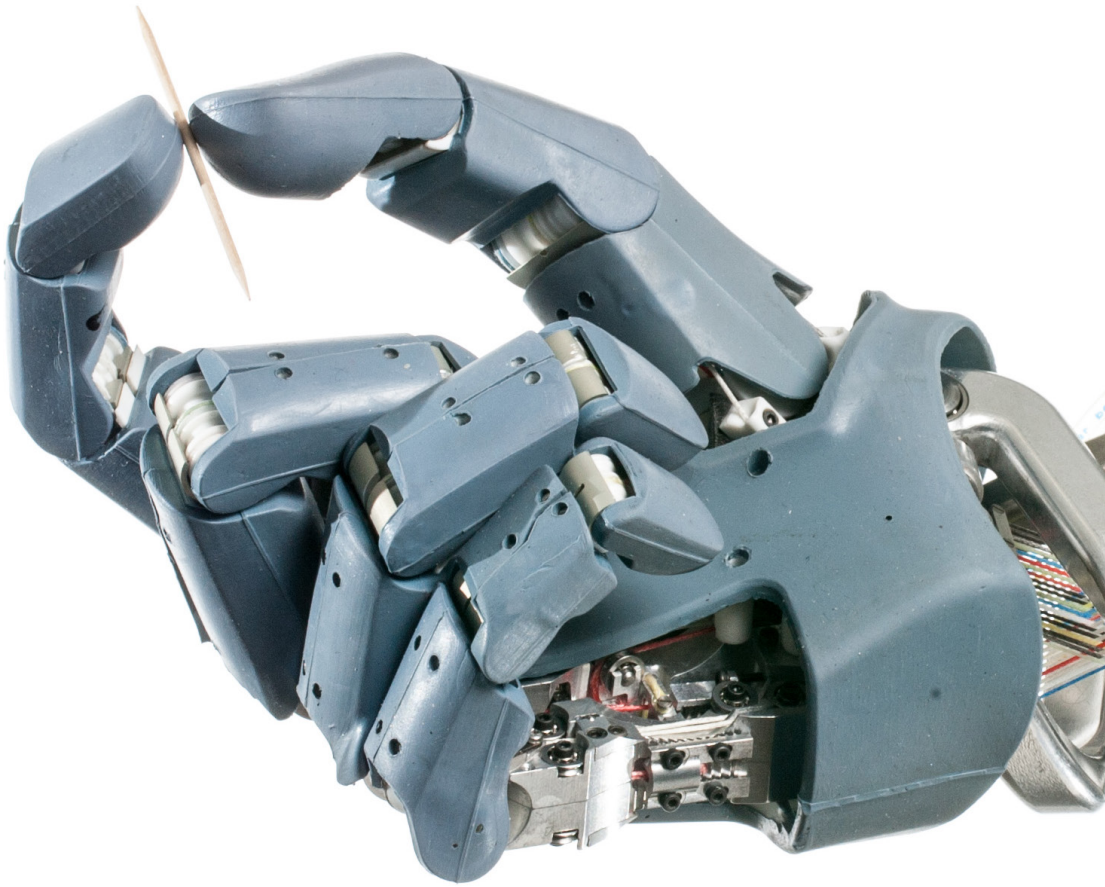

Diss. ETH N^{o} 20471

APPROACHING HUMAN PERFORMANCE: THE FUNCTIONALITY DRIVEN AWIWI ROBOT HAND

A dissertation submitted to

ETH ZURICH

for the degree of

Doctor of Sciences

presented by

MARKUS GREBENSTEIN

Dipl. Ing., Technische Universität München

born on September 27nd 1969

citizen of Germany

accepted on the recommendation of

Prof. Dr. Roland Siegwart, supervisor
Prof. Dr. Gerd Hirzinger, co-supervisor

2012

Acknowledgment

This thesis summarizes my research in the field of robot hand development and variable impedance anthropomorphic robots carried out at the German Aerospace Center (DLR), Robotics and Mechatronics Center (RMC).

I want to thank Prof. Roland Siegwart for giving me the possibility and trust to write this thesis under his advice and guidance in an extremely busy time for him. Nevertheless, he shared his time whenever I needed advice and assistance.

I would like to cordially thank all my colleagues who shared their time with me to discuss ideas, give their valuable opinions or to help me. Thank you Max Fischer for the inspiring discussions during the drive to DLR, which I think have been the birth of the idea of the *DLR Hand Arm System*.

In particular, I would like to thank Prof. Gerd Hirzinger for his invaluable faith in me and my research. He gave me the freedom to realize the idea of the *DLR Hand Arm System* and the *Awiwi Hand* starting from 2003 until now.

The idea would have been just an idea without the *DLR Hand Arm System team*:
Alin Albu-Schäffer, Thomas Bahls, Maxime Chalon, Werner Friedl, Robin Gruber, Oliver Eiberger, Sami Haddadin, Ulrich Hagn, Robert Haslinger, Hannes Höppner, Stefan Jörg, Mathias Nickl, Alexander Nothhelfer, Florian Petit, Josef Reill, Jens Reinecke, Benedikt Pleintinger, Nikolaus Seitz, Thomas Wimböck, Sebastian Wolf, and Tilo Wüsthoff.

You made a dream come true and I am not sure if I have been able to express my heart felt gratitude as much as I would have liked to.

Thanks are also due to the invaluable support from our mechatronic labs:

Mechanics lab: Harald Wagner, Jacqueline Böhne, Michael Dreer, Michael Heumos, Manfred Leichtenstern, Alexander Regner, Mario Sünderman, Thuan van Tran.

Electronics lab: Bernd Hartman, Markus Breu, Hans Buchner, Paul Ebner.

A warm thank you to my friend and long time former roommate Ulrich Hagn for always having an ear when I needed somebody to discuss with. His opinions have been invaluable. Thank you for encouraging me to take a different –and long lasting– route in hand and robot design and finally write the thesis. Cordial thanks to Mathias Nickl for all the inspiring and enthusiastic discussions throughout the years. Not to forget my colleagues Alin Albu-Schäffer, Michael Suppa and Christoph Borst for keeping me free from additional obligations as much as possible in the critical phase of writing.

I also would like to thank all the people who energetically helped me finalizing the thesis: Maxime Chalon, Jens Reinecke, and Werner Friedl for supporting me with the experiments. Alin Albu- Schäffer, Sami Haddadin, Werner Friedl, and Sebastian Wolf for the very qualified reviews and input. Melissa von Harrach, Alessa Krempel and in especial Neal Y. Lii —who proofread the whole thesis within a really short time having a newborn baby— for their valuable corrections. And last but not least Holger Urbanek for the brilliant photography.

Thank you Margot Fox- Ziekau for your incredible support in all administrative matters.

Finally, I would like to thank my family for all the incredible support and patience. There would not have been a thesis without them.

Markus Grebenstein

Dedicated to my beloved family Stefanie, Hannes, and Otto

Kurzfassung

Die humanoide Robotik hat einen bemerkenswerten Stand erreicht. Humanoide Roboter können Treppen steigen, Kaffee zubereiten und servieren, Bälle fangen und werfen sowie mit dem Menschen interagieren. Nichtsdestotrotz werden humanoide Roboter weitestgehend in speziellen, für Roboter angepassten, oder zumindest geeigneten Umgebungen eingesetzt. Um jedoch als Assistenten für den Menschen fungieren zu können ist es erforderlich diese Roboter auch in unbekannten und veränderlichen Umgebungen einsetzen zu können. In derartigen Umgebungen ist die Vermeidung von Kollisionen kaum realisierbar. Deswegen wird in dieser Dissertation davon ausgegangen, dass der Roboter für den universellen Einsatz in a priori unbekannter Umgebung in der Lage sein muss eine Aufgabe auch im Falle einer Kollision fertig zu stellen.

Von besonderer Bedeutung ist diese Anforderung für Roboter- Hände. Die Hand eines Roboters ist dessen wichtigste,[1] exponierteste und gleichzeitig fragilste mechanische Komponente. Demzufolge sollten humanoide Roboter für die Anwendung in unbekannten Umgebungen anthropomorph sein im Sinne von "menschliche Eigenschaften besitzen" und nicht lediglich eine menschenähnliche Erscheinung vorweisen. Im Speziellen sollen diese

- robust gegen Kollisionen sein
- hoch dynamisch sein
- menschenähnliche Greif- und Manipulations- Fertigkeiten besitzen

Insbesondere um robust gegen Kollisionen und gleichzeitig hoch dynamisch zu sein erscheint dem Autor ein Paradigmenwechsel erforderlich:

Zukünftige Roboter- Assistenten müssen in der Lage sein Energie zwischen zu speichern. [Morita et al. 1999]

[1] Ausgehend von Manipulations- Aufgaben

Inhalt dieser Dissertation ist daher die Entwicklung einer Roboter Hand, der *Awiwi Hand*, die aufgrund Ihres elastischen Antriebsstranges mit einstellbarer Steifigkeit mechanisch Energie speichern kann und demzufolge sowohl menschenähnlich dynamisch und robust gegen Kollisionen ist, als auch die Greif- Fertigkeiten der menschlichen Hand weitestgehend erreicht.

Um diese hoch gesteckten Ziele zu erreichen erscheint es dem Autor notwendig die menschliche Hand, sowie die bestehenden Roboter- Hände, bezüglich der grundlegenden Funktionalitäten zu analysieren. Im Sinne von *"kapieren statt kopieren"* ist das abstrakte Verständnis dieser Funktionalitäten die Voraussetzung für einen Anthropomorphismus im eigentlichen Wortsinn. Die menschliche Hand zu replizieren erscheint dem Autor weder zielführend noch technisch durchführbar.

Aufbauend auf den abgeleiteten abstrakten Funktionalitäten wird in dieser Arbeit eine Roboter- Hand entwickelt. Die *Awiwi Hand* als zentrales Ergebnis der Arbeit wird in zahlreichen Experimenten bezüglich der als Ziel definierten anthropomorphen Eigenschaften evaluiert. Die *Awiwi Hand* übersteht Schläge mit einem 500 g schweren Hammer ohne Schaden und hält Objekte fest gegriffen, selbst, wenn diese mit einem circa 4 m/s schnellen Objekt von 750 g Masse kollidieren.

Die Fähigkeit Energie zu speichern, die Grundvoraussetzung für die gezeigte Robustheit ist, ermöglicht der *Awiwi Hand* Gelenkwinkel- Geschwindigkeiten von mehr als 3500 °/s zu erreichen, indem die gespeicherte potenzielle Energie in kinetische Energie umgewandelt wird. Dies entspricht dem mehr als fünffachen der maximalen Motor- Geschwindigkeit der Hand. Nach dem Wissen des Autors ist die *Awiwi Hand* die erste Roboter- Hand, die in der Lage ist alle Griffe der von *Cutkosky* vorgeschlagenen Taxonomie [Cutkosky 1989] durchzuführen.

Einerseits ermöglichen die Robustheit, die Dynamik und die Greif- Fähigkeiten der Hand es zukünftigen humanoiden Robotern außerhalb speziell dafür geschaffener Labore eingesetzt zu werden. Andererseits bedeutet diese Robustheit, dass bedeutend weniger Rücksicht auf die, meist aufwändige und kostspielige, Hardware genommen werden muss. Dies erleichtert und beschleunigt, nach Auffassung des Autors, insbesondere im Bereich der Planung und Autonomie die Entwicklung von Applikationen und Methoden und ermöglicht den Einsatz von Herangehensweisen, wie zum Beispiel Reinforcement Learning, welche ein Scheitern des Roboters und damit auch Kollisionen für Ihren Erfolg benötigen.

Die vorgeschlagene Methode ist keineswegs beschränkt auf die Entwicklung von Roboter- Händen. Sie unterstützt die Entwicklung von humanoiden Assistenz- Robotern, die anthropomorph im eigentlichen Wortsinn sind und zum Beispiel eines Tages in der Lage sein könnten zu stürzen ohne nennenswerten Schaden zu nehmen. Diese Robustheit ist Voraussetzung für den Einsatz von Roboter-Assistenten in schwierigen und für den Menschen schädlichen oder gefährlichen Umgebungen. Das allgegenwärtige Interesse der Menschen an humanoiden Robotern zeigt nur zu deutlich, dass die Gesellschaft nach derartigen Assistenten mit robusten, schnellen und gut funktionierenden Händen verlangt.

Stichworte: Roboterhand, Design, Anthropomorphismus, Funktionale Abstraktion, Antagonismus, Robustheit, Dynamik, Elastische Antriebe, Humanoid

Abstract

Humanoid robotics have achieved a remarkable state in recent years. Nowadays humanoids can walk stairs, serve coffee, throw and catch balls and interact with human beings. However, most of these demonstrations and applications take place in well known environments or even in surroundings that have been adapted to the robots capabilities and needs. However, in order to assist the human in every day tasks, the robot has to operate in (partially) unknown environments in most cases. In these unknown environments and in interaction with moving obstacles as well as human beings, collision avoidance is vague notion. Consequently, this dissertation hypothesizes that the operation of humanoid robots outside of environments dedicated to operate the robots implies that robots have to be able to complete tasks even in case of collision. This especially applies to robot hands, since they are the most exposed and fragile part of a humanoid robot. Humanoid robots have to be anthropomorphic in sense of providing not only human-like appearance but also human characteristics. In particular they have to provide:

- Robustness against impacts
- Fast dynamics
- Human-like grasping and manipulation performance

To achieve this robustness and fast dynamics, from the author's point of view, a paradigm change has to be done

Future robots have to be able to store energy

as suggested by *T. Morita* [Morita et al. 1999].

In this thesis the anthropomorphic *Awiwi Hand* is developed, which provides human-like robustness and dynamics as well as grasping performance. To achieve these characteristics, the human anatomy as well as existing robot

hands are analyzed. The goal of this analysis is to derive the functionalities needed to achieve real anthropomorphism rather than to blindly copy the human being. These abstract functionalities are then implemented to a robotic hand. The achieved anthropomorphic characteristics of the *Awiwi Hand* are demonstrated in several experiments. The *Awiwi Hand* is able to withstand the impact of a 500 g hammer at high velocity without any damage. It can still keep objects firmly grasped even when struck by an 750 g object at a speed of approximately 4 m/s. The energy stored in the elastic elements of its antagonistic drive train allows the fingers of the hand to achieve a maximum finger speed of approximately 3500 °/s which is more than five times the speed provided by the drives alone. The *Awiwi Hand* is, to the author's knowledge, the first robot hand able to perform all grasps of *M. Cutkosky's* grasp taxonomy [Cutkosky 1989].

The robustness, fast dynamics and grasping performance of the *Awiwi Hand* is thought to enable future humanoid robots to operate in "field robotics" rather than in laboratories built for the robots. It will speed up the development of robotic applications since developers will no longer have to bother to avoid possibly costly collisions of the robot. Methods such as reinforcement learning, which need failed task execution attempts to succeed, can be used without fears of severely damaging the robot. The method underlying this development is not limited to robot hands. The proposed methodology will help realize a new generation of humanoid robots that can assist the human being even in harsh environments without damage and for example might fall over without damage. They will hopefully accommodate the demand of the human society for robot assistants that is well documented by the public interest in humanoid robotics.

Keywords: Robot hand, Design, Anthropomorphism, Functional abstraction, Antagonism, Robustness, Fast dynamics, Compliant actuation, Humanoid

Organization of the Thesis

The following gives a short overview of the structure of the thesis as given in figure 1.

Chapter one highlights the bottlenecks of current humanoid robots and gives the motivation of the thesis based on the comparison of the human and robots in case of collision, and a short discussion of the stiffness strategies of the human being. They help illuminate the goals and the contribution of this thesis. Finally, the methodology underlying this dissertation is described.

Based on the given methodology, *chapter two* analyzes recent hand developments, hand kinematics design methodologies, and variable stiffness actuated robots and hands, to derive guidelines for the design of the *Awiwi Hand*.

The same methodology is used to analyze the human archetype in *chapter three*. The anatomy, the motion capabilities of the human hand, as well as characteristic grasps are investigated to help identify a set of basic functionalities necessary to design the *Awiwi Hand*.

Chapter four describes the design of the *Awiwi Hand* based on the guidelines derived in *chapter two* and *chapter three*. In the beginning the *DLR Hand Arm System* is described shortly to show the context of the hand design. The choice of the antagonistic actuation concept as a central part of the hand is discussed subsequently. Two important aspects of the actuation concepts are investigated: the hyperactuation concept used to investigate suitable couplings for future versions of the hand, and the energy storage capabilities that are hypothesized to be paramount to achieving robustness and fast dynamics. A description of the *DLR Hand Arm System* forearm that provides these characteristics concludes the actuation section.

The approach used to design the *Awiwi Hand* kinematics is introduced in the following section. Its application to the kinematics of the *Awiwi Hand* is described and the final kinematics is presented shortly.

Based on this kinematics the friction of several finger design concepts is

estimated and compared. This estimation guides the whole design process to guarantee near optimal friction characteristics of the *Awiwi Hand*.

The design of the fingers, the thumb, and the palm as well as a description of the housing concept closes the last part of *chapter four*.

Experimental results gained with the *Awiwi Hand* prove that the goals of this thesis

- Robustness
- Fast dynamics
- Human-like grasping performance

are achieved. *Chapter five* describes impact and dynamics evaluation experiments on the finger testbed as well as on the *DLR Hand Arm System*. The grasping performance is demonstrated by performing the grasps of *M. Custkosky's* grasp taxonomy [Cutkosky 1989]. Finally impacts on grasped objects are performed to demonstrate the robustness of power grasps.

Chapter six concludes the thesis by reflecting the achievement of the goals and contribution of the thesis. Future works and ongoing research in robotic hands are described and an outlook to humanoid robotics is given from the author's perspective.

Figure 1. Organization of the thesis (next page)

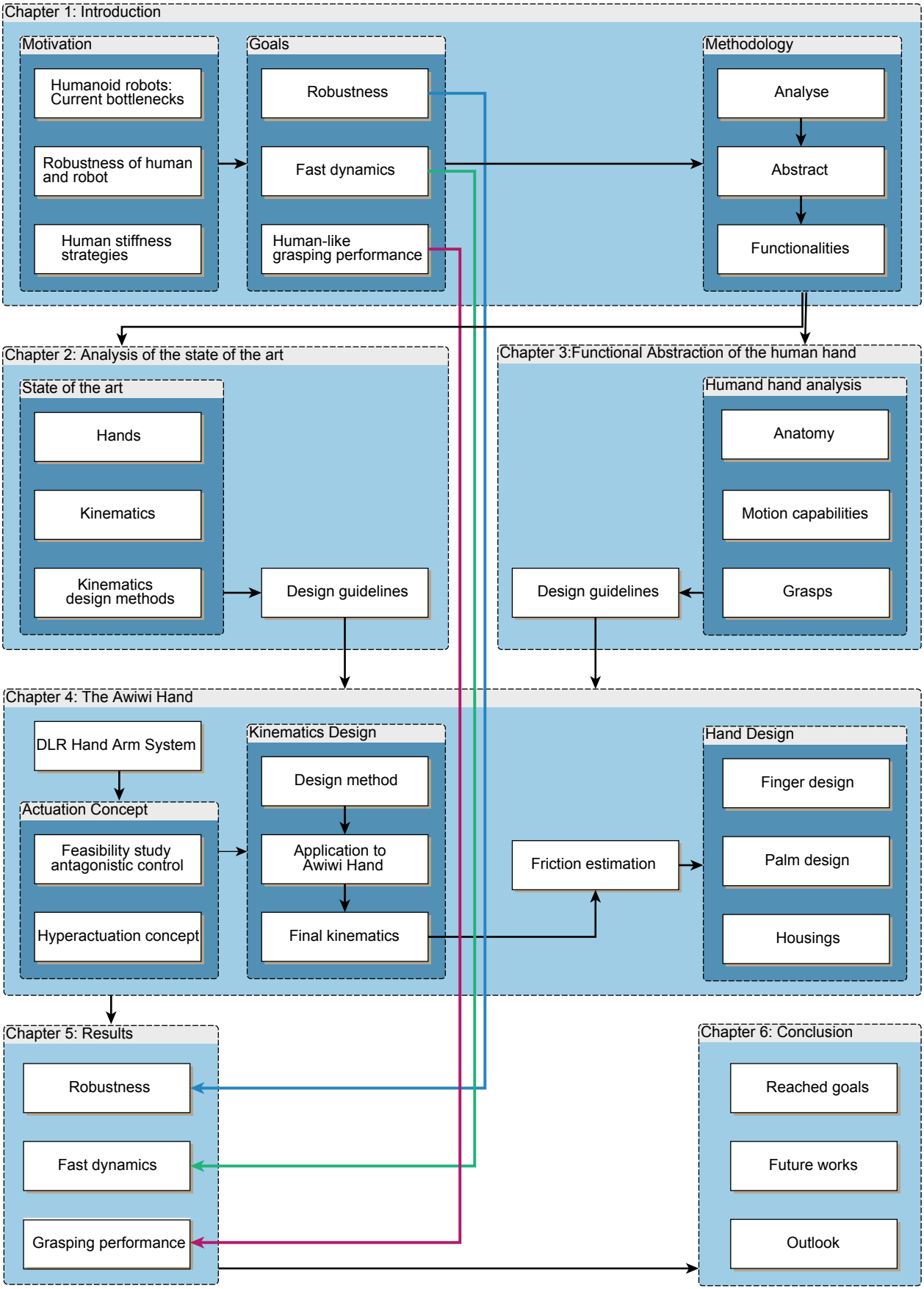
Chapter 1: Introduction
Motivation
Humanoid robots: Current bottlenecks
Robustness of human and robot
Human stiffness strategies
Goals
Robustness
Fast dynamics
Human-like grasping performance
Methodology
Analyse
Abstract
Functionalities
Chapter 2: Analysis of the state of the art
State of the art
Hands
Kinematics
Kinematics design methods
Design guidelines
Chapter 3:Functional Abstraction of the human hand
Humand hand analysis
Anatomy
Motion capabilities
Grasps
Design guidelines
Chapter 4: The Awiwi Hand
DLR Hand Arm System
Actuation Concept
Feasibility study antagonistic control
Hyperactuation concept
Kinematics Design
Design method
Application to Awiwi Hand
Final kinematics
Friction estimation
Hand Design
Finger design
Palm design
Housings
Chapter 5: Results
Robustness
Fast dynamics
Grasping performance
Chapter 6: Conclusion
Reached goals
Future works
Outlook

Contents

List of Figures

List of Tables

Notation

The notation used in this thesis will be given in the following. In the beginning, the anatomical terms will be given, followed by a list of acronyms. Finally, the used symbols are listed and explained.

Anatomical Terminology

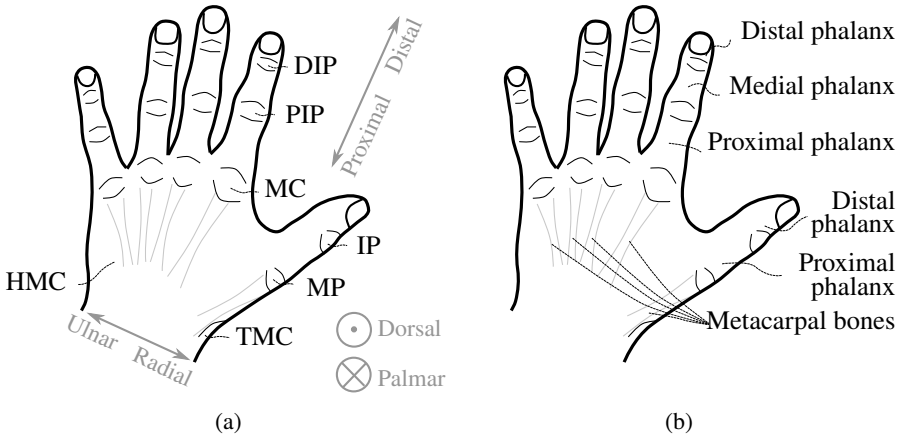

Figure 2. Nomenclature of hand joints, bones, and orientations as used within this thesis. *a*, joints and positioning; *b*, bones

This section will explain the anatomical terms relevant for this thesis. Figure 2 depicts the nomenclature of the joints in the human hand, important bones and terms indicating orientation/location. Additionally, table 1 provides a short definition of the anatomical terms used here (see also [Napier 1993; Benninghoff 1994; Gray 1999; Gosling et al. 2002]).

Since most readers will be robotics researchers, only a minimal set of anatomic terms will be used.

Table 1. Anatomical terms used in this work

Term	Definition
Joints of the human hand	
CMC	Carpometacarpal (see fig. 2a)
HMC	Hamatometacarpal (see fig. 2a)
TMC	Trapezometacarpal (see fig. 2a)
MC	Metacarpophalangeal; also used as *metacarpal joint* in case of the fingers to disambiguate (see fig. 2a)
MP	Metacarpophalangeal[2] (see fig. 2a)
IP	Interphalangeal; singular used only for the thumb to disambiguate (see fig. 2a)
DIP	Distal interphalangeal (see fig. 2a)
PIP	Proximal interphalangeal (see fig. 2a)
Regions and orientations	
Distal	Closer to the fingertip (see fig. 2a)
Medial	Middle part / between proximal and distal
Proximal	Closer to the torso (see fig. 2a)
Dorsal	Towards the back of the palm (see fig. 2a)
Frontal	Towards the inner surface of the palm; synonym for palmar
Palmar	Towards the inner surface of the palm (see fig. 2a)
Radial	On the side of the radius bone of the forearm (or thumb) (see fig. 2b)
Ulnar	On the side of the ulna bone of the forearm (or little finger) (see fig. 2b)
Sagittal	Middle (plane)
Motions	

(continued on next page)

[2]The anatomically correct nomenclature for the thumb and the fingers is identical. Since the metacarpophalangeal joint of the thumb has a different structure and function, different acronyms are used to avoid confusion.

Anatomical terms (continued)	
Abduction	Sideways motion that spreads the fingers away from the sagittal plane. Thumb: sideways motion that spreads the thumb away from the palm
Adduction	Sideways motion that pulls the fingers toward the sagittal plane. Thumb: sideways motion toward the palm
Extension	Motion of the finger that opens the hand
Flexion	Motion of the finger that closes the hand
Cupping	Motion within the palm that moves the little finger towards the thumb. In this configuration the palm takes on the shape of a cup.
Bones, muscles, and tendons of the human hand	
Adductor	Tendon/muscle that moves the finger towards the midline of the hand (see adduction)
Abductor	Tendon/muscle that spreads the fingers (see abduction)
Extensor	Tendon/muscle that moves the finger joint towards the back of the hand
Flexor	Tendon/muscle that moves the finger joint towards the palm
Metacarpal	The bones building the palm (from lat. “metacarpus”: the middle part of the hand) (see fig. 2b)
Phalanx	Finger bone

Acronyms

CMC	Carpometacarpal joint.
DIP	Distal interphalangeal joint.
DLR	German Aerospace Center.
DoF	Degree of freedom.
FAS	Flexible antagonistic spring element.
FSJ	Floating spring joint.
HMC	Hamatometacarpal joint.
IP	Interphalangeal joint.
LWR III	DLR light-weight robot III.
MC	Metacarpophalangeal joint.
MP	Metacarpophalangeal joint of the thumb.
PIP	Proximal interphalangeal joint.
RMC	Robotics and Mechatronics Center.
SEA	Serial elastic actuation.
TMC	Trapezometacarpal joint.

List of Symbols

A	Wrap around angle matrix.
α_i	Wrap around angle at default joint position of joint i.
$\vec{\Delta}_{f.act}(\alpha, f_{pre})$	Vector of active tendon force errors.
Δ_s	Linear spring deflection of elastic element.
ϵ	Inclination angle: deviation angle (within frontal plane) of the joint axis with respect to the normal position.
E_{spring}	Potential energy stored in spring.
f_{fc}	Capstan friction force.
f_{n_i}	Joint normal force of joint i.
$\vec{f}_{nsum_i}$	Vector of summed up normal forces.
$\vec{f}_n$	Vector of joint normal forces.
f_t	Input tendon force.
$f_{t.act}$	Active part of tendon force on motor side. Produces the fingertip force f_{tip} assuming no friction.
$f_{t.act.joint}$	Active part of tendon force on joint side.
$f_{t.act.link}$	Active part of tendon force at link side.
$f_{t.ext}$	Extensor tendon force.
$f_{t.fc}$	Capstan friction force at tendon.
$f_{t.flex}$	Flexor tendon force.
f_{tip}	Fingertip force.
$f_{t.joint}$	Joint side tendon force.
$f_{t.pre}$	Tendon pretension force.
γ	Wrap around angle. Equals $\alpha + \theta$.
i	General index; used for joints, motors, and tendons.

k_d	Proportional gain of damping controller.
$k(\phi)$	Stiffness function of elastic element.
$\vec{l}$	Vector of finger segment lengths l_i.
μ	Coulomb friction coefficient.
$\mu_c(q)$	Joint angle dependent capstan friction coefficient.
n	Number of joints/ tendons.
ϕ	Elastic deflection angle in joint coordinates.
$\phi_{des\ i}$	Desired deflection of elastic element i.
ϕ_i	Deflection of elastic element i.
Q	Diagonal matrix of joint angles $q_1 \ldots q_n$.
q_i	Joint angle of joint i.
q_{link}	Link position.
R_l	Matrix of pulley radius to friction bearing surface radius leverage.
r_{p_i}	Pulley radius of joint i.
r_{s_i}	Radius of friction bearing surface at joint i.
$\vec{r}$	Vector of finger joint pulley radii r_i.
σ	Angle between deflection force and tendon in "side pull mechanism".
τ_i	Torque at the elastic element of tendon i.
$\tau_{des\ i}$	Desired torque at elastic element i.
$\tau_{ff\ i}$	Feed forward torque at tendon i to compensate for elastic deflection of the joint.
τ_{link}	Link output torque.
θ	Motor position in joint angle coordinates. For stiff joints θ is equal q.
$\theta_{des\ i}$	Desired position of motor i.

θ_i	Position of motor i.
ζ	Twist angle: deviation angle of the joint axis around the longitudinal axis of the more proximal phalanx with respect to normal position / frontal plane.

1 Introduction

The starting point of this research was the insight that a humanoid robot has to operate in surroundings that are hard to predict or even unknown, making collisions with other objects inevitable. On the other hand, as it is of paramount importance for a robotic system to successfully and reliably complete its task, it needs to be able to withstand collisions and impacts without suffering severe damage or functional impairment [Grebenstein and Smagt 2008; Grebenstein et al. 2011; Grebenstein et al. 2012].

Within the previous decades service and humanoid robotics research has reached a remarkable maturity level. Nevertheless, the results within the community regarding major challenges such as grasping and manipulation, remain limited. The progress seems to have stagnated in some aspects. In the author's opinion, this is related to major shortfalls in the tool chain, and especially, the hardware. Since robotic systems get increasingly complex, the risk of damage increases. A single collision during operation may consume significant amounts of money and time. Therefore, application developers have to be very conservative when testing new methods and strategies, which slows down progress dramatically. Furthermore, this makes it difficult to develop radically different control / motion planning strategies, or to use failure based methods, such as reinforcement learning. In robotic hands, impact tolerance

plays an even more dominant role than in robot arms. In service robotics applications, the hand is the most exposed part of the robot, even though it is designed for relatively small forces (typically a few newtons). In highly unstructured environments, the maximum velocity of most robotic hand arm systems is limited by the ability of the hand to withstand impacts [Grebenstein et al. 2010b].

An impressive example of robot hands lacking robustness is the German Aerospace Center (DLR) ball catching demonstration performed by DLR's humanoid robot *JUSTIN* [Bäuml et al. 2010]. Its hands (*DLR Hand II*, see sec. 2.1.6), which are used to catch the ball, are able to produce a maximum fingertip force of 30 N, which makes them one of the strongest hands used in service robotics today. However, it reaches its mechanical limits catching a ball of 80 g, hitting the fingertips at a speed of 25 km/h, whereas a goalkeeper in handball withstands the impact of a 480 g ball at 120 km/h, introducing an amount of energy more than a hundred times higher without causing severe damage [Grebenstein et al. 2011]. Comparing the typical service robotic systems to the average human, one finds the maximum joint torques and even the maximum power of the human and the robot to be comparable (conf. [Panzer et al. 2008; Hirzinger et al. 2000]). However, in terms of the dynamic properties and the robustness against impacts in particular, robot hands are clearly inferior to the human hand. Therefore, there must be a substantial difference between robots and humans that is expected to be the key to more robust robots. The next section will show this difference by analyzing the characteristics of both systems in case of collision.

Moreover, the dynamic abilities of state of the art robots do not suffice to fulfill several human tasks. Particularly when it comes to cyclic tasks (e.g. running) or highly dynamic tasks (throwing), the actuators cannot provide sufficient energy during peak loads without getting too bulky and heavy, making it necessary to augment energy short-term. Therefore, the author is convinced that major steps in space and service robotics are only possible if a paradigm change is made [Morita et al. 1999]:

Future robotic systems have to be able to store energy

1.1. Robot in Collision

To reach maximum positioning accuracy during manipulation and to reduce the amplitude of vibrations, robots (including lightweight robots) are built to be as stiff as possible. To realize compliance, impedance control is used for most of these robots [Hogan 1984; Khatib 1987; Albu-Schäffer 2001]. Impedance control enables "active compliance" by measuring the actual force respectively torque and the position of the joints. As a result, the robot's physical stiffness equals its mechanical stiffness until the actual force and position are measured, the control output is calculated and the inertia of the robot and the drives[1] is accelerated to the desired position and speed. *S. Haddadin* [Haddadin et al. 2008; Haddadin et al. 2010] has shown that during impact, the peak load of the impedance controlled *DLR light-weight robot III (LWR III)* is reached so quickly that it cannot be measured by the joint torque sensor. Therefore, even an impedance controlled *stiff robot* can be assumed stiff in case of collision.

1.2. Human Behavior During Collision

This section provides a more detailed analysis of the strategies of the human in case of collision in order to show the importance of variable stiffness.

As human muscles can only develop tensile force, every degree of freedom (DoF) must have an agonist and an antagonist muscle (see figure 1.1). Since the compliance of the muscles, tendons and ligaments in sum has non-linear characteristics, the human being adjusts the stiffness of its joints by activating agonist and antagonist.

Depending on the respective situation, humans can adjust the stiffness of their joints to any given situation in order to prevent damage to their muscles, joints, bones, tendons and ligaments. Depending on the impact situation, at least two major strategies can be identified. The main criteria for these strategies are:

- Avoid joint damage
- Reduce muscle load

[1] The projected inertia of the drive including axis, bearings etc. is in the order of magnitude of the link side inertia.

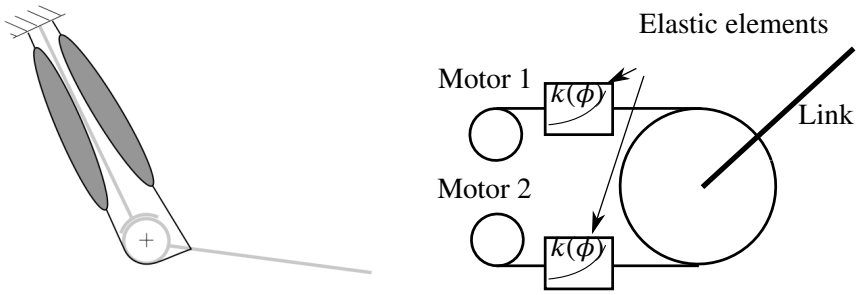

(a) Antagonistic muscles (b) Antagonistic drive setup

Figure 1.1. Schemes of antagonistic setups

The following provides an interpretation of human stiffness strategies to meet the two, somewhat contradictory, criteria.

1.2.1. Known Impact Energy

Examples for the first strategy to adjust the joint stiffness can be seen when catching a heavy medicine ball, or jumping off from great height (fig. 1.2). In both cases, the amount of energy to be expected during the impact is known/ predictable. The human being uses that knowledge to adjust the stiffness of its joints in order to utilize a maximum range of motion for dissipating the introduced energy. Thus, a minimum drive force/torque is used without reaching the motion range limits of the joints. In these situations, the criterion for adjusting the stiffness characteristics of the muscles/joints is to keep the muscle load minimal, and as a result, avoid muscle damage by overload. The minimum load applied to the muscle is obviously restricted by the joint motion range limits.

1.2.2. Unknown Impact Energy

The second type of stiffness adjustment strategy is used in situations when the amount of energy[2] is unknown for example during an unexpected crash while skiing, mountain biking, or running. In those situations, the human uses the maximum load of the muscles to minimize the range of motion needed to

[2] And in most cases even the direction of the to be expected force

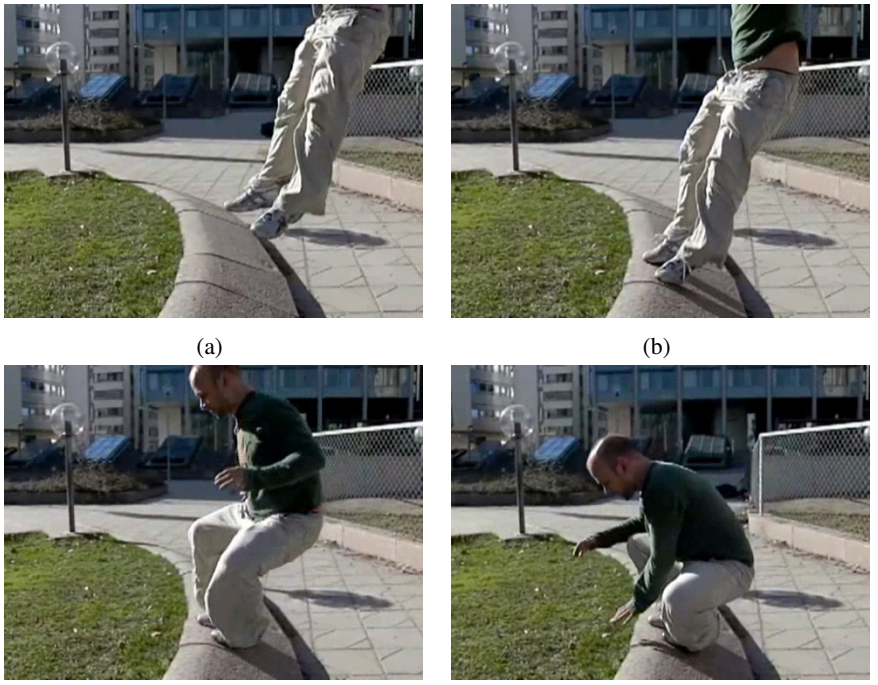

(a) (b)

(c) (d)

Figure 1.2. Stiffness strategies: jump from great height. A known amount of energy is absorbed by using full joint motion range. This strategy reduces the muscles stress to a minimum: *a*, approaching with fully extended legs; *b*, preparing for impact by avoiding singularities (stretched knee); *c*, absorbing energy; *d*, end of motion range [slowmoparkour 2008]. (courtesy of *www.youtube.com*)

dissipate the impact energy. The latter in consequence minimizes the joint motion. Here, the focus lies on avoiding the joint motion range limits, even if it means risking severe muscle damage,[3] in order to prevent often irreparable damage of the joint or bones which was a frequent cause of death during the evolution of mankind.[4]

1.3. Storing Instead of Dissipating Energy

The following section will discuss the functionality of the human archetype on which the strategies developed during the evolution of mankind are based. Compliance, which is the prerequisite to store a reasonable amount of energy in the drive train, is the essential difference between human arms and *stiff robots* that makes the human arm at least one order of magnitude more robust. The elasticity provided by the muscles, tendons and ligaments decouples the link position from the drive position (as will be discussed in more detail in sec. 4.2) and enables to store energy for a short amount of time.[5] Therefore, it is mandatory to follow the stiffness adjustment strategies mentioned above in order to approach human performance.

Generally, the energy introduced to the drives and their elastic elements, whether caused by a collision, external forces or acceleration of the robot link inertia, is converted to potential energy. The latter can be used to regain kinetic energy and thus enhance the dynamics of the system. In the case of the *DLR Hand Arm System* (see fig. 1.3), an anthropomorphic hand arm system, intended to approach its human archetype in size, weight, performance, and dexterity [Grebenstein et al. 2011], *S. Wolf* shows that the variable stiffness actuation systems used can produce a link speed 2.6 times the drive speed by utilizing the energy stored in the elastic elements [Wolf and Hirzinger 2008].

In case of collision, the drives can actively dissipate the stored potential energy over a longer period of time, resulting in significantly lower peak forces at the drives or the energy can even be stored in the elasticity. *Stiff robots* cannot store potential energy,[6] therefore, energy that is introduced externally

[3] Victims of car crashes can be found to have sore muscles over a large period of time [Cowing 2012; Hildingsson and Toolanen 1990].

[4] In contrast, muscle damage in many cases is self-healing.

[5] Without active motion of the drives, the joint acts as a nonlinear spring.

[6] Neglecting the low elasticity of standard robot joints

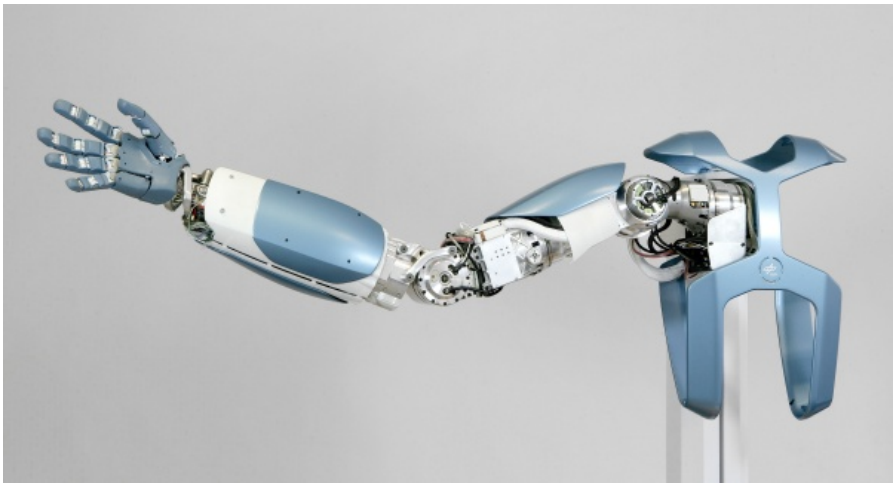

Figure 1.3. The *DLR Hand Arm System*: An anthropomorphic hand arm system using variable stiffness actuation developed at the German Aerospace Center (DLR). It is intended to approach its human archetype in size, weight and performance. The focus of the development is on robustness, dynamic performance and dexterity [Grebenstein et al. 2011].

must be simultaneously and actively dissipated by the drives. Moreover, in case of hard impacts, the resulting forces far exceed the maximum load of the drive train and can seriously damage the *stiff robot*.

1.4. Motivation and Goals

This section will discuss the main motivation for this thesis, based on the shortcomings of current robots shown above, as well as a basic understanding of human stiffness strategies described beforehand. Finally, the objective of the thesis as well as the expected contribution to robotics research are derived.

First of all, two terms commonly used to classify robots need clarification: *humanoid* and *anthropomorphic*. In the author's experience the term *anthropomorphic* is often used as a less concise form of *humanoid*. But being *humanoid* is comprised by being *anthropomorphic*. In this thesis these terms

will be used in their original meanings, defining *humanoid*[7] as:

> "having an appearance or character resembling that of a human" [Oxford University Press 2012b]

in contrast, *anthropomorphism* will be defined as:

> "the attribution of human characteristics or behavior to a god, animal, or object." [Oxford University Press 2012a]

In the author's opinion a more concise interpretation of *anthropomorphism* is required to improve robot hardware, especially robot hands, since:

future "humanoid" robots need hands that are rather anthropomorphic in the original meaning, than humanoid.

Such an interpretation will lay the focus on what is actually missing in humanoid robots. Apart from being *humanoid* in terms of shape and size, being *anthropomorphic* includes characteristics of the human archetype that are of major significance in unstructured environments:

- Robustness against collisions
- Fast dynamics and human-like force properties
- Enhanced grasping performance

The major objective of this thesis is to apply these *anthropomorphic* characteristics to a human sized robot hand for the *DLR Hand Arm System* called *Awiwi Hand* (Awiwi: Hawaiian for fast)[8] in the following.

Hence, a new approach to hand design is necessary to be able to transfer the capabilities and functional properties of the human hand to a robotic system, using cutting edge technology. The hand should be designed sharing the anthropomorphic design principles given above with the *DLR Hand Arm System*. The drives have to be integrated into the forearm to meet the spatial restrictions. Furthermore, the transmission between forearm and hand has to be routed through the palm and wrist without limiting the wrist's range of motion.

[7] The word is composed from the Latin word "homo" (human) and Greek "eidos" (appearance, gestalt).

[8] The name is inspired by the name of the *Wiki* hypertext system. The latter is derived from the Hawaiian word *wikiwiki* and is a synonym for *awiwi*.

1.5. Contribution

This work contributes to robotics research in the following areas:

- An new approach to robot hand design is proposed that analyzes the anatomy of the human hand to derive the functionalities it provides. Based on this abstraction of the human hand, the robot hand is designed to achieve real anthropomorphism, in particular, in terms of robustness, fast dynamics, as well as grasping, and manipulation performance (see fig. 1.4). This approach can also be used to analyze existing robot hands.
- A functionality based kinematics design approach is proposed that uses proven and easy to apply tests derived from surgery as well as grasping tests. It enables a real synergy between hand design and kinematics design.
- The enhanced robustness of the hand will enable task completion even after collisions, and therefore, contribute to more robust applications in unstructured and a priori unknown environments.
- The robot hand will enable application developers to concentrate on the development of the application itself rather than to consider the hardware by being robust against impacts.
- Significantly enhanced dynamics and human-like grasping abilities will enable the development of complex manipulation tasks and applications.

1.6. Methodology

This section will describe the methodology used to design the hand for the *DLR Hand Arm System* developed at DLR. The *DLR Hand Arm System* is an anthropomorphic hand arm system (fig. 1.3) using variable stiffness actuation [Grebenstein et al. 2011]. It shares the design philosophy of the *Awiwi Hand* and is intended to reach its human archetype regarding size, weight and performance [Grebenstein and Smagt 2008]. The main focus of the development is put on robustness, fast dynamic performance and dexterity to enable completion of challenging tasks even after collision.

The human hand is clearly superior to the existing robot hands regarding almost all aspects relevant for grasping and, in particular, manipulation. It serves as the archetype and reference for the intended robot hand.

The gap between the basic principles and solutions of bio-mechanical systems and the capabilities of technical systems is too wide to develop a proper hand design by simply copying the human hand using methods and solutions of the current robotics state of the art. It is currently still not possible to construct an exact copy of the human hand. For example, technical materials are not able to regenerate like human tissue does. Therefore, the key to developing a robust and highly dynamic robot hand is to understand the human hand by looking at it from a functional abstraction viewpoint rather than to attempt to copy the human archetype [Grebenstein and Smagt 2008; Grebenstein et al. 2010a; Grebenstein et al. 2010b]. Subsequently, the required extracted functionalities have to be transferred to the robot in a meaningful way.

By making this abstraction and transfer, it will be avoided to copy not only the assets of the biological solution but its drawbacks as well. It also avoids transferring biological solutions that are useless/irrelevant for the robot hand.

This thesis works out basic principles and functions of the human anatomy focusing on kinematics, joints and drives. These will be verified in experiments and transferred to the technical system to develop a robot hand for the *DLR Hand Arm System*.

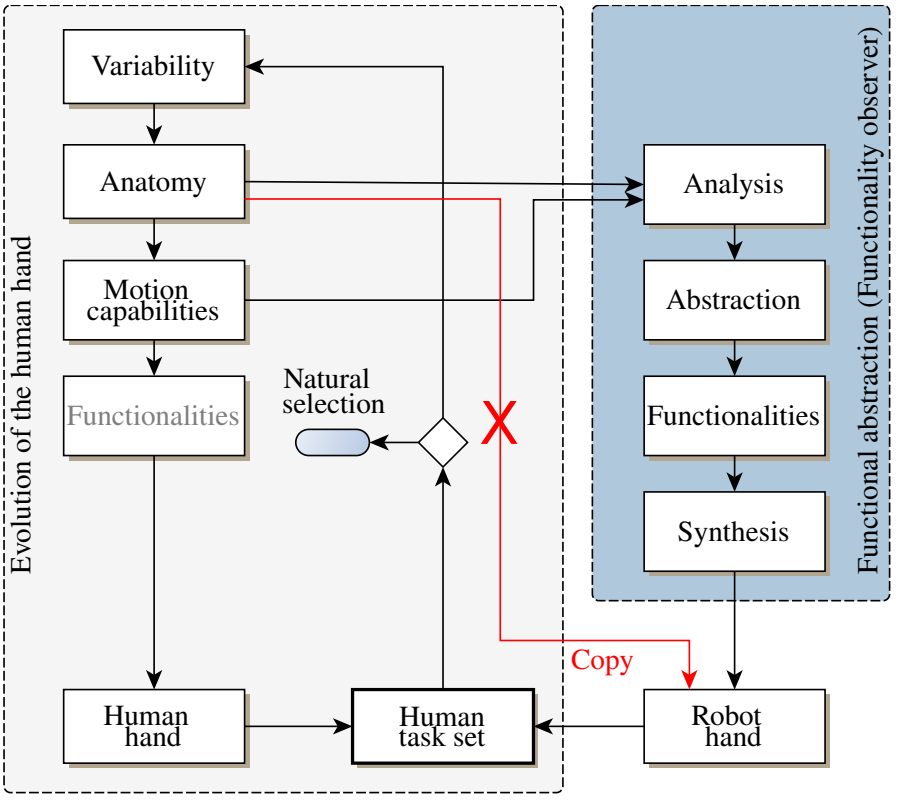

Figure 1.4. Design approach used for the *Awiwi Hand*. The author hypothesizes that the functionalities of the human hand are the (hidden) criteria of failure or successful task execution (and, in the history of mankind, even survival). In contrast, suitable anatomy is merely the prerequisite of the functionalities provided by the hand, and might be even a limiting factor. Thus, the design approach for the *Awiwi Hand* is to understand the functionalities in an abstract manner. Anatomy and the motion capabilities of the human hand are used to *observe* the underlying functionalities by functional abstraction. These functionalities are the basis for the hand design to achieve a real anthropomorphism.

2

Analysis of the Current State of Robot Hands

Designing an anthropomorphic hand is a multidisciplinary challenge that comprises several key aspects such as kinematics, actuation and the design of the hand itself. The following gives an overview of the most relevant existing hands. It will present current methods to synthesize hand kinematics followed by a short overview of recent passively compliant robots as well as existing variable stiffness actuation concepts and joints. The nomenclature of the joints used in the following is illustrated in figure 2.1.

Finally, the significance of the presented state of the art for the design of the hand of the *DLR Hand Arm System* will be discussed.

2.1. Hands

This section will begin with an overview of important robot hand developments before moving on to describe those hands that are of particular relevance to this thesis.

Over the last decades, several multi-fingered dexterous robotic hands have been developed. A summary of important hands is given in table 2.1. Apart

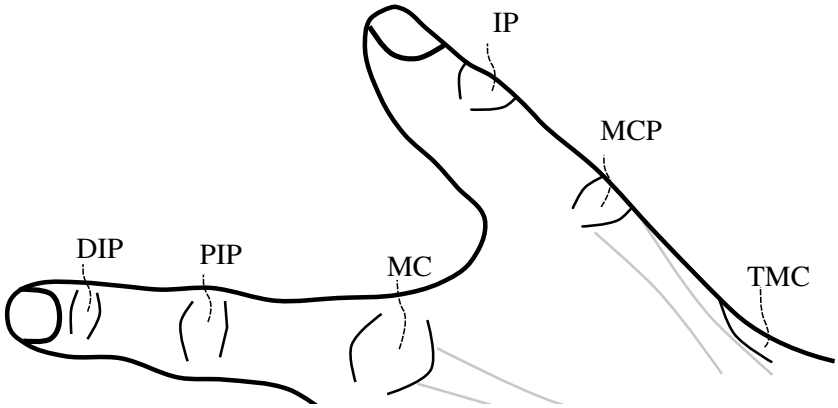

Figure 2.1. Joints of the human index finger and thumb. Abbreviations: DIP: Distal interphalangeal joint, PIP: Proximal interphalangeal joint, MC: Metacarpophalangeal joint, IP: Interphalangeal joint, MP: Metacarpophalangeal joint of the thumb, TMC: Trapezometacarpal joint

from some early, groundbreaking designs, only hands with at least 4 fingers have been selected. The hands relevant for the design of the intended hand are marked with a * and described subsequently. A more general overview of robot hands can be found in [Birglen et al. 2008, pp. 7-13] and an overview focusing on anthropomorphism in [Biagiotti et al. 2002]

Table 2.1. Selection of existing robot hands. The hands are grouped by categories integrated actuation / remote actuation and by the number of fingers. The respective number of degrees of freedom (DoF) does not include wrist DoF. († released after final design of the *DLR Hand Arm System*)

name	year	DoF		short description / references
		act.	tot.	
Remote actuated, 3 fingers				
Okada Hand	1977	11	11	Fully actuated, 3-fingered hand with 2 ”fingers” (4-DoF) and a ”thumb” (4-DoF). Actuated remotely using tendons.[1]
Stanford/JPL Hand	1983	9	12	Modular 3-fingered gripper with integrated fingertip force sensors and tactile sensors.[2]
Remote actuated, 4 fingers				
Utah/M.I.T. Hand⋆	1983	16	16	Tendon (belt) driven, highly integrated hand with 38 antagonistic drives and tendon tension control. Thumb has a rotational DoF parallel to the index finger metacarpal enabling thumb opposition/reorientation similar to e.g. LMS Hand, Elu Hand, I-Limb Hand, Twendy-One Hand, etc.[3]

[1] Okada and Tsuchiya 1977; Okada 1982.
[2] Salisbury and Roth 1982; Mason and Salisbury 1985.
[3] Jacobsen et al. 1984.

Selection of robot hands. (continued)

name	year	DoF		short description / references
		act.	tot.	
LMS Hand	1998	16	16	Tendon driven hand by Université de Poitiers with electric motors fully integrated into the forearm to develop fine manipulation algorithms. Kinematics similar to UTAH/M.I.T. Hand.[4]
Remote actuated, 5 fingers				
Robonaut Hand⋆	1999	12	20	Dexterous hand built by NASA/JPL. Aimed for space applications. Provides soft skin on hand and fingers and ”cupping” DoF for little and ring finger.[5]
Robonaut 2 Hand†	2010	12	20	Successor of Robonaut Hand with improved kinematics. The first robot hand in space.[6]
Shadow Hand⋆	2003	18	22	Commercial antagonistically driven hand using “artificial muscles”. Available with electric drives starting 2009.[7]

[4] Gazeau et al. 1999; Gazeau et al. 2001.
[5] Lovchik and Diftler 1999.
[6] Diftler et al. 2011.
[7] ShadowRobotCompany 2003; ShadowRobotCompany 2008.

Selection of robot hands. (continued)

name	year	DoF		short description / references
		act.	tot.	
ACT Hand⋆	2003	20[8]	23	Anatomically Correct Test-bed Hand developed at Carnegie Mellon University to study the human hand in terms of neuromuscular control and anatomy. Antagonistic tendon setup.[9]
UB Hand 3⋆	2004	15	20	Anthropomorphic hand by University of Bologna focused on simplicity while being dexterous and providing a soft skin for grasp stability. All fingers of equal length but with different kinematics.[10]
UB Hand IV†	2009	?[11]	20	Successor of UB Hand 3 with 5 identical fingers and remote actuation. Transmission by ”sliding tendons”.[12]

[8] Currently only the thumb, index and ringfinger are actuated

[9] Wilkinson et al. 2003; Vande Weghe et al. 2004; Gialias and Matsuoka 2004; Chang and Matsuoka 2006; Matsuoka et al. 2006; Balasubramanian and Matsuoka 2008; Deshpande et al. 2009.

[10] Lotti et al. 2004a; Lotti et al. 2004b; Lotti et al. 2004c; Lotti et al. 2005.

[11] Depending on drive setup

[12] Ficuciello et al. 2011.

Selection of robot hands. (continued)

name	year	DoF act.	DoF tot.	short description / references
Cyberhand	2006	6	16	Underactuated hand developed at the Univerity of Naples (UNINA) using tendon transmission intended as a prosthesis. Thumb abduction/adduction axis within palm but in contrast to e.g. UTAH/M.I.T Hand inclined with respect to outstretched index finger.[13]
Integrated actuators, 4 fingers				
DLR Hand I	1998	12	16	Modular hand with integrated motors, tendon transmission, and tactile sensors as well as 6-DoF fingertip force sensors.[14]
DLR Hand II ⋆	2001	13	18	Successor of DLR Hand I. Added ”cupping” degree of freedom and notably increased maximum speed and fingertip force.[15]
Twendy-One Hand⋆†	2009	13	16	Hand of Waseda University’s humanoid robot Twendy-One with re-orientable thumb, soft skin, tactile sensors and serial elastic actuation (SEA) to enhance robustness.[16]

[13] Carrozza et al. 2006.
[14] Butterfaß et al. 1998.
[15] Liu et al. 2001; Butterfaß et al. 2004.
[16] Iwata and Sugano 2009; Sugaiwa et al. 2009.

Selection of robot hands. (continued)

name	year	DoF		short description / references
		act.	tot.	
MEKKA hand†	2009	5	12	Commercially available compliant hand using SEA.[17]
Integrated actuators, 5 fingers				
Fluidhand⋆	2001	13		Lightweight prosthetic hand with internal hydraulic actuation and anthropomorphic kinematics developed at Forschungszentrum Karlsruhe.[18]
ARMAR's Hand⋆	2006	8	11	Successor of Fluidhand aimed at service robotics tasks on humanoid robot ARMAR.[19]
Gifu Hand II	2002	16	20	Dexterous hand with modular fingers. Almost completely covered by tactile sensors.[20]
Gifu Hand III⋆	2002	16	20	Successor of Gifu Hand II with improved thumb opposition.[21]
I-Limb ultra[22]	2008			Commercial prosthetic hand based on the Fluidhand of the Forschungszentrum Karlsruhe. Integrated drives and first thumb axis similar to UTAH/M.I.T. Hand.[23]

[17] Meka Robotics LLC 2009.
[18] Schulz et al. 2001.
[19] Kargov et al. 2005; Kargov et al. 2006.
[20] Kawasaki et al. 2002.
[21] Mouri et al. 2002.
[22] No official information about active and passive DoF available
[23] Touch Bionics Inc. 2012; Guizzo 2008; Adee 2008.

Selection of robot hands. (continued)

name	year	DoF act.	DoF tot.	short description / references
ELU2 Hand[24]	<2009	9	17	Commercial modular hand with fully integrated drives using several couplings (e.g. knuckle, cupping)[25]

The hands marked with ⋆ are described in more detail below, in the same order as they appear in table 2.1.

2.1.1. UTAH/M-I.T. Dexterous Hand

The *UTAH/M.I.T. Dexterous Hand* (see fig. 2.2) was developed as a research tool [Jacobsen et al. 1984]. Built in 1983, it is already anthropomorphic and targeted to have the static and dynamic performance of the human hand. It has 16 DoF and three fingers with four active DoF each, plus a thumb with four DoF. The fingers each have a proximal joint allowing abduction/adduction. The proximal joint is followed by three parallel axes to provide "curling action" (flexion and extension). The distance between the abduction/adduction axis and the flexion/extension axis of the MC joint is rather large (63 mm). The thumb kinematics is similar to the finger kinematics except for the first axis of the MC joint. The latter is arranged approximately in parallel to the outstretched index finger to allow power grasp as well as pinch grasp using abduction/adduction. For more details on the kinematics please also see figure 2.3a.

In the first version of the drive box, the hand is driven by 36 electric actuators[26] located in a remotely antagonistic setup. The transmission was accomplished by belts instead of tendons (see fig. 2.2b). This setup did not use

[24] No information on the release year available; number of overall DoF estimated from datasheet pictures

[25] Elumotion ltd. 2010; Elumotion ltd. 2012.

[26] Two more actuators drive the wrist

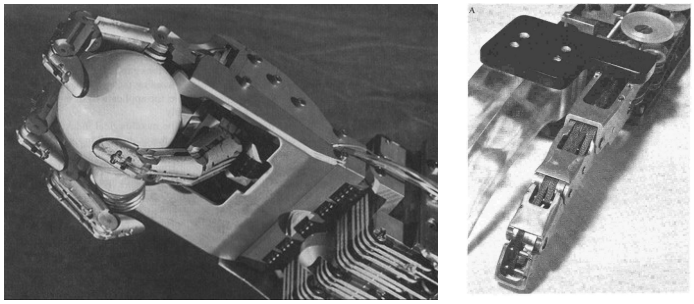

(a) (b)

Figure 2.2. UTAH/M.I.T. Hand [Jacobsen et al. 1984]: *a*, complete hand; *b*, finger with the characteristic belts used instead of tendons

elastic elements to store energy, but ensured tendon tension by tension sensors and control. In a later version, it was driven by pneumatic actuators in a similar setup.

2.1.2. Robonaut Hand

The *Robonaut Hand* of NASA is a human sized five-fingered hand designed for space based operations and extra vehicular activities (EVA) in particular [Lovchik and Diftler 1999]. It consequently mimics the grasping and manipulation abilities of astronauts (see fig. 2.4). The force requirements of the hand are derived from typical tasks performed by astronauts, such as handling of orbital replacement units (ORUs). The hand itself has 12 DoF and two additional DoF in the wrist. All actuators are located in the forearm. The hand is logically divided into *grasping fingers* (ring and little finger; mainly used to grasp objects), *dexterous fingers* (index and middle finger; used for manipulation tasks also), the palm and the thumb. The actuation of each active joint is accomplished by a flexshaft transmitting the rotary motion of the motors to a nut that converts the rotary motion to linear motion. Linear transmission is done by one short cable in both directions.

The *dexterous fingers* (index and middle finger) each has a two DoF MC joint, with the first axis pointing to the front, as seen from the palm, and a coupled PIP and DIP joint DoF. The MC, PIP, and DIP joint of the *grasping fingers* have parallel axes and are coupled. They are actuated by one motor

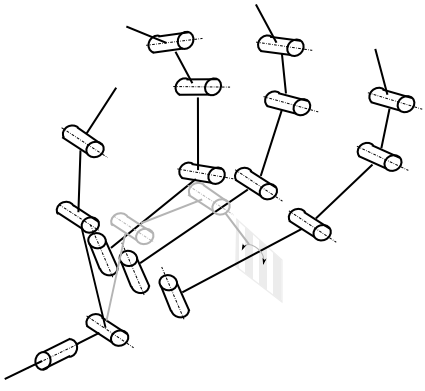

(a) MIT Hand: The suggested orientation of the first thumb axis is used by several other hands, such as the Twendy-One Hand, and Elu 2 Hand. The gray position of the thumb shows the limitations due to the singularity of the first axis.

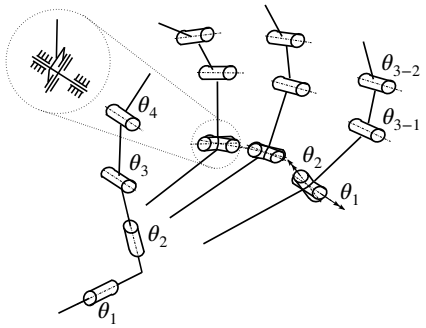

(b) Twendy-One Hand: The first thumb axis is similar to the UTAH/M.I.T- Hand, but the second joint is a roll joint and avoids the thumb tip singularity close to the index MC. Please note that, in contrast to the MIT Hand, the Robonaut Hand and most other hands, the first MC axis of the fingers points sideways.

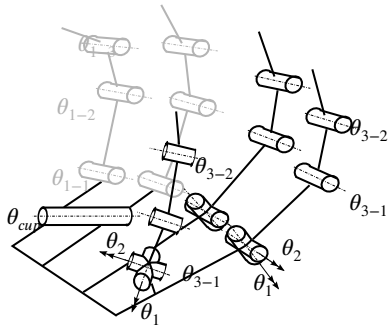

(c) Robonaut Hand: The thumb has a skew first axis of the thumb and points toward the middle of the palm enabling proper opposition. The palm can also perform "cupping motion" of the "grasping fingers" (grey) to improve opposition. The Shadow Hand uses an almost identical kinematics with more active joints, but the palm DoF only moves the base of the little finger

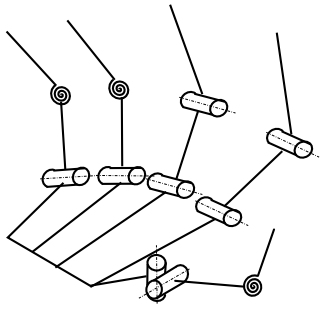

(d) ARMAR's hand: The abduction/adduction axis of the thumb is the first axis of the TMC joint. Thus, the thumb does not have a singularity when the thumb gets in palm contact. All fingers lack a DIP and MC (there exist versions with a passive MC joint). The springs, used in the 3 passive joints, are denoted by spirals. (As described in [Kargov et al. 2005]; there exist multiple versions of ARMAR's Fluidhands).

Figure 2.3. Reconstructed kinematics of the UTAH/M.I.T- Hand, Twendy-One Hand, Robonaut Hand, and ARMAR's hand. Joints that are coupled share the first index.

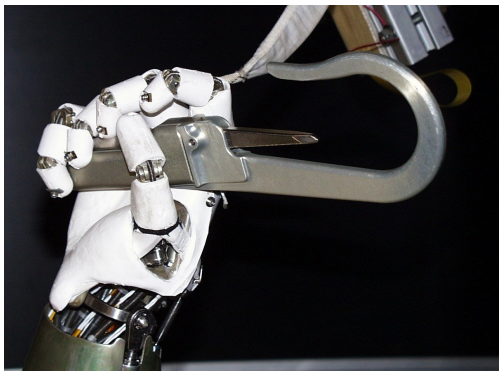

Figure 2.4. Robonaut Hand of NASA grasping a tether hook (courtesy of *NASA*)

each. The MC joints of these two fingers can be moved inward along an inclined axis that enables improved opposition of the ring and little finger as well as "cupping" of the palm itself by one additional drive[27]. The thumb of the *Robonaut Hand* has a human-like two-DoF TMC joint with an enhanced range of motion (70°/110°), and two coupled DoF within the MP and IP joint. The first axis runs nearly parallel to the frontal plane of the palm but inclined with respect to the outstretched index finger similar to the *Cyberhand* [Carrozza et al. 2006]. For further details on the kinematics see also figure 2.3c. The robustness against collisions is enhanced by allowing a buckling of the cables connecting the lead screw and the finger segments[28] and additionally shock mounts between the fingers and the palm.

2.1.3. The Shadow Hand

The *Shadow Hand* (fig. 2.5) is a commercially available anthropomorphic hand with 18 DoF and two additional wrist DoF [ShadowRobotCompany 2003; ShadowRobotCompany 2008]. It is mainly used as a research platform. The thumb and the little finger each have five DoF, whereas the other fingers have four DoF. Besides the thumb IP joint, all distal joints of the fingers are

[27] The MC joint of the little finger is moved actively, whereas the motion of the ring finger MC is accomplished by torsional springs attached to the little finger MC and the palm.

[28] Only possible in push direction of cables enabling additional flexion of fingers in case of collision.

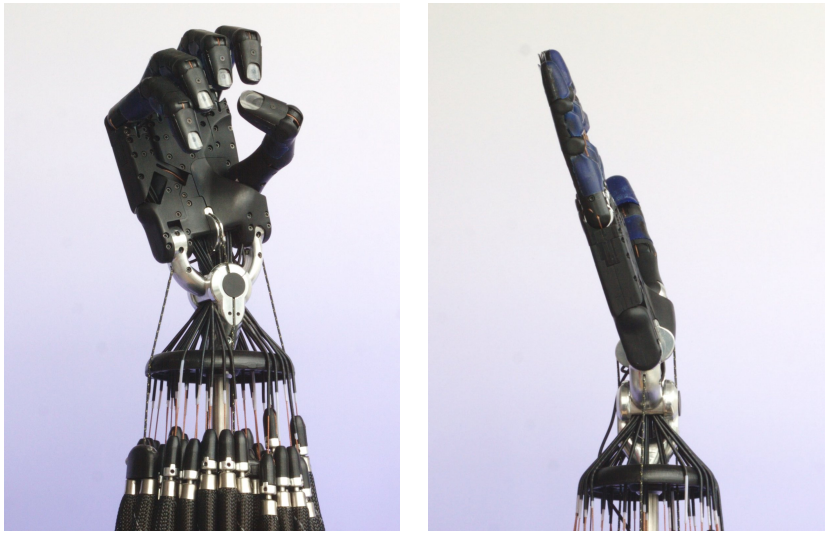

(a) (b)

Figure 2.5. The pneumatically driven Shadow Hand C5: *a*, thumb in opposition; *b*, flat configuration (courtesy of *Shadow Robot Company Inc.*)

coupled with the PIP joints. Just as the *Robonaut Hand* and the *DLR Hand II* (introduced in section 2.1.6), the MC joint of the little finger can be moved toward the thumb to enable "cupping motion" and proper opposition. The thumb is placed close to the frontal surface of the palm to allow for a flat configuration of the hand in order to push against objects, for example (fig. 2.5b). The abduction/adduction axis of the thumb is approximately adjacent to the front of the palm but inclined with respect to the outstretched index finger, as is the case with the *Cyberhand* and the *Robonaut Hands*.

It is necessary for the hand to be driven antagonistically, since the applied McKibben-type pneumatic actuators (so-called "artificial muscles") [C. Chou and Hannaford 1996; Kothera et al. 2009] are only able to pull by contraction. The hand is driven by 36 pneumatic muscle actuators[29] which allow for variable stiffness in a limited way since the range of achievable stiffness is position dependent [C.-P. Chou and Hannaford 1994]. From 2009 on, the *Shadow*

[29] Four additional actuators are used for wrist motion

Hand has also been available with 20 electric motor drives [ShadowRobot-Company 2009]. In that version, the fingers are not actuated antagonistically.

2.1.4. Anatomically Correct Testbed Hand

The *Anatomically Correct Testbed Hand (ACT Hand)* (fig. 2.6a) is intended to be an exact copy of the human archetype, modeling the passive and active dynamics of the human hand [Wilkinson et al. 2003; Vande Weghe et al. 2004; Gialias and Matsuoka 2004; Chang and Matsuoka 2006]. Its research focus is on functionality, neuromuscular control and surgeon training [Matsuoka et al. 2006; Balasubramanian and Matsuoka 2008; Deshpande et al. 2009]. The anatomically correct design allows it to be used as a training test bed for surgeons to develop new reconstruction techniques. Furthermore, it is intended to be a telemanipulator as well as a prosthesis.

The bones of the fingers are built as a 1:1 copy[30] of the human bones, based on human MRI data. The tendon apparatus of the hand is also designed in analogy to the human hand, as depicted in figure 2.6b [Wilkinson et al. 2003; Chang and Matsuoka 2006]. The hand has 23 DoF (thumb five, fingers four; one additional palm DoF for the ring and little finger). Currently, only the thumb, index, and middle finger of the hand are actuated (see fig. 2.6a). The thumb is actuated via the humanlike tendon apparatus by eight tendons, whereas the fingers are actuated by six tendons/motors each. The actuation is accomplished by electric motors [Deshpande et al. 2013].

2.1.5. UB Hand 3

Several anthropomorphic hands have been developed at the University of Bologna [Melchiorri and Vassura 1992; Eusebi et al. 1994; Ficuciello et al. 2011]. The *UB Hand 3* [Lotti et al. 2004a; Lotti et al. 2004b; Lotti et al. 2004c; Lotti et al. 2005] has four structurally identical fingers covered by soft tissue (see fig. 2.7a) to improve grasping performance, plus an opposing thumb. The design is focused on reducing the hand's complexity while at the same time aimed at good grasping performance and dexterity. In contrast to all the other hands discussed, this hand has elastic joints (see fig. 2.7b).

The linear motion generated by the drives is transferred to the fingers by sheath routed tendons. Depending on the configuration, the hand can be run

[30] Besides some cutouts needed for the pin- joints

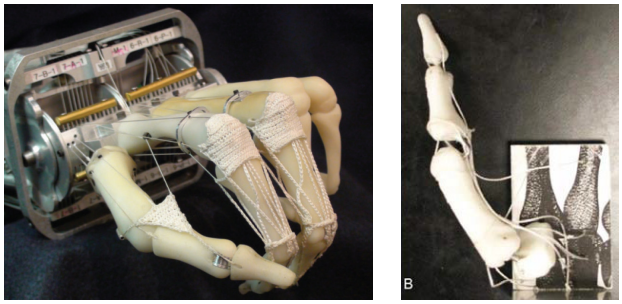

(a) (b)

Figure 2.6. The Anatomically Correct Testbed Hand of the Carnegie Mellon University: *a*, ACT Hand with forearm [Deshpande et al. 2013]; *b*, thumb design with human-like tendon routing [Chang and Matsuoka 2006]

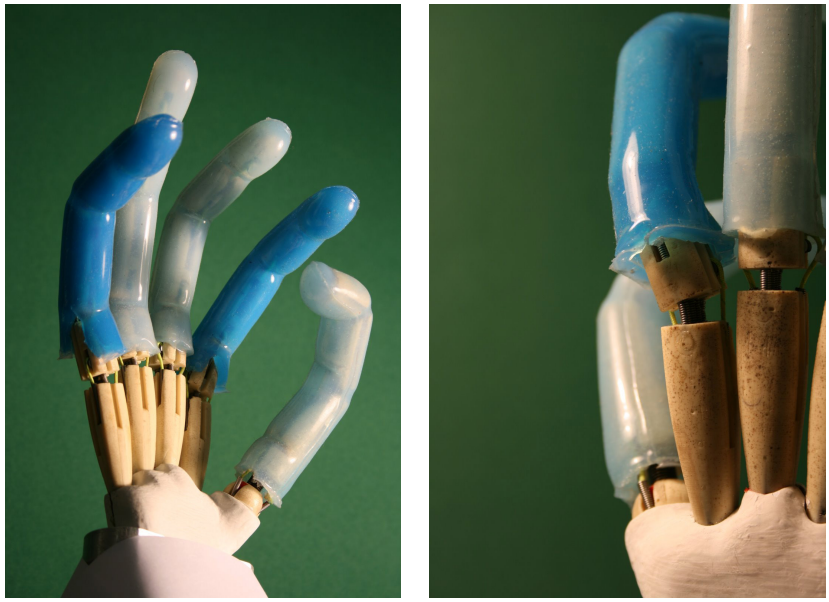

(a) (b)

Figure 2.7. University of Bologna Hand 3: *a*, hand covered with soft tissue; *b*, elastic joints (courtesy of *Gianni Borghesan*)

by a full set of antagonistic drives, or by one tendon at every joint. In the configuration *F. Lotti* presented, extension is achieved by the restoring forces of the joint elasticities [Lotti et al. 2005]. The index finger is the only fully actuated finger, and the number of actively actuated DoF (totaling at 15) is different in every finger (see table 2.2).

finger	MC 1	MC 2	PIP	DIP
little	actuated	actuated	actuated	coupled with PIP
ring	fixed	actuated	actuated	coupled with PIP
middle	fixed	actuated	actuated	actuated
index	actuated	actuated	actuated	actuated
thumb	2DoF joint		actuated	coupled with PIP[31]

Table 2.2. DoF of the UB Hand 3

2.1.6. DLR Hand II

DLR Hand II [Haidacher et al. 2003; Borst et al. 2003; Butterfaß et al. 2004] (see fig. 2.8b) is the successor of *DLR Hand I* [Hirzinger et al. 1998; Butterfaß et al. 1998] (fig. 2.8a). It is a modular, belt driven, four-fingered hand aimed to be a research platform for robot grasping. Each finger has a differential bevel gear cardan MC joint allowing abduction/adduction in the first axis and flexion/extension in the second. The PIP and DIP joint are coupled by tendons. The hand is approximately 1.5 times the size of the human hand, as all necessary drives and electronics are integrated into the hand to enable its use on standard robots. A thirteenth DoF similarly to the *Robonaut Hand*, enables "cupping motion"[32] of the palm as well as improved opposition of the thumb and the ring finger. The hand allows for 30N maximum fingertip force and a maximum speed of 540 °/s in the MC joints.

2.1.7. Twendy-One Hand

The hand of the humanoid robot *Twendy-One* (the successor of the first humanoid robot providing passive variable stiffness *Wendy* ; see section 2.3.2

[32] motion of the basejoints that changes the almost flat shape of the palm to a more closed, cup-like shape

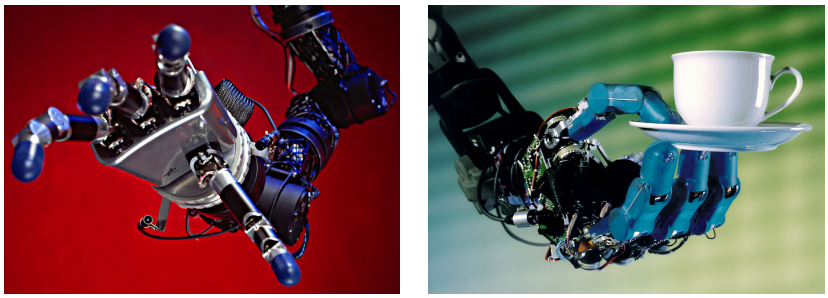

(a) (b)

Figure 2.8. DLR Hands: *a*, DLR Hand I; *b*, DLR Hand II

and figure 2.15a) developed by *H. Iwata* in the Sugano Labs of the Waseda University, is a human-sized four finger hand with a "bio-mechanism design" [Iwata and Sugano 2009; Sugaiwa et al. 2009]. Like with the *Gifu Hand* and the *DLR Hands*, all drives are integrated into the hand. In contrast to the latter, the *Twendy-One Hand* provides passive compliance by serial elastic actuation (SEA).

The hand has 16 joints and 13 drives. The fingers of the *Twendy-One Hand* all have the same length and three active DoF. In contrast to the thumb joints, the DIP and PIP joints of the fingers are coupled by a linkage. Within the first DoF of the MC joint and the DIP joint, a passive compliance is integrated to compensate position errors during grasps in position control. In contrast to several other robotic hands like the *Robonaut Hand*, the *Gifu Hand* and *DLR Hand II* the first axis of the finger MC joint is the flexion/extension axis resulting in a different shape of the fingertip range of motion (see sec. 3.2).

The first axis of the four-DoF thumb enables abduction/adduction and is aligned with the longitudinal axis of the index finger like e.g. in the *UTAH/ M.I.T. Hand* (sec. 2.1.1), the *LMS Hand* [Gazeau et al. 2001] and the *Elu2 Hand* [Elumotion ltd. 2010]. In contrast to these hands, however, the second joint of the thumb is a roll joint whose axis is aligned with the first phalanx of the thumb. Functionally, it is used to align the grasping surfaces as well as the distal phalanx of the thumb with the grasped object (see figs. 2.9a, 2.9b). A scheme of the kinematics is depicted in figure 2.3b.

The hand is equipped with tactile sensors spread across the palm and the frontal finger surfaces, as well as a six DoF force/torque sensor in every fin-

(a) (b) .

Figure 2.9. The hand of Twendy- One developed in the Sugano Lab: *a*, grasping a bottle. The thumb is opposing index and middle finger; *b*, holding a cup. The thumb is in pinch grasp position and touching the index finger laterally (courtesy of *Sugano Lab Waseda University*)

gertip. All grasping surfaces of the fingers and the hand are covered with thick silicone pads to improve grasp stability.

2.1.8. Fluidhands of Forschungszentrum Karlsruhe

The *Fluidhands* of the Forschungszentrum Karlsruhe (see fig. 2.10) are characterized by their humanlike size and the low weight of less than 20 g per finger in the first version, due to the actuation by fluidic actuators driven by a micro pump [Schulz et al. 2001]. The latter is integrated into the palm of the hand. The first version (fig. 2.10a) is developed as a full replacement hand prosthesis. It has 18 joints and 13 actuators, allowing for a more natural motion than that of prosthesis with fewer DoF. The extension of the finger joints is done fully passively by springs. The thumb has a three-DoF base joint followed by two coupled joints. The fluidic actuators designed specifically for the *Fluidhands* allow for more than 3 N fingertip force.

ARMAR's Hand[33] (fig. 2.10b) is the successor of the *Fluidhand* and is intended as an endeffector for the humanoid robot *ARMAR* [Kargov et al. 2005; Kargov et al. 2006]. It is strongly focused on handling objects designed for humans in home surroundings such as kitchens. Like the *Fluidhand*, it features five fingers and the characteristic fluidic actuation in a redesigned version. All

[33] In the original publication, the hand is not named.

(a) (b)

Figure 2.10. The hands of the Forschungszentrum Karlsruhe: *a*, first version of the Fluidhand (courtesy of *Stephan Schulz*); *b*, the hand of ARMAR [Kargov et al. 2005]

drives and electronic components are integrated into the palm. In contrast to its predecessor, it has eight active DoF and three passive DoF. All fingers have a one-DoF MC joint and only the PIP joint. The ring and the little finger have one passive and one active joint, whereas the index and middle finger have two DoF. The thumb has one passive "middle joint" (merge of IP and MP) and two active joints in the base (TMC) joint (see fig. 2.3d for a kinematics scheme). The hand has humanlike size, a weight of approximately 0.5 kg, and an average contact force of 1 N.[34]

2.1.9. Gifu Hand III

The *Gifu Hand III* (fig. 2.11) is designed for robotics research with a focus on the use of tactile sensors for grasping and manipulation [Mouri et al. 2002]. It is largely covered by tactile sensors (fig. 2.11a). Regarding its predecessors

[34] There is no mention of a maximum fingertip force in the publications.

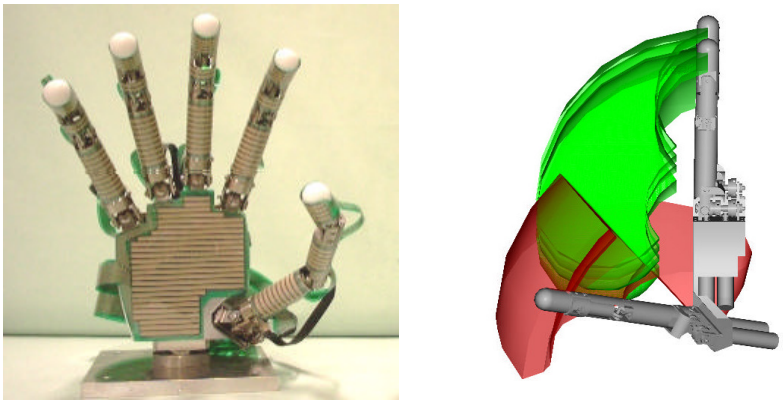

(a) (b)

Figure 2.11. Gifu Hand III : *a*, hand with tactile sensors; *b*, motion range of the fingers and the thumb. Please note that the thumb cannot reach the MC/base joints of the fingers [Mouri et al. 2002].

Gifu Hand I and *Gifu Hand II* [Kawasaki and Komatsu 1998; Kawasaki and Komatsu 1999; Kawasaki et al. 2002], it was optimized especially in regard to the quality of thumb opposition (fig. 2.11b).

The motors of the *Gifu Hand III* are all located in the hand to reduce inaccuracies by e.g tendon transmission. The five fingers should enable "human like grasping" and have 20 DoF (four per finger including the thumb). In contrast to the thumb, the DIP and PIP joints of the fingers are coupled by a planar four bar linkage with a transmission ratio of approximately 1:1. The thumb design of the *Gifu Hand III* is different from the fingers to improve thumb opposition (fig. 2.11b). It has four independent DoF and a higher (3.7N) maximum fingertip force than the fingers (3.4N). The hand is actuated by 16 servo motors.

2.1.10. A Natural Hand Model

The hand model developed by *O. van Nierop* [Nierop et al. 2008], based on the body hand dimensions of eight test persons of both sexes, is not a full robot hand. Nevertheless, it is a remarkable hand model gained by measurement of human specimen, analysis of the gained data, interpretation, and finally modeling of the kinematics. *Van Nierop's* work focuses on a hand model that

"looks good" and is used for a visual representation of hands in animations and computer games for example. Therefore, this "virtual hand" is relevant for the design of a robot hand and is discussed shortly in the following.

The structure of the human hands was measured using calipers, rulers, compasses, and also radiographies of the thumbs. To analyze the motion of the joints, the motion of the fingers is captured separately for each joint by fixing all other joints. The motion curve of the joints has been recorded using a pencil clamped to the phalanx parallel to the joint axis. The authors show that there are basically two types of joint motion:

- Circular motion
- Conical motion

Circular motion is the exact motion around an axis perpendicular to the phalanx. Conical motion is a motion where the phalanx is moving along the lateral surface of a cone. This motion results in a non-planar motion of the phalanx and an additional coupled motion of the phalanx around its longitudinal axis. The plots done using the above method, showed to be modeled best by circular or conical motions having two different radii and being tangent to each other (see fig. 2.12). The authors found the radius of the motion curve to change at a neutral position[35] of the joint. The motion trajectories of the human joints are resulting mainly from the shape of the (non rotationally symmetric) joint articulate surfaces sliding on each other.[36] These motions of the human fingers are modeled closely on the approximated curves suggested by *van Nierop*. To develop a hand model including kinematics, *van Nierop* proposes a joint model (see figs. 2.12a,2.12b) using "natural joint axes" which enable a rotational motion around the joint axis as well as a superposed translation (elongation) of the fingers phalanx. The translation is said to occur in a neutral position and to allow only two values (zero elongation and full elongation).

Van Nierop claims that the hand model allows for natural motion. Some exemplary poses can be seen in figure 2.13.

[35] The neutral position is defined as the position of the fingers when the hand is inactive (not outstretched).

[36] and of course the constraints resulting from the ligaments

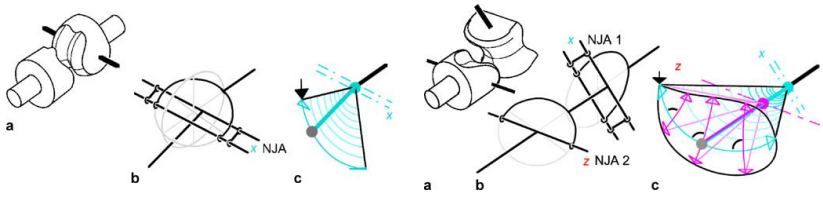

(a) (b)

Figure 2.12. Models of the joints of the human hand [Nierop et al. 2008]: *a*, model of IP, PIP, and DIP joint; *b*, TMC/MC joint model

2.2. Kinematics Design Methods

The development of robot hand kinematics has been a research topic for several decades, resulting in several methods of synthesis. They will be described in the following. This section is based on [Grebenstein et al. 2010a].

2.2.1. Empirical Kinematics

A large number of kinematics mainly based on empirical results can be found. They are designed to fit the special needs of existing robot hands (see section 2.1), data glove calibration or animation purpose. *W. B. Griffin* designed a kinematics to help develop a calibration scheme for data gloves [Griffin et al. 2000]. He added longitudinal axes of rotation in the proximal phalanx of the thumb to enable the rotation of the thumb during flexion (this feature can also be found in the thumb of the *Twendy-One Hand*, see sec. 2.1.7). The first axis of the thumb is adjacent to the metacarpal bone of the index finger. This orientation of the first axis of the thumb can also be found in several robot hands discussed in section 2.1.

2.2.2. Kinematics Analysis

D. Giurintano and *A. Hollister* [Giurintano et al. 1995] developed a five link kinematics for the thumb based on cadaver analysis [Hollister et al. 1992; Hollister et al. 1995] to reproduce the motion of the human thumb as closely as possible. *G. Stillfried* [Stillfried and Smagt 2008] measured the kinematics of a human hand using MRI data and segmentation algorithms to extract the motion of the bones and, as a result, the hand kinematics (see fig. 2.14).

Figure 2.13. Three hand poses including Kapandji test (see section 4.3.2) performed by *van Nierop's* hand model [Nierop et al. 2008].

The Technical University of Munich's Institute of Ergonomics synthesized a kinematics model of the whole human body to realize the *RAMSIS* system[37] [Geuss 1994; Purschke et al. 1998].

2.2.3. Kinematics Optimization

V. Santos and *F. J. Valero-Cuevas* [Santos and Valero-Cuevas 2003] modeled the kinematics of *Giurintano* and *Hollister* using Denavit Hartenberg (DH) -

[37] The RAMSIS model is used mainly to design ergonomic interfaces, e.g. in automobile industry.

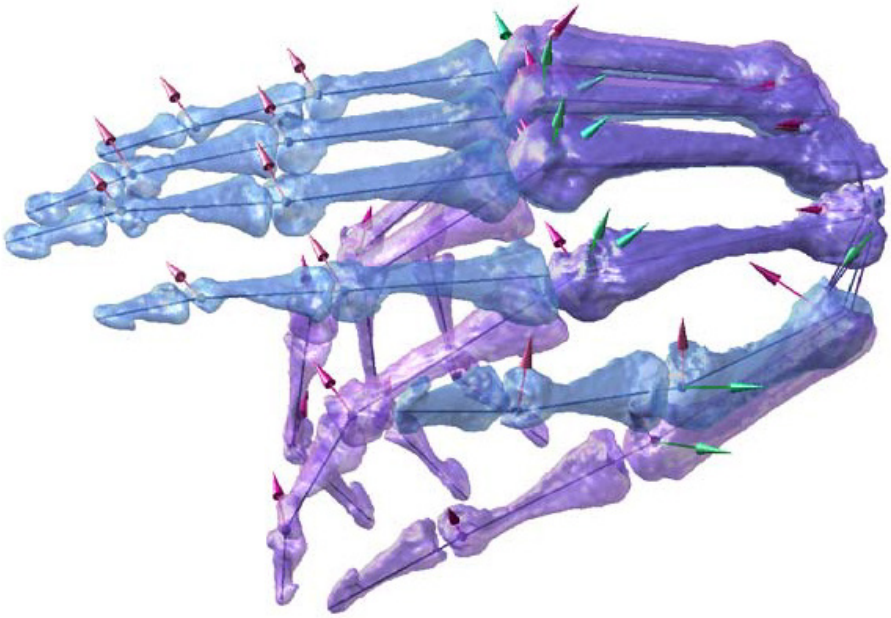

Figure 2.14. Human hand kinematics modeled by *Stillfried* [Stillfried and Smagt 2008]

parameters and optimized it using cadaver test data from [Hollister et al. 1992; Hollister et al. 1995]. They optimized the results using Markov Chain Monte Carlo Simulation within a 50D parameter space [Santos and Valero-Cuevas 2004].

2.2.4. Kinematics Evaluation Criteria

To optimize and prove the kinematics, it is paramount to have verified and reliable optimization criteria / cost functions. Several different approaches can be used for optimizing as well as evaluating existing kinematics. Examples for such methods are:

- Mathematical criteria
  - Manipulability ellipsoids [Yoshikawa 2003; Rosenstein and Grupen 2002]
  - Dexterous workspace [Craig 2004]

  - Grasp stability [Arimoto et al. 2003]

- Hand and grasping simulation tools

For grasping research, *A. Miller* developed a complete environment called "GraspIt!" to simulate hands-in-contact situations, which could be used as an alternative (or in addition) to the cardboard prototypes to execute the tests proposed in section 4.3.2 [Miller and Allen 2004].

2.3. Compliant Robots and Actuation

This thesis aims to develop a hand with increased robustness and dynamics. To meet these goals, the drive train has to be able to store energy, as well as to provide variable stiffness. The drive system is located in the forearm of the *DLR Hand Arm System* and is not a topic of this thesis. However, in order to elaborate the requirements for the hand actuation, knowledge of the current state of variable stiffness actuation and in especial compliant robots is indispensable. The section, partly based on [Grebenstein et al. 2011], provides an overview of those requirements as well as references.

2.3.1. Variable Stiffness Actuation

In recent years, there has been a lively discussion on how storage of potential energy in robot joints can contribute to "intrinsically safe robots", while enhancing robot dynamics [Bicchi and Tonietti 2004; Zinn et al. 2004; Tonietti et al. 2006; Tonietti et al. 2005; Surentu et al. 2007; Park et al. 2007; Haddadin et al. 2009a; Bicchi et al. 2004].[38] In general, both goals can be achieved by serial elastic actuation (SEA). Nevertheless, to be able to use stiffness strategies as discussed in section 1.2 as well as to adapt the eigenfrequencies of the robot to the requirements of cyclic tasks at varying speeds in particular, variable stiffness will become necessary. Several variable stiffness actuators have been proposed [Laurin-Kovitz et al. 1991; English and Russell 1999a; Eiberger et al. 2010; Palli et al. 2007; Ham et al. 2006]. They range from fully antagonistic joints in different variations [Laurin-Kovitz et al. 1991; English and Russell 1999a; Petit et al. 2010; Filippini et al. 2007] to variable stiffness

[38] This is contradictory in the authors eyes, since a fast moving robot stores much more kinetic energy and therefore is, by far, more dangerous (see [Haddadin et al. 2010]).

joints that use a separate motor to adjust the stiffness of the joint [Laurin-Kovitz et al. 1991; Wolf and Hirzinger 2008; Schiavi et al. 2008; Grebenstein 2006a].[39] A wide spectrum of these actuators can be found e.g within the VIACTORS EU Project (http://www.viactors.eu). An overview of the actuators developed specifically for the *DLR Hand Arm System* can be found in [Grebenstein et al. 2011].

2.3.2. Physically Compliant Robots and Hands

In relation to the number of existing robot hands, the number of robots and, particularly, robot hands using physical compliance or variable stiffness, is quite limited.

S. Sugano points out the importance of finger compliance in robot hands to achieve stable grasps [Sugano et al. 1992]. He suggests introducing variable mechanical stiffness into the drive train instead of compliance control to improve the mechanical bandwidth and the characteristics of the stiffness achieved. *Sugano* successfully designed and controlled a finger with variable stiffness actuation in a serial setup where one motor changes the stiffness characteristics of the drive train and another motor independently changes position.

Nearly a decade later, Waseda University's robot, *Wendy* designed by *T. Morita et. al.* (fig. 2.15a) became the first humanoid with adjustable mechanical joint stiffness [Morita et al. 1999]. *Wendy's* successor *Twendy-One*, presented in [Iwata and Sugano 2009], still uses elastic elements in the drive train, but does not have variable stiffness in order to save space and weight in the arms.

Recently, NASA has presented the second version *R2* (fig. 2.15b) of the *Robonaut*. In contrast to its predecessor, the arm of *R2*, in contrast to its hand, provides mechanical compliance by SEA to enhance the robustness of the robot [Diftler et al. 2011].

The humanoid *Kenta* provides a tendon driven spine as well as elastic elements within the drive train used as tendon tension sensors. These elastic elements, which have linear spring characteristics, also provide robustness against impacts. The stiffness of the joints is adjusted by tendon force control. It is aimed at resembling a human being and providing human-like motion

[39] This enables to us motors of different characteristics

(a) (b) (c)

Figure 2.15. Compliant robots: *a*, the first humanoid variable stiffness robot WENDY (courtesy of *Sugano Lab Waseda University*); *b*, Robonaut R2, the first humanoid robot in space (courtesy of *NASA*); *c*, Kojiro legs and torso during load tests [Mizuuchi et al. 2007];

[Mizuuchi et al. 2002]. Its successor *Kojiro* (see fig. 2.15c) is driven by even more drives, 109 tendon drives in total, to closely mimic the human archetype and its muscle and tendon structure [Mizuuchi et al. 2007].

2.4. Significance for *Awiwi Hand*

The next paragraph will discuss the relevance and the use of the recent work shown in the sections 2.2, 2.1, 2.3 for the *Awiwi Hand* focusing on the aspects kinematics and grasping performance, kinematics design methods, and actuation with respect to robustness and dynamics of the hand.

2.4.1. Hand Kinematics and Grasping Performance

The grasping and manipulation capabilities of hands are primarily a matter of well designed hand kinematics. Therefore, several hand designs will be discussed in regard to their kinematics and their applicability to the desired hand in terms of grasping and manipulation performance. The discussion will focus on the following aspects of the kinematics design:

- Finger length and kinematics
- Applied joint couplings and number of DoF
- Thumb position and kinematics
- Applicability to a robot hand

Several robot hands, such as the *Gifu Hand* (sec. 2.1.9), *UB Hand 3* (sec. 2.1.5), *Twendy-One Hand* (sec. 2.1.7) and, naturally, all modular hands like *DLR Hand I* and *DLR Hand II* (sec. 2.1.6), have fingers of equal length and kinematics. While it simplifies the design in terms of cost reduction and e.g maintainability, this approach limits the performance of the robot hand. The human thumb is quite different from the fingers in terms of kinematics, size and strength, as will be shown in section 3.2.5. For example the base (TMC) joint of the human thumb allows for a much bigger range of motion than the fingers with regard to abduction/adduction and provides an inward/outward rotation of the thumb. These two characteristics of the TMC joint are essential for the opposition of the thumb and the ability to perform both, fine manipulation as well as power grasp.

To deal with the problems resulting from non ideal thumbs, several robot hands have been equipped with a thumb that significantly differs from the fingers. For example, the *UTAH/M.I.T. Hand* (sec. 2.1.1), the *Twendy-One Hand* (sec. 2.1.7) and the *Elu2 Hand* [Elumotion ltd. 2010] use a thumb whose first axis runs in parallel or even adjacent to the metacarpal bone of the index finger, as depicted in figure 2.3a and 2.3b. This allows for the thumb to be positioned in opposition to the palm for a power grasp or to touch the palm, respectively the index finger, laterally, as needed, for instance, to perform a key grasp as depicted in the pictures of the *Twendy-One Hand* (figs. 2.9a,2.9b). However, this orientation of the first axis results in a near singular position of the thumb tip when it touches the palm (see fig. 2.3a). For this reason, such a thumb fails the Kapandji test (see section 4.3.2). This failure signifies that the thumb is neither able to touch the basis of the ring and little finger, as used e.g. to fix an object in the palm using only the thumb, nor to properly oppose the ring and little finger, as the sagittal plane of the thumb always has to include the axis of the first joint.[40] The *Twendy-One Hand* avoids that problem

[40] Assuming the 2nd to last joint axes are parallel

by putting a rotational joint into the first phalanx of the thumb as depicted in figure 2.3b. That way, the thumb is able to rotate out of the sagittal plane. However, the missing flexion/extension of the TMC joint limits the range of motion of the thumb and therefore e.g. the size of the objects which can be grasped.

An equally important aspect is the position of the thumb relative to the rest of the hand. If the positioning of the thumb does not fit its length, the grasping and manipulation performance of the hand is impaired. If the thumb is too long[41] or the thumb base is too close to the MC joints of the fingers, as like e.g. in *DLR Hand I* and *DLR Hand II* (see fig. 2.8), the fingertips of all fingers and the thumb can only contact an object located distally to the palm. This requires extensive wrist or elbow motion to achieve a suitable position and orientation of the hand, for example to pick up a flat cylindrical object from a table. Furthermore, the power grasp performance of such hands is poor as the fingers cannot close around the object properly. On the other hand, a thumb that is too short or placed too far away from the MC joints, as found in chimpanzee [Napier 1993, pp. 57-60] or gorilla hands [Flatt 2002], allows for very effective power grasp[42] but impairs manipulation of objects that are distally to the hand[43] or too small.

The longitudinal position of the thumb is not the only important criterion. A thumb TMC placed within or very close to the palm as seen in the *Shadow Hand* (see fig. 2.5b) will be able to push against flat surfaces, but impair the opposition of the thumb as well as power grasp of large objects.

The (virtual) hand proposed by *van Nierop* (sec. 2.1.10) is able to perform the required grasps and motions in a natural way,[44] but the hand model is designed to *mimic* the motion of the human hand. It is not intended to provide the functionality of the human hand with a minimal amount of DoF. Hence, the joint models used to achieve this behavior are not applicable to robot hands without making the hand too complex and bulky.

In contrast to *van Nierop´s* approach, the reduction of active DoF by introducing couplings or omitting DoF, like in the *Elu2 Hand*, the *UB Hand 3*, the *DLR Hands*, as well as the *Fluidhands*, without a rather complete un-

[41] The latter is a typical problem of modular hands since the drives of their MC joints are placed proximally to the joint itself.

[42] That is the main purpose of most monkey's hands

[43] E.g screwing a nut or turning a knob fixed to the wall, with an almost stretched-out arm

[44] E.g. it is able to perform the Kapandji Test

derstanding of manipulation and grasping and the role of couplings in human hands (see sec. 4.2.2) can drastically reduce the capabilities of a robot hand as a universal grasping and manipulation tool. In the author's opinion, that understanding has not been fully reached yet. The lacking joint in the fingers of *ARMAR's* hand,[45] for example, drastically limits their ability to wrap themselves around objects (see fig. 2.3d).[46] Hence, the use of synergies and couplings in robot hands, as described by *M. Santello* [Santello et al. 1998], is a current research topic of for example the THE project (http://www.thehandembodied.eu).

Consequently, all kinematics previously discussed are somehow tailored to the intended field of use, ranging from research on neuromuscular control to prosthetic hands. They are in part influenced by the boundary conditions ranging from robot interfaces, maximum weight, power consumption all the way up to the available resources for the hand or even aesthetic aspects. None of these kinematics fully meet the goals set for the hand of the *DLR Hand Arm System* in a satisfactory way. Therefore, a new kinematics for the *Awiwi Hand* is designed in this work.

2.4.2. Kinematics Design Methods

Since no fitting kinematics has been found for the aimed hand, it is important to select appropriate methods to design the kinematics. The recent work on kinematics design methods and evaluation criteria will be discussed in the following based on [Grebenstein et al. 2010a; Grebenstein et al. 2012].

The design space of a hand is extremely large and, unfortunately, the existing optimization results are focused on the analysis of single fingers or subsets of the parameter space. *Santos* used seven experiments from *Hollister* to optimize a model of the thumb composed of hinge joints [Santos and Valero-Cuevas 2004; Hollister et al. 1992]. Hinge joints do not completely represent the real joint motion, since the human joint axes of rotation are configuration-dependent.[47] Because the outcome of any optimization effort

[45] Focussed on simplicity and light weight rather than perfect grasping performance

[46] The frontal surface of the human fingertip can completely oppose the frontal surface of the proximal phalanx. That range of motion is not possible using only one finger joint.

[47] The use of cadaver measurements also increases the errors in bone position measurement, since rapid tissue deterioration allows for unnatural movements. Moreover, only passive ranges of motion can be measured (for grasping, only the active range of motion is used).

is strongly dependent on the initial kinematic model, the optimization results represent the funtionalities and motions needed for a hand only in a limited way. Furthermore, the interaction of the fingers and the thumb is crucial for a well performing hand. Therefore, the thumb kinematics has to fit the finger kinematics as well as the palm geometry. In consequence, the proposed kinematics unfortunately cannot be applied to the *Awiwi Hand*.

Approaches to reproduce the exact kinematics of human hands are not suitable for the design of the desired hand either. The robotic system has to use technologies that are not equivalent to biological solutions (tissue regeneration, drive speed/power density). Furthermore, packaging constraints hinder the implementation of a large number of actuators, which in turn limits the total available DoF in the hand design.

The main focus of the intended hand is on an anthropomorphic service robotic system which means the grasping and manipulation performances of the hand as a whole is a central goal. Therefore, for the *Awiwi Hand*, it is of little relevance to optimize the kinematics of a single finger. The design should rather focus on the synergies between the five serial robots, that are the five fingers, and the underlying functionalities of the hand. To find a functional optimal kinematics using optimization algorithms, optimizations have to be performed over the complete hand. Consequently, functional parameter sets have to be defined.[48] A fundamental understanding of the entire grasping and fine manipulation process, as well as a transcription of this understanding into a set of mathematical properties would be required to apply the methods described earlier. Otherwise, poor performance in unconsidered tasks due to incomplete subsets of parameters, comparable to the over fitting in neural network learning, is likely to occur. Up to now, there is no clear definition using objective functions/criteria of what “a good hand” means in regard to grasping and manipulation abilities, and it has never been practically applied apart from some basic examples, to the author’s knowledge.

Therefore, this thesis will use a simple and effective approach to design the kinematics of the *Awiwi Hand*. As a starting point, rough kinematic models based on a functional understanding of the human hand will be established and improved iteratively, using intuitive tests and fast prototyping. The tests

[48] The well known criteria to evaluate serial robots like dexterous workspace and manipulability and even grasp stability criteria have not proved suitable for hand kinematics optimization or even functional evaluation.

are based on medical evaluation tests used in surgery, as well as everyday grasping tasks. More details will be given in section 4.3.

2.4.3. Actuation

The design of the forearm actuating the hand is not part of this work (see [Grebenstein et al. 2011; Friedl et al. 2011a; Friedl et al. 2011b]). However, selecting an appropriate actuation concept for the hand remains a key issue. Since the hand is aimed to be anthropomorphic in terms of size and force, integrated actuators as in the *Fluidhand* and *ARMAR's* hand of the Forschungszentrum Karlsruhe, *DLR Hand II*, the *Gifu Hands* or in the remarkable *Twendy-One Hand* as well as in commercial hands like the *Elu2 Hand*, are not applicable. All these hands are either much weaker or significantly bigger than the human hand. Consequently, the range of relevant recent hands regarding actuation is limited to remotely actuated hands.

Furthermore, the *DLR Hand Arm System* is intended as a mobile system. Therefore, the use of pneumatic actuators like in the *UTAH/M.I.T. Hand* or the *Shadow Hand* is not favorable due to the necessity of a bulky pressurized air source or tank[49] and hence spatial restrictions.

Robustness Considerations

Robustness of the robot hand is one of the key goals of this work. It has been partially achieved so far by several approaches discussed in the following. The hand of NASA's *Robonaut* is built to be robust with integrated shock mounts. Furthermore, the bidirectional cable transmission is constructed to buckle when external impacts force the finger into increased flexion, thus absorbing the impact.

The *UB Hand 3* as well as several other hands such as the *Robonaut Hand* and the *Twendy-One Hand*, are covered with thick and soft, shock absorbing tissue which also improves the grasp performance.

The compliant finger presented by *Sugano* [Sugano et al. 1992] uses its compliance to enhance robustness and is also able to vary the passive joint stiffness. It comprises an elastic element that is able to store energy, and therefore, dynamically decouples the drives and the fingers. The latter protects the

[49] Using a pressurized air tank raises control issues caused by variying air pressure due to e.g. changing Reynolds- number etc.

structure as well as the drive train from damage from impacts, and thus, enhances the robustness of the finger significantly. The concept of storing energy is also used for the humanoid robot *Wendy* and its successor *Twendy-One*. The actuation of the pneumatically driven version of the *UTAH/M.I.T. Hand* as well as the actuation of all other pneumatically driven hands like the hands of the Forschungszentrum Karlsruhe, the pneumatic version of the *Shadow Hand* and the *I-Limb Hand* by Touch Bionics Inc., are also intrinsically able to store energy in the compressed air and thus to withstand impacts.

None of the previously mentioned hands provides the desired robustness. Their robustness remains significantly less than that of the human archetype.[50]

Dynamics Considerations

Another objective of this work is to significantly enhance the dynamics of the hand. Approaches are discussed in the following. *Kaneko* presented a three finger gripper that achieves 100 g acceleration and moves "almost too fast" for the human eye when catching a ball [Kaneko et al. 2003]. This remarkable performance is achieved by high power and high speed motors in combination with a low inertia finger design. On the other hand, this approach is not applicable to an anthropomorphic five-fingered hand, since the size of the motors would make the forearm of the robot much too bulky.

The finger built by *Sugano* [Sugano et al. 1992] does not only provide robustness by storing energy short-term, but it also permits using the energy stored in the elastic elements to enhance the dynamics of the finger as shown for a robot joint, for example by *Haddadin* [Haddadin et al. 2009b]. Of course, all the hands mentioned above that are able to store potential energy provide enhanced dynamic performance.

Consequently, to achieve the targeted dynamical performance as well as robustness against impacts, the *Awiwi Hand* has to utilize energy storage. Since the quality of grasps as well as the fine manipulation capabilities of robot hands largely depend on a compliance suitable for the task as shown by *Sugano* [Sugano et al. 1992], the use of variable stiffness in combination with the intended kinematics is expected to provide the desired enhanced grasping performance. However, the design of the drive train *Sugano* has chosen,

[50] It can be assumed that the human hand is equipped with an ideal degree of robustness for the tasks it needs to fulfill, as it has been optimized for that specific use for hundreds of thousands of years.

specifically the non-antagonistic setup that makes a tendon tensioning mechanism necessary to eliminate tendon length changes, is not suitable for the hand of the *DLR Hand Arm System* due to spatial restrictions.

To drive the *UTAH/M.I.T. Hand*, *Jacobsen* used an antagonistic setup without energy storage and adjusted the tendon tension by a controller [Jacobsen et al. 1989; Jacobsen et al. 1984]. Nevertheless, the antagonistic setup allows for simplicity regarding the drive train design, since all actuators can be designed the same way with no additional tendon tensioner.

Combining the antagonistic drive train approach shown by *Jacobsen* with the elastic elements of the drive train suggested by *Sugano* and *C. E. English* turns out to be a promising approach for the actuation of the *Awiwi Hand* as shown in the experimental results to be discussed in detail in chapter 5 [Sugano et al. 1992; English and Russell 1999a; Grebenstein 2006b].

2.5. Conclusion

The analysis of the state of the art shows that, to achieve the goals of this work, it is necessary to gain a deeper understanding of the human hand on a functional and abstracted basis.

The kinematics implemented in the hands shown beforehand do not achieve the grasping performance required for the intended hand. For hand designers, the methods for designing hand kinematics are not only dissatisfying in terms of applicability, but also in regard to the actual outcome.

On the other hand, the principles of the designed drives and the designs of the transmission allow neither for the necessary robustness to use the hand in an unstructured environment where collisions will occur, nor for a robustness comparable to that of the human archetype that also provides variable stiffness.

Based on the approach of understanding rather than copying the human archetype, the following chapter will analyze the human hand in order to depict the underlying and necessary functions as a basis for hand design.

3

Analysis of the Human Hand

The previous chapter discussed the state of the art of robot hand design and elaborated its key aspects. As a basis for hand design, insights have been deduced by analyzing the assets and drawbacks of existing hands and kinematics design methods. Since the human hand by far outperforms all existing robot hands, the thorough analysis of the human hand is fundamental for finding the essential functionalities needed for the design of a robot hand.

This chapter presents the human anatomy and analyzes the underlying functionalities that are essential for the performance of a hand, using the methodology presented in section 1.6 as depicted in figure 3.1.

The first part of this chapter gives an overview of human hand anatomy based on [Grebenstein et al. 2010b; Grebenstein et al. 2012].

The aspects relevant to elaborate the functionalities the human hand anatomy provides, will be highlighted. The first section discusses the skeletal and ligament structure. Subsequently, the joint anatomy of the hand, the fingers and the thumb is presented. The most important anatomical terms used in the following are depicted in figure 3.2. The complete anatomical terminology used in the following is given in the prelims (chap. Notation).

The second part of the chapter analyzes the human anatomy using the methodology presented in section 1.6 and is based on [Grebenstein et al.

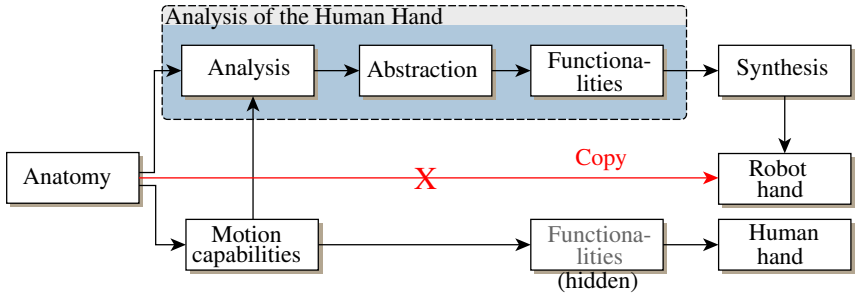

Figure 3.1. Functional abstraction scheme. To derive the functionalities needed for a well performing hand, the anatomy and the resulting motion capabilities give valuable hints since they are the basis of the (hidden) functionalities needed for a well performing hand.

2010b; Grebenstein et al. 2012]. Fundamental functionalities provided by anatomy and necessary for robustness, fast dynamics, and in particular, good grasping performance are derived by abstraction and functional understanding of the hand. Initially, the anatomy and functionality of the finger joints are analyzed, followed by the analysis of the axis orientations in the fingers. Next, the anatomy of the finger MC joints (excluding the thumb) is of special interest, since the characteristics and axes orientations of these joints have a large impact on the functional interaction of the fingers and thus the functionalities the hand provides. The thumb, as the strongest finger of the hand and the opponent of the fingers, plays a central role in hand functionality. Hence, the functionalities provided by the thumb joints are subsequently analyzed. The human hand is able to arch the palm of the hand by moving the little finger MC joint towards the thumb, which is achieved by the HMC joint. The functionality of the latter will be abstracted and interpreted. Finally, the importance of the skin and the surrounding tissue of the human hand is discussed, followed by a short resume of the functional abstraction that sums up the aspects that are most important for hand design.

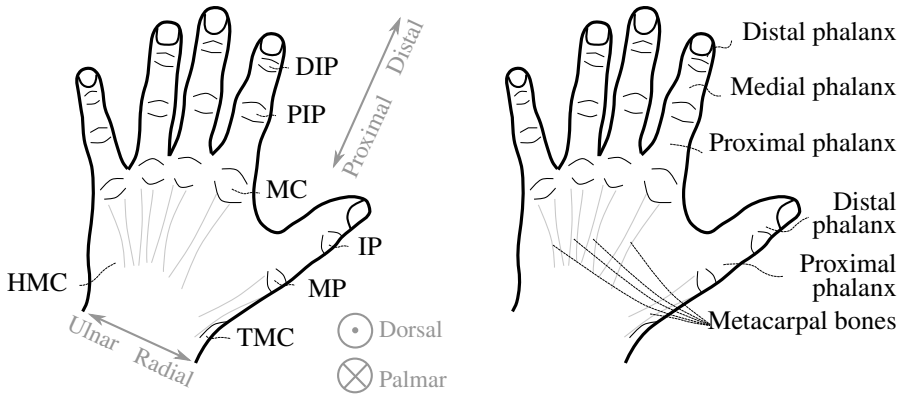

(a) Joints and positioning

(b) Bones

Figure 3.2. Anatomical terminology used in the following chapters. The full terminology is given in the prelim (chap. Notation). Abbreviations: DIP: distal interphalangeal, PIP: proximal interphalangeal, MC: metacarpophalangeal, IP: interphalangeal, MP: metacarpophalangeal, TMC: trapezometacarpal, HMC: hamatometacarpal

3.1. Anatomy of the Human Hand

Anatomy and the resulting motion capabilities are the basis of the functionalities the human hand provides. By implication, the analysis of the human anatomy gives valuable insights into the functional principles a robot hand should be capable of. Following the methodology from chapter 1.6, understanding these functionalities in terms of functional abstraction in the author's opinion is a more promising path than the plain copying of the anatomy of the human hand, which is for example described by *A. Kapandji*, *A. Benninghoff*, *H. Gray* or *J. A. Gosling* [Kapandji 1982, pp. 164-281; Benninghoff 1994, pp. 441-468; Gray 1999, pp. 158-170,263-268,401-409; Gosling et al. 2002, pp. 118-120]. In this thesis, this abstraction will be the basis of the development of the technical system. With this approach, the advantages of the human hand can be merged with the beneficial properties of a technical system. The attempt to replace all biological materials with technical ones, as necessary to copy the anatomy of the human hand, will lead to a hand that will not achieve

the goals of this thesis. As a starting point of the functional abstraction this section presents the anatomy of the fingers and highlights the elements that are important in terms of functionality. It is partly based on [Grebenstein and Smagt 2008; Grebenstein et al. 2010b; Grebenstein et al. 2012].

3.1.1. The Skeletal Structure of the Human Hand

The human hand skeleton consists of the bones of the wrist, palm, fingers and thumb (the term "fingers" does not include the thumb in this thesis). The palm is based on the wrist bones, which mainly enable the wrist movements. The metacarpal bones of the fingers span the palm and are connected with each other by the so-called interossei ligaments (see fig. 3.3). The fingers consist of the proximal, medial, and distal phalanges (see also fig. 3.2), whereas the thumb only has two phalanges (proximal and distal phalanx; see fig. 3.3).

All bones of the hand are connected by joints. Their range of motion varies significantly. The carpometacarpal (CMC) joints connect the metacarpal bones to the bones of the wrist (see fig. 3.3). Within the index finger, the middle finger and, in part the ring finger,[1] the joint motion range is negligible with regards to the function of the hand and for that reason, will not be discussed in the following. Their motion is limited or even disabled by ligament structures.

The CMC joint of the little finger is called HMC and provides a significant range of motion due to the less rigid ligament structure. The fingers are connected to the metacarpals by the MC joints. The PIP and DIP joints of the fingers link the phalanges of the fingers to each other (see fig. 3.2). The fingers are similar regarding their structure, joints and tendons, but differ significantly from the thumb [Gray 1999, pp. 166,265,404]. The thumb is stronger and shorter than the four fingers. Since the thumb plays an extraordinary role in human grasping [Napier 1993, pp. 55-60; Flatt 2002; Chalon et al. 2010] and manipulation and further, differs significantly from the fingers in anatomy, it will be described separately in section 3.2.5 [Grebenstein et al. 2010b].

[1] The mobility of the ring finger CMC is small and therefore does not play a dominant role in grasping.

Figure 3.3. The structure of the palm. The four vertical bones *(right)* are the metacarpal bones of the fingers. The interossei ligaments *(top)* connect the metacarpal bones right at the MC joints located at their distal end. The thumb is seen on the left of the picture. The proximal bone of the thumb is the thumb metacarpal *(bottom left)*. Thus, the thumb has only two phalanges. Its proximal phalanx is seen in the upper left of the picture. The CMC joints, which connect the metacarpal bones to the wrist bones, are partly hidden behind the massive ligament structure of the wrist *(bottom)* (courtesy of *Primal Picture Ltd.* [McGrouther et al. 2000]).

3.1.2. Joint Types of the Human Hand

Biological joints are very different from their technical counterparts. Hence, a thorough understanding of the hand joints is imperative for the proper design of an anthropomorphic hand. The analysis of the joints gives valuable insights into underlying functionalities. The human hand is mainly composed of three kinds of joints (fig. 3.4):

1. Hinge joints
2. Condyloid joints

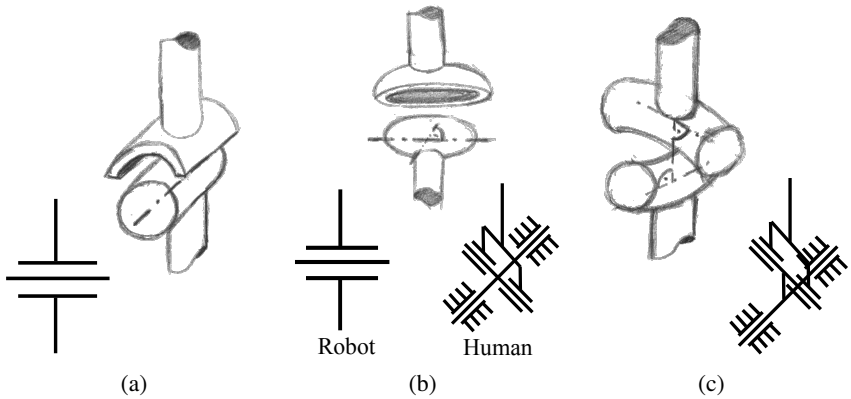

Figure 3.4. Joint types of the human hand and their equivalents: *a*, hinge joint; *b*, condyloid joint. From a geometrical perspective, the condyloid joint is a 1-DoF hinge joint, but is used as a 2-DoF joint in biology. *c*, saddle joint

3. Saddle joints

These can be categorized into one-DoF and two-DoF joints. The one-DoF joints (PIP, DIP, and thumb IP) of the human hand are hinge joints. The ridge in the middle of the joint (figure. 3.5a), which could be misinterpreted as a saddle joint head, prevents the finger from being dislocated by axial loads. The human hand provides two types of two-DoF joints: the finger MC joints, the CMC joints of the fingers, and the HMC joint are of the condyloid type (see figure 3.4b) [Gray 1999, p. 267]. In contrast, the TMC joint of the thumb is a saddle joint [Gray 1999, p. 265], however, with non-orthogonal axes. *K. Kuczynski* described its geometry similar to the saddle of a scoliotic horse [Kuczynski 1975] as depicted in figure 3.6 [Kuczynski 1975; Tubiana 1981].[2] The functionality of the different joint types is discussed in section 3.2.

3.1.3. Joints of the Finger and the Thumb Joints

The joint types described above exist in several variations. In the following, the joint characteristics specific to dedicated joints are discussed, starting with

[2] Scoliosis is a "abnormal lateral curvature of the spine"[Oxford University Press 2012c]

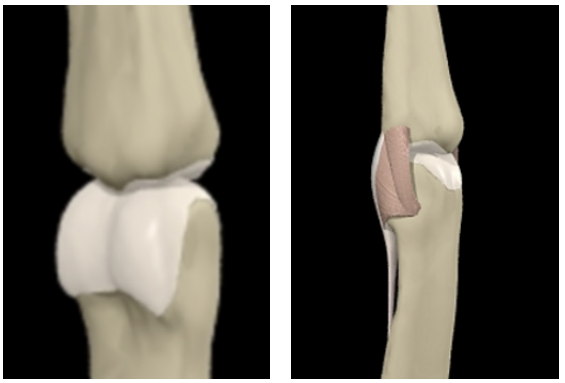

(a) (b)

Figure 3.5. The Human PIP- Joint: *a*, the PIP joint; *b*, supporting ligaments of the PIP joint. The white frontal (*left*) structure prevents overstretching of the finger.

the little finger moving distally and towards the thumb. The little finger differs from the other fingers and the thumb. It has a bone structure similar to the index, middle, and ring finger, but its tendons, ligaments, and muscles resemble those of the thumb. As stated before, the motion range of the metacarpal bone in the CMC joint (or more specifically HMC joint) is considerably larger than in the index, middle, and ring fingers. The so-called opponens digiti minimi muscle moves the metacarpal bone palmar and towards the center of the palm. This movement shapes a ridge (called the palmar arch) between little finger and thumb [Kapandji 1982, pp. 174-175].

Following *Kapandji*, the axes of the human finger joints are not orthogonal to the sagittal plane. The so-called inclination of a joint is defined as the angle of deviation of the axes from the normal position within the frontal plane (fig. 3.7a). The inclination of the axes increases from the index to the little finger [Kapandji 1982, p. 188] (fig. 3.7b).

The kinematics of the human thumb, regarding the TMC and MP joint (please see figure 3.2 for nomenclature of joints), is not described consistently in anatomical literature. *Kapandji* [Kapandji 1982, pp. 208-236] hypothesizes two DoF in the TMC joint and two DoF in the MP joint, while *Benninghoff* [Benninghoff 1994, p. 448] suggests three DoF in the TMC joint and one in

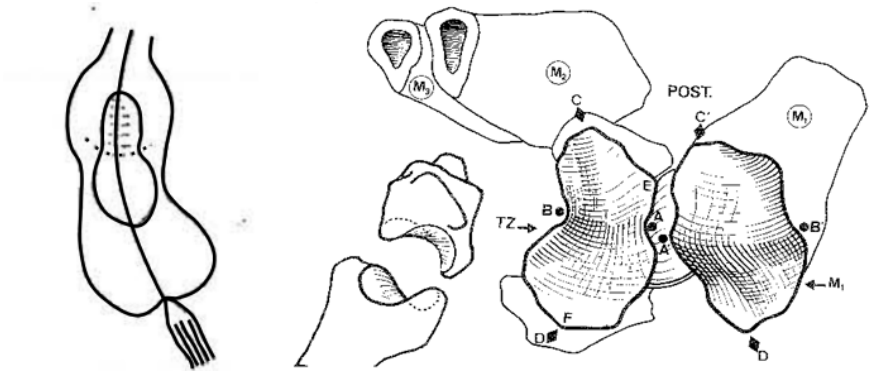

Figure 3.6. The saddle of the human thumb TMC [Kuczynski 1975]. The vertices of the horse saddle are located on a curved line. The dotted line on the horse back marks the trajectory of the contact point during joint motion *(left)*. This "saddle of a scoliotic horse" describes well the articulate surfaces of the thumb TMC joint *(right)*.

the MP joint.[3] Following *Kapandji*, the TMC joint of the thumb is considered a two-DoF saddle joint.

According to *Kapandji* [Kapandji 1982, pp. 232-235], the thumb MP joint has, in addition to its main axis of motion (flexion/extension), a range of motion of about 25 ° around the longitudinal axis of the medial phalanx described in more detail in section 3.2.5. Most people are, however, not able to actuate this DoF separately.

Analogue to the finger DIP joint, the IP joint of the thumb is a one-DoF hinge joint. The range of motion of the thumb IP joint is much bigger than that of the finger DIP joints and varies extremely amongst individuals (see fig. 3.8).

3.1.4. Ligaments, Tendons, and Muscles

The joint capsules, ligaments, tendons, and muscles are of paramount importance for the function of the human hand. However, these structures are ex-

[3] Especially the joints of the thumb have large flexibility even in non-articulated axes. All of these can move, at least passively, in allmost every direction. Therefore, the discussion boils down to which joints generate the five largest movements.

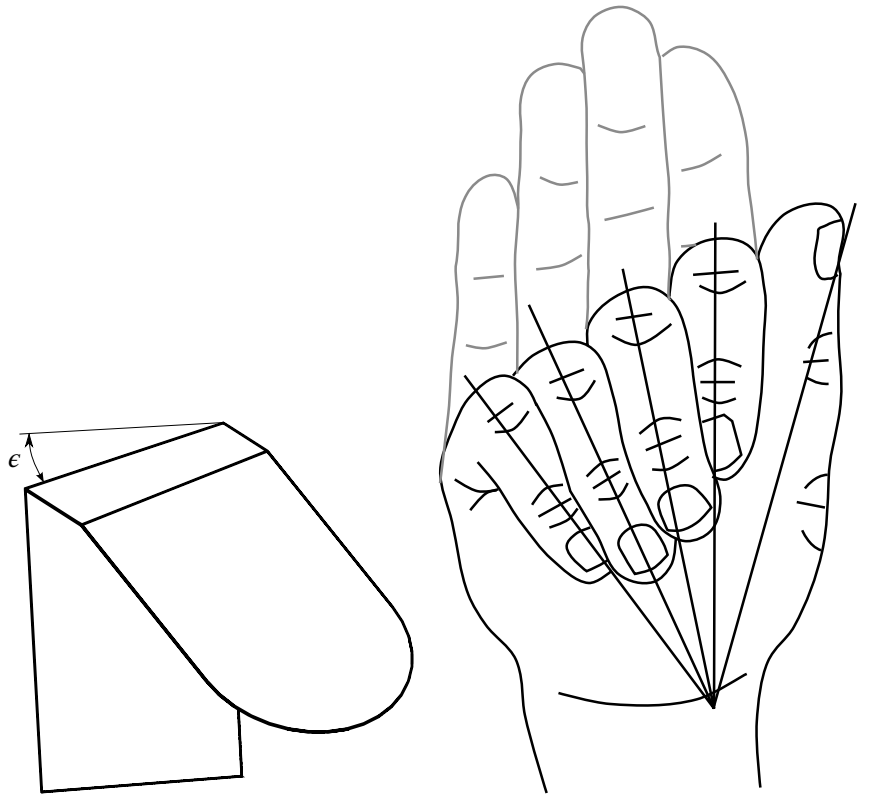

Figure 3.7. The effect of joint axis inclination: *a*, rotation of the distal phalanx and reorientation of the medial and distal phalanx due to inclination angle ϵ: The angle between the phalanges has a maximum of 2 times the inclination angle at 180° flexion. In contrast, the reorientation angle of the frontal surface of the finger maximizes to the inclination angle at 90° deflection; *b*, change of distal phalanx orientation: stretched-out and fully flexed (PIP) fingers as shown by *Kapandji* [Kapandji 1982]. The lines of the finger phalanges meet in one point at full flexion of the PIP due to the inclination angles ϵ_i.

Figure 3.8. Thumb maximum passive extension of the IP of two team members

tremely complex and vary between individuals [Leijnse 1997]. An example of the complexity of the tendon apparatus is the extensor mechanism, see figure 3.9. This, in comparison to the structures in the palm and forearm, relatively simple structure is still under investigation in robotics and bio-mechanics research [Miller et al. 2005; Wilkinson et al. 2003; Leijnse and Spoor 2012]. This is further complicated by the fact that all these structures are flexible and, in particular ligaments, capsules and tendon sheaths, degenerate within a couple of hours if being dissected. This makes cadaver experiments very difficult and extremely expensive. In consequence, a complete understanding of the functions of these structures is still an open and challenging research topic. Therefore, no general overview of the human tendons, muscles, and ligaments will be given in this thesis. Nevertheless, the function of important ligaments, will be considered in order to deduce, for example, joint functionalities.

3.2. Functional Abstraction of the Human Hand

The previous section roughly outlined the anatomy of the human hand. This anatomy, in turn, has been optimized by natural selection until it enabled the

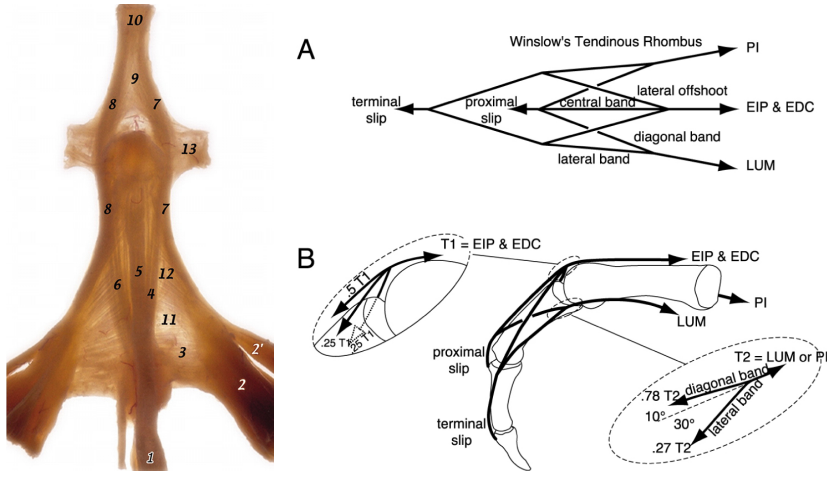

(a) (b)

Figure 3.9. The extensor mechanism of the human finger: *a*, the photo of the unwrapped (easily deformed and flexible) extensor mechanism web demonstrates the complexity of the functional analysis of the ligament structures [Clavero et al. 2003]; *b*, the *Winslow* model is an exemplary model of the extensor mechanism and the resulting finger motion [Miller et al. 2005].

functionalities needed to survive. For example, the location, length, and orientation of the human thumb, in contrast to monkey thumbs which are mainly used for power grasp, are a result of the necessity of opposition to handle tools [Napier 1993, pp. 55-60]. Thus, the analysis of the hand anatomy and its motion capabilities described in the following sections, allows to "observe" the functionalities of the hand and deduce guidelines for the design of the anthropomorphic *Awiwi Hand*.

3.2.1. Joints of the Human Hand: Functionalities and Technical Equivalents

As mentioned in section 3.1.2, the human hand consists of three different joint types: hinge joints, condyloid joints, and saddle joints (see fig. 3.4). In the following, the underlying functions and manifestations of the joints are

discussed.

Human bones are relatively weak regarding shear and tensile stress and they degenerate if no load is applied. Therefore, the articular surfaces of human joints are not protruding and rather roundish. This results in low guidance of the joints in all but normal directions. This characteristic has to be compensated by the ligaments, capsules, and tendons (see fig. 3.10). In contrast, technical materials, such as alloy or steel, enable much more guidance due to their tensile strength. This makes it possible to build well guided joints without capsule and additional "ligaments". Since the capsules of the human joint also prevent the joints from falling apart at zero tendon load, a technical solution has to be found that keeps joints in place even when the system is switched off.

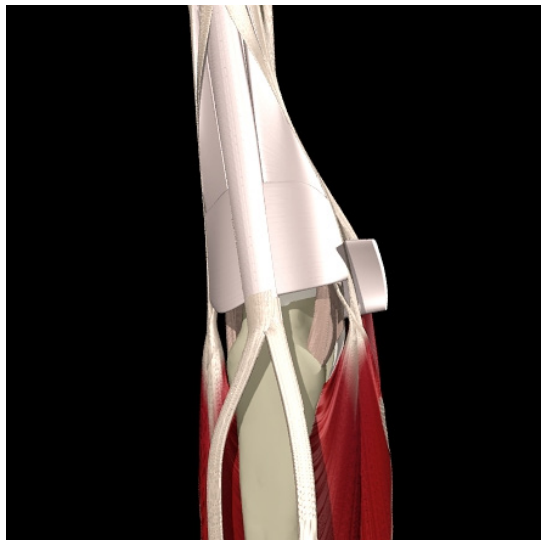

Figure 3.10. The ligaments and tendons supporting the human MC joint. The joint is supported by several layers of strong ligaments. In consequence, the functional joint characteristics is greatly influenced by the ligaments. (courtesy of *Primal Picture Ltd.*) [McGrouther et al. 2000]

3.2.2. Functionalities of the Interphalangeal Joints

The DIP and PIP joints of the fingers and the thumb IP joint are of the hinge joint type. From a functional perspective, these joints consist of a (more or less) cylindrical joint head and a joint pan.[4] The joint pan has significantly less than 180° enclosure. Therefore, these joints are able to luxate. Luxation can harm the (regenerating) capsules and tendons. However, it avoids structural damage of the joint heads and the bones. This behavior is also favorable for the joints of a robot hand as it significantly improves robustness, in particular against sideways collision. The ridge in the middle of the joint (figure 3.5a), together with the joint capsule and the ligaments, prevents the finger from being dislocated by axial loads. This functionality has to be technically represented in the robot hand.

3.2.3. The Role of Inclination

Besides the characteristics of the joints themselves, their orientation is crucial for the performance of the hand. This section describes the role of the so-called inclination of the IP joints.

Following *Kapandji*, the axes of human IP joints are not orthogonal to the sagittal plane [Kapandji 1982, p. 188]. The inclination of a joint is defined as the angle of deviation of the axes from the normal position within the frontal plane (see fig. 3.7a). The axis inclination increases from the index to the little finger (fig. 3.7b).

A serial column of orthogonal axis joints does not change the fingertip orientation nor does it move the fingertip out of the sagittal plane. Therefore, from a functional perspective, the inclinations of the axes enable the fingers to be straight in a stretched-out position of the joint. This is important, for example, for carrying a heavy box on the edge or pushing against an object with the flat hand without collision/overlap of the fingers (see figures 3.17b, 3.17a). On the other hand, the inclination causes the phalanges of the finger to point towards the palm middle for flexed position (see figure 3.7b). This effect increases with flexion angle, which is e.g. important in grasping a palm sized or small ball (fig. 3.11). Furthermore, it enables opposition of the little

[4] According to *van Nierop* [Nierop et al. 2008], the shape of the human joint can be approximated by tangentially fitted lateral surfaces of cylinders (or even cones) with different diameters. Of course, this shape causes a moving joint axis.

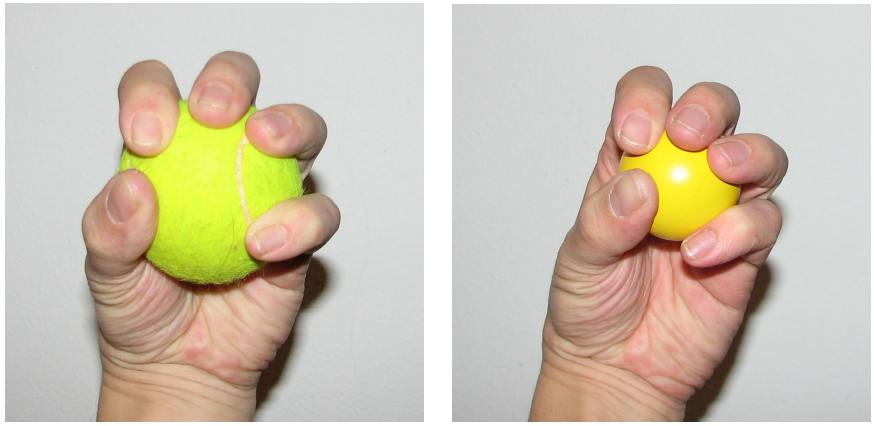

(a) (b)

Figure 3.11. Grasping of small balls: the inclination of the DIP and PIP joint supports the inward orientation of the first axis of ring and fifth finger MC joint: *a*, palm size ball: The fingers are in well distributed contact with the object. The ring and little finger are in opposition to the thumb. *b*, small ball: The inclination of the ring finger enables proper opposition. Its distal phalanx meets the thumb fingertip. The inclination of the little finger cannot prevent the finger from touching the ball sideways anymore. Without inclination it would have no or very weak contact with the ball.

finger and thumb. In addition, the inclination rotates the phalanges toward the inside of the palm (figure 3.7a, 3.11). This rotation prevents (painful) contact of the sides of the fingers and enables contact of the pulp with the object. Performing small object power grasp, it also prevents lateral forces within the joints due to laterally oriented contact forces.

3.2.4. Metacarpal Joint of the Fingers

The finger MC joints enable a large workspace of the fingers. This property makes them the most important joints of human fingers. This section discusses the functionality of the MC joints in detail.

The MC joints of the human fingers, unlike the thumb TMC[5] (see sec.

[5] Anatomically correct the thumb has no MC joint. Consequently, the TMC is the base joint

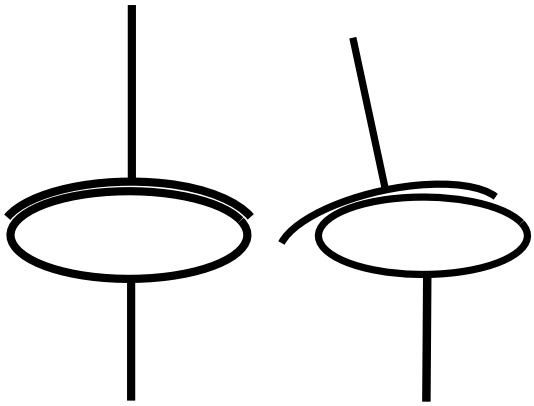

Figure 3.12. Condyloid joint motion around second axis. The contact changes from *a*, line/surface contact to *b*, point contact.

3.2.5) are condyloid or spherical joints. In classic anatomy they are often interpreted as condyloid (ellipsoidal) joints (fig. 3.4) [Gray 1999, p. 267; Kapandji 1982, p. 176]. The ellipsoidal geometry allows only for one-DoF movements, whereas within the human hand it is used as a two-DoF joint. Motion of such an ellipsoidal joint, around any but the main axis, inevitably changes surface contact to point contact (fig. 3.12). Presupposing a condyloid joint, the rotation about the longitudinal axis of the joint link is blocked by the ellipsoidal geometry of both, the joint socket and the joint head.

In contrast, in the extensor mechanism model of *J. Leijnse* [Leijnse and Spoor 2012; Leijnse et al. 1992], the MC joint is interpreted as a three-DoF ball joint. It is limited to two DoF by the ligament structure (so-called collateral ligaments; see figure 3.13b).[6] The rather small contact surfaces of the MC joint and the almost spherical joint head geometry of the metacarpal bone, do not shed light on the correct interpretation of the MC joint from a *skeletal view* (see fig. 3.13a). Taking into account the supporting ligaments (*musculoskeletal view*), as well as the functional point of view, the MC joint will be

of the thumb as the MC is for the fingers. Thus, the TMC joint can be interpreted as an equivalent to the finger MC joints.

[6] Some anatomists also interpret the MC joint as a ball joint, cfr. [Benninghoff 1994, p. 449].

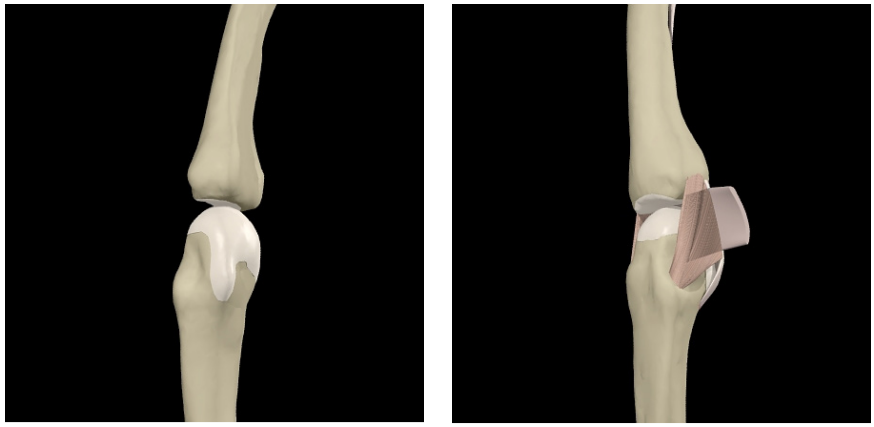

(a) (b)

Figure 3.13. The human MC joint: *a*, the MC joint head. The small area of contact does not give information about the joint characteristics (*skeletal view*). *b*, the collateral ligaments stabilize the joint and limit it to 2 DoF. (*musculoskeletal view*) (courtesy of *Primal Picture Ltd.*) [McGrouther et al. 2000]

interpreted as a two-DoF joint in the following.

Due to high contact pressure, a technical copy of a condyloid joint would cause excessive wear on the joint surfaces. In human joints, the elasticity of the cartilage surfaces in addition to the joint fluid together compensate for geometrical inaccuracies of the joint heads. On the other hand, complicated mechanisms or ligament-like structures would be necessary to disable the third DoF of a spherical/ ball joint.

From the kinematics perspective, replacing a condyloid or spherical joint by a two-DoF cardan joint is not correct. The second axis of a cardan joint changes its function from pitch to roll at 90° flexion of the first axis and is singular in this position. Therefore, the workspace of the cardan joint has the shape of an "orange segment" (fig. 3.15b), unlike a spherical or condyloid joint, which has the shape of a conical section of a sphere (fig. 3.15a). A simple experiment gives valuable hints about how to replace the condyloid joint or spherical joint: If one moves the MC of the stretched out finger sideways from one motion limit to the other (adduction/abduction) when the finger is

increasingly flexed, the resulting range of motion is shaped similar to the one of a cardan joint. In contrast, the anatomy of the joint itself gives reason to expect a cone-shaped sphere section (see fig. 3.15a). At 90° flexion, the human fingers have a very restricted sideways motion range but are able to roll about their longitudinal axis (see fig. 3.16).[7] Additionally, the limited lateral motion range enables the carrying of lateral forces by the structure instead of the muscles e.g climbing a rope or a pole (see fig. 3.14).

Figure 3.14. Climbing a pole: The MC joints, in particular of the little and ring finger, are locked sideways. Thus the lateral force largely is carried by the joint structure (and the thumb). Structural damage of the joints by these lateral loads is very unlikely, since the (tangential) lateral forces are transmitted by friction and thus, are limited.

In full flexion ($\approx 90°$) the fingers perform mainly two tasks:

- Fixing an object in the palm by wrapping around it and pressing it

[7] Every finger of the human hand reaches its singularity at 90° flexion.

Figure 3.15. Schematic range of motion of MC joints: *a*, spherical joint; *b*, cardan joint. The motion range of the cardan joint depends on the maximum elevation angles of abduction/adduction and flexion/extension.

against the palm (power grasp fig. 3.17b), even at high lateral loads (fig. 3.14)

- Locking the MC joint position with out-stretched DIP and PIP of the finger, for example in order to hold large objects at their edges (fig. 3.17a)

Hence, from a functional perspective, the fingers should not have any motion range in the MC joint at 90° flexion.

The condyloid joint can be replaced by a cardan joint without any functional impairment, assuming that the finger functionality in the fully flexed position is limited to the cited cases. Nonetheless, care must be taken in the choice of the reference frame for the "orange segment" [Grebenstein et al. 2010b; Grebenstein et al. 2012].

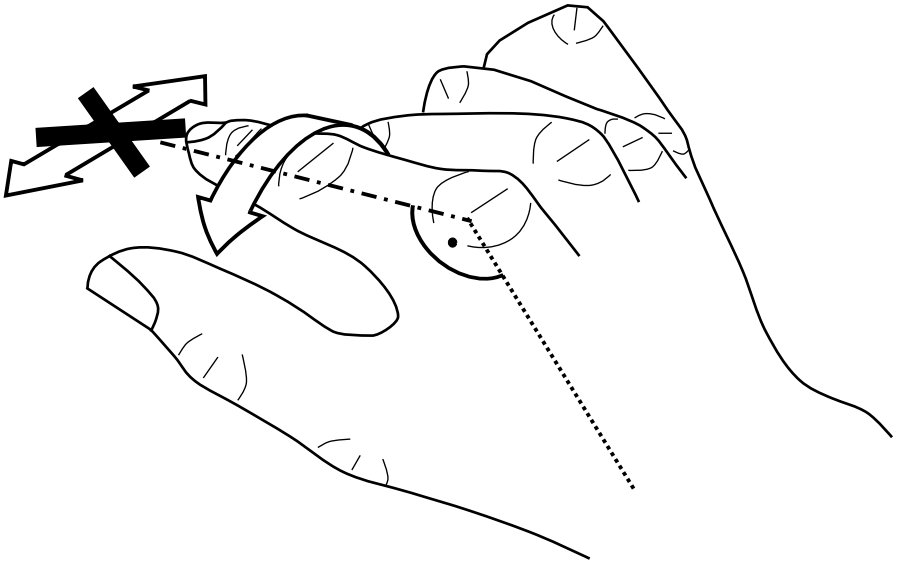

Figure 3.16. The first axis of the index finger MC joint changes its function to a roll axis at the singularity (90° flexion). The motion range of this roll motion is quite small and does not provide important functionality. In this pose, no lateral motion of the finger is possible.

3.2.5. The Joints of the Thumb

> *The hand without a thumb is at worst, nothing but an animated fish-slice, and at best a pair of forceps whose points don't meet properly.*
>
> –J. Napier [Napier 1993, p. 55]

The thumb has a key role in the human hand. As early as in the 10th century, King Canute of Denmark laid down the importance of the thumb in the compensation to be paid for the loss of the fingers and the thumb. His rates match the ones defined by the British Department of Health and Social Security (DHSS) surprisingly closely: "They range from 30 percent for the loss of thumb (DHSS) and 30 solidi or shillings (Canute), to 7 percent for the loss of

(a) (b)

Figure 3.17. Main functions of the fingers at 90° MC joint flexion. The first axis of the MC joint is singular in this position. Therefore, the fingers have no motion capabilities sideways. *(a)* Carrying an object *(b)* Enclosing an object (power grasp)

the little finger."[Napier 1993, p. 22].[8]

Furthermore, the importance of the thumb for human grasping and manipulation is reflected in the effort put into the reconstruction of the human thumb to regain the grasping capabilities of the human hand. Surgeons nowadays replace a lost or missing thumb in a surgery named pollicisation by a finger (mostly index finger) or a toe. Almost the complete grasping abilities of an average human hand can be regained by pollicisation [Flatt 2002; Chalon et al. 2010].

Interpretation of the Thumb TMC

The equivalent to the MC joint of the finger within the thumb is the TMC joint.

The "scoliotic horse saddle" shape of the TMC joint (see sec. 3.1.2), which

[8] Solidus is believed to match percentage [Napier 1993, p. 22].

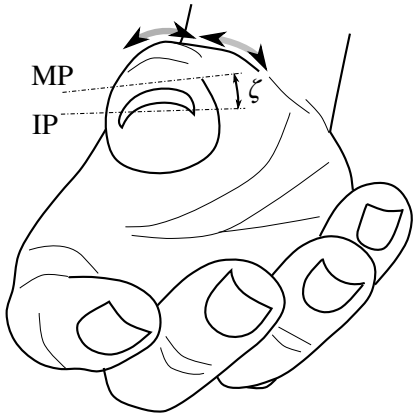

Figure 3.18. Rotations and twist of thumb joints and axes. The motion of the TMC joint and the MP joint around the longitudinal axes of the thumb bones (gray arrows) determines the inward rotation of the thumb fingertip. It is neither completely known which joint is the main source of the inward rotation, nor whether it is an active or passive motion [Kapandji 1982]. ζ denotes the twist between the axes of the MP and IP joint, which supports the inward rotation of the pad in the stretched-out position.

is technically not representable in a meaningful manner,[9] causes a two-DoF motion coupled with an additional rotation of the proximal bone along its longitudinal axis. It produces an inward rotation of the thumb [Gray 1999, p. 265], increasing with abduction angle to provide an opposition function (see figure 3.18).

Thumb MP Pronation and Suppination

The previously described inward rotation of the TMC joint during flexion is supported by an inward rotation, called pronation, of the MP joint that increases with flexion. *Kapandji* describes this inward rotation as an additional DoF of the MP joint (see figure 3.18) [Kapandji 1982, pp. 232-235]. Few humans, are able to actuate this DoF separately. Therefore, it acts similarly to a

[9] A contact surface fitting to such a curved saddle would not enable any relative motion between the joint surfaces without losing the initial contact configuration. This would produce excessive wear due to point contacts. In human thumbs the latter is known as "arthrosis of the carpometacarpal joint" of the thumb or "Rhizarthrosis".

coupled DoF, adding an inward rotation of the pad to flexion. In particular, the unloaded MP is extremely flexible regarding rotation around the longitudinal axis. The strong muscles and ligaments that articulate the flexion of the thumb are attached to the back of the phalanges and wrapped around the outside of the bones (see fig. 3.4). They turn the thumb inward, using the flexibility of the joint to get in frontal contact with the surface of objects such as large cylinders during power grasp. Furthermore, this inward rotation of the TMC and MP enables pinch grasps with the index, middle, and ring finger without limiting the ability to perform key grasps (see fig. 3.20). Key grasps and pinch grasps, in particular, use the passive range of motion of the MP extensively in order to provide better contact.

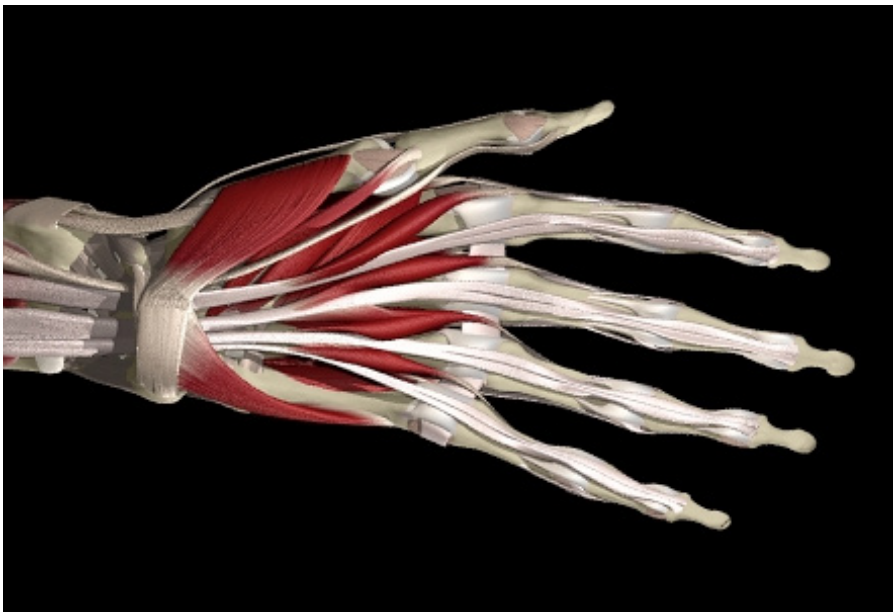

Figure 3.19. Attachment of the tendons and muscles performing thumb opposition (left hand). The large muscle attached to the metacarpal bone is the "opponens policis brevis". It turns the metacarpal bone inward during contraction (courtesy of *Primal Picture Ltd.*) [McGrouther et al. 2000].

(a) (b)

Figure 3.20. Reorientation capabilities of the thumb: *a*, pinch grasp. The thumb makes frontal contact with the index finger. *b*, key grasp. The thumb is in lateral contact with the index finger.

Function of the Thumb IP

The axis of the thumb IP is turned around the longitudinal axis of the proximal phalanx (the middle bone of the thumb) with respect to the MP axis [Kapandji 1982, pp. 236-237]. This axis orientation, called twist in the following (fig. 3.21b), rotates the thumb tip inward in stretched-out position (see figure 3.18 angle ζ and section 4.3.3) [Chalon et al. 2010].

In contrast, the IP of the thumb provides an inclination of its axis of rotation (fig. 3.21a), which causes an inward motion of the finger tip during joint flexion. This reorients the frontal pad of the fingertip to be almost parallel to the opposing part of the palm (please see also 4.3.3). The latter is used for example to power grasp cylindrical objects of medium diameter and, in extreme cases, to "clamp" a small cylindrical objects with the thumb (fig. 3.22). As already mentioned, this inward rotation is supported by the MP joint during flexion.

The combination of twist and inclination of the thumb IP allows for tuning the orientation of the fingertip in fully flexed position as well as in stretched-out position. Therefore, twist and inclination is of major importance for the design of the thumb (see section 4.3.3) [Chalon et al. 2010].

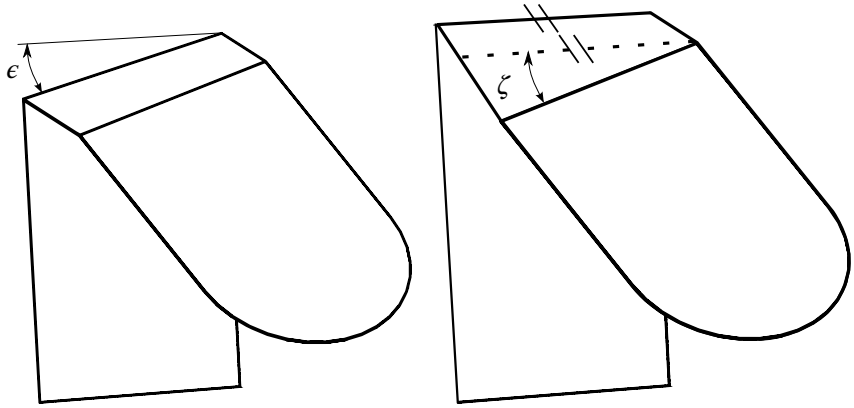

Figure 3.21. Axis angle variation and its effects: *a*, inclination; *b*, twist

3.2.6. Kinematics of the Hamatometacarpal (HMC) Joint

The function of the HMC joint enables proper opposition of the thumb and the little finger. The movement of the HMC is a combination of translation and rotation (see fig, 3.24). The translation, which is dominant in the beginning of the trajectory, enables the little finger MC to get in front of the ring finger MC. As such, the finger base and, therefore, the whole workspace of the finger can rotate inward without collision with the ring finger. Furthermore, the HMC motion arches the palm, which is important to perform power grasp of medium diameter objects with an abducted thumb, such as a screwdriver (see fig. 3.23) [Kapandji 1982, pp. 174-175].

3.2.7. Human Skin and Tissue

In the human archetype, the tissue and skin of the hand is of major importance for the grasping and manipulation abilities of the hand [Napier 1993, pp. 29-40,42-44]. It provides the contact surfaces to the object and locates the object within the hand firmly, in particular when performing power grasp.

The pads of the human hand are a complex combination of the skin, the underlying muscles and a ligament structure. This ligament structure, fastens the skin in order to be able to transfer stress to the skeletal structure. In contrast, it also allows for a direction dependent range of motion of the skin with

Figure 3.22. Clamping an object with thumb IP joint in full flexion and therefore inward rotated fingertip. This pose keeps the remaining four fingers free for manipulation tasks. This pose is rarely used but illustrates the functionality of thumb tip reorientation.

respect to the hand skeleton.

For example, within the palm, as described trenchantly by *Napier*, the

> […] skin of the palm is firmly bound to the underlying, packing tissue of the hand. There are areas, over the ball of the thumb and the ”heel” of the hand, where the skin is relatively mobile. This is because the underlying fibrous tissue, which is heavily loaded with fat, forms a distinct pad. But elsewhere—as in the central area of the palm—the underlying tissues are fat-free and the skin is firmly adherent. [Napier 1993, p. 29]

The importance of this partially firm connection of the skin to the underlying tissue has been seen after full skin grafts of the palms of soldiers who burned their hands on guns. Due to the missing connection between subcutaneous[10] fat and underlying fibrous structures, the power grasping of the soldiers became insecure and felt slippery [Napier 1993, pp. 29-30]. This clearly

[10] Lying under the skin

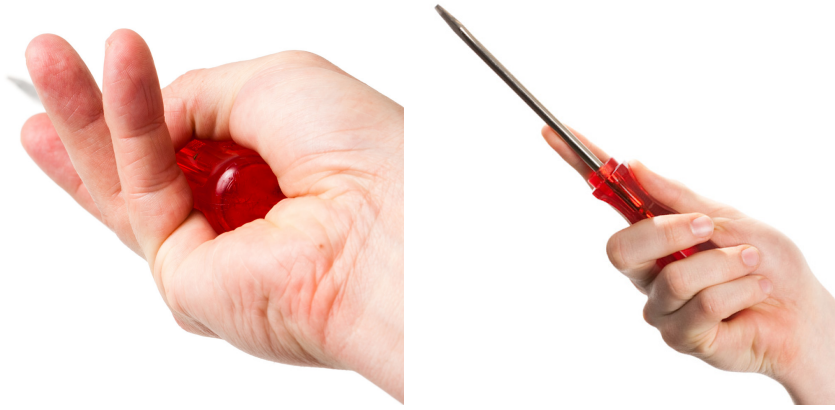

(a) (b)

Figure 3.23. The palm is arched by HMC motion to grasp a screwdriver: *a*, the palmar arch wraps the screwdriver to fix its location. The palm is quite concave in its lower part, which enables it to carry the axial forces in order to operate the screwdriver. *b*, the fingers enclose the object firmly. The little finger distal phalanx points to the thumb base due to the inward rotation and pushes the ring finger inward.

shows that at least the partial, firm connection of the skin and the underlying structures is functionally necessary.

Functionally, the skin and the underlying tissue have to provide sufficient tangential force transmission from the grasped object to the hand skeleton. Therefore, it has to be able to adapt to the object surface, to enable local force closure and provide high friction with a majority of objects. Last but not least, the pads of the hand have to distribute stress uniformly to reduce surface pressure on the contact areas.

3.3. Summary: Functional Hand Design Guidelines

According to section 1.6, the functional abstraction of the human hand is the basis of the hand design. Therefore, the most important functionalities of the human hand, mandatory to meet the goals of this work are given in the fol-

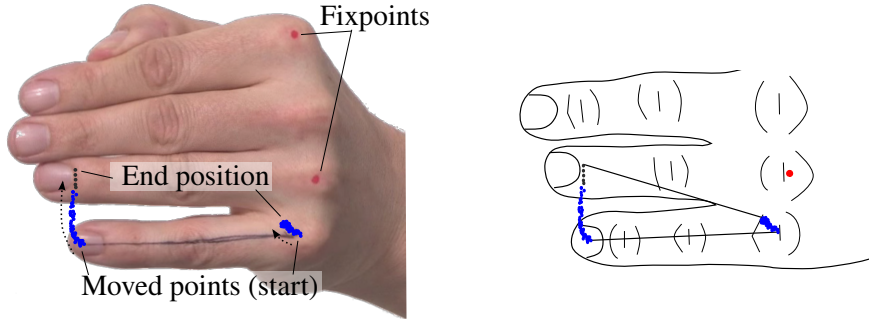

(a) (b)

Figure 3.24. HMC motion: the trajectory has been tracked by video recording and manually interpreted. Accuracy is not an issue in this experiment, since it is intended to gain a functional understanding of the motion, rather than an accurate trajectory to copy. *a*, single frame of motion analysis. The additional two red points (fixpoints) enable orientation validation of the particular frames, whereas the blue points track the trajectory (points repainted for visualization purpose). *b*, trajectory of the little finger base and fingertip. The gray tracking points have been extrapolated using the finger length and the orientation of the proximal phalanx, since the fingertip is hidden under the ring finger in extreme positions.

lowing. The section where the analysis is performed is given as reference followed by the section the guideline is relevant for.

- The location and orientation of the thumb TMC is the most important aspect in thumb design, if not even in hand design. In particular, the TMC is decisive in the following grasp situations, see sections 3.2.5, 4.6.1:
  - Key grasp
  - Pinch grasp
  - Power grasp of large diameter cylindrical objects
  - Grasping of spherical objects of different sizes

Figure 3.25. Example of stress distribution functionality of the skin: a Fakir [Ponting 1907]. The contact pressure at the nails would easily damage the underlying structures, such as nerves, veines, and muscle fibres without the stress distribution functionality of the skin.

- In addition to these grasps, a more general and proven test of the hand functionalities is needed. It should be reliable and easy to implement, see sections 2.2.4, 4.3.2.

- The reorientation of the thumb fingertip (in the human hand, provided by the fifth DoF / coupled motions, as well as the laxity of the capsules and ligaments) must be provided as a function of the flexion angles of the MP and IP joints. The thumb fingertip has to meet the object properly even in contradictory grasps, such as the key grasp and the large diameter power grasp, see sections 3.2.5, 4.3.3.

- To provide key and power grasps, the thumb has to be able to meet the fingertip of the index finger frontal, as well as lateral, see sections 3.2.5, 4.6.1.

- The fingers of the hand have to be locked against sideways motion in full flexion of the MC joint, in order to carry large lateral forces during power grasp of objects having small diameters (such as climbing a pole or using a hammer). The characteristics of cardan joints meet these re-

quirement if the first axis is pointing out of the palm, see sections 3.2.4, 4.5.1.

- To achieve good grasping performance of sphere shaped objects, in particular of small size, the distal and medial phalanges of the little and ring finger have to increasingly reorient towards the thumb with flexion (thumb opposition), see sections 3.2.3, 4.7.5.
- The fingers have to be straight in stretched-out position to avoid intersection of the fingers and to avoid lateral forces in the joints, see sections 3.2.3, 4.3.3.
- The hand has to be able to shape "the palmar arch" to grasp cylindrical objects of smaller diameter firmly and repeatable, see sections 3.2.6, 4.7.5.
- The workspace of the little finger needs to be able to turn towards the thumb to grasp small spherical objects, whereas it needs to be "in parallel" to the workspace of the other fingers during power grasp to avoid collisions of the fingers. To avoid collision with the ring finger, the MC joint of the little finger has to move in front of the palm before rotating inward, see sections 3.2.6, 4.7.5.
- To provide robustness against lateral impacts, the joints of the hand have to be dislocatable as the human joints are. The actuation has to be able to compensate the resulting changes in tendon length, see sections 3.2.2, 4.2, and 4.5.1.
- The housings of the hand, in particular, have to guarantee secure and firm grasping, see sections 3.2.7, 4.8:
  - Locate the object firmly
  - Have soft "skin" that is able to adapt to the object shape, provide good tangential force transmission, and distribute stress uniformly

The following chapter describes the hand design, based on these guidelines gained from the functional analysis of the human anatomy.

4

The Awiwi Hand: An Artificial Hand for the DLR Hand Arm System

The previous chapter analyzed the human hand to derive the underlying functionalities necessary to design the robotic hand. This chapter describes the design of the *Awiwi Hand*.

In the first part an overview of the *DLR Hand Arm System* is given since the hand is intended to be an integral part of it.

The second part describes the design of a fitting actuation concept that is integrated into the *DLR Hand Arm System*. First, the drive concept is selected according to the goals and requirements of the hand and the interfaces to the *DLR Hand Arm System*. The feasibility is then proven using a basic controller providing force control as well as vibration damping.

The design of the kinematics based on the functionalities derived from state-of-the-art hands (see sec. 2.4), as well as from the analysis of the human anatomy (see sec. 3.2), is described in the third part of this chapter. A practical approach used to design the hand kinematics is described. It uses an initial rough kinematic skeleton, based on functional understanding, which is improved through iteration, using intuitive and easy to apply medical tests, as well as selected daily grasping tasks.

Using the designed kinematics, the expected friction is estimated to guarantee the performance of the hand, as well as to derive design rules, in particular for the joint design and the tendon routing.

The fifth part outlines the transfer of the design guidelines to the design of the fingers of the hand with a focus on the joint design, as well as the structure and the tendon routing and tendon actuation.

The thumb is the most important digit of the hand, and a central part of this work. The thumb specific design details, as well as the implementation of the needed functionality is described in the sixth part of this chapter.

The kinematics designed beforehand predetermines the integration of the fingers and the thumb into a complete hand and therefore the boundary conditions for the palm design, which is described in the seventh part of this chapter. The functionalities of the HMC joint as well as the thumb described in section 3.2 drives the design of the palm. A practical approach, driven by the goal to minimize friction and to maximize accessibility and maintainability, to route all 38 tendons (having a combined load of >6 kN) from the wrist to the fingers and the thumb is discussed.

In the final part of this chapter, the housing design concepts, which have to provide the functional contact surfaces of the hand for proper grasping and manipulation, as well as the final housings, are presented.

4.1. Context of the Hand Development: The *DLR Hand Arm System*

The *Awiwi Hand* is an integral part of the *DLR Hand Arm System*. Therefore, a short description of the *DLR Hand Arm System* partially based on [Grebenstein et al. 2011] is given, and the resulting requirements for the desired hand are derived. The *DLR Hand Arm System* is a robotic system mimicking the kinematic, dynamic, and force properties of the human arm using modern mechatronic technologies. Furthermore, it should allow to make a next major step toward autonomy in service robotics by its significantly improved robustness and dynamic properties. It is based on variable stiffness drive concepts for all joints of the arm and the hand.

The system (see fig. 4.1) is designed as a fully integrated, human-sized hand arm system that no longer allows the isolated use of the hand or arm, unlike previous modular hands. Nevertheless, it still can be logically divided into a

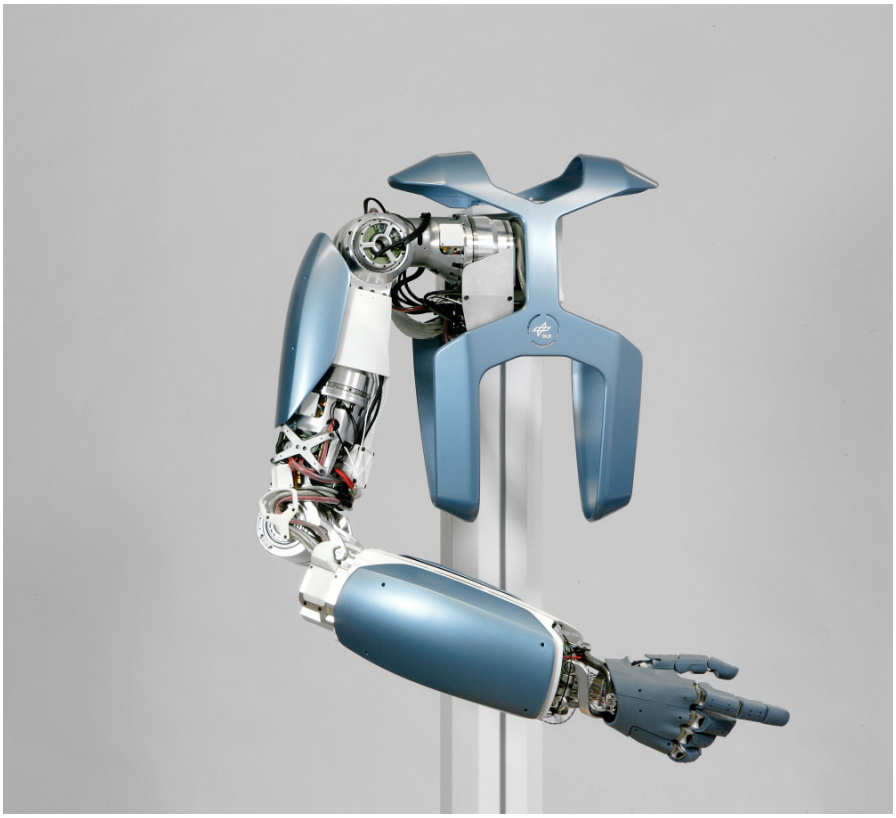

Figure 4.1. DLR Hand Arm System

forearm and hand, including the wrist, on one side, and the arm consisting of a three-DoF shoulder and a two-DoF elbow, on the other.

The *DLR Hand Arm System* is as close to the human archetype as possible in terms of kinematics, dynamics, and forces. The arm requirements are rather different from the hand requirements. The arm has to carry much higher loads than the fingers. In addition, the actuators have to apply the necessary force to counter gravity torques for the whole arm, which are negligible for the fingers. Furthermore, compared to the fingers, higher angular accuracy is necessary, and the dynamic forces within the system are significantly higher (finger dynamics are negligible relative to the total applied forces). Consequently, vibration damping performance is essential for proper functioning

of the whole *DLR Hand Arm System*. Variable stiffness actuation principles have been found to meet the requirements for the shoulder and the elbow best [Grebenstein et al. 2011].

To ensure the capability of the arm to perform human tasks in every position within the workspace, ergonomics data for every joint of the human arm were analyzed [Panzer et al. 2008]. Based on this analysis, the final dimensioning of the drives has been derived [Wolf and Hirzinger 2008]. The actuation of the arm has to be capable of storing short-term energy. To help achieve this, the joints of the arm use four Floating Spring Joints (FSJs) described in [Wolf et al. 2011] for all four DoF.

Since the *Awiwi Hand* itself has no drives or electronics, they have to be integrated into the forearm, together with the drives needed for forearm rotation and the wrist motions. Like the arm, the forearm is intended to have human-like size, and proportions. Its design constraints heavily influence the design of the hand, and is therefore described in more detail in section 4.2.4.

A wrist, providing a large motion range in all three axes, is paramount to enabling human-like workspace and bimanual manipulation. Furthermore, all the tendons necessary to articulate the hand, have to be routed through the wrist at minimal friction. The wrist is actuated by four motors located between the elbow and forearm base frame [Grebenstein et al. 2011]. Its roll axis is intergrated into the proximal end of the forearm. A four-bar mechanism wrist, forming a three-dimensional anti-parallelogram, has been developed (fig. 4.2). It allows the routing of the tendons as close to the neutral position as possible. This allows the angle of tendon deflection to be kept low to reduce friction, and reduces the coupling between wrist and finger motion to a minimum. In addition, due to the non-linear transmission ratio,[1] the wrist centers and is stabilized if maximum tension (totaling >6 kN) is erroneously applied to the tendons.

4.2. Hand Actuation Concept

The actuation concept is crucial for the performance of a robot hand. In the following, the selection of a suitable actuation for the desired hand is discussed. In a second step, the feasibility of the chosen concept is proven. Finally, a

[1] The wrist has minimum length in stretched-out position.

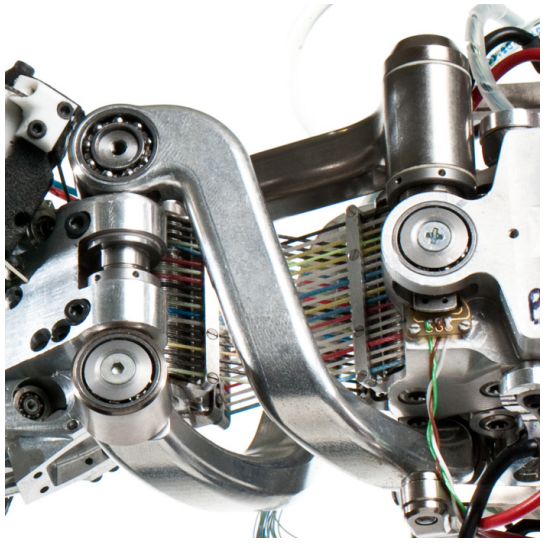

Figure 4.2. The wrist of the *DLR Hand Arm System*. The four-bar mechanism design enables the routing of all 38 tendons through the center of the wrist. The nonlinear transmission of the wrist stabilizes the wrist if high tendon forces (max. $> 6\,\mathrm{kN}$) are applied. The wrist hands over the tendons at the pulley array *(left)* in the palm. The tendons are not allowed to lose contact with the pulleys within the whole motion range.

short overview of the actuation integrated in the forearm of the *DLR Hand Arm System* is given.

As already mentioned, the actuation of the *Awiwi Hand* must meet the following requirements:

- Energy storage capabilities
- Variable stiffness
- Remote actuation

Due to the spatial restrictions, in particular within the wrist, and the large, two-DoF range of motion of the wrist (see sec. 4.1), the transmission of the forces from the forearm to the 19 DoF of the fingers is only possible via tendon

actuation. Furthermore, the friction along the tendon path must be as low as possible. Consequently, sheath tendon transmission (as e.g. within *UB Hand 3*, see sec. 2.1.5 [Lotti et al. 2004a]) is also not suitable (in addition the sheaths need additional space; if using sheaths, the tendons would need to be free running within the wrist).

Tendon driven hands that are not antagonistically driven, such as the electromechanical version of the *Shadow Hand* (sec. 2.1.3), need a closed tendon loop to provide bidirectional force transmission from the motors to the links [ShadowRobotCompany 2009]. Hence, they have to compensate misaligned axes and other geometrical errors within the drive train and tendon path by tensioning mechanisms. They prevent overstretched or slack tendons, which would result in tendon damage or jumped off tendons. These tensioners introduce an additional compliance, at least in one of the tendons actuating a joint. This elasticity introduced by the tensioner has to be low to compensate for tendon length changes without excessively changing the tendon load.[2] This limits the grasping and, in particular, the manipulation abilities of these hands. To circumvent these limitations, in the most important motion directions, a tensioner can be applied in just one of the two necessary tendons. In this case, external forces in the "wrong" direction cause a slack tendon, since the length of only one tendon is compensated by the tensioner. This increases the risk that the tendon jumps off, which possibly results in tendon damage. In addition the joints of the *Awiwi Hand* should be able to be dislocated (see sec. 3.2.2), which implies a notable elongation of the tendons. The latter is not possible using a tensioner without getting too bulky.

Antagonistically driven hands do not have a closed tendon loop, since there is no direct connection between the agonist and antagonist tendon besides the link attachment. Assuming that the actuators are fast enough to compensate tendon length changes and provide force control, no additional tensioners are needed, even if the drive train does not provide notable elasticity, as shown by *Jacobsen* [Jacobsen et al. 1984]. Antagonistic actuation provides intrinsic tensioning by the drive train itself. Furthermore, to provide the desired robustness and grasping performance the hand has to use variable stiffness actuation. Consequently, the fingers of the hand are actuated antagonistically using one motor and a non-linear elastic element (see fig. 4.3) for each ten-

[2] Which would change the characteristics of the hand, regarding e.g. friction and stiffness, introduce cross coupling torques/forces, etc.

don [Grebenstein 2006b]. To prevent unintended dislocation of the joints, a minimum tension of 5-10 N is applied by an admittance controller [Chalon et al. 2011; Grebenstein et al. 2012] to each tendon during operation. Since the drive train is not backdrivable, the tendons remain under tension in power-off mode. All 38 motors, necessary to actuate the 19 active DoF of the hand, are located in the forearm.

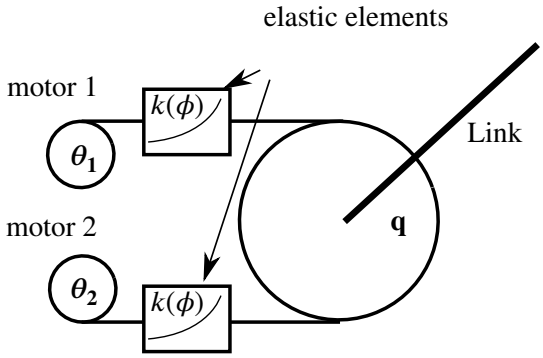

Figure 4.3. Antagonstic actuation scheme. The joint is actuated by two motors which are connected to the link by a non-linear elastic element with the stiffness characteristics $k(\phi)$, where ϕ is the elastic element deflection, θ denotes the motor positions, and q is the link position.

4.2.1. Feasibility of Antagonistic Actuator Control

The control of antagonistically driven robots, starting in the late 80s, has been investigated intensively by *Jacobsen et al.*, *English and Russel*, and others [Jacobsen et al. 1989; English and Russell 1999a; English and Russell 1999b]. Nevertheless, the actuation of the *Awiwi Hand* differs significantly from the investigated actuation. The elastic elements of the actuation use non-linear and non-quadratic elastic elements with high energy storage capabilities (sec. 4.2.3) and small link side inertia. Consequently, a simple controller for the antagonistic actuators (see fig. 4.5, 4.4), providing position control, force control, and basic vibration damping has been designed and is described in the following. Please note that all values are mapped to link torques/positions and follow the flexible joint notation given in figure 4.3.

The antagonistic testbed has two control modes:

- position control
- force control

Position Control

In an antagonistic system, position control of the output position q_{link} is not desired since it would try to compensate for the deflection of the elastic elements and thus "disable" the elastic element. Consequently, position control is performed on the drive positions θ_i. To reach the desired output position with external disturbances, feed-forward control is necessary (see fig. 4.4).

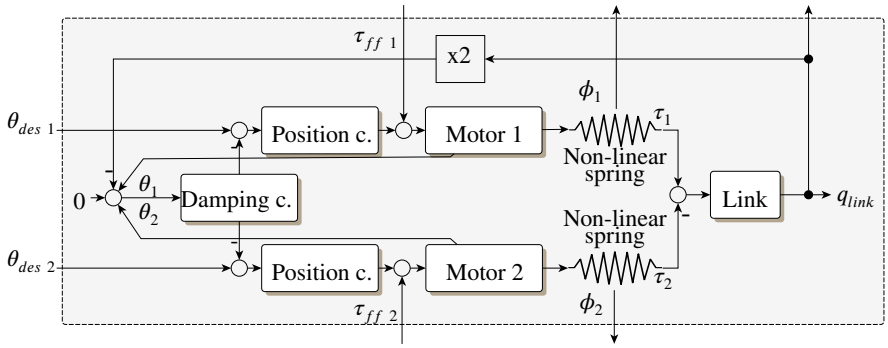

Figure 4.4. *Position control* structure of antagonistic testbed. Control of the output position q_{link} would bypass the elastic elements. Thus, positioning accuracy has to be achieved by feed-forward control input torques $\tau_{ff\ i}$ to compensate external forces. The joint stiffness as well as the position is changed setting the motor position control input (state feedback controller) to the respective input positions $\theta_{des\ i}$. Vibration damping is achieved with a PD controller by reducing the difference between the linkside position and the average motor position to zero.

Force Control

The link output torque τ_{link} equals the difference of the "tendon torques" τ_i at the elastic elements. The torques τ_i at the elastic elements are a (non-linear)

function of the stiffness characteristics $k(\phi)$ which is dependent of the elastic element deflection ϕ_i. Hence, the output torque τ_{link}, as well as the tendon pretension, can be controlled using the motor position controllers if the input torques $\tau_{des\ i}$ are transformed to desired elastic element deflections $\phi_{des\ i}$. The measured elastic element deflections ϕ_i are used as feedback signal. To increase pretension, both input torques τ_i have to be raised. Increasing their difference increases the output torque τ_{link}, see figure 4.5.

In both control modes, a simple PD damping controller is used to control the difference of the average of the motor positions θ_i and the output position q_{link} to zero.

A testbed has been set up to validate (see fig. 4.6) the feasibility of antagonistic actuation and control for the desired hand. The results have been published in [Grebenstein and Smagt 2008].

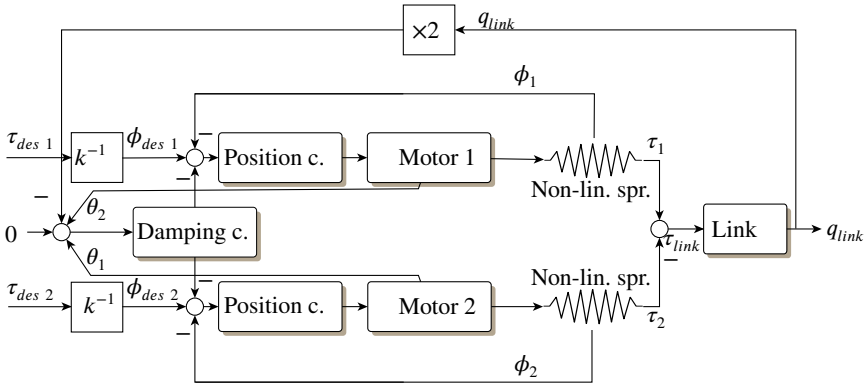

Figure 4.5. *Torque control* structure of the antagonistic testbed. The tendon pretension ($min(\tau_i)$) as well as the link side torque $\tau_{link} = \tau_1 - \tau_2$ is achieved by control of the elastic element deflections ϕ_i, and thus position control of the motors (state feedback controller). The desired element deflections $\phi_{des\ i}$ are calculated using the stiffness function $k(\phi)$. The vibration damping controller is identical to the one used with the position controller in figure 4.4.

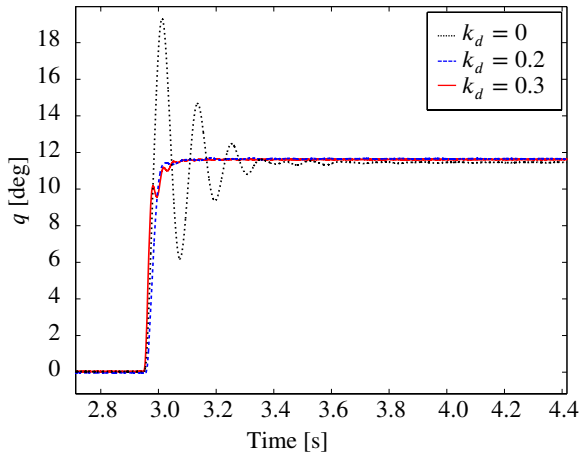

Figure 4.6. Step response of antagonistic testbed with different damping proportional gain parameters k_d. The given angle is the link side position q_{link}.

4.2.2. The Hyper Actuation Concept

In human anatomy, the placement and function of the tendons and muscles of the hand is well known. Nevertheless, functional understanding of the coupled joint movements in the human hand and their relevance for grasping, and manipulation tasks in particular, is incomplete. When the number of actuated degrees of freedom of the desired hand is not identical to the number of DoF of the human hand, introducing couplings may degrade the grasping and manipulation performance of the hand drastically. On the other hand, the introduction of joint couplings can reduce the number of needed drives, and thus system complexity. To enable future complexity reduction by couplings, the *Awiwi Hand* is designed to be "hyper-actuated". Every actuated joint of the hand can be moved independently, allowing to investigate numerous couplings by software as investigated for the *DLR Hand II* in [Wimböck et al. 2011]. The most relevant couplings could later be implemented mechanically, thus reducing complexity, size, and cost of the hand and its actuation [Grebenstein et al. 2012].

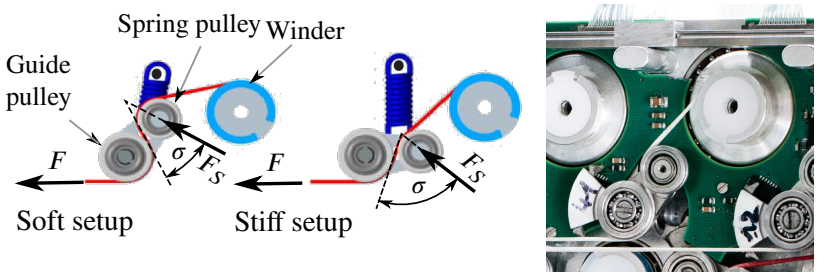

(a) (b)

Figure 4.7. Antagonistic drive compliance mechanism ("tendon side-pull mechanism"): *a*, the pulley located at the spring loaded lever rotates around the center of the guiding pulley and exerts F_S. Due to this design, a non-linear relation between tendon force and spring elongation is obtained. Low mechanical stiffness is achieved by small σ, large σ results in high stiffness. *b*, final elastic element design. The winder is located on the upper right in the photo.

4.2.3. Energy Storage Capabilities

The energy storage capabilities of the elastic elements within the forearm are crucial. On one side, the amount of energy that can be stored determines the maximum allowable impact forces in collision and by this, the robustness of the hand, as well as the necessary reaction time of a controller. On the other side, the amount of stored energy defines the maximum speed of the joints. The maximum energy that can be stored is limited by the spring characteristics and the maximum elongation of the elastic element. Within the *DLR Hand Arm System*, a linear spring in different configurations is used to represent the elastic elements (sec. 4.2.4). Due to the nonlinear lever mechanism (fig. 4.7), the overall elastic behavior is nonlinear. Example spring characteristics of different tendons are shown in figure 4.8.

The maximum energy storage capabilities E_{spring} can be calculated using the characteristics of the linear spring by:

$$E_{spring} = \frac{1}{2} * k * {\Delta_s}^2, \tag{4.1}$$

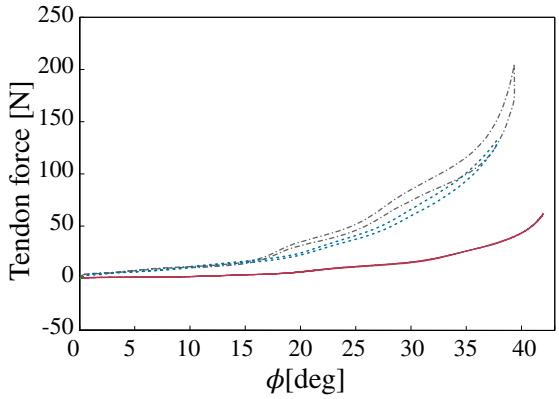

Figure 4.8. Spring characteristics of three different tendons during calibration cycle. ϕ is the deflection angle of the elastic element lever. (—) HMC extensor; (·····) index MC extension/adduction tendon; (-·-··) index flexor PIP

where k is the stiffness of the spring and Δ_s denotes the travel of the spring

Table 4.1. Maximum energy storage of the implemented springs

	low	medium	high
k [N/mm]	10.8	15.08	15.8
Δ_s [mm]	3.0	3.4	4.4
E [mJ]	48.6	87.2	152.9

4.2.4. The Forearm of the *DLR Hand Arm System*

The previous section described the prerequisites to design the actuation of the finger. Subsequently, a short overview of the forearm, based on [Friedl et al. 2011a; Grebenstein et al. 2012], is given.

Logically the forearm can be divided into two sections: the forearm rotation joint, which is a separate structure and the forearm itself. The latter actuates the two-DoF wrist and the 19-DoF hand. All 42 motors and 42 nonlinear compliance mechanisms are integrated into the forearm (fig. 4.9). Each

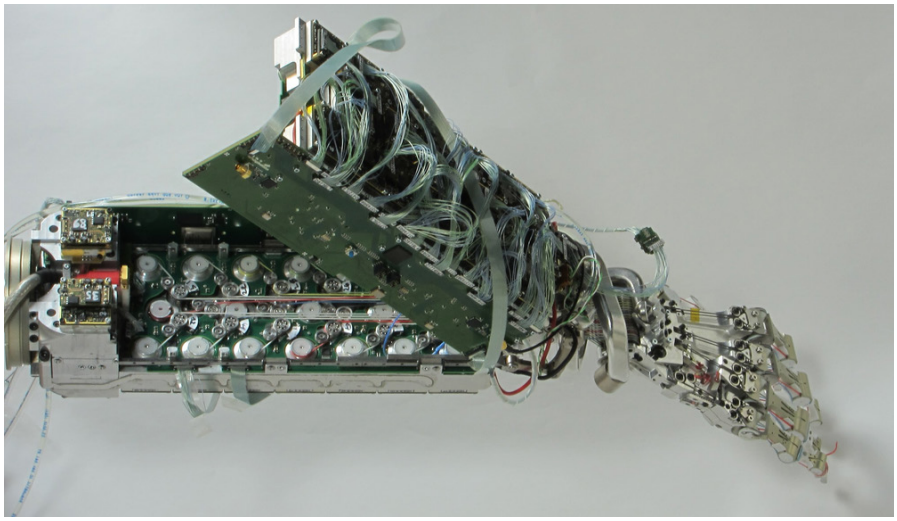

Figure 4.9. Forearm with ServoModules: the ServoModules are located on the outside of each half and thus easy to reach. The tendons and elastic elements are located in the middle layer between both halves. This "split design" protects the tendons in the middle of the forearm and enables easy access to the tendons for maintenance. The forearm is fully operational (at limited tendon loads) if open. To replace a ServoModule, only two screws have to be released and the low level bus connector has to be disconnected.

of the "ServoModules" that drive the fingers contains a motor, position sensor, electronics, and wave generator of the harmonic drive gear (HD) (see fig. 4.10). Every compliance element is adapted to the different finger and joint characteristics. The "split design" of the forearm enables free access to the tendons for fast maintenance and replacement (fig. 4.9). Furthermore, the ServoModules can be replaced quickly, which is helpful for maintenance.

The availability of highly integrated motor modules played an important role in the design decision, whether a full set of tendons ($2n$ routing; every joint has 2 motors) or rather $n + 1$ tendon routing (underactuation approach as described, for example, by *L. Birglen* [Birglen et al. 2008]) should be used. In the case of an underactuated tendon routing ($n + 1$ routing), modules with several different motor subsystem sizes are needed.

Due to the compact packaging of the electronics and the power density of the motors, the generated thermal energy exceeds the technical limits of typical air cooling. The heat can effectively be transferred out of the system with water cooling.

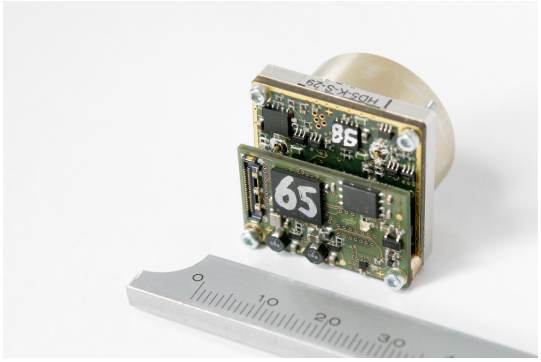

Figure 4.10. The ServoModules consisting of the motor, the position sensors, the electronics, and the "wave generator" of the harmonic drive gear (HD)

Actuation of the Fingers

The fingers are actuated with the ServoModules. A multiturn winder transfers the rotational gear motion to the tendons. The compliance mechanism is similar to the one described in [Grebenstein and Smagt 2008], but the winder acts also as the first pulley of the "tendon side-pull mechanism" (fig. 4.7). This reduces the number of required pulleys to a minimum.

The characteristics of every finger joint can be adapted by selecting the equilibrium point, the spring rate, and the spring position. The tendon length and its serial elasticity need to be modeled to appropriately design the target "stiffness to deflection characteristics". A more detailed description of the elastic elements has been published in [Friedl et al. 2011a].

4.3. Kinematics

The previous section discussed the actuation concept of the *Awiwi Hand*. Once the actuation of the hand and, by this, the number of DoF is defined, the kinematics can be designed. Defining the kinematics of the hand is the most important part of the design process and implies most of the design criteria and requirements for the fingers, the thumb, and the palm. This section is based on [Grebenstein et al. 2010a; Grebenstein et al. 2012].

Section 2.4.2 discusses the state of the art in kinematic design methods. It shows that mathematical optimization approaches cannot be used to design the kinematics of the *Awiwi Hand*, since the parameter space of the hand is too large. The kinematics presented in literature, for example, the thumb kinematics of *Santos* and *Valero-Cuevas* [Santos and Valero-Cuevas 2004; Valero-Cuevas et al. 2003; Hollister et al. 1992; Giurintano et al. 1995; Hollister et al. 1995], focus on the representation of single fingers. These remarkable works do not take into account the interaction of the fingers, the thumb, and the palm. Furthermore, the cost functions / evaluation criteria, to the author's understanding do not represent the full task set of the intended hand.

Kinematic models of the exact human hand, as suggested by *Stillfried* (sec. 2.2.2) also are not suitable for the *Awiwi Hand*, since the hand has a reduced number of DoF [Stillfried and Smagt 2008]. Unfortunately, a mapping of the suggested human kinematics to a different set of DoF does not exist yet.

In the following, a practical approach to design the kinematics of the *Awiwi Hand* is presented. It consists of building a rough kinematic skeleton, based on functional understanding, as described in section 3.2 and improving the kinematics design through iteration, using intuitive tests and rapid prototyping. The tests are based on medical evaluation criteria as well as daily grasping tasks. They are simple and fast and thus allow for very short iteration cycles. Hence, a real synergy between the hand design and the hand applications is created.

In the first part, the methodology and the tests used to evaluate the performance are presented in details.

The second part applies the method to an example. First, an initial model, with a set of free parameters is described. Then, the model is used on different tests and the parameters are modified accordingly. Appropriate measures to improve the kinematics according to the test results are given.

The relevance of the parameters obtained in section 4.3.3 is limited to the

specific case of the *Awiwi Hand* hand [Grebenstein et al. 2010a]. Therefore, it is suggested to hand designers, to apply the method to the specific objectives.

4.3.1. Kinematics Design Process

There is no optimal kinematics but a variety of almost 7 billion well working ones [Grebenstein et al. 2010a]

Figure 4.11. Two clearly different hands selected from a group of less than twenty people. The exact geometrical properties are not of prime importance but rather the functions they create.

A quick scan of different human hands highlights one often neglected fact: The hands of human individuals cover a very wide range of segment length, joint locations, length to width relationships (fig. 4.11), joint limits (fig. 3.8), and even tendon arrangements without major impacts on the persons grasping abilities. Consequently, optimal design for the *Awiwi Hand* is a vague notion. The focus for the design is to fulfill all functional needs of a hand. Therefore, a suitable set of medical tests, derived from decades of hand surgery, and

daily life object grasping tests seems more effective than a set of mathematical abstractions. Indeed, expressing the quality of a grasp can be easily assessed under human supervision but is difficult in quantitative terms. Therefore, the hand kinematics is designed by an empirical, iterative process using a set of tests selected for the *Awiwi Hand* needs. This process guarantees that the final design will fulfill all the functional needs (human supervision prevents the risk of over fitting to the training data). Taking this into account, appropriate kinematics having a given number of DoF for robot hands can be found by:

- Understanding the basic functionalities of the human hand and transferring them to an initial kinematic skeleton
- Prototyping the kinematics in reality or simulation
- Analyzing the resulting kinematics using a set of tests
- Iterative redesign of the kinematics repeating the process until satisfaction

4.3.2. Evaluation Tests

This section describes a set of short but reliable tests used to design the kinematics of the hand. To improve the kinematics within the iterative process, the quality of the realized kinematics is evaluated by these tests under human supervision. The tests can be grouped into:

- Tests derived from hand surgery
- Grasping tests
- Aesthetic tests

Medical Tests

The loss of a finger or even hand dramatically limits the human's ability to interact with the environment and impairs the individual's quality of life. Thus, there have been tremendous achievements in hand surgery in the past decades. For example, the loss of a thumb can be partially compensated by replacing the missing thumb by the middle or the index finger (having only four DoF). The hands capabilities can be restored almost completely by these surgeries

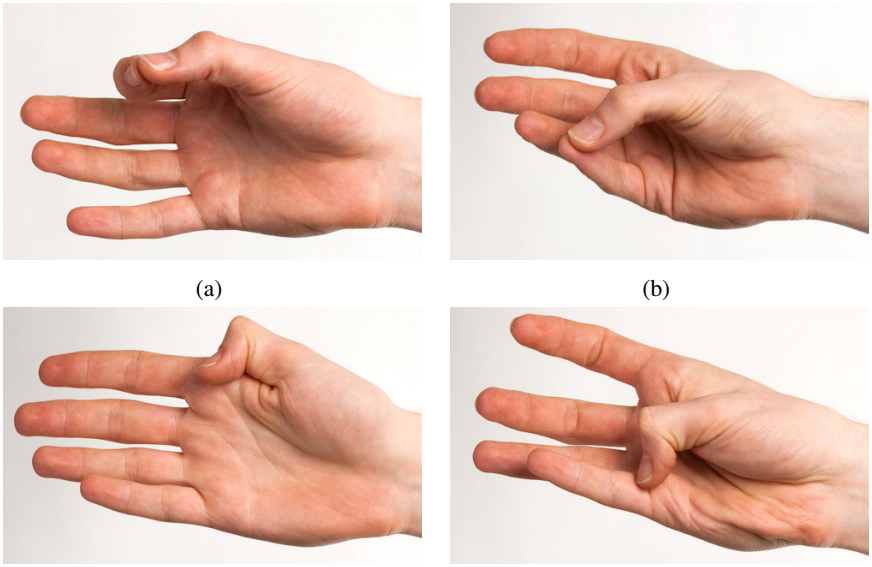

(a) (b)

(c) (d)

Figure 4.12. Most important positions of the Kapandji test: *a*, fingertip of index finger test; *b*, fingertip of little finger; *c*, base of index finger; *d*, base of little finger

called policization [Flatt 2002]. Hand surgeons developed a set of fast and reliable tests to evaluate the success of the surgery and therefore grasping ability. These tests can be applied to robot hands as well since they evaluate the grasping and manipulation capabilities of the hands regardless whether they are human or robot hands. A well known example of such test is the one developed by *Kapandji* (fig. 4.12). It is a testing routine to evaluate the reachability of several partially combined finger positions [Kapandji 1986; Kapandji 1982, pp. 248-255] and will be called Kapandji test in the following. The positions used for the design of the *Awiwi Hand* are:

- Contact of thumb fingertip with the MC joint / base of all fingers, see figures 4.12c, 4.12d)
- Contact of the thumb fingertip pad to the tip of index and little finger without reconfiguration of PIP and DIP joint positions (fifth finger test), see figures 4.12a, 4.12b.

For more accurate investigation of the grasping abilities and in order to account for natural grasp distribution, a more advanced scoring scheme can be applied to the Kapandji test [Soras et al. 1994].

Grasping Tests

The variety of grasps existing is tremendous and would go beyond the scope of this work, but a subset of them are commonly used to evaluate the capabilities of hands. Only few examples are listed which are representatives of the most important grasping functions:

- Pinch grasp (fig. 3.20a)
- Key grasp (fig. 3.20b)
- Grasping of cylindrical objects in different sizes
- Grasping of spherical objects in different sizes (fig. 3.11)

An overview of several grasping tasks can be found e.g. in [Tubiana 1981; Kapandji 1982, pp. 256-273; Cutkosky 1989; Schulz et al. 2001; Feix et al. 2009].

Aesthetics

The overall appearance of the hand is important when performing human interaction. The hand should look balanced and should be easily accepted by humans (in line with the prosthesis design philosophy). It is recommended to perform every-day grasping tasks using the prototypes within the natural surroundings (desk, home etc.) since it provides a good scaling reference and supports intuition. Even non-experts can easily recognize, whether a kinematics performs well by seeing the hand in motion. The great efforts taken in hand animations used in movies and games exemplifies this ability [Nierop et al. 2008].

4.3.3. Kinematics Design

The previous section introduced the tests used to evaluate the kinematics designed. These tests will be applied to kinematics of different stages of the design process until satisfactory in the following section.

Initial Kinematics

The *Awiwi Hand* should have anthropomorphic grasping and manipulation abilities, but should be limited in its DoF to fit the restricted design space of the forearm. Therefore, the number of active DoF is selected to be 19 [Grebenstein et al. 2010b; Grebenstein and Smagt 2008]. Consequently, the thumb can only afford four DoF instead of five. However, this reduction should not impair the abilities of the hand. The impressing results of policization (see e.g. [Flatt 2002]) prove that a four-DoF thumb is sufficient for a majority of grasping tasks [Chalon et al. 2010]. Nevertheless, the omitted fifth DoF has to be compensated based on the functional knowledge described in section 3.2.5. Following *Kuczinsky* and *Kapandji* the TMC geometry of the five-DoF thumb, in addition to the second degree of freedom in the MP results in an inward orientation of the pad during TMC and MP flexion [Kapandji 1982; Kuczynski 1975]. This change of orientation is crucial for proper opposition of the thumb to the fingers while grasping, for example, a cylindrical object and has to be achieved by tuning the parameters of the kinematics in a suitable way [Grebenstein et al. 2010b; Chalon et al. 2010].

The experiences with *DLR Hand II* have shown that coupling the PIP and DIP of the little and ring finger is not problematic and reduces the number of active DoF [Butterfaß et al. 2004].[3] The starting configuration can be seen in table 4.2. As a starting point several prototypes are built based roughly on [Kapandji 1982; Purschke et al. 1998] and direct measurements of a human hand. Given that the thumb is by far the most important finger within the hand, the location and the orientation of the axes of the TMC joint as well as the PIP and DIP joint angles (of the thumb) have been set up in variety of configurations:

- Thumb base joint located within the palm
- Thumb base in front of the palm
- Thumb axes of TMC orthogonal
- Thumb axes of TMC non-orthogonal
- Thumb IP without twist and inclination

[3] The coupling was not taken into account for the kinematics prototypes.

- Thumb IP with twist
- Thumb IP with inclination
- Thumb IP with twist and inclination

The inclination and twist (fig. 3.21 values of the IP axis are used as parameters during the the second phase of the kinematics design. It has to be noted that, to start, it is important to realize a wide range of different prototypes. It prevents local extrema, as a randomized process does in numerical optimization.

Table 4.2. DoF of the fingers (*: coupled DoF)

Joint	thumb	index	middle	ring	little
MC/TMC [DoF]	2	2	2	2	2
PIP/MP [DoF]	1	1	1	1	1
DIP/IP [DoF]	1	1	1	1^*	1^*
$\sum$ [DoF]	4	4	4	$3+1^*$	$3+1^*$+HMC

Prototyping

Inspired by *Kapandji* cardboard prototypes are used (fig. 4.13) [Kapandji 1982, p. 253]. Fast prototyping methods (stereolithography or equivalent) can also be utilized. Software prototyping [Miller and Allen 2004; Borst et al. 2003], is another alternative, but lacks the physical interaction needed for the designer and roboticist to "feel" the design. The card board prototypes have the advantage of being low cost, as well as very fast, and easy to modify. However, their structural flexibility and relatively low precision limit their use to the first but important development steps. Using physical prototypes, grasping common objects can be performed without any additional modeling effort. "Playing around" with the prototypes is important and helps because the human being, even having limited or no grasping/kinematics knowledge, has a strong intuition about "good" or "bad" kinematics through a life time of using human hands to perform these tasks. For the thumb joints, a final refinement is done using simulation. It also is recommended to make final refinement of

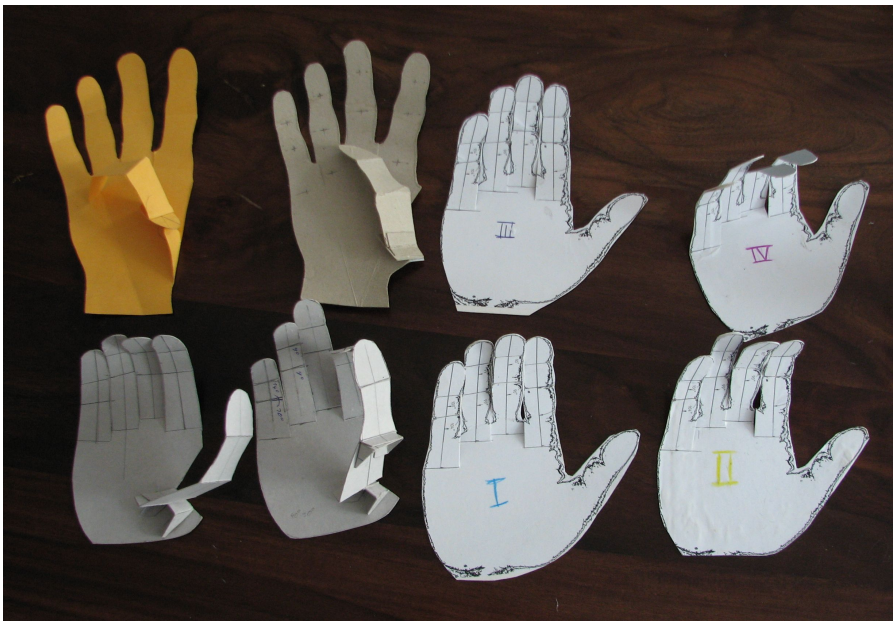

Figure 4.13. Hand cardboard prototypes: four samples on the left have been built for the evaluation of thumb parameters. The four hands on the right are used to investigate the inclination of the ring and little finger. These hands lack a movable thumb for handling reasons. This is not advised since the prototypes selected as suitable cannot be reused for the Kapandji test.

the kinematics using simulation. Certainly, collisions of the fingers are best detected using a 3D simulation.

Application of the Tests/ Kinematics Improvement

In the following, representative results of the applied tests, as well as the corresponding measures are given. This enables hand designers to use the method for their own purpose. Furthermore, the incompatible sets of tests are highlighted. Trade-offs have to be selected depending on the relative tests importance. Kinematics prototypes of an early, intermediate and mature stages of the kinematics are shown. The prototypes are modified or rebuilt repeatedly based on the tests described in section 4.3.2 until a satisfactory solution is

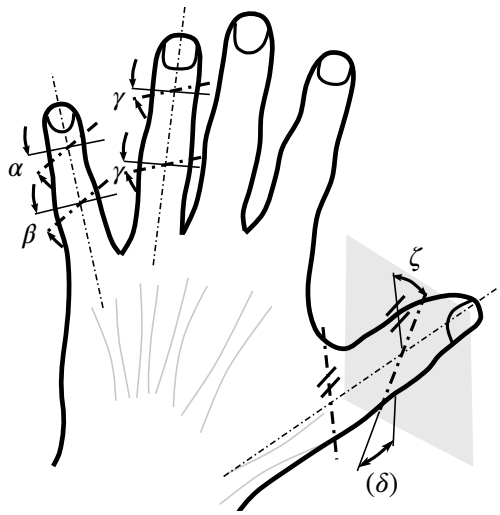

Figure 4.14. Varied parameters of kinematics prototypes

found. The iterative process relies on the functional abstraction deduced in section 3.2 and in part on the designer's intuition in the beginning. However, once the main parameters, such as joint location or order of axes, are fixed, the tuning can be done by taking appropriate measures as given in the respective sections in the following to improve the kinematics. The parameters modified within the examples are shown in table 4.3 and figure 4.14.

Kapandji Test with Different Thumb Configurations The Kapandji test has been developed for hand capabilities evaluation in surgery [Kapandji 1986; Kapandji 1982, pp. 248-255]. It enables a fast and reliable method to evaluate the thumbs ability to move to all necessary positions for proper grasping (see fig. 4.12 and sec. 4.3.2). Therefore, it is the first test performed with every thumb configuration. The Kapandji test should be performed with every prototype even in later "fine-tuning" stages. The capability of the thumb to reach all finger bases is dominated by the point of intersection of the first axis of the thumb and the palm.[4] If the point of intersection is located at the base of one finger, the thumb is within its singularity (see fig. 4.15, sec. 2.4.1). Therefore,

[4] A first axis not pointing towards the palm, leads to unnatural motion of the thumb and fails almost all test. Therefore it is not reported.

Table 4.3. Varied parameters within shown hand

Finger	Parameter	Range
Thumb	TMC position	20mm distal and palmar
	TMC 1st axis orientation	
	TMC angle between axis	[60… 90]
	Inclination MP	[0… 5]
	Twist between MP and IP	[0… 9]
Ring finger	Inclination PIP	[5… 9]
	Inclination DIP	[5… 9]
little finger	Inclination PIP	[10… 14]
	Inclination DIP	[10… 14]

the thumb is not able to reach any other position of the palm (fig. 4.16a).[5] Furthermore, a thumb TMC placed too close to the palm leads to sideways collision of the thumb and the index finger / the index metacarpal bone (fig. 4.16b). Measures to improve Kapandji test results are:

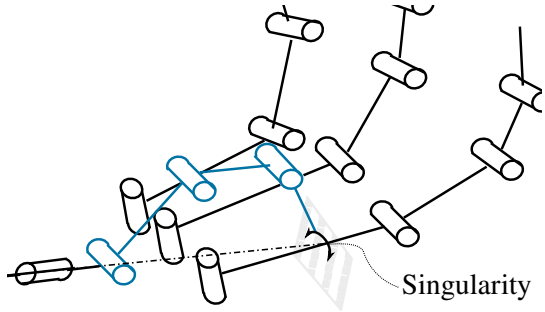

Figure 4.15. Thumb TMC singularity: The first axis of this thumb kinematics (modified *MIT hand* thumb kinematics) meets the palm close to the index MC joint. The thumb becomes too close to its singularity. It cannot reach the finger bases of the other fingers frontally.

- To enlarge the range of reachable finger bases, the intersection point of

[5] If the thumb fingertip is located within or nearby the middle (sagittal) plane of the thumb

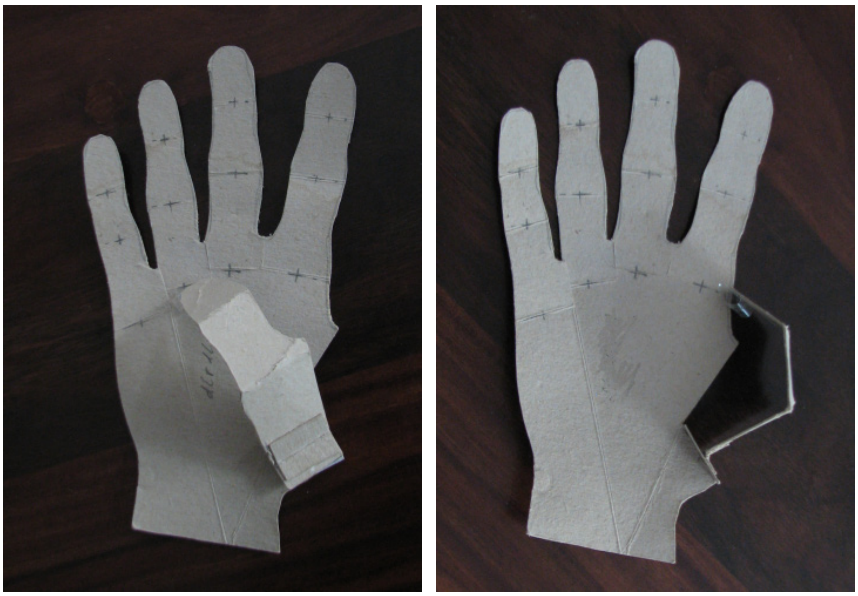

(a) (b)

Figure 4.16. Kapandji test of a configuration with thumb MC placement in the palm plane: *a*, the first axis of the thumb meets the palm plane on the base of the ring finger (the thumb is in its singularity at the ring finger base). Thus, the thumb is not able to reach any other finger base. *b*, since the thumb axis coincides with the palm, the thumb can touch the index MC only lateral.

first axis and palm has to be more distant from the finger bases.

- If the thumb collides with the index finger sideways the TMC base has to be placed further in front of the palm.

The improved configurations shown in figure 4.17 achieve better results, since their TMC joints are placed in front of the palm and the first axis meets the palm distant from all metacarpals. Both hands use the final thumb position and identical axes orientations. The thumb on the left (fig. 4.17a) has inclination and twist within the IP axis[6] to improve grasping of large cylindrical

[6]Which moves the thumbs tip out of the sagittal/middle plane in flexed position

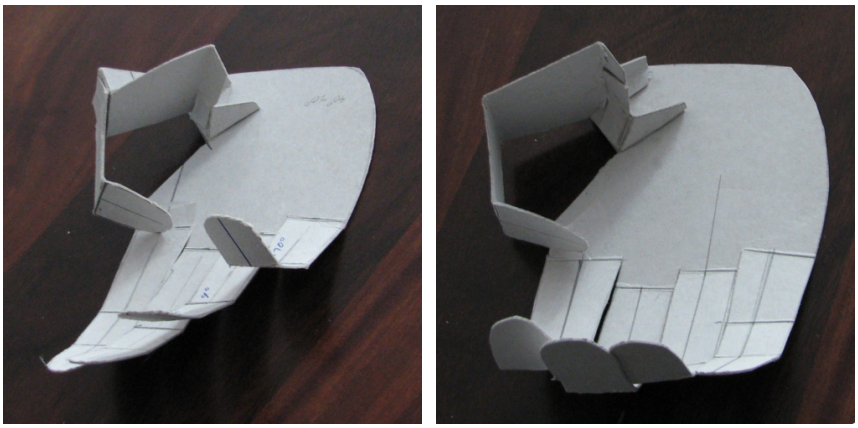

(a) (b)

Figure 4.17. Two configurations with identical TMC placement in front of the palm performing the Kapandji test: The configuration with twist and inclination *(a)* meets the palm at the index base more frontal than the prototype without twist and inclination *(b)*.

objects (see sec. 4.3.3). Performing the Kapandji test at the base of the index finger (see fig. 4.12c), the pose of the thumb lacking twist and inclination (fig. 4.17b) is less natural than the one of the design having inclination and twist (fig. 4.17a). The latter configuration (fig. 4.17a) also performs better for power grasps of large objects (sec. 4.3.3) due to the more inward oriented pose of the thumb.

Grasping Tests Application of the Kapandji test and the related measures described beforehand mainly improve the thumb and its base joint parameters. The grasping tests described in the following are used to improve the kinematics of the fingers and the thumb MP and IP. The two more striking of the four grasping tests (see sec. 4.3.2) performed are presented in the following for clarity.

Finger Joint Axis Inclination Evaluation Performing Power Grasp Since obviously larger inclination of the PIP and DIP joint of the ring and little finger leads to better opposition of the thumb (within a meaningful range), a

single test checking incongruous configuration is sufficient to identify proper inclinations. Too large inclinations increase overlapping of the fingers while performing power grasps, since their proximal phalanges are parallel during power grasp [Grebenstein et al. 2010a]. Therefore, a simple power grasp test was performed. The initial value for the joint inclinations was adopted from [Kapandji 1982, pp. 170-189]. The initial values were clearly too large (identical values for little and ring finger) for the chosen length of segments. As a result, a considerable overlapping occurred between the middle and the ring finger (fig. 4.18b). Hence, the values have been decreased to reduce overlapping (fig. 4.18a), while still enabling proper opposition to the thumb. For fine tuning of inclinations, collision checks are performed in simulation to improve accuracy. Overlapping must be avoided since it prevents proper power grasp. Measures tuning PIP/DIP inclination:

- Start with large inclination angles
- To reduce overlapping of the fingers reduce inclination
- To improve opposition increase inclination
- Start with the finger closest to the index

Tuning Twist and Inclination of Thumb Joints As shown in section 3.2.5, the missing fifth DoF within the thumb of the *Awiwi Hand* has to be compensated for, see section 4.6. The introduction of axis inclination and twist is an effective solution. New prototypes with and without joint inclination have been built. These have to undergo the already mentioned tests as well as everyday object grasping tests. Two contradictory grasping tasks are shown in the following: key grasp, and power grasp of a cylinder. To perform a key grasp, the pad of the thumb has to be tangent to the longitudinal axis of the distal or medial phalanx of the index finger (see fig. 3.20b, 4.19). In contrast, to perform a power grasp, the sagittal (middle) plane of the thumb has to be almost parallel to the sagittal plane of the index/middle finger to bring the pad of the thumb in contact to the object. The pad is much softer than the side of the thumb and therefore offers better grasping. Contact of the side of the thumb during strong power grasps also would be painful.

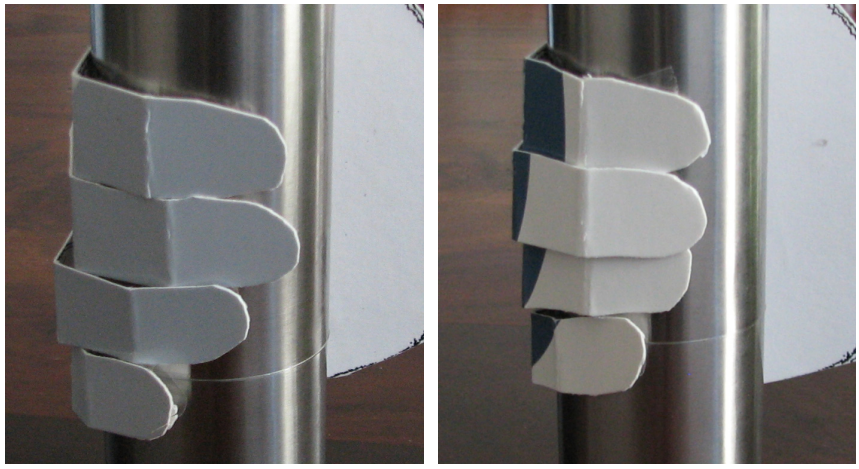

(a) (b)

Figure 4.18. Testing inclination of PIP and DIP joints performing power grasps on a pepper mill: *a*, the hand with medium inclination of ring and little finger has only few intersection of the fingers; b, the prototype providing the inclination reported by *Kapandji* [Kapandji 1982] has notable intersection between middle and ring finger for the assigned finger base parameters. The prototypes have no mobility within the thumb. The MC joints of the fingers are fixed using tape for visualization purpose, which is not optimal for positioning of the fingers.

Key Grasp Performing a key grasp, it can be seen that the thumb without inclination and twist performs a good key grasp (fig. 4.19a), whereas the thumb with inclination and twist[7] does not bring the front of the thumb's tip in perfect contact to the side of the index finger (fig. 4.19b). However, the angle of the inclined and twisted version is small enough to be compensated by the soft materials of the finger housings.

Power Grasp of Large Cylindrical Object If the thumb lacks inclination and twist, the angle between the frontal surface of the thumb and the object is far from ideal during power grasps (fig. 4.20a). During this type of grasp, the

[7]The inclination of the joint axis does not change orientation of the thumbs tip during key grasp since PIP and DIP are in (almost) stretched-out position.

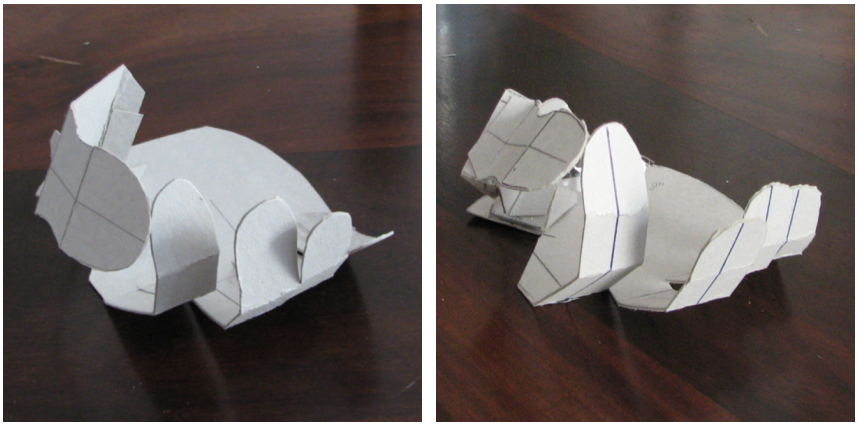

(a) (b)

Figure 4.19. Key grasp with a thumb without and with inclination and twist: *a*, the thumb lacking twist and inclination touches the index finger more lateral than the one providing twist and inclination *(b)* and thus, performs key grasp better.

thumb is almost fully stretched out. Therefore, a twist of the thumb joint axes is more effective than inclination to correct the orientation of the thumb fingertip. Due to the superior performance during power grasp (which is a much more common grasp in robotic applications than key grasp) the thumb configuration using inclination and twist has been chosen. In detail, inclination and twist can be tuned by the following rules:

- To improve contact of a key grasp, twist IP joint outward from the palm.
- To improve contact performing large object grasps, twist IP inward.
- To improve power grasp of small objects increase/ decrease inclination of thumb IP to achieve proper opposition.[8]

Balancing the values for inclination and twist of the thumb joints is the most difficult part of the design requiring several iterations due to conflicting

[8]Inclination of in especial DIP does not affect key grasp and large object power grasp too much since DIP is almost stretched out.

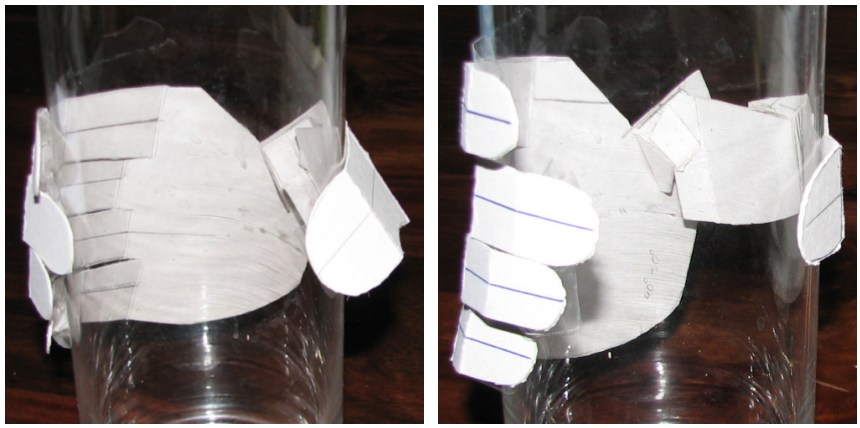

(a) (b)

Figure 4.20. Power grasp of large cylindrical flower vase to test thumb inclination and twist. The prototypes are the ones used in figure 4.19. *a*, the thumb without inclination and twist meets the cylinder quite laterally and thus, does not bring the frontal pad of the thumb in contact leading to poor object contact and lateral forces on the joints. *b*, the prototype providing twist and inclination is in perfect frontal contact to the vase.

goals. Final fine tuning is performed in simulation in parallel to the cardboard tests to help the visualization of the finger pad shape.

Contrary Tests/ Measurements Conflicting test results of the kinematics evaluation require further attention as discussed here:

- Kapandji test *versus* grasping of large objects: If the intersection point of the first axis of the thumb is located too low and close to the thumbs base joint, the singularity on the backside of the thumb gets closer to large objects surface of contact to the thumb. This results in limited motion range of the thumb doing this kind of grasp. Therefore, a suitable compromise between both has to be reached. The Kapandji test should be passed completely, as it relates to the most frequently used grasp and manipulation situations.

- Key grasp *versus* grasping of large objects: No general rule can be given to solve this conflict. IP tiwst/inclination parameters must be balanced out according to use case/requirements.
- Inclination: Kapandji test *versus* overlapping: Overlapping hinders power grasp. The inclination should not create any overlapping.

Kinematics of the Hamatometacarpal Joint

This section will describe the kinematics design of the HMC joint, which belongs to the palm itself. As section 3.2.6 described, the HMC joint function is to turn the workspace of the little finger inward to enable opposition with the thumb, eg. to grasp small spherical object as seen in figure 3.11. Additionally, it arches the palm and therefore, shapes the palmar ridge, which is used for example when grasping a screwdriver or a shovel (see fig. 3.23).

To turn the workspace of the little finger towards the thumb, it is inevitable to bring the MC joint of the little finger in front of the palm to avoid collision of the little finger with the ring finger. Thus, the motion of the MC joint is composed of translation, dominant in the first part of the motion (to bring the MC joint in front of the palm), and rotation (to rotate the workspace), which prevails the second part of the motion. With this combination of motions, collision of the little finger and the ring finger is avoided. Therefore, a non-linear motion characteristics is needed. This property is achieved by using a four-bar mechanism with links of unequal length as shown in figure 4.21a. The criteria for the design have been to achieve a translation of roughly 12 mm (as measured in section 3.2.6) and an inward rotation of approximately 10°. The achieved trajectory is depicted in figure 4.21b.

The reproduction of the exact trajectory, as discussed previously, is of minor importance. Furthermore, the space available is quite limited. Therefore, the goal of the design of the HMC DoF is to find a suitable design, that provides the motion characteristics mentioned above.

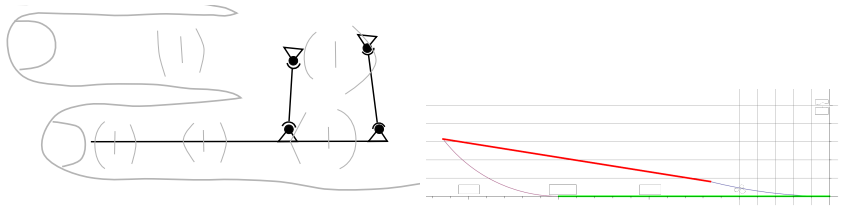

(a) (b)

Figure 4.21. HMC four-bar mechanism kinematics: *a*, HMC kinematics scheme; *b*, calculated trajectory of the four-bar mechanism seen from distally. The green line in *(b)* represents the little finger in 90° MC flexion and power grasp configuration. The red line depicts the finger in opposition configuration: The little finger base is in front of the palm, and the workspace of the little finger is rotated toward the thumb.

Conclusion and Final Kinematics

This section introduced an efficient and fast method to design a hand kinematics and described the design process with examples performed for the design of the *Awiwi Hand*. The measures to improve the kinematics during the design process have been derived from the functional understanding of the human hand gained in section 3.2.

A kinematics (see fig. 4.23, 4.22) has been designed to provide inclination of the finger PIP and DIP joints, in particular within the ring and little finger. With this feature, proper opposition to the thumb, which is important for power grasp of palm size and smaller spherical objects is achieved on one hand. On the other hand, it still enables to perform power grasp of cylindrical objects well, which demands for parallel fingers.

The thumb TMC placement and the twist and inclination of the thumb IP has been optimized to meet the requirements of the Kapandji test, used by surgeons to check grasping ability of human hands. Furthermore, grasping tests such as key grasp and large cylinder power grasp have been used to further fine tune these parameters. The combination of proper TMC joint placement and IP joint twist and inclination has shown to be able to adequately compensate the missing fifth thumb DoF of the *Awiwi Hand*.

The following section will show the design of the hand using the obtained kinematics.

Figure 4.22. Rendering of the hand in later stage of kinematics iteration process (the final thumb design is rotated more inward) grasping a beer glass to check the thumb IP twist parameters as well as the MP inclination. The palm has not yet been designed at this design stage.

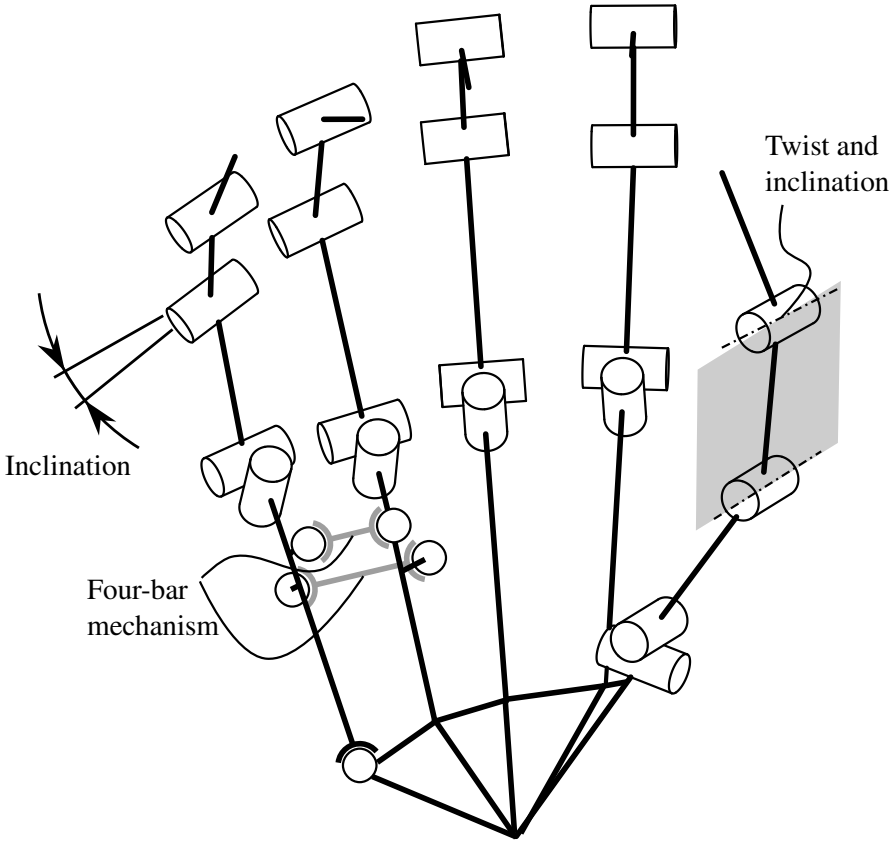

Figure 4.23. Kinematics scheme of the *Awiwi Hand*. All fingers other than the index and middle finger have inclination in all hinge joints to improve opposition and power grasp of spherical objects. The thumb IP provides inclination as well as twist to compensate the missing fifth DoF of the thumb and improve key grasp and power grasp performance. The MC joints, as well as the thumb TMC have orthogonal, but non intersecting axes. The little finger HMC is designed as a four-bar mechanism and a spherical joint on the proximal end of the metacarpal. This enables inward rotation of the little finger, as well as palmar motion of the MC joint itself, which arches the palm to locate cylindrical objects of smaller diameter firmly during power grasp.

4.4. Internal Friction Estimation

Before starting the design of the fingers, a rough estimate of the friction within tendons and joints is performed to study the feasibility of tendon actuation in combination with sliding guidances. Furthermore, many decisions still have to be made during the design, which would heavily influence the friction and thereby the grasping and manipulation performance, as well as the dexterity of the hand. Within the drive train, two types of friction have to be addressed: tendon friction and joint friction. Since tendon friction is dependent on the wrap-around angle, whereas joint friction is dependent on the normal force in the joint friction surfaces, a good knowledge of the amount and proportion of the two types of friction is necessary to make the right design decisions in terms of grasping performance, such as tendon routing concept, joint friction surface diameters, choice of materials and maximum tendon load. The next section presents this estimation. Some example results are also given to help derive design guidelines. The runable calculation is available online at http://www.sagenb.org/home/pub/4684.

Since the parameters of the fingers, such as wrap-around angles in default position, are design dependent, this estimation is performed iteratively with repeatedly adjusted parameter sets during the design process.

To estimate the friction within the tendon path and the joints, a forward mapping of the tendon forces to the fingertip force is made for the tendon routings shown in figure 4.24.[9] Additional joint torques, introduced by the tendon routing, are relatively low, thus neglected for ease of calculation. Furthermore, since the tendon routing is not yet defined, all tendon forces are assumed to be in parallel to the phalanges[10] (even for crossed tendon routing) and the pretension forces are set equally for every joint. The change in the capstan friction of the MC tendons, when the angle q_1[11] of the first axis of the MC joint (abduction/ adduction; noted as *MC1* in the following) changes from 0° to 30° is lower than 0.15% (using the values given in table 4.4), and is therefore neglected. Instead the default configuration ($q_1 = 0°$) is taken into account as the constant offset angle for the estimation. For clarity of pre-

[9] The PIP and DIP tendons are routed through the center of the flexion/extension axis *(MC2)* axis for the crossed tendon setup in the calculation.

[10] Which is conservative since the normal forces in the joint decrease if not parallel

[11] The notation of the flexible joint model, see figure 4.3, is used in this calculation for consistency reasons.

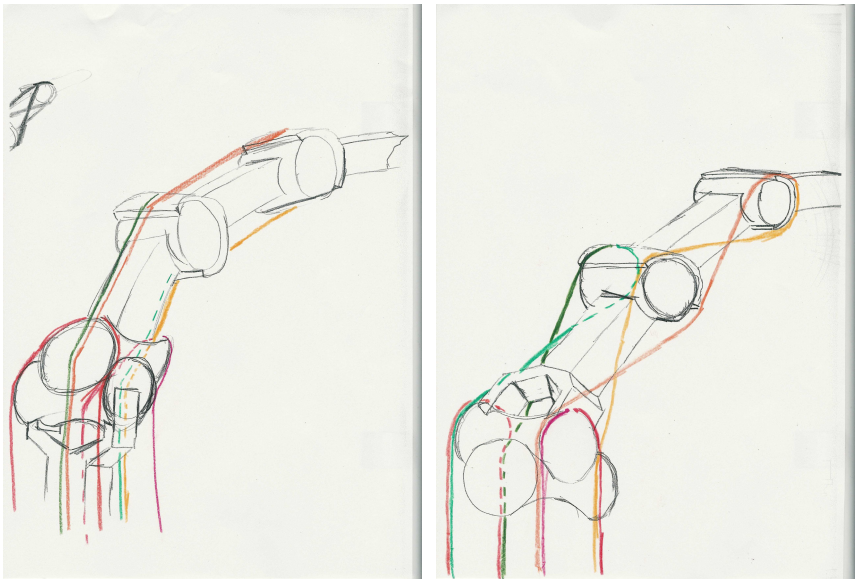

(a) (b)

Figure 4.24. Two tendon routing concept sketches: *a*, parallel tendon routing. The change in tendon length sums up during flexion. *b*, crossed tendon routing. The DIP joint tendon length changes during 1:1 ratio flexion of the PIP and DIP joint cancel each other out. Thus, there is relative motion between PIP guidances and DIP tendons in this case.

sentation all forces are mapped to the tendons. The estimation does not take into account on which sliding surface the capstan friction acts. In addition, it is assumed that the complete capstan friction reduces the normal force in the joint surface.[12] Finally, a tendon is assumed, as soon as it is completely unwrapped on one surface, to be wrapped on the opposite surface, since the tendons should not change their path (with respect to the respective segment of the finger) within the whole range of motion.

In a first step, the tendon force necessary to exert the fingertip force without

[12] In reality the capstan friction is distributed over all guidances along the whole tendon path and is a tangential force at the cylindrical guidances, rather than a force directed in parallel to the tendon force.

any friction is calculated. Subsequently, all friction forces that diminish the *active* part of the tendon force (the part of the tendon force that exerts a force at the fingertip; pretension forces only result in structural / internal forces) along the tendon path are calculated, as depicted in figure 4.25.

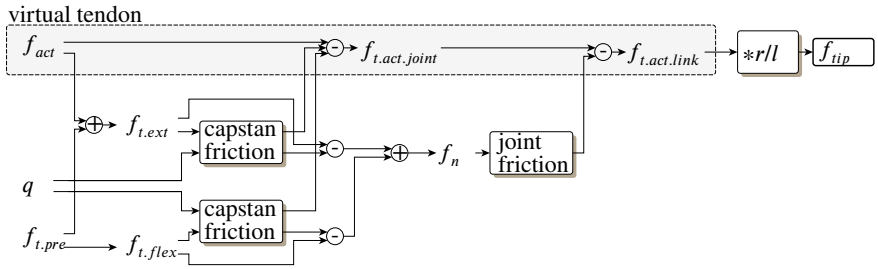

Figure 4.25. Calculation scheme of the friction estimation: All forces are calculated with respect to the *active* part $f_{t.act}$ of the tendon force that exerts f_{tip} without any friction (virtual tendon). The pretension forces of the flexor and extensor add an additional capstan friction component that has to be calculated at tendon level and diminishes the active tendon force. In addition, the pretension and the *active* tendon force sum up to the normal force. Therefore, the joint friction is pretension dependent. Force components introduced by the tendons of other joints are not shown for clarity of presentation.

Using the assumptions given above, the *active* tendon force of a joint $f_{t.act}$, necessary to exert the fingertip force $f_{tip} = 30\,\mathrm{N}$ is

$$\vec{f}_{t.act} = f_{tip}\frac{\vec{l}}{\vec{r}}, \tag{4.2}$$

where $\vec{l}$ is the vector of distances l_i from the respective joint i to the fingertip and $\vec{r}$ is the vector of radii r_i of the tendon attachment at the joint i. Since the tendons can only transmit tension forces and a frontal fingertip force is assumed (see fig. 4.28), only the flexors can contribute to the necessary joint torques. Furthermore, to avoid tendon slack or change joint stiffness, every tendon has to have an additional pretension force $f_{t.pre}$. Hence, as depicted in figure 4.26, the tendon forces of the flexor $f_{t.flex}$ and extensor $f_{t.ext}$ of a single joint are

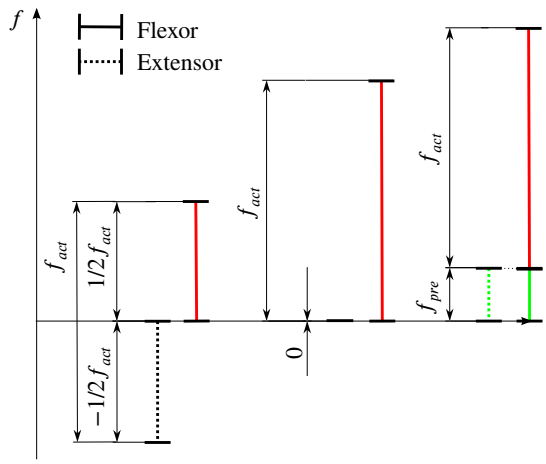

Figure 4.26. Active and passive parts of tendon forces. On the left, no pretension force is applied. The desired tip force cannot be exerted, since the extensor cannot transmit negative forces. In the middle, the minimum pretension necessary to exert the desired tip force, is added. On the right a pretension force is added to change the joint stiffness and to prevent slack tendons (green).

$$f_{t.flex} = f_{t.pre} + f_{t.act} \qquad \text{with} \quad f_{t.flex} \geq 0 \tag{4.3}$$

$$f_{t.ext} = f_{t.pre} \qquad \text{with} \quad f_{t.ext} \geq 0\,. \tag{4.4}$$

If these forces are applied to the tendons of the joint, the capstan friction f_{fc} on both tendons diminishes the tendon forces acting at the tendon path to the joint. According to the Euler-Eytelwein Equation [Meriam and Kraige 2007, p. 381], a given tendon force T_0 due to the capstan friction becomes

$$T(\phi) = T_0 e^{-\mu\phi} \quad \text{with} \quad T_0 > T(\phi) \tag{4.5}$$

Hence, the friction force is

$$F_{fc} = T_0 - T(\phi) = T_0 \left(1 - e^{-\mu\phi}\right). \tag{4.6}$$

T_0 is substituted with the tendon force on the motor side (proximal), f_t and $T(\phi)$ with the joint side tendon force $f_{t.joint}$ and ϕ by γ for compatibility with the flexible joint model. This is used for solving for the relationship of the motor side tendon force f_t to the capstan tendon friction $f_{t.fc} = (f_t - f_{t.joint})$ that defines the joint angle dependent capstan friction coefficient of the tendon $\mu_c(q)$. Hence,

$$\mu_c(q) = \frac{f_{t.fc}}{f_t} = \frac{f_t - f_{t.joint}}{f_t} = 1 - e^{-\mu\gamma} \quad \text{with} \quad f_t > f_{t.joint}, \tag{4.7}$$

where γ is the summed up wrap-around angle of the respective tendon. Within an agonist antagonist tendon pair, this coefficient is only valid for the specific tendon, since the opposing tendon does have different tendon forces f_t (see fig. 4.25, 4.26). It is assumed that the wrap-around angles of all tendons in a specific joint i are identical and define a matrix A of the wrap-around angles from joint 1 to n in default configuration

$$\mathrm{A} = \begin{vmatrix} 0 & 0 & 0 & 0 \\ \alpha_{MC1} & 0 & 0 & 0 \\ 0 & \alpha_{MC2} & 0 & 0 \\ 0 & \alpha_{MC2} & \alpha_{PIP} & 0 \end{vmatrix} \tag{4.8}$$

which maps the wrap-around angles of the joints to the tendons. Joint motion of a joint wraps or unwraps the tendons of all more distal joints, and therefore, contributes to the summed up wrap-around angle γ. Thus the vector $\vec{\gamma}$ of the wrap-around angles γ_i is

$$\vec{\gamma} = (M * Q + \mathrm{A}) * \begin{pmatrix} 1 \\ 1 \\ 1 \end{pmatrix} \qquad \text{for extensors and} \tag{4.9}$$

$$\vec{\gamma} = (M * -Q + \mathrm{A}) * \begin{pmatrix} 1 \\ 1 \\ 1 \end{pmatrix} \qquad \text{for flexors,} \tag{4.10}$$

where Q is the diagonal matrix of the joint angles $q_1 \dots q_n$ and M is the matrix that maps the joint angles q_i to the wrapping of the tendon and becomes

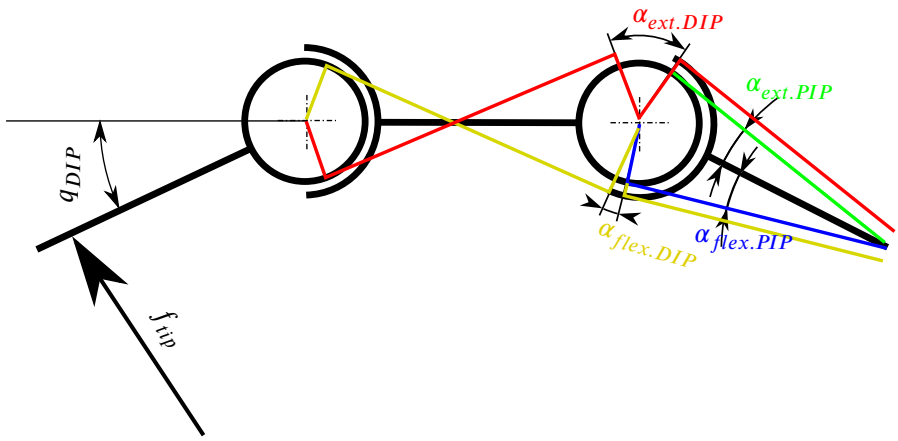

Figure 4.27. Tendon routing and wrap-around angles of tendons. The joint angle of the joint itself does not change the wrap-around angle of the respective tendons of the joint. Flexion of the joints corresponds to an positive joint angle.

$$M = \begin{vmatrix} 0 & 0 & 0 & 0 \\ 0 & 0 & 0 & 0 \\ 1 & -1 & 0 & 0 \\ 1 & 1 & -1 & 0 \end{vmatrix} \tag{4.11}$$

e.g. for a crossed tendon routing.[13]

The summed up wrap-around angle γ_i of joint i is only dependent of the joint angles $q_1 \ldots q_{i-1}$ and offset angles $\alpha_1 \ldots \alpha_{i-1}$ of the more proximal joints, since there is no relative motion between the tendon of the respective joint and the link-side (see eq. (4.8)).

The capstan friction force of a single tendon is then

$$f_{t.fc} = \mu_c(\gamma) * f_t \tag{4.12}$$

Using equation (4.7), the *active* tendon force $f_{t.act.joint}$, which is diminished by the capstan friction force of each tendon of the antagonistic pair (extensor and flexor) becomes

[13] The MC 2 tendons are assumed to not wrap with q_{MC1}. The tendons of PIP and DIP both wrap with increasing joint angle q_{MC1}.

$$\begin{aligned} f_{t.act.joint} &= f_{t.act} - \left(f_{t.fc.flex} + f_{t.fc.ext}\right) = \\ &= f_{t.act} - \left(\mu_{c.flex} f_{t.flex} + \mu_{c.ext} f_{t.ext}\right) = \\ &= f_{t.act} - \left(\mu_{c.ext} f_{t.pre} + \mu_{c.flex}\left(f_{t.pre} + f_{t.act}\right)\right). \end{aligned} \tag{4.13}$$

The *active* force $f_{t.act.joint_i}$ acting at the joint pulley of joint i has to overcome the friction in the joint surface caused by the normal force f_{n_i} (see fig. 4.28). The part of f_{n_i} that is caused by the pretension force $f_{t.pre}$, as well as the active tendon force part, is also reduced by the tendon friction.[14] Hence,

$$f_{n_i} = f_{t.pre}\left(2 - \mu_{c.ext_i} - \mu_{c.flex_i}\right) + f_{t.act.joint_i}\,. \tag{4.14}$$

Since $\mu_{c.ext_i}(q)$ and $\mu_{c.flex_i}(q)$ are always positive, f_{n_i} can be simplified conservatively as

$$f_{n_i} = 2 f_{t.pre} + f_{t.act.joint_i}\,. \tag{4.15}$$

The tendon loads of all more distal joints introduce an additional normal force in the respective joint. Hence, the summed up normal forces $\vec{f}_{nsum_i}$ becomes

$$\vec{f}_{nsum_i} = \sum_{i}^{n} \vec{f}_{n_i}\,. \tag{4.16}$$

Since friction forces should be estimated for the worst case, all normal forces are conservatively assumed to have the same direction. As a result, equation (4.16) becomes

$$f_{nsum_i} = \sum_{i}^{n} f_{n_i}\,. \tag{4.17}$$

To gain the vector of all normal force sums of equation (4.17) in the respective joint, the vector $\vec{f}_n$ of all joint normal forces is multiplied with a lower triangular matrix of ones $\in \mathbb{R}^{n \times n}$ to obtain

[14] This representation is not fully conservative, since it does not take into account that the (tangential) capstan friction force is distributed to all sliding contacts. Therefore, it also introduces normal forces on previous joints. Nevertheless, the effect of the capstan friction reducing the normal force should be considered by the calculation.

$$\vec{f}_{n\ sum} = \vec{f}_n \begin{vmatrix} 1 & \dots & 0 \\ \vdots & \ddots & \vdots \\ 1 & \dots & 1 \end{vmatrix}. \tag{4.18}$$

Using equation (4.15), equation (4.18) becomes

$$\vec{f}_{n\ sum} = \left(2\vec{f}_{t.pre} + \vec{f}_{t.act.joint}\right) \begin{vmatrix} 1 & \dots & 0 \\ \vdots & \ddots & \vdots \\ 1 & \dots & 1 \end{vmatrix}. \tag{4.19}$$

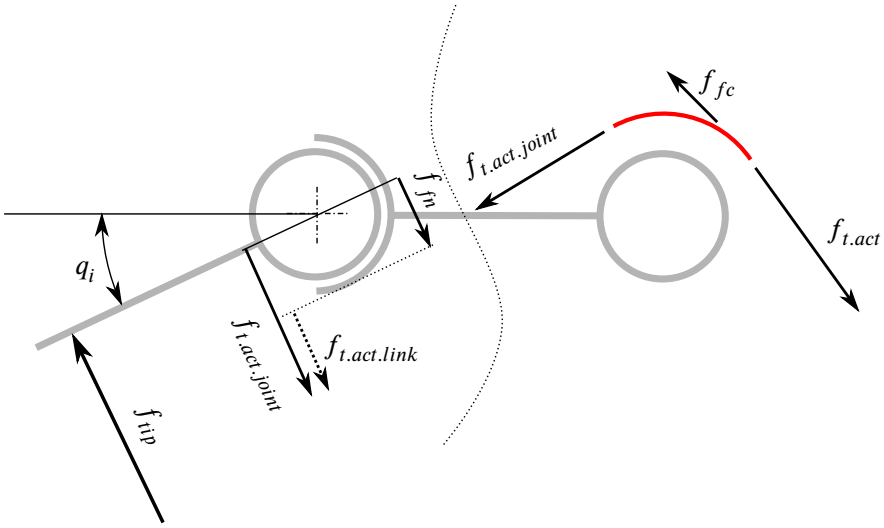

Figure 4.28. Tendon forces. $f_{t.act.link}$ (dotted) is not an existing force at the tendon. f_{fn} denotes the joint friction force and f_{fc} the capstan friction.

In case the radius of the joint surface r_s is not designed identically to the radius of the pulley r_p, the leverage has to be taken into account, to calculate the friction force mapped to the tendon $f_{fn} = (r_s/r_p)\mu f_n$ to finally obtain the (virtual[15]) active force at the link $f_{t.act.link}$ (see fig. 4.28)

$$\vec{f}_{t.act.link} = \vec{f}_{t.act} - \vec{f}_{fn} = \vec{f}_{t.act} - \mu R_l \vec{f}_{n\ sum}, \tag{4.20}$$

[15] $f_{t.act.link}$ does not exist at tendon level, since joint friction acts on the joint surface and therefore the linkside. It is only used for calculation and illustration purpose.

where μ is the coulomb friction coefficient of the joint surface and

$$R_l = \begin{vmatrix} \frac{r_{s_1}}{r_{p_1}} & \dots & 0 \\ \vdots & \ddots & \vdots \\ 0 & \dots & \frac{r_{s_n}}{r_{p_n}} \end{vmatrix} \tag{4.21}$$

is the diagonal matrix $R_l \in \mathbb{R}^{n \times n}$ of the leverages of r_{s_i}/r_{p_i}.
Finally, the dimensionless *error factor* $\Delta_{f.act}\left(\alpha, f_{pre}\right)$ is calculated:

$$\vec{\Delta}_{f.act}(\alpha, f_{pre}) = \frac{\vec{f}_{t.act.link}}{\vec{f}_{t.act}}, \tag{4.22}$$

relates the summed up friction forces of a joint to the *active* tendon forces, provided by the drives. $\Delta_{f.act}$ gives a quality measure for the force transmission of every joint of the finger. Example calculation results are given in the following.

Figure 4.29 gives examples showing the dependencies of the combined friction within the DIP joint (the DIP is selected, since it has the highest friction of all joints) for the parameter set given in table 4.4 and the maximum desired fingertip force f_{tip} (30 N). The friction, starting from less than 16% at zero pretension and in full extension position, increases with flexion of the PIP joint due to the growing wrap-around angle of the flexor tendon (having a higher load than the extensor) as well as the extensor tendon. The knee at approximately 22° results from the extensor DIP being completely unwrapped and getting wrapped again with increasing flexion angle. Increasing tendon pretension raises the overall friction, as it directly results in a growing normal force, and therefore, joint friction.

The joint friction, compared to capstan friction, is dominant within the DIP joint, see figure 4.30. In fully extended position, the joint friction makes up more than 72% of the overall friction. In contrast the capstan friction exceeds joint friction, which contributes less than 24% to the overall friction at maximum flexion. The proportions of friction are much more dependent of the joint angles than of the pretension force since the joint friction is roughly proportional to the applied tendon force.

To achieve good performance of the hand, the overall- friction of the hand has to be as low as possible. To reduce friction, it is essential to know which friction-relevant parameters, such as tendon routing / wrap-around angles, and

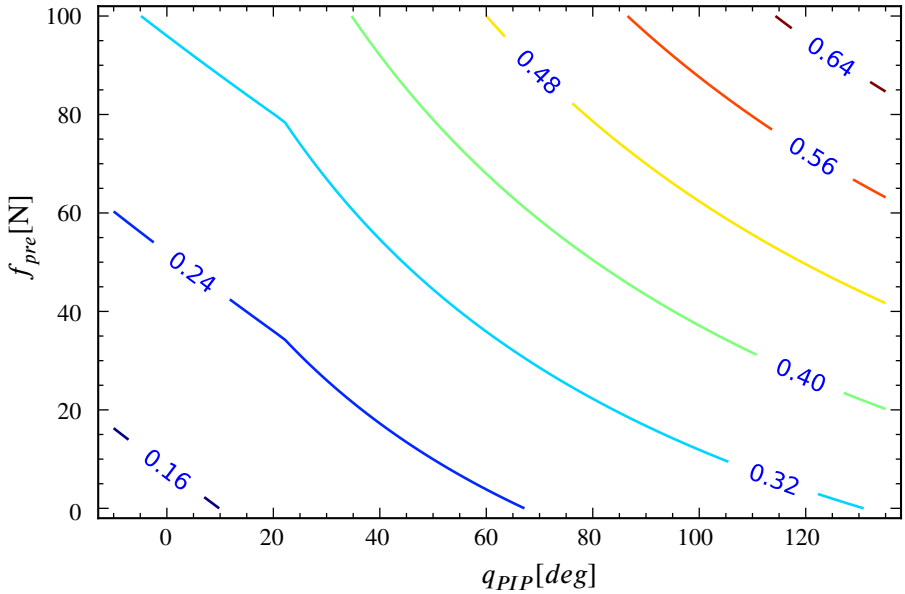

Figure 4.29. Estimated fingertip force error due to friction in the DIP joint with respect to the PIP angle q_{PIP}. The friction increases with flexion of the PIP joint due to the growing wrap-around angle of the flexor tendon as well as the extensor tendon. At $\approx 22°$ the extensor DIP becomes completely unwrapped and wrapped again with increasing flexion angle resulting a knee in the friction error is. Increasing tendon pretension raises the overall friction, as it directly results in a growing normal force.

joint surface diameters are most important for the hand design. Thus, in the following the influences of the sliding bearing surface diameter as well as the tendon routing on the overall friction is discussed.

Figure 4.31 compares the friction of two setups. Within the first setup, the friction surface is reduced to 3 mm radius (as for the hyperboloid joint design discussed in sec. 4.5.1), whereas the pulley radius is 8.2 mm. Therefore, the leverage of pulley radius and friction radius, according to eq. 4.20, reduces the friction force drastically in comparison to the second setup providing equal radii of pulley and sliding bearing surface.

The tendon routing has an equally important influence as the friction sur-

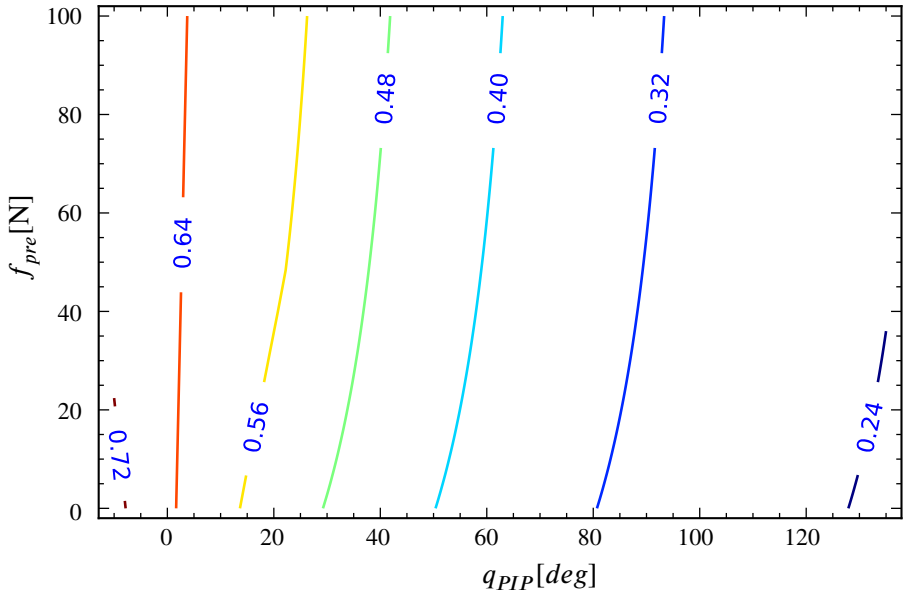

Figure 4.30. DIP portion of joint friction relative to the overall friction with respect to q_{PIP}. Joint friction is dominant within the DIP joint in fully extended position. At maximum flexion the capstan friction exceeds joint friction by far. The proportion of frictions is much more dependent on the joint angles than of the pretension force since joint friction is roughly proportional to the applied tendon force.

face diameters on the overall friction. If the tendons are routed in parallel as seen in figure 4.24a, all extensor tendons are wrapped around the joints with increasing flexion of the finger, leading to a steep increase of the tendon friction, and consequently, overall friction.[16] The crossed tendon routing (see fig. 4.24b) does not show such behavior. Furthermore, the friction is less pretension dependent for low joint angles in absolute values, since the flexor is almost unwrapped which results in a lower capstan friction portion. On the other hand, the overall friction is lower for parallel routing, since the tendons do not have "offset angles" α_i.

[16] In addition, the needed drive speed, in particular of the DIP increases, since the wrapping has to be compensated by the drive.

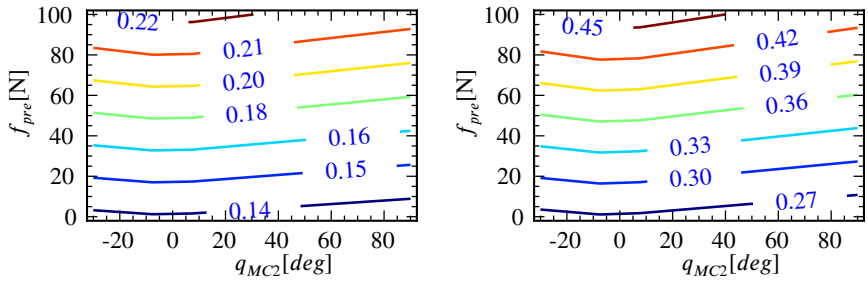

Figure 4.31. Comparison of overall MC 2 friction with respect to MC 2 joint angle q_{MC2}: *a*, MC friction surface reduced to 3mm radius; *b*, sliding surface radius equal to pulley radius (8.2mm), which drastically increases joint friction and, by this, overall friction. The decrease of the friction with increasing joint angle is caused by the reduced normal force due to increasing tendon friction in more distal tendons at constant input tendon force.

Finally, it has to be guaranteed that the fingers move properly, even in worst-case configurations. Thus, worst-case scenarios are calculated as well. Figure 4.33 depicts the overall friction of the DIP joint in full flexion of all joints, besides the PIP. In this position, no precision grasp or fine manipulation can be achieved.[17] Consequently, accuracy and sensitivity is not an issue in this configuration. Nevertheless, the fingers have to be able to at least move back from such poses independently, to ensure operation within the full motion and force range of the fingers. The DIP joint has by far the highest friction and exceeds 80% friction in the worst-case pose at a pretension force of 100 N[18] and in crossed tendon routing setup.

The friction estimation shows that the ratio of joint friction and capstan friction largely differs in relation to the joint angles, the tendon routing and the related wrap-around angles, as well as the pretension force. Consequently, the calculation parameters need to be modified and the calculation performed again within the design process, to balance out the design parameters. Nev-

[17] The human hand is not able to perform this motion due to the coupling of the PIP and DIP joint.

[18] This value can never be reached without exceeding critical tendon load.

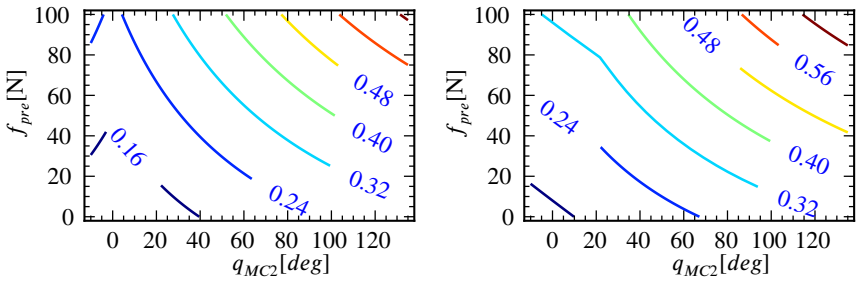

Figure 4.32. Comparison of overall DIP friction with respect to PIP joint angle q_{PIP} using different tendon routing concepts: *a*, parallel tendons. Flexion wraps all extensor tendons; *b*, crossed tendon routing. Tendons alternately are wrapped or unwrapped by flexion of all joints as depicted in fig. 4.27. Overall friction is lower for parallel routing *(a)* since the tendons do not have "offset angles" for the latter. The friction of crossed routing *(b)* is less pretension dependent for low joint angle absolute values since the flexor is unwrapped.

ertheless, the analysis gives valuable hints for the joint design.

For example, in parallel tendon routing setup, the flexion angles of all joints sum up and produce a rather large wrap-around angle value (255° at the extensors for the given motion range) leading to high pretension force sensitivity to friction.[19] In contrast, the wrap-around angles compensate for each other during flexion of the finger in a crossed tendon routing, as depicted in figure 4.27 and reaches only 155° for the extensors. In addition, to reduce joint friction, in particular in more proximal joints, having large normal forces (>1.3 kN in the MC joint), the relation of sliding bearing surface diameters and the pulley diameters has to be reduced as much as possible.

[19] If the "offset angles" are designed similarly to the crossed tendon setup, the tendon friction is significantly higher than for the crossed setup.

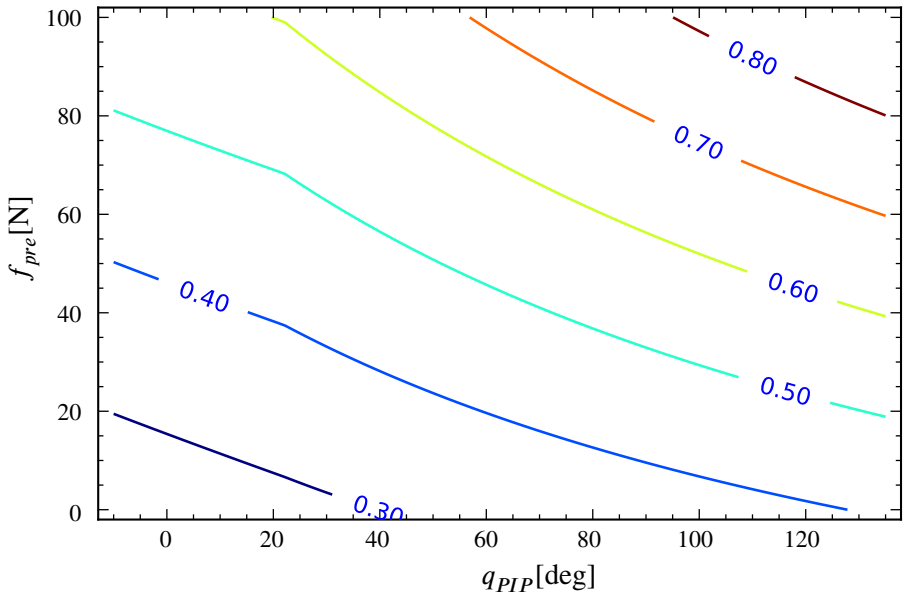

Figure 4.33. DIP friction force error estimated for worst case. The first axis of the finger is in full abduction (30°) and all other joints besides the moved PIP are in full flexion (90°/90°), which results in maximum wrap-around angle.

Table 4.4. Example parameter set used for the friction plot calculation. q_{DIP} is without any influence to the results. The friction values are measured and rounded up.

Parameter	value	description
q_{MC1}	[-30° … 30°]	MC 1 (abd./add.) joint angle
q_{MC2}	[-30° … 90°]	MC 2 (ext./flex.) joint angle
q_{PIP}	[-10° … 135°]	PIP joint angle
q_{DIP}	[-30° … 90°]	DIP joint angle
α_{MC1}	30°	Summed up wrap-around angle MC 1
α_{MC2}	≈7.6°	Summed up wrap-around angle MC 2
α_{PIP}	≈22.1°	Summed up wrap-around angle PIP
μ	0.1	Coulomb friction coefficient
μ_c	0.1	Capstan friction coefficient
l_{mc}	0 mm	Distance between 1^{st} and 2^{nd} MC axis
l_{prox}	40 mm	Length of proximal phalanx
l_{med}	30 mm	Length of medial phalanx
l_{dist}	20 mm	Length of distal phalanx
r_{pMC} / r_{sMC}	8.2 mm / 3.0 mm	Radius of pulley/ of sliding surface MC
r_{pPIP} / r_{sPIP}	5.3 mm / 5.3 mm	Radius of pulley/ of sliding surface MC
r_{pDIP} / r_{sDIP}	3.75 mm / 3.75 mm	Radius of pulley/ of sliding surface MC

4.5. Design of Anthropomorphic Fingers

The term anthropomorphic design has been overused throughout the past decades and therefore, is not only perceived positively. This, on one side, results from designing empirical copies of the human archetype that do not take into account that the underlying design principles in biological and technical systems are fundamentally diverse. For example the long lasting lifetime of human joints containing articulation surfaces as well as cartilage, tendons etc. is strictly related to the self healing and self lubrication abilities of biological systems as discussed in section 1.6. On the other side, the word is misused for systems that are falsely referred to as anthropomorphic to valorize them.

The fingers of the *Awiwi Hand* are intended to be anthropomorphic in the original definition (see sec. 1.6). They should have the characteristics of the human archetype in all relevant aspects, such as robustness, dynamics, grasping performance and size. They are antagonistically driven and are of average human size (within 25^{th} and 75^{th} percentile). They are intended to withstand large lateral impacts and collisions by allowing a subluxation of each of the joints. This section presents the design of the joints with a strong focus on the MC joint, the finger structure, the tendon routing, and finally, the coupling of the ring and little finger PIP and DIP joint. This section is based on [Grebenstein et al. 2010b; Grebenstein et al. 2012]

4.5.1. Finger Joints

The following describes the design of the joints of the finger based on the fundamental functionalities elaborated in section 3.2. The finger joints have to fit the kinematic structure designed in the previous section.

DIP and PIP Joint

The design of the DIP and PIP joints is a direct transfer of the human hinge joints to the robotic hand. The main design constraint is that the fingers have to withstand large impacts without damage. They also require a range of motion of 90° for the DIP joint and 135° for the PIP. Moreover, in order to reduce the control complexity of the fingers, no additional non-linearities should be introduced by the tendon actuation. Therefore the tendons are, in contrast to the human hand [Kapandji 1982, p. 194; Wilkinson et al. 2003; Deshpande

et al. 2008] fixed on a cylindrical pulley providing a constant moment arm. The external loads at the joints are relatively small with respect to the loads introduced by the pretension of the tendons. For example, the index finger provides 30 N force at the fingertip in the stretched-out position, which is in the vicinity of what a human can exert. The relation of the phalanx length to the maximal pulley diameter, which is constrained by the targeted outer geometry of the hand, is in between 5.7/1 (DIP of little finger) and 10.8/1 (PIP of middle finger). The overall load of the middle finger reaches more than 1.3 kN at the MC joint. Furthermore, the joints of the finger, as in the human archetype, should be dislocatable. Therefore, it is not possible to use standard, fixed axis, ball bearing setups (considering a bearing size compatible with the packaging constraints). The tendon pretension forces enable to use an open hinge joint, consisting of a cylindrical joint head and a joint pan of less than 180°. This open hinge joint does not prevent dislocations by form closure. Hence, the joint can be dislocated by external loads, that produce longitudinal forces larger than the actual tendon forces, without structural damage. Axial movement of the joint is constrained by ridges in the cylindrical shape of the joint head and pan similarly to the human PIP and DIP joints (see fig. 4.34).

The ridges in the joint pan and head have to be rounded to prevent point or edge contacts to prevent damage of the joint surfaces in case of dislocation. Torques resulting from forces parallel to the joint axis have to be carried by force closure. Therefore, the insertion points of the tendons, in particular the flexors, have to be located as far from the opposed end of the cylinder as possible. Indeed, it increases the relationship of the levers. Because tendons can only pull, two flexors and one extensor (which is placed within the sagittal plane; see fig. 4.34) are used to create a force triangle and increase the joint stability.

Metacarpal Joint

As shown in section 3.2.4, the MC joint of the human hand can be approximated by a cardan joint without degrading the functionality, if provided that the orientation of the first axis is chosen properly. Since the singularity of the human metacarpal joint is at about 90° flexion, the first axis of the metacarpal has to be oriented approximately orthogonal to the palm. As the MC joint has to carry the complete tendon load of the finger column, the applied load on the joint can reach 1.3 kN in the middle finger. As a result of the potential high

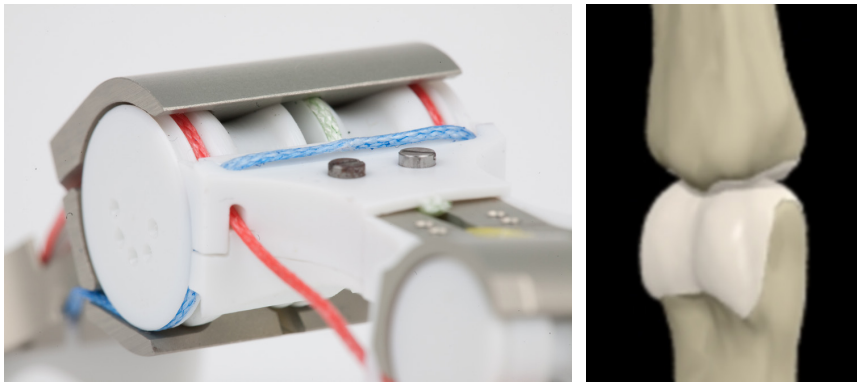

(a) (b)

Figure 4.34. PIP joint design: *a*, the open hinge joint design of the robot finger PIP; *b*, its human archetype. The ridges of both joints keep the joint in place axially. The two PIP flexor tendons (blue) in *(a)* are routed as far as possible from the sagittal plane of the finger to provide the leverage necessary to withstand lateral forces. The PIP extensor tendon (green) is placed close to the sagittal plane.

loads, together with the spacial restrictions, a cardan joint cannot be used. Inspired by the human thumb (sec. 3.1.3, 3.2.5), the MC joint is designed as a saddle joint with two orthogonal, but non-intersecting axes (see fig. 4.35). The surface pressure in a saddle joint is much lower than in a condyloid joint. Moreover, the saddle joint is geometrically exact and can remain in line contact within the whole range of motion. Therefore, a pair of hyperboloids is chosen for the metacarpal joint sliding surfaces building a hyperboloid saddle joint (see fig. 4.36).

The tendons actuating the metacarpal joint are connected to the hyperboloid with a maximum, constant moment arm, thus reducing tendon loads and providing a linear coupling. Additionally, the hyperboloid shape enables a reduction of the friction bearing diameter with respect to the pulley diameter, if the hyperboloids are designed such that the tendon load is mainly carried in the center of the hyperboloid. The joint friction can be then reduced drastically as shown in section 4.4 (at the cost of higher contact pressure).

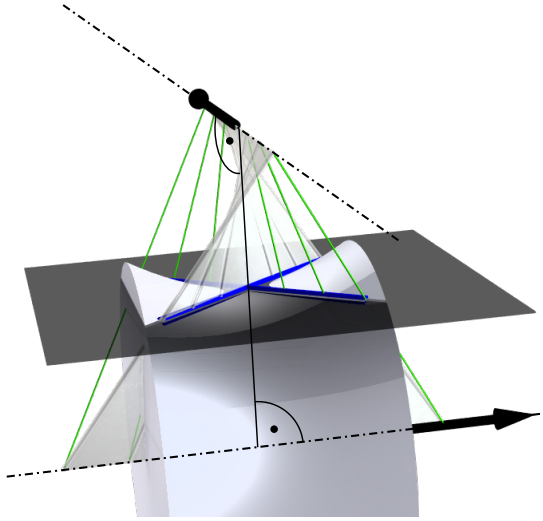

Figure 4.35. Hyperboloid generatrix. A line of contact between two rotational geometries with orthogonal, non-intersecting axes can be found connecting equidistant points on both axis of rotation by straight lines (green) and intersecting these with a plane orthogonal to the perpendicular to both axes. If the line of contact (blue) is rotated around one of the axes of rotation, it generates a hyperboloid.

4.5.2. Structure

The design of the finger structure is rather straight forward. The use of an endoskeleton (see fig. 4.37), as in the human archetype, reduces the number of parts and allows the addition of pads between the structure and the outer surfaces of the finger. This is crucial to improve the grasp quality and distribute stress uniformly.

4.5.3. Tendons and Tendon Routing

The tendons of the hand have a central role in the design of the hand and its fingers and are discussed in the following based on [Grebenstein et al. 2010b].

The friction estimation (see sec. 4.4) showed that, regarding friction, a crossed tendon coupling reduces the overall wrap-around angle drastically.

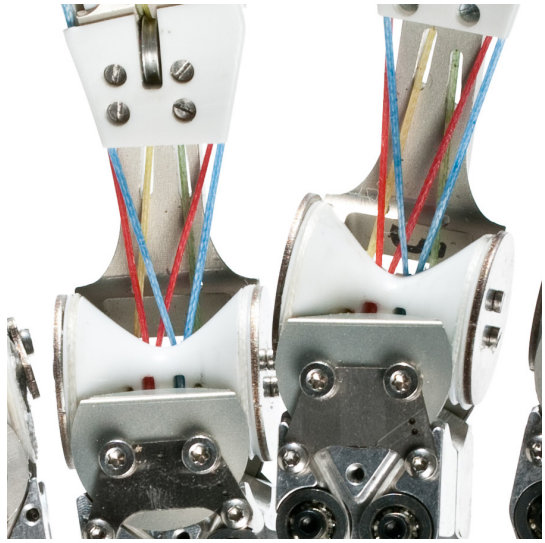

Figure 4.36. Hyperboloid based anthropomorphic MC joint. The hyperboloid shape reduces the joint friction drastically since, assuming the load is mainly promoted in the center of the joint, the lever of the pulley (white tendons) is much larger than that of the coulomb friction (see sec. 4.4).

This reduction is even more important regarding tendon travel and drive speed. A parallel tendon setup drastically reduces the maximum possible speed during full finger flexion or extension, since the drives must provide the additional speed to compensate the additional tendon travel introduced by the coupling on one hand. On the other hand, the tendon travel, necessary to provide the range of motion is much smaller in the crossed tendon setup and thus, enables more compact design of the drives. It has to be pointed out that, with respect to travel and maximum joint speed, a tendon routing through the axis of the joint is generally favorable. Due to the large range of motion of the joints, in particular the PIP and DIP, the cutouts necessary to route the tendon through the center of the joint have to be too large. Hence, a crossed tendon setup is chosen for the finger design.

In contrast to most of the tendon driven hands, as discussed in detail in section 4.2, the proposed design does not need a tensioning mechanism. Consequently, it does not suffer from tendon length changes caused by the geometric

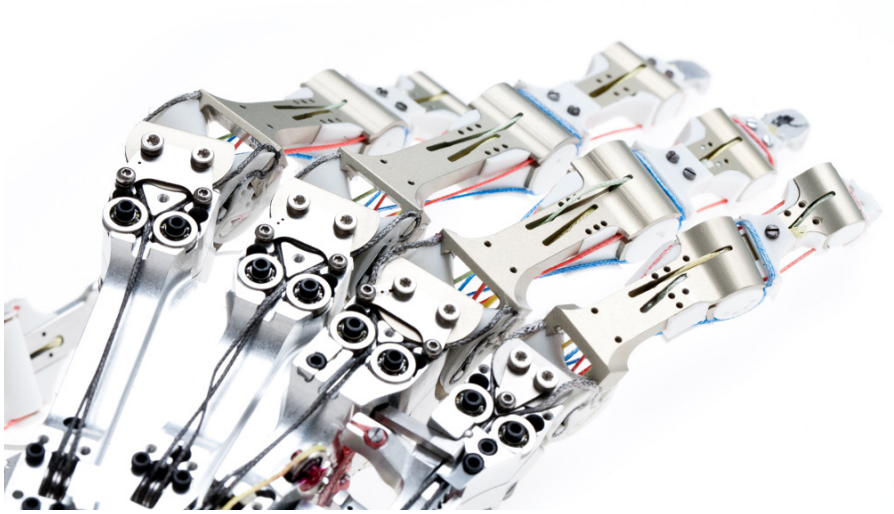

Figure 4.37. Endoskeleton structure of the fingers, providing low component count and abundant space to apply soft pads to improve grasping performance. The white tendon guidances are made from friction bearing plastics to reduce capstan friction.

inaccuracies associated with pulleys, wrist motion, etc. As a result, the creep properties are not taken into account in the selection of the tendon material. After some preliminary experiments on different tendon types it appears that the most important parameters are:

- Possibility for termination/fixation of the tendons
- Robustness against folding during assembly
- Component wear (tendons and guides)
- Color coding, which is important for clarity during assembly and maintenance

In order to fit in the desired envelope, especially within the little finger, the termination and the fixation of the tendons are crucial. The terminations have to be compact, reliable and repeatable. The steel cables used within the first finger prototype turned out to be inapplicable, as the terminals created at production time are too bulky to be inserted into the palm and, in particular the

hyperboloids during assembly and maintenance. Folding of the tendons during assembly drastically reduces the tendon lifetime and is unfortunately not avoidable. Kevlar or Aramid tendons are much better regarding wear and folding. However, their termination is complicated since knots weaken the tendon significantly and are difficult to design. The tendons braiding prevents splicing, which is the best termination technique in our observation. Tests of the Dyneema tendons published by *Friedl* [Friedl et al. 2011a], revealed significantly less wear than steel or Kevlar tendons (especially in sliding contact) as depicted in figure 4.38. Termination can be placed accurately by splicing, which is easy to do and reliable. Therefore, in contrast to [Palli et al. 2009] Dyneema is selected as the tendon material. The tendon routing from the insertion points in the joint toward the palm (fig. 4.40) has to fulfill the following constraints:

- Linear transmission characteristics
- Minimal friction
- Easy maintenance

When redesigning the routing in the MC joint with the Dyneema tendons, it has been decided to route the tendons internally (see fig. 4.40). As a result, the coupling of MC joint motion and DIP/PIP motion is reduced drastically (i.e. a motion of the finger base has little, if any, influence on the PIP and DIP joint positions). This routing also reduces the wear of the tendon since the tendons are changing direction only in a planar way (in the first design the tendon "rolled" on the guiding surface). The Y-shaped flexor tendons, necessary to carry lateral loads (see sec. 4.5.1), split from one tendon into two within the palm.[20] If the splitting would be located between the MC and the PIP joint, it would have introduced a non linearity in the transmission characteristics. Furthermore, one of the two parts of the "Y" would run slack when the connection point moves, if the PIP of the finger has inclination. The guidance of the tendon toward the insertion points is provided via sliding surfaces. The guiding parts (see fig. 4.40) have been machined out of low friction bearing plastics, to reduce overall tendon friction to a minimum. The

[20] In detail, the tendons are spliced to form a loop around the guidance part distally of the joints, such that the splice is located between the proximal MC hyperboloid and the most distal pulley within the palm.

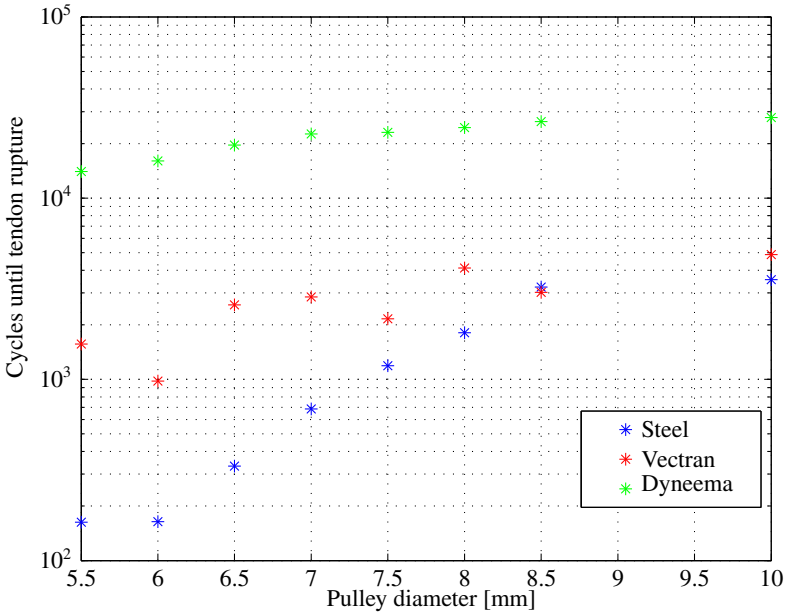

Figure 4.38. Lifetime of different tendons with respect to pulley diameter [Friedl et al. 2011a] (logarithmic scale). The implemented Dyneema tendons (0.6 mm diameter) show more than one magnitude longer lifetime than steel cables of comparable maximum load (Carlstahl 8×19 + 7×7 0.57 mm diameter, uncoated). The Dyneema tendons are also less prone to small pulley diameters.

friction coefficient of the Dyneema tendons at constant velocity on the bearing plastics was measured (using a load cell) to be 0.09 on a cylindrical surface of 12 mm diameter.

4.5.4. Coupling of Ring and Little Finger PIP and DIP Joint

Section 3.2 shows that coupling the PIP and DIP joint of the ring as well as of the little finger does not impair the grasping and manipulation performance of the hand considerably. Furthermore, such coupling reduces the number of necessary actuators within the forearm. The coupling cannot be designed

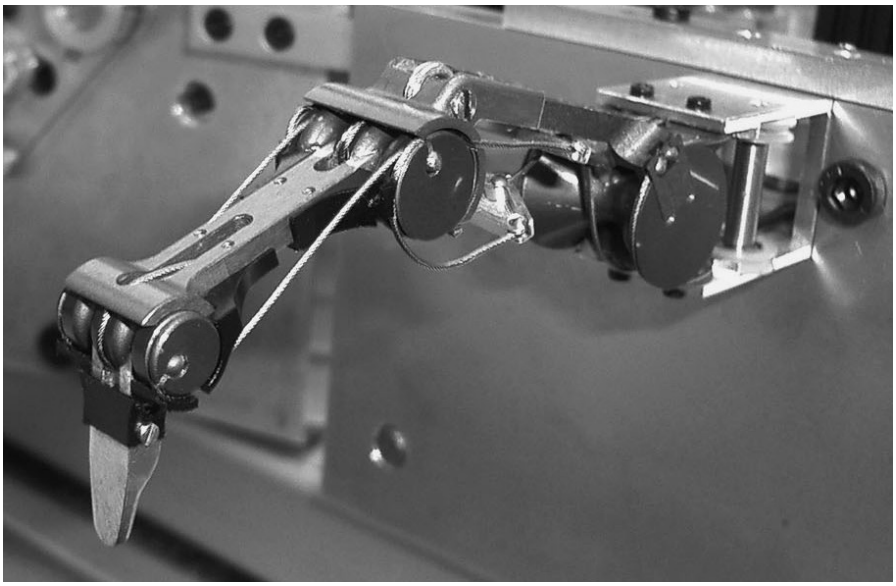

Figure 4.39. Tendon routing of the first finger using steel tendons. Due to the large diameter of the tendon terminals an internal routing of the tendon is not possible. The external routing increases coupling of the PIP and DIP joint motion with MC motion which reduces the maximum joint speed. The tendons are not planar in the MC guidance. Therefore, the tendons roll/slide on the surface which increases wear. (see Appendix B.2 for more pictures)

within the fingers themselves and has to be part of the palm, due to spacial restrictions in the fingers. The coupling tendons are not length invariant since they cannot be routed through the neutral points of the MC joint in a sharp edge. This length variation has to be compensated by a tensioning mechanism providing the necessary travel. The tensioner of both fingers is applied to the extensors of the DIP joint.[21] The agonist tendon (flexor) of the DIP is fixed rigidly in the distal hyperboloid of the MC joint. The tensioner of the ring and little finger is depicted in figure 4.41.

[21] The extensor of the DIP is thought to rarely have external loads that cause noteworthy compression of the tensioner and therefore tendon slack in the flexor tendon. In case of slack tendons the tendon is kept in place by the housings.

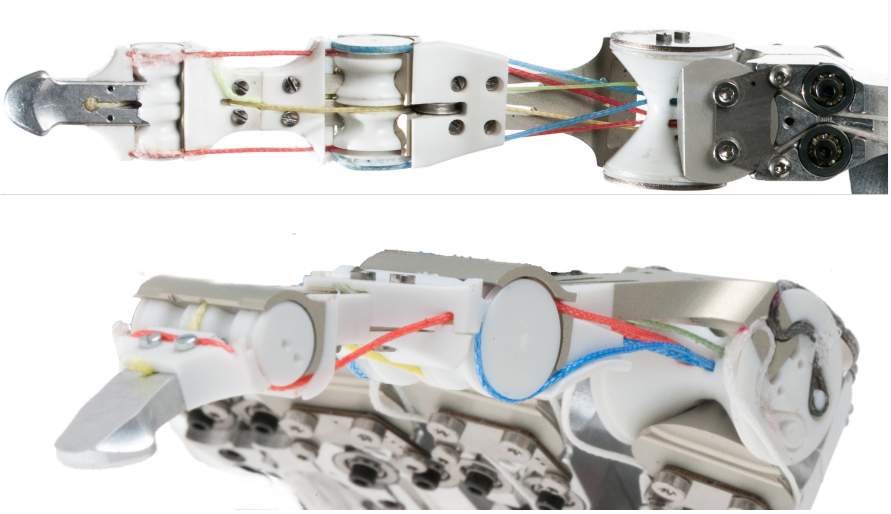

Figure 4.40. Internal Tendon routing of the PIP and DIP joint tendons at the MC joint. The tendons are routed through equivalent slots in the proximal hyperboloid.

4.6. Thumb Design

As shown in section 3.2.5, the human thumb is the most important digit of the human hand. It must be significantly stronger than the fingers, to be able to oppose multiple fingers especially during power grasp and thereby carry the loads exerted onto the object by the fingers. Furthermore, as described in section 3.1.3, the human thumb has five DoF. The thumb of the *Awiwi Hand*, however, must be implemented with four DoF to meet the constraints of the *DLR Hand Arm System* without major functional impairments (sec. 4.3.3).

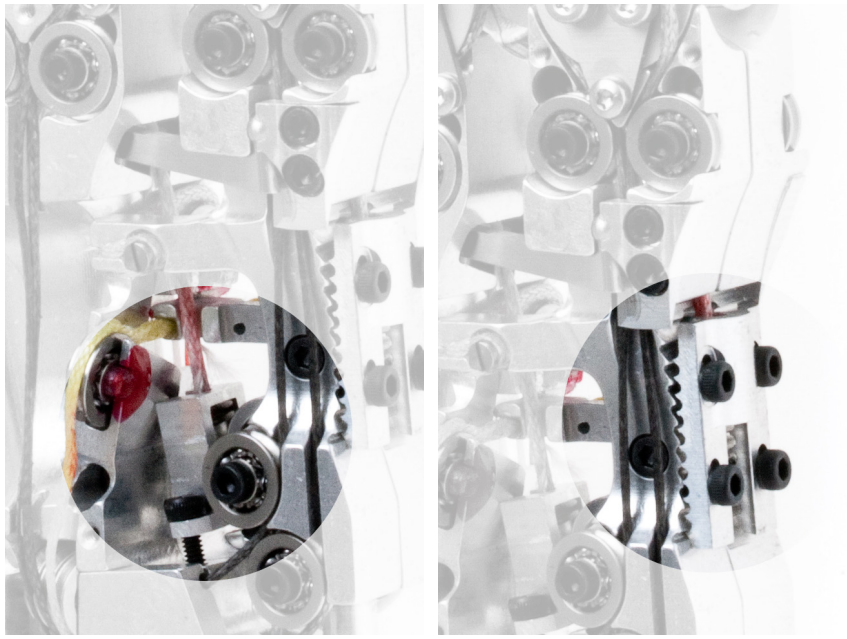

(a) (b)

Figure 4.41. Tensioner of the ring and little finger integrated into the palm. Both tensioners act on the red tendon (flexor DIP). The fingers point toward the top on the photo. *a*, ring finger tensioner providing large travel of the tensioner and the spring (the spring is integrated in the alloy part in the center of the circle and almost as long as the alloy part itself); *b*, little finger tensioner based on "Nonius" principle to enable fine adjustment. The integrated spring (not visible) is identical to the one used in the ring finger.

4.6.1. Joints of the Thumb

The TMC Joint

The TMC joint uses the hyperboloids of the finger MC joints.[22] In contrast to the finger MC joints, the desired fingertip force of the thumb is 40 N. Due to spacial restrictions the tendons have to be attached directly to the thumb structure itself and to be led by guides attached to the palm to provide sufficient moment arms (see fig. 4.42).

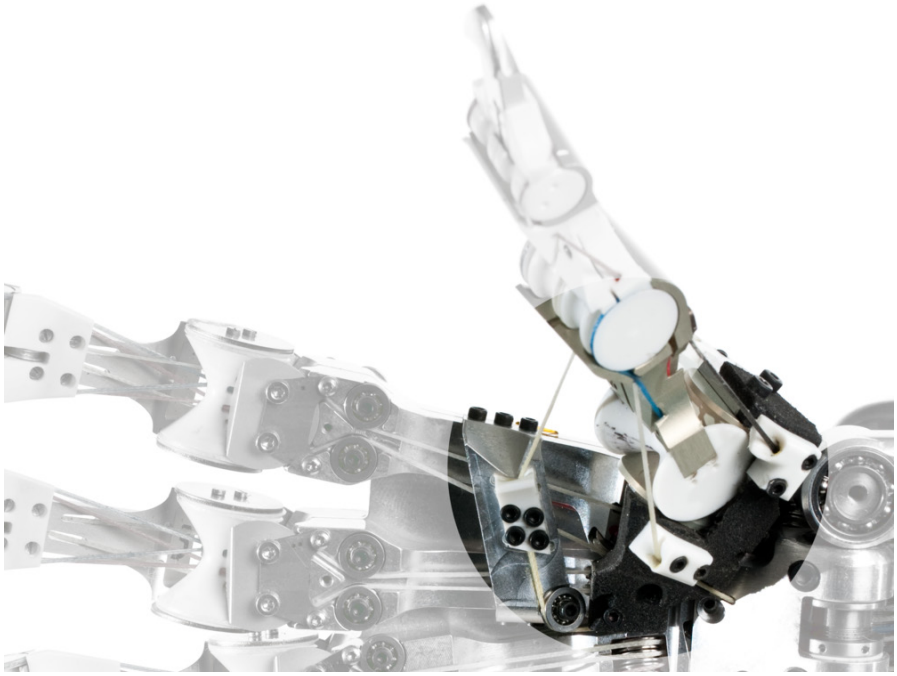

Figure 4.42. Tendon routing of the thumb. The guidances of the flexor tendons are placed more distant than the extensors, to maximize the available tip force, in particular for power grasp. By this, the maximum force at the IP joint location is greater than 80 N.

[22] The hyperboloids themselves are machined all together in a first step. In a second step, the tendon guidings as well as the pulley profiles are machined. The latter are omitted and the inner tendon guidings are adapted to the different range of motion for the thumb hyperboloids.

Thumb MP and IP Joint

The MP and IP Joint design of the thumb is identical to the finger joints, aside from the diameters of the joint bodies to provide the necessary joint torques by larger moment arms, in particular in the thumb MP. To compensate for the missing fifth DoF of the thumb of the *Awiwi Hand*, the IP is turned inward around the longitudinal axis of the proximal phalanx with respect to the MP axis (twist; see fig. 4.43), which improves the power grasp performance as discussed in section 4.3.3. Furthermore, the IP joint provides inclination, see also section 4.3.3.

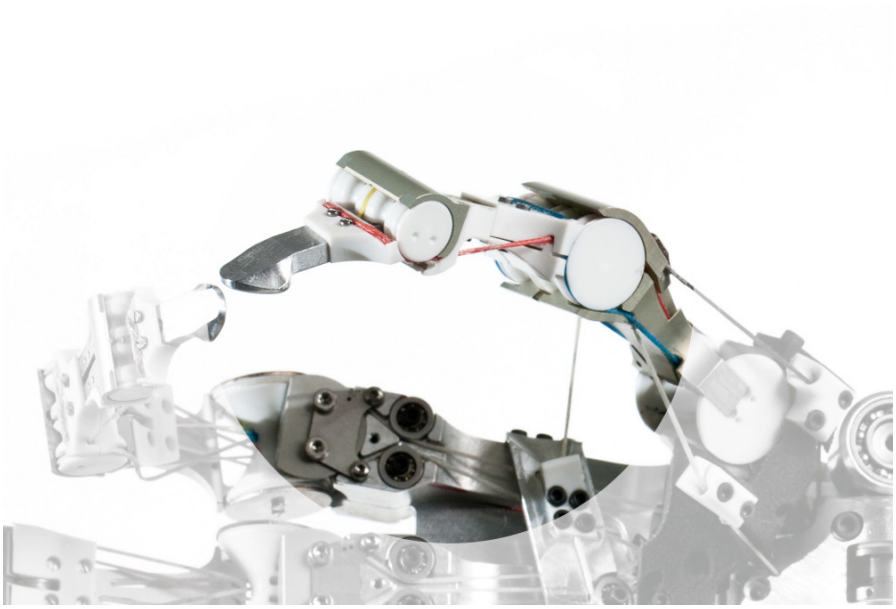

Figure 4.43. Photo of the twist between IP and MP joint (inward rotation of the IP axis with respect to the MP axis). It enables the thumb to make a more frontal contact, in particular, with large cylindrical objects during a power grasp (sec. 4.3.3)

4.6.2. Thumb Structure

The structure, like in the fingers is an endoskeleton structure. To enable proper tendon attachment, the proximal phalanx differs from the design used in the fingers (see fig. 4.44). The medial phalanx, in contrast to the fingers, has to be twisted as discussed in section 4.3.3 and 4.6.1 to compensate for the missing fifth DoF of the thumb, and to enable a good compromise between key grasp and power grasp performance (see fig. 4.43).

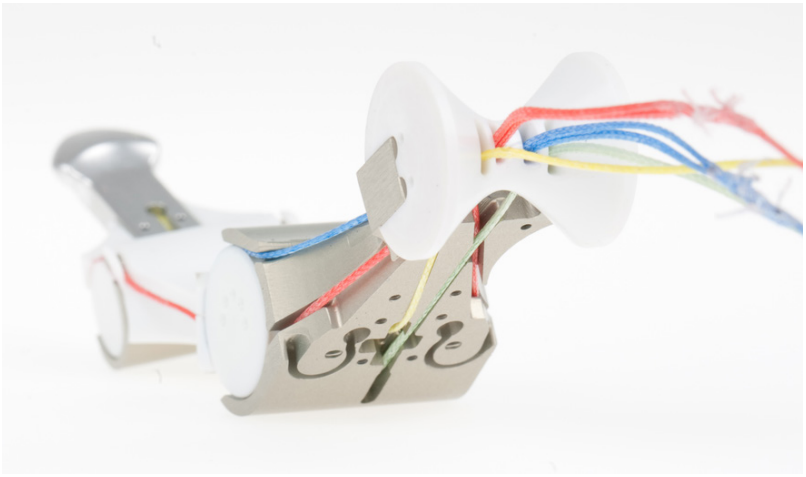

Figure 4.44. Structure of the thumb: the tendons of the TMC joint are attached to the, relative to the fingers, much wider and stronger “bone”. The tendons of the MP (green and blue) and IP joint (red and yellow) are routed through the hyperboloid similar to the fingers.

4.6.3. Tendons and Tendon Routing of the Thumb

The routing of the flexor and extensor of the MP and IP joint (see fig. 4.44) is identical to the tendon routing of the fingers, see section 4.5.3.

Similar to the human thumb, the tendons actuating the TMC are directly inserted into the metacarpal bone as discussed in section 4.6.1. Proximally, the tendons are guided at four points of the palm. To enable abduction, adduction, flexion, and extension, the flexors and the extensors have to be placed around the TMC (see fig. 4.42). As a result, the tendon kinematics are non-

linear, which implies the need of appropriate control algorithms as presented by *M. Chalon* [Chalon et al. 2011]. The tendon routing of the TMC tendons allows for much higher forces (>80 N) at the IP joint location. Nevertheless, the fingertip force of the thumb is limited to 40 N by the PIP diameter. The guidances of the flexors are placed more farther than the extensor ones, as depicted in figure 4.42, since extension of the thumb needs, significantly less force than flexion, to provide the needed functionalities of the hand.

4.7. Design of the Palm

The palm has two main functions. First, it has to route the tendons from the wrist to the fingers with minimal friction losses. Second, it has to provide the functional surfaces, in particular to perform power grasp of objects of different sizes and shapes (spherical, cylindrical, ropes etc.) and it has to shape the "palmar arch" (see secs. 3.2.6 and 3.3) [Kapandji 1982, pp. 174-175]. This is an important functionality, which is crucial for the grasping performance of the hand.

4.7.1. Tendon Routing Requirements

The tendon routing of the palm, in particular, has to provide:

- Minimal friction
- Good maintainability and access to the tendons
- No contact between tendons

Friction within the palm has to be as low as possible. The friction along the whole tendon path, including joint friction, is crucial for the grasping, and manipulation performance of the hand. As shown in section 4.4, even an optimal design of the guidances and joints leads to a non negligible amount of friction, ranging up to 80% friction in worst case configuration at high tendon pretension. Consequently, any additional friction along the tendon path has to be reduced as much as possible. Hence, all (notable) redirections should be ball bearing mounted pulleys if possible. Due to the spacial restrictions the number of pulleys has to be reduced as much as possible. Additionally, the

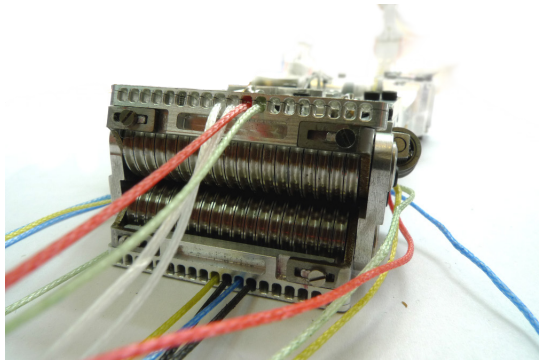

Figure 4.45. Wrist pulley array: to reduce wrist torques due to asymmetric tendon load and to save design space, the tendons are placed as close together as possible. The tendons assembled in the figure are thumb tendons providing large tendon forces, and therefore placed close to the sagittal plane.

tendons are reshaped in every additional contact with a pulley, which dissipates energy, and thus adds to the friction.

As described in section 4.2.4, the forearm uses two types of drives, providing different maximum tendon forces (250 N, 350 N). The tendons providing maximum forces are placed as close as possible to the sagittal plane of the hand on the wrist pulley array shown in figures 4.45 and 4.46, to achieve a compact design of the forearm. In addition, this design reduces unwanted wrist torques resulting from asymmetric tendon load. On the other hand, the thumb, index and middle finger have the longest phalanges and the highest maximum fingertip forces resulting in high tendon loads. As a result, their tendons have to be routed from the center of the wrist to the radial (thumb) side of the hand. Furthermore, the tendons should not have (loaded) contact to each other, since tendon contact at high velocity leads to non negligible heat development. The latter have been shown to be able to damage or even brake the Dyneema tendons.

Finally, the tendons have to be routed in a way that enables easy access and in especial replacement of the tendons. This requirement, also applies to the design of the palm mechanics, which is described in detail in the following section.

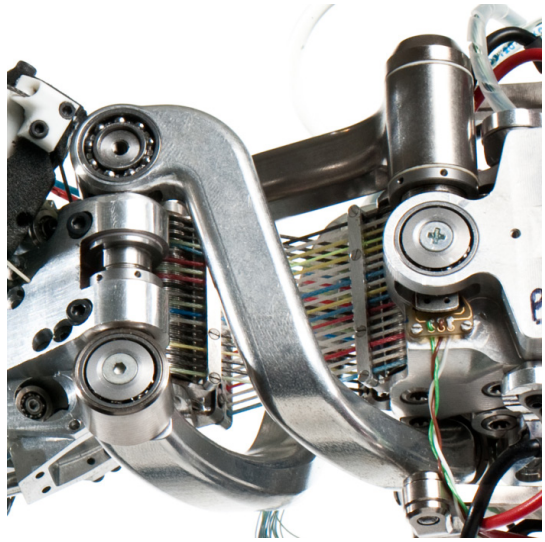

Figure 4.46. Tendon routing within the wrist: the tendons are guided by pulley arrays on the proximal (forearm) side (*right*) as well as on the distal (hand) side of the wrist (*left*). The tendons providing maximum force are placed in the middle of the wrist to reduce (unwanted) torques on the wrist.

4.7.2. Assembly and Maintenance Concept

A major challenge of the palm mechanics design is the assembly and maintenance of the tendons as tendon wear and breakage is likely due to the amount of the tendons and the large tendon loads. The tendon routing (within the finger) of the index, middle and ring finger is similar, whereas the tendon routing of the little finger and the thumb differs significantly. To recall, the thumb tendons do not act on pulleys, but are attached directly to the first phalanx of the thumb. The guides of the TMC tendons are part of the palm. In contrast, the metacarpal bone of the little finger is movable and therefore not part of the central palm.

Within the fingers the tendons can be grouped into the DIP and PIP tendons running through the center of the MC joints, and the tendons actuating the MC joint itself. The latter are running toward the palmar and dorsal end of the MC joints. On the wrist side of the palm, the tendons coming from the wrist are all

routed over a pulley array of two times 19 pulleys in two layers (see fig. 4.45, 4.46). Due to the wrist design it is not possible to lead the tendons directly toward the fingers. To avoid the tendons losing contact to the pulleys during wrist flexion and extension, the minimum contact angle at the pulley arrays is 22.4° (see fig. 4.47).

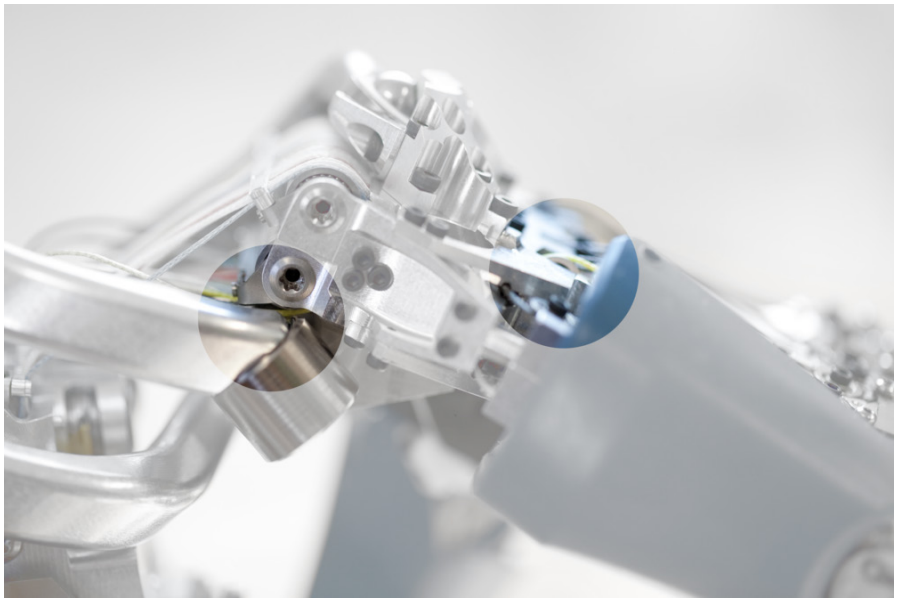

Figure 4.47. Tendons at the wrist in maximum flexion: The tendons should not lose contact with the pulley array in this position to avoid tendon damage. The yellow tendon *(lower left)* on the pulley array is routed to the opposite side of the palm *(upper right)* to prevent losing contact with the pulley.

Consequently, the tendons cannot be directly routed to the MC joints. As a result, at least one pulley is needed. Furthermore, the lateral distance between the tendons within the wrist has to be as small as possible to reduce coupling of wrist and finger motion as well as to fit into the available design space as shown in figure 4.45. It is not possible to place the pulleys that redirect the tendons next to each other due to these spacial constraints. A tendon routing in three layers as shown in figure 4.48 is advantageous. It enables alternating placement of the pulleys in two rows, a proximal one redirecting the tendons

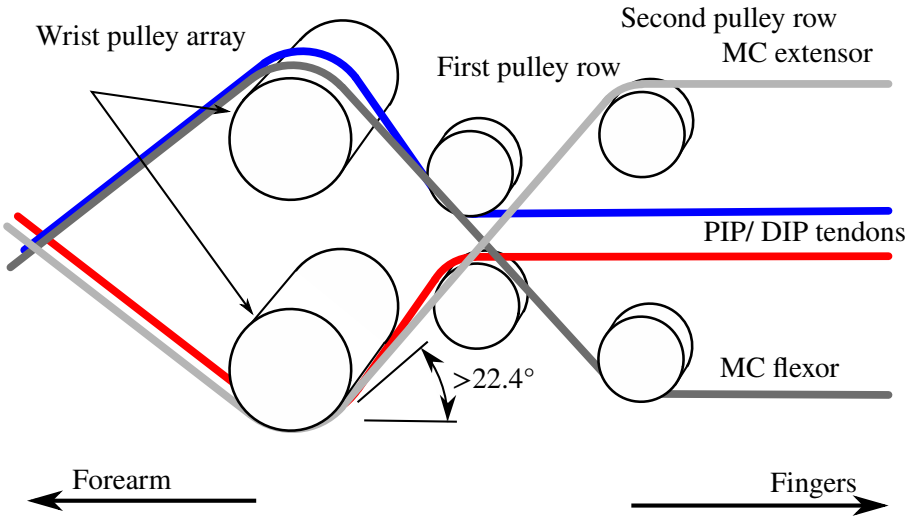

Figure 4.48. Three layered tendon routing concept. The tendons have to enter the palm at an angle of >22.4°. Depending on their destination, they are routed to the respective layer by a single, three DoF oriented, pulley, to reduce friction and design space.

to the middle plain of the palm towards the MC center and a distal one that routes the tendons through the palm to the opposite side of the palm (see fig. 4.47). With this design strategy, the palm can be designed such that the tendons actuating the MC joints are freely accessible for maintenance and inspection as seen in figure 4.49.

To improve tendon lifetime, the pulleys are oriented in three DoF for exact fits to the intended tendon pull directions. [23]

4.7.3. Central Palm Mechanics

To achieve the three layered tendon routing, the palm itself is constructed in four layers parallel to the frontal plane of the palm (see figs. 4.50, 4.51). The metacarpal bones make up the two middle layers. They are split in a palmar and a dorsal halve, to enable assembly of the tendons, as well as machining of the tendon grooves, and end at the distal side of the first pulley row of the palm

[23] Diagonal pull reduces tendon lifetime drastically and has to be avoided if possible.

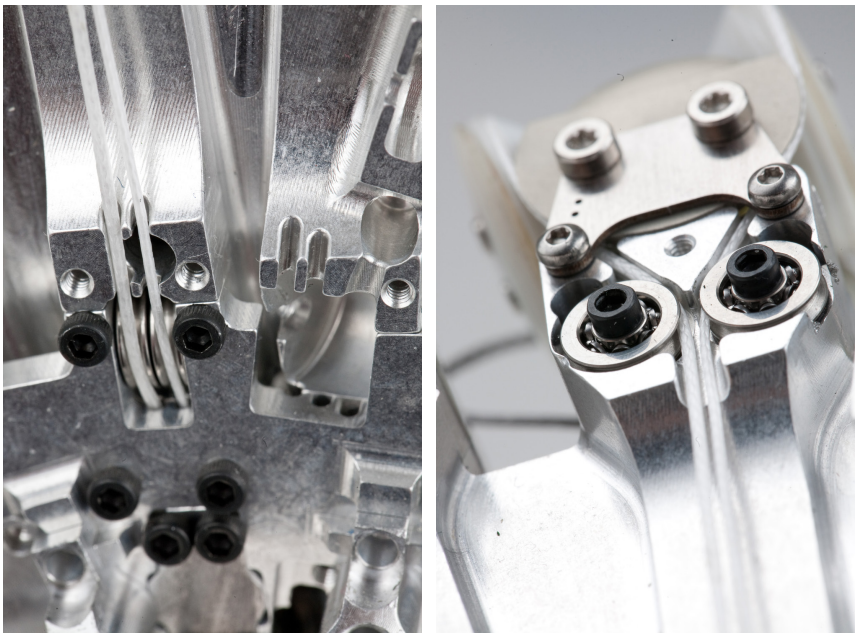

(a) (b)

Figure 4.49. Routing of MC tendons: The pulley located at the proximal end of the metacarpal bone *(a)* redirects the tendon from the wrist pulley array to the opposite side, where it is fully accessible and free running on the complete path to the MC joints pulleys *(b)*.

(see fig. 4.48). The metacarpal bones carry the base hyperboloid of the index, middle, and ring finger. The three metacarpal bones of the palmar section are built as one piece and thus, laterally connect the fingers, whereas the dorsal metacarpal bones are three separate parts. The latter enables maintenance of the PIP and DIP tendons of one single finger and significantly simplifies the assembly process. Only four tendons have to be kept in place to assemble the metacarpal bones instead of twelve.

A palmar and a dorsal plate connect the metacarpal bones to the wrist attachment points. The pulleys redirecting the MC tendons are placed in the proximal end of the metacarpal bones (see fig. 4.49b). Thus, these tendons enter the palm underneath the dorsal/palmar plate and leave the lower part of the palm right between the opposite (palmar/dorsal) plate and the “metacar-

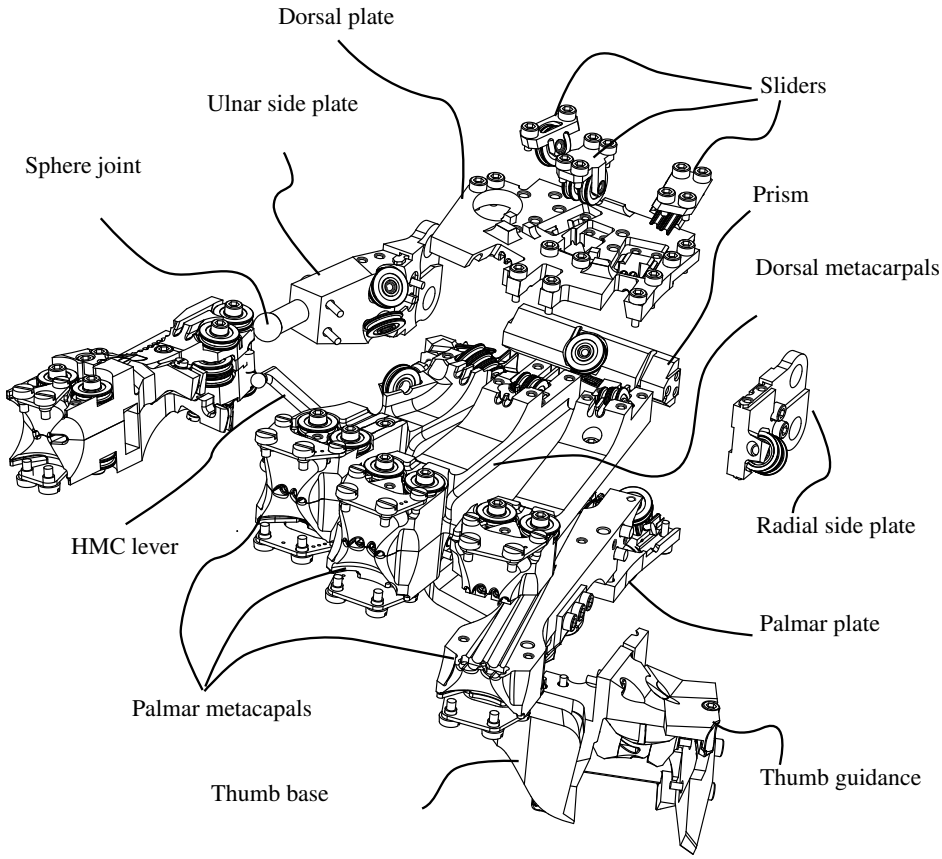

Figure 4.50. The palm assembly: The proximal finger MC hyperboloids are carried by the dorsal and the palmar metacarpal bones. The three palmar metacarpal bones are connected, whereas the dorsal metacarpal bones are separate and allow for assembly and maintenance of one single finger. The metacarpal bones are again connected to a palmar and a dorsal plate which provide grooves on the inside to guide the tendons. Sliders are implemented to carry the pulleys to redirect the tendons into the three tendon routing layers. The side plates carry the little finger HMC sphere joint as well as the thumb base. The little finger four-bar mechanism is connected to the MC joint of the ring finger laterally. The parts connecting the wrist with the palmar and dorsal plate are not shown.

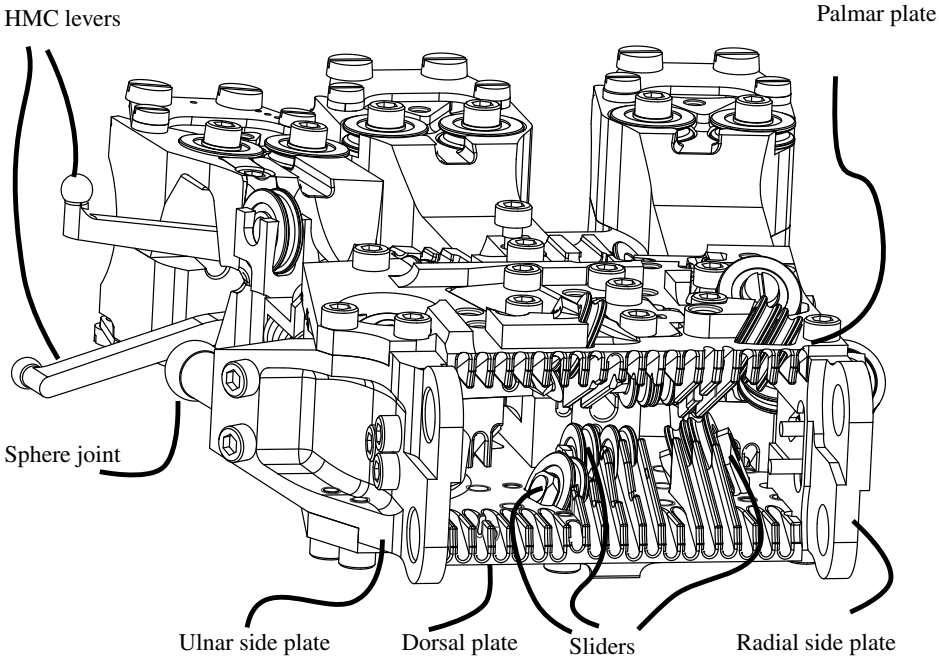

Figure 4.51. Central palm assembly with internal tendon guides. The tendons coming from the view point are guided by the palmar and dorsal plate grooves and the sliders along the whole tendon path to ease maintenance and keep the tendons in place even when slack. The dorsal and palmar plate together with the side plates form a closed cross section to carry torsional loads around the longitudinal axis of the palm. As visible in the illustration, a large amount of screws is necessary to provide sufficient force closure connections. The prism is not shown.

pal bones" (see fig. 4.49a). "Sliders" that guide the tendons in the intended direction using one or more of the ball bearing mounted pulleys mentioned beforehand are installed with the palmar and the dorsal plate.[24] These sliders fit into slots within the palmar and dorsal plate (see fig. 4.52) and enable access to the tendons for assembly, maintenance and inspection. The slots are directed in parallel to the pulley middle plane to guarantee proper alignment of pulley and tendon during insertion.

On the inside of the palmar and dorsal plate, the tendons are fully guided by grooves. This avoids that tendons jump off the pulleys in case of tendon slack, and keeps them in place during assembly, particularly for the insertion of the sliders.

The load of all tendons (>6 kN) is transferred from the hyperboloids to the metacarpal bones, to the palmar and dorsal plate, and finally to the wrist connection parts. Every part connection transfers the load by form closure as well as force closure. To withstand torsional loads between wrist and hand, the dorsal and the palmar plate are connected with the side plates (also by form and force closure) to achieve a closed cross section as seen in figure 4.51. Furthermore, these side plates carry the pulley-arrays introducing the tendons from the wrist into the hand.

The base of the little finger HMC joint (see sec. 4.7.5) is attached sideways to the ulnar side plate, whereas the thumb TMC hyperboloid is attached to the palmar plate and to the radial side plate, which will be discussed in the following.

4.7.4. Thumb Base

The tendons actuating the MP and IP joint of the thumb have to provide a maximum load of 350 N each performing power grasp. To reduce the resulting torque in the wrist, the latter are located close to the sagittal plane, whereas the thumb is placed radially. The thumb MP and IP tendons are routed inside the triangular prism shaped space inside the other tendons coming from the wrist pulley array. This avoids intersection with the grooves that guide the other tendons within the palm plates. They exit the palm side plate proximally of the thumb, at the double pulley shown in figure 4.52b. As described in section 4.6.3 the flexors of the MP and IP, as within the fingers, are double

[24] If the ideal angle of pulleys only differs single degrees, they share one axis of a slider to reduce design space.

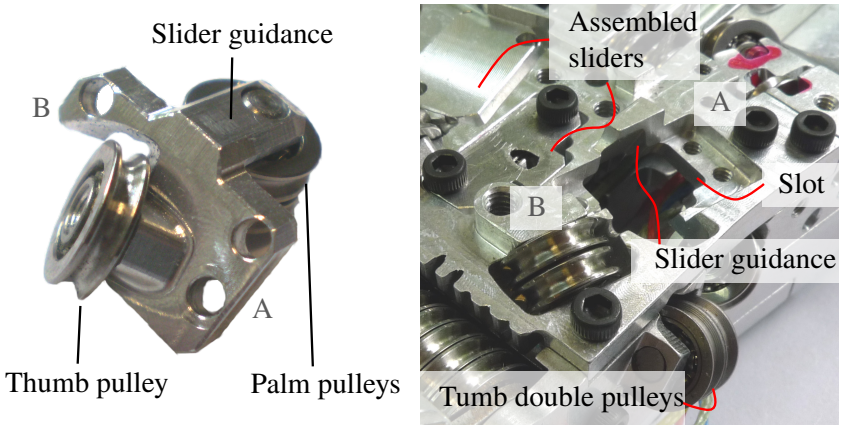

(a) (b)

Figure 4.52. Palm pulley sliders and slots: *a*, the slider carries two parallel, ball bearing mounted pulleys redirecting the PIP and DIP tendons to the middle plane of the palm and towards the index finger. The depicted slider, located on the thumb side of the palm, carries an additional pulley that redirects an abductor tendon of the thumb. *b*, the slider insertion direction into the slot is parallel to the middle planes of the pulleys, to exactly meet the tendon on insertion, and to minimize slot and slider size. The two parallel pulleys in the side plate redirect the flexor of the thumb IP and MP joint.

tendons to increase the maximum force during sideways contact. The branching of the tendon is located in between the first pulley located within the above mentioned prism and the second pulley of the flexor, as seen in figure 4.53.

The motion of the TMC tendons in the guiding points is three dimensional. Due to spacial restrictions, a ball bearing based guidance of the tendons with two bearings for each tendon is not suitable. The tendons of the TMC are routed by pulleys toward the tendon guidances. The location of these pulleys is constrained by the available design space and can be seen in figure 4.54.

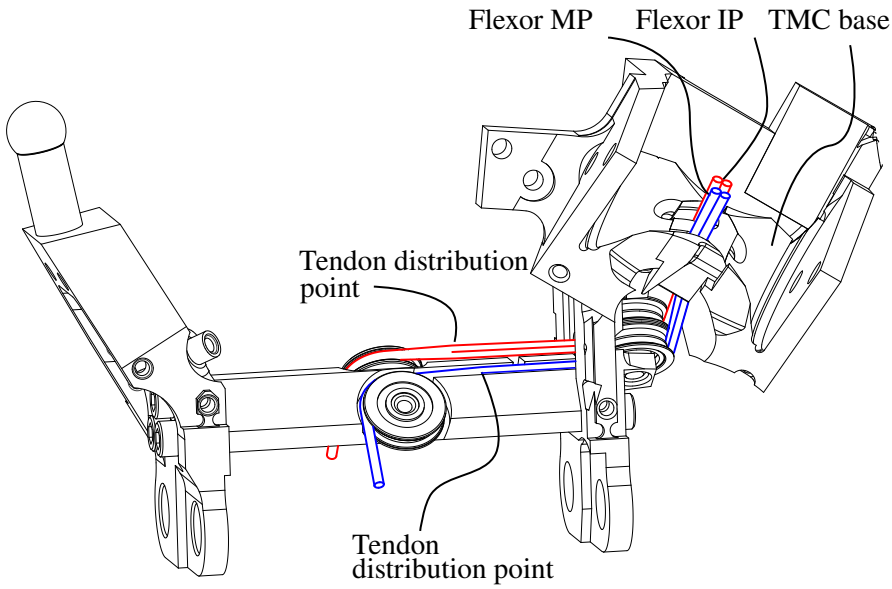

Figure 4.53. Routing of the thumb MP and IP flexor tendons. These highly loaded tendons have to be routed from the center of the palm to the thumb. To avoid intersection with the grooves guiding the finger tendons and to gain space for the proximal pulley row, the tendons are routed within the prism shaped space inside all other tendons coming from the pulley arrays of the wrist. The distribution of the tendon to the double tendon is placed between the first and the second pulley (starting from the wrist) to provide the necessary travel for the splice.

4.7.5. Little Finger Metacarpal and Hamatometacarpal Joint

As discussed in section 3.2.6, the movement of the HMC joint is crucial for proper opposition. This non-linear motion is enabled by a four-bar mechanism depicted in figure 4.55 and figure 4.51. The levers connecting the palm to the distal part of the little fingers metacarpal are connected by spherical joints on both ends, as their motion is not planar. The joint at the proximal end of the metacarpal bone, also has to be a spherical joint for the functionality of the HMC joint itself. The levers at the proximal end are analogous to the ligaments linking the little finger and ring finger MC joints. The tendons

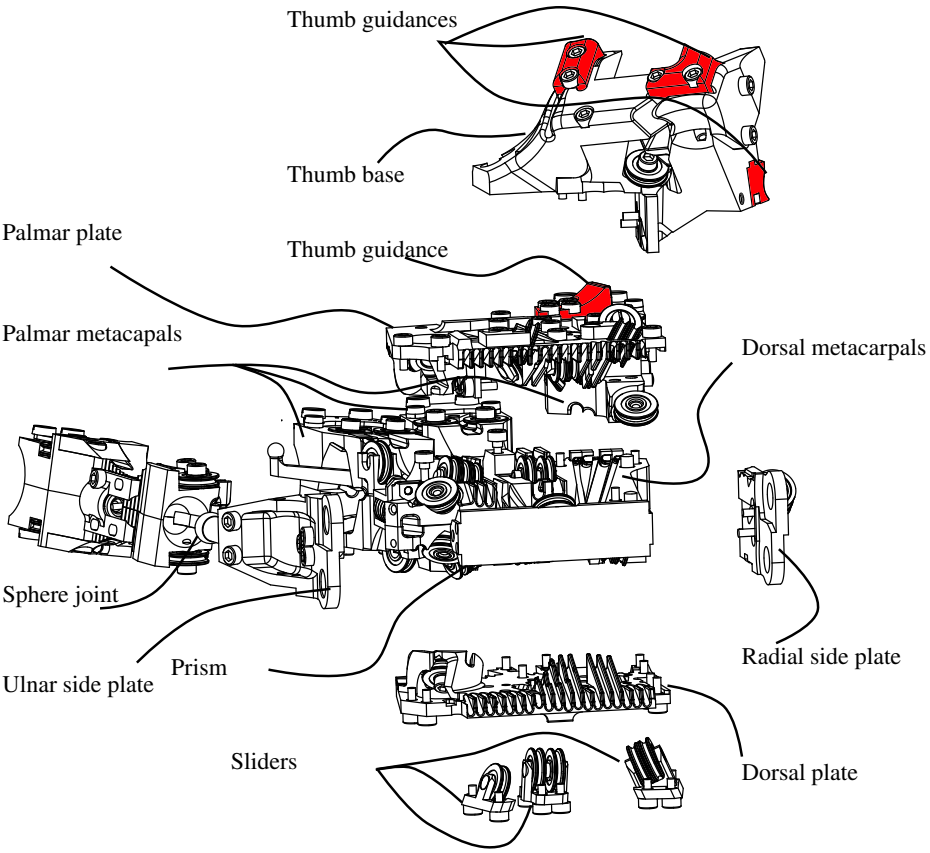

Figure 4.54. Exploded view of the palm and thumb guidances (red) in a proximal palmar view. The flexor abductor of the thumb is attached to a bridge mounted on the metacarpal bone of the index and middle finger at a rather large distance to the thumb to provide large opposition forces. The notably weaker flexor adductor, as well as the extensors are mounted on the thumb base in smaller distance.

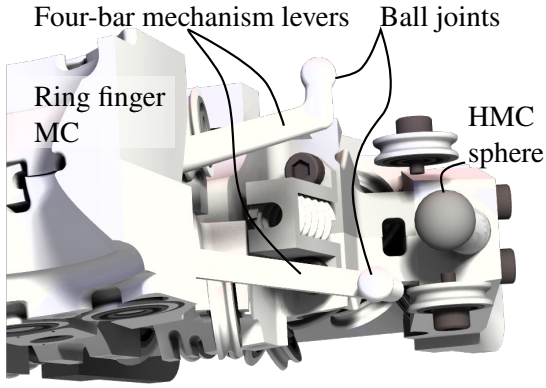

Figure 4.55. Rendering of the HMC four-bar mechanism without the little finger metacarpal bone. The mechanism consists of the two levers of unequal length and the sphere joint at the proximal end of the little finger metacarpal bone. The mechanism causes a nonlinearly coupled movement combining a translational and a rotational motion. This enables the little finger MC joint to get in front of the palm and turn toward the thumb in the last part of the trajectory.

of the PIP and DIP joint are routed to the ulnar side of the palm and enter the metacarpal as close as possible to the spherical HMC joint to reduce coupling between PIP/DIP motion and motion within the HMC joint. The tendons actuating the HMC joint are directed approximately orthogonal to the palm to enable the mostly translational motion of the little finger MC (see fig. 4.56).

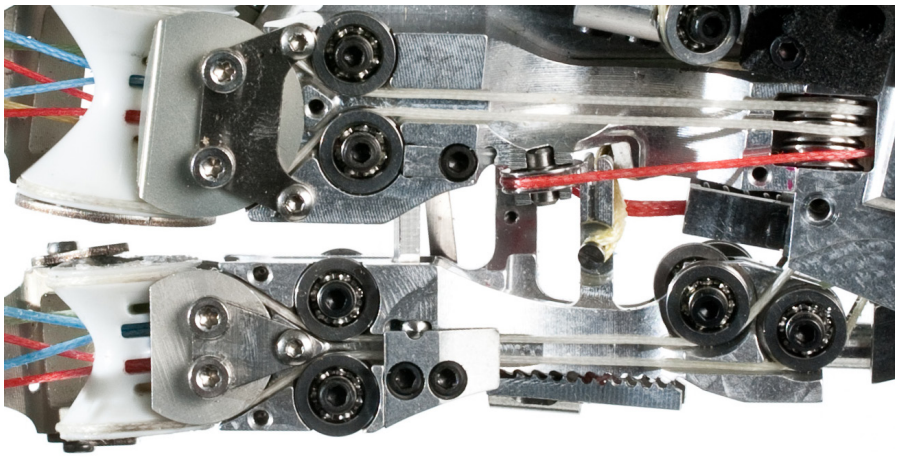

Figure 4.56. Routing of little finger and HMC tendons (frontal view). The red tendon moves the MC joint of the little finger inward and towards the thumb, whereas the yellow tendon (not correctly mounted on the picture for visualizations purpose) extends the HMC joint. As in the fingers, the tendons actuating the MC joint (white) are routed on the outside of the "metacarpal bone". The PIP tendons enter the "metacarpal bone" slightly on the left of the MC tendons.

4.8. Housings Design

The design of the housings of the hand is not a part of this work, but nevertheless, the housing concept has to fit the functional needs of the designed hand to provide the needed grasping performance. Thus, the housing concepts are outlined in the following and the final housings design is shown.

As described in section 3.2.7, the functional surfaces of the hand are of major functional importance. As with the hand design itself, it is not possible to copy the human "housings", due to the high complexity and the large gap between biological and current engineering technology. To recall from section 3.3, the housings of the hand, have to provide the following functionalities:

- Locate the object firmly by the housing geometry
- Adapt to the object shape and thus form closure by the soft skin

- High friction coefficient for a majority of surfaces
- Avoid contact of rigid and stiff parts of the hand with the object to prevent
  - Damaging the object
  - Insecure grasp due to low friction and lacking shape adaption to the object surface

The design of "good" housings is an iterative process, since the performance of the housings, as in the case of *DLR Hand II*, often largely differs from the expected results. Indeed, the calculated contact mechanics of the fingers, the palm, and the object use several parameters that are objective to large uncertainties, such as friction coefficients,[25] deformation of the soft parts of the housings, and thus, adaption to the object. Consequently, the housings of the hand have to be easy to modify and change, as well as cheap and fast for production.

Two concepts have been investigated:

- Gloves
- Rigid housings with soft surface

The gloves concept as seen in figure 4.57, is similar to the housings of *Robonaut R2* [Diftler et al. 2011] and provides fully closed housings consisting of a skin and underlying soft and thick pads that are connected to the structure of the hand. The gloves have to be rather flexible or foldable in the joint regions and firmly connected to the pads in the grasping regions. The glove concept has not yet been realized, since the design of the skin covering the joints, having a rather large range of motion of up to 145° and being dislocatable, is a big challenge. On one hand, the forces needed to stretch the elastic parts of the glove have to be low, but the glove still has to be robust. On the other hand, pinching of the skin has to be avoided, in particular at joint limits and after (partial) dislocation of the joint.

Consequently, a concept similar to the housings of several hands, such as the *Twendy One Hand* (sec. 2.1.7), *UB Hand 3* (sec. 2.1.5), *Robonaut Hand* (sec. 2.1.2), and *DLR Hand II* (sec. 2.1.6) has been chosen. Every segment of the fingers, the thumb and the palm, has a separate housing, see figure 4.58.

[25] For example, a can previously grasped by a human can have largely reduced friction coefficients because of greasy fingers.

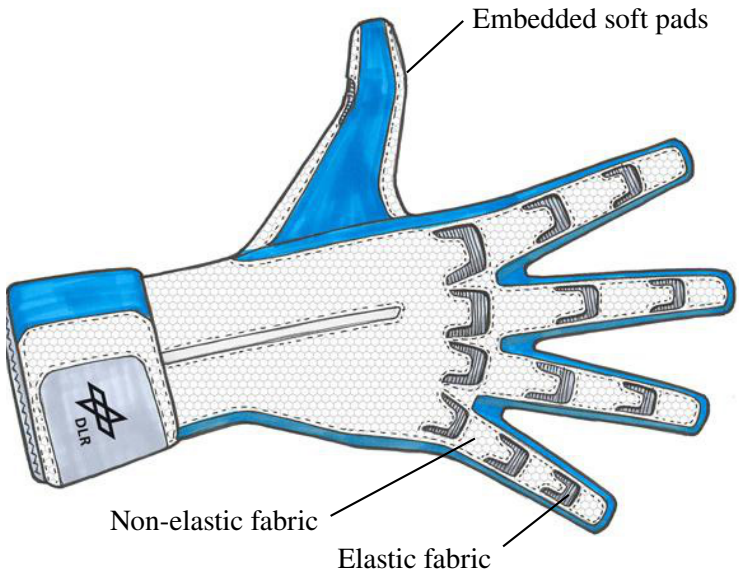

Figure 4.57. Glove concept sketch. The gloves consist of an outer skin with highly elastic or foldable tissue in the joint regions, and stronger tissue, firmly connected to the underlying thick elastic pads. The elastic pads distribute the force uniformly, adapt to the object surface and transfer the external load to the hand structure.

The housings of the hand consist of, partly multiple, rigid inner parts that prevent contact of the tendons with the soft housings if external forces are applied and transfer the stress to the structure. A soft and thick outer part, made from polyurethane, ensures good contact of the hand and the objects, and distributes stress uniformly, see figure 4.59.[26] The housings are not intended to cover the joints. As a result, they have to be shaped such that the majority of objects does not get into contact with the joints, and in particular with the tendons.

The transition between the palm and the thumb TMC joint, similar to the human ball of the thumb has to be soft to enable full contact of the thumb

[26]The distal housing of the fingers and the thumb do not have a ridged inner part, since the tendons do not move in this segment.

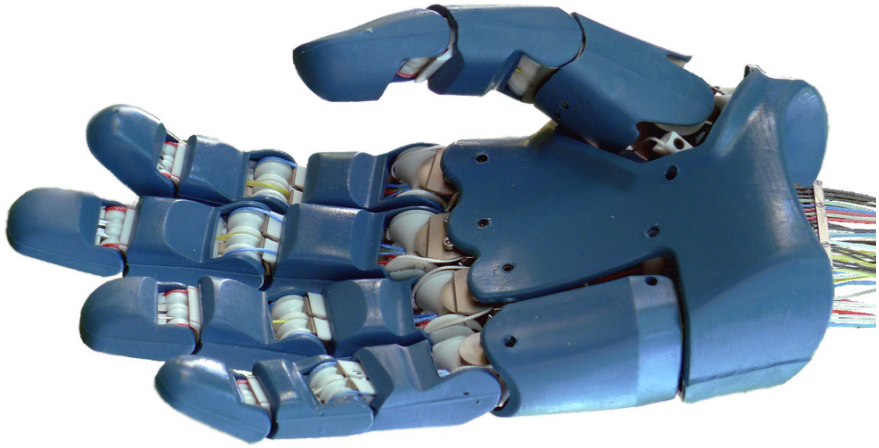

Figure 4.58. Hand with housings, consisting of rigid parts transferring the stress to the structure, and a thick soft polyurethane skin. The housings do not cover the joints themselves. The transition between palm and thumb is fully flexible to improve power grasp performance.

when executing power grasp, rather than with the transition surface from the palm to the thumb. The latter would result in forces to the object directed out of the palm (e.g. for large cylindrical objects), and thus, in an insecure grasp.

4.9. Summary

In this chapter, the design of the hand has been presented. The actuation concept has been selected and its feasibility along with a first validation of the control concept has been proven.

A hand kinematics design method to achieve an appropriate kinematics, providing the needed functionalities of the hand, has been proposed. It uses fast and easy to build prototypes and a practical, easy to perform and effective set of tests, derived from surgery validation procedures and daily grasping. It

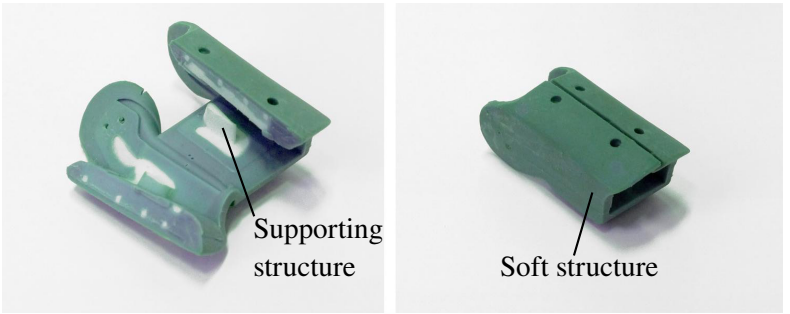

Figure 4.59. Final housings of the hand (housing of the proximal phalanx). The housings consist of rigid structural parts (white) that transfer load to the skeletal structure and protect the tendons from getting in contact with the soft outer shell. The outer shell (blue) is produced from thick and soft polyurethane to distribute stress uniformly and adapt to the grasped object surface providing optimal tangential force transmission. Since the screws would impair the grasping performance, the housings are wrapped around the finger and screwed to the phalanges from the back of the finger.

allows for a true synergy between hand design and kinematics design. This method has been applied to the *Awiwi Hand* to obtain a 19-DoF hand kinematics, meeting the requirements of the hand given in section 1.4.

Based on the kinematics design, a short estimation of the expected friction has been presented and measures to reduce friction within the design process have been derived.

The design of the fingers, using dislocatable anthropomorphic joints and an endoskeleton structure, has been presented. The thumb is actuated by four tendons that are routed similar to the human ones and attached to the metacarpal bone. They provide asymmetric force exertion, to take into account the different functionalities of the hand.

The design of an anthropomorphic palm that is able to provide the functionality of arching the functional surfaces of the palm, as well as bringing the little finger into proper opposition to the thumb, has been presented. The palm routes the tendons from the wrist to the fingers with close to minimal friction losses.

Finally, two housing concepts and the final housings, consisting of a rigid

inner structure and thick and soft polyurethane covering tissue, have been described.

The design of the *Awiwi Hand* is the main contribution of this work. To demonstrate its performance with respect to the goals defined in section 1.4, experimental validation results are presented in the next chapter.

5 Results

The previous chapter described in detail the embodiment of the *Awiwi Hand*. Experimental results that prove the performance of the hand with respect to the goals set in section 1.4 are presented in the following chapter. In the first part, the characteristics of the hand is evaluated with focus on the robustness and the fast dynamics. The second part gives an evaluation of the grasping performance. The medical tests used to help design the kinematics are performed as a first test of the *Awiwi Hand*. Subsequently, the grasping performance is evaluated by performing grasps of objects based on the grasp taxonomies presented by *M. Cutkosky* [Cutkosky 1989] and by *T. Feix* [Feix 2010] to enable a system of comparison with other hands that performed these , as for example the *Robonaut Hands* [Diftler et al. 2011]. Finally, the robustness of power grasps against disturbances is evaluated through impacts tests on grasped objects.

A complete left and right hand have been built. A right hand (fig. 5.1) is assembled to the robot and in full operation. Some key data of the hand are given in table 5.1. Example elastic element characteristics are shown in figure 4.8. As an early proof of concept, an index finger prototype using steel cables and the final index finger design, using Dyneema tendons, have both been tested on the finger testbed (see fig 5.4 and Appendix B.1).

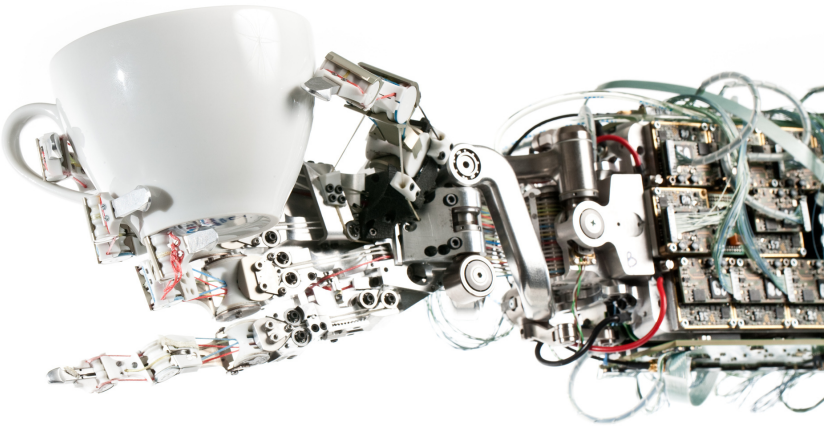

Figure 5.1. The *Awiwi Hand* without housings.

5.1. Actuation Concept

The first set of experiments aims at the validation of the chosen actuation and its properties regarding two of the goals defined in section 1.4, which are, robustness and fast dynamics. The tests have been performed on the finger testbed as well as on the *DLR Hand Arm System* to take into account the properties of the differing drive trains.

5.1.1. Robustness Due to Mechanical Compliance

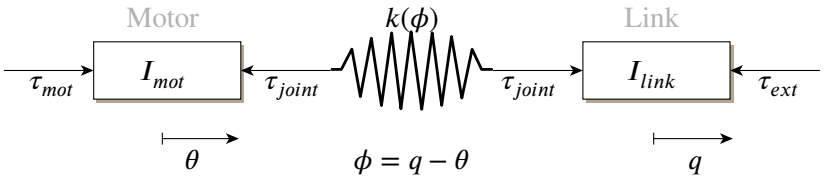

Figure 5.2. 1 DoF variable stiffness joint model. All coordinates are generalized joint coordinates.

Robustness has motivated this work as it is believed to be the key to the successful completion of tasks in unknown or unstructured environments. A simple task performed to demonstrate the robustness of the hand as well as the fast dynamics of the *DLR Hand Arm System*, is to hammer a nail into wood. The impact of the hammer on the nail introduces large impact forces into the robot hand and would easily damage e.g. the *DLR Hand II*, since the drives of the hand would not be able to follow the finger deflection fast enough. The image sequence (25 frames/s) shown in figure 5.3 clearly shows the large relative motion between the hammer and in particular the little finger of the *Awiwi Hand* during the impact. The resulting deflections are enabled by the energy storage capabilities and hence the decoupling of the link and the drives.

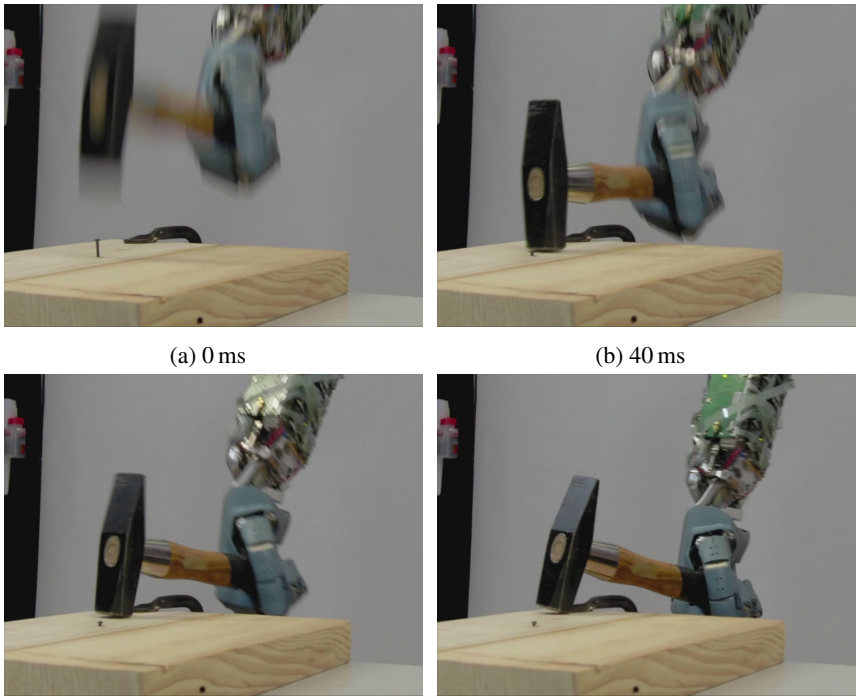

(a) 0 ms (b) 40 ms

(c) 80 ms (d) 120 ms

Figure 5.3. Image sequence of the *DLR Hand Arm System* hammering a nail into a piece of wood (spruce).

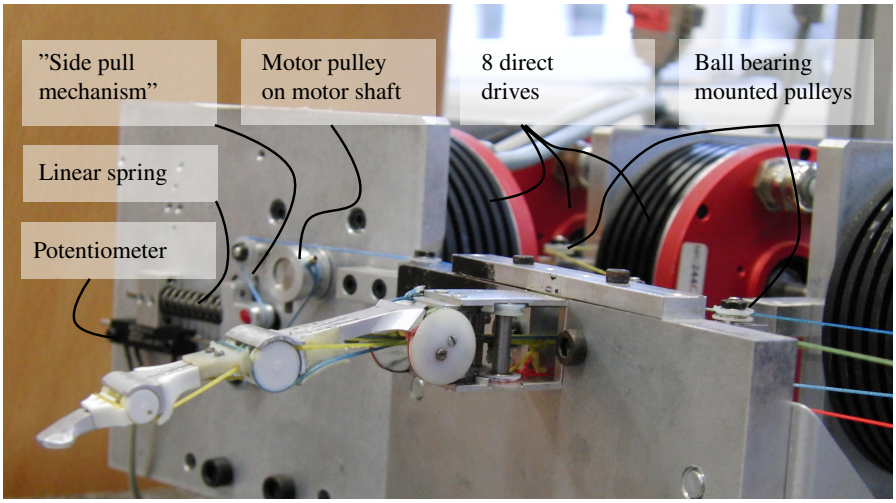

Figure 5.4. The antagonistic finger testbed. The finger is driven by eight direct drive motors to reduce the influence of gears in terms of friction, backlash etc. One of the eight elastic element mechanisms is seen in the background. As in the forearm, they are from the “tendon side-pull mechanism” type.

Robustness Against Impact on Finger Testbed Since the hammering demonstration has been performed without any measurement, experiments performed on the finger testbed are described in the following for more quantitative analysis. All given angles and velocities are generalized angles calculated with respect to the joint. The symbols used in the following are illustrated in figure 5.2.

The finger testbed (fig. 5.4) consists of eight direct drive motors that drive the fingers. The direct drives are chosen to reduce parameters within the drive train that are difficult to model. Thus, the characteristics of the fingers can be analyzed more accurately. The tendons of the finger are connected to winders directly attached to the motors. “Tendon side-pull mechanisms” as within the fingers are used as non-linear elastic elements. Both, the motor position as well as the absolute elastic element deflection, are measured by absolute sensors. The spring characteristics are similar to the ones used in the forearm. Further information about the testbed is given in Appendix B.

To evaluate the robustness of the final finger design on the testbed, the

tendon pretensions were set to a minimum (≈10 N tendon force).[1] The direct drive motors were controlled in position mode and the finger was impacted by a cylindrical bar at a speed of approximately 3.8 m/s. Still frames of the impact test have been captured by a high speed camera (see fig. 5.5).

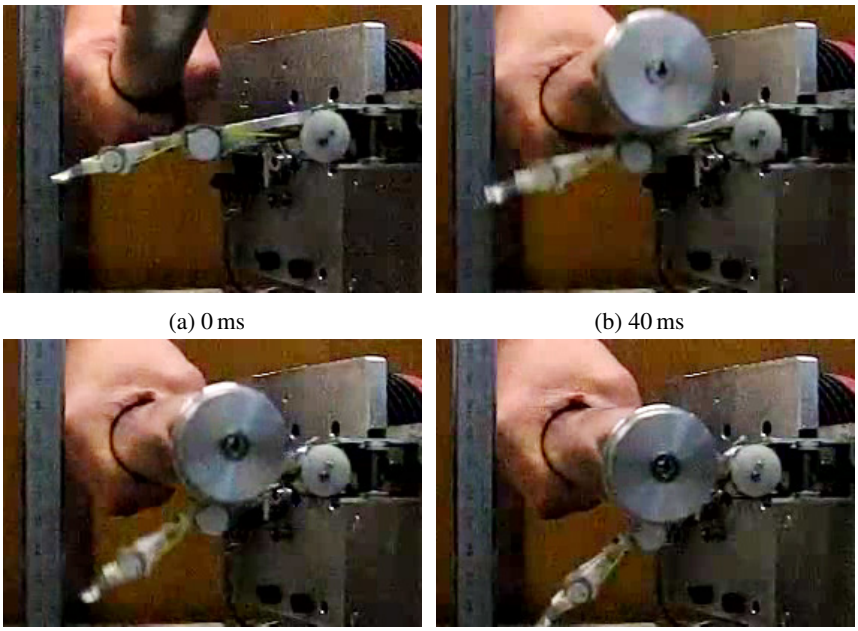

(a) 0 ms (b) 40 ms

(c) 50 ms (d) 60 ms

Figure 5.5. High speed pictures of a fast collision. The finger is hit with a 788 g aluminum cylinder at a speed of ≈3.8 m/s without any damage.

The finger withstood the collision without damages of the structure, the joints, or the tendons. As expected, the energy of the impact was shortly stored in the springs and restored on a longer time span, thus reducing the structural loads (fig. 5.6).

The elastic elements stored the impact energy at short-term, reducing the required motor speed to 490 °/s (fig. 5.7b). In contrast, the joint speed reached a value of approximately 2950 °/s as estimated from the elastic elements de-

[1] The minimum pretension is selected to prevent tendon dislocation at the pulleys.

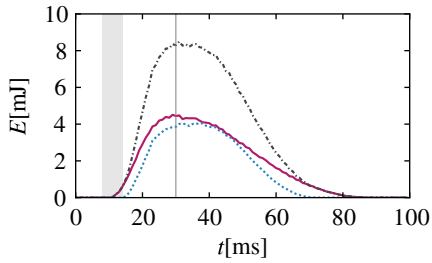

Figure 5.6. Testbed results: The impact force is stored as potential energy within the elastic elements of the two springs of the MC extensor joint during impact (·-·-·). They decouple the link side and the drive side. Thus, the maximum force on the drive side is reduced significantly. The stored energy in each of the two elastic elements of the MC flexors are shown as (—) and (·····), respectively. It can clearly seen that the finger is not hit completely frontally.

flection (fig. 5.7d).

The acceleration phase of the motors[2] during the impact is extended from 6 ms at the elastic elements (fig. 5.7c) to 22 ms at the motors (fig. 5.7a). The drives of the hand would not be able to follow the displacement imposed by the impact without the elastic elements due to their limited maximum velocity of 640 °/s (MC joint). This would severely damage the structure, tendons or gearbox.

Robustness Using Hand and Forearm In addition to the testbed experiments, the robustness of the *Awiwi Hand* against impacts has been investigated using the *Awiwi Hand* assembled to the *DLR Hand Arm System* forearm, since the forearm actuation differs from the testbed in particular in terms of backdriveability and the elastic element properties.[3] A hammer (500 g) hits the finger at the DIP joint of the index finger as seen in figure 5.8 with the complete forearm rigidly anchored. Figure 5.9 shows the resulting torques

[2] The forces caused by acceleration of the drive train are the limiting factor during impact neglecting drive efficiency.

[3] As described in 4.2.4 the stiffness characteristics of every elastic element is adapted to specific joint requirements.

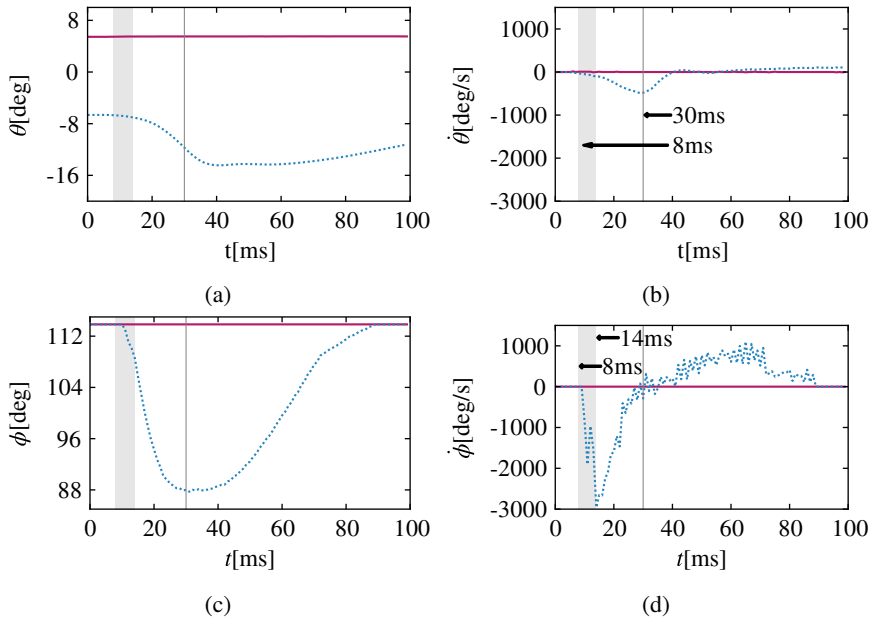

Figure 5.7. Impact of a 788 g alloy cylinder (see fig 5.5). Positions *(left)* and velocities *(right)* of *motor (top)* and *link (bottom)*. The MC joint accelerates to a maximum velocity of approximately 3000 °/s within the first 6 ms, whereas the motor accelerates to only ≈490 °/s within 22 ms. The motor would not be able to follow the (6 times faster) link. Consequently, the drive train or structure would be damaged by the impact. The elastic element increases the acceleration phase by a factor of more than 2.5. All positions and velocities are calculated as the average of both flexor (——) / extensor (·····) motors / elastic elements and transformed to MC joint speed.

and joint velocities. All motors are in position control mode. In comparison to the finger testbed (see sec. 5.1.1), the spring energy is distributed more evenly because the characteristics of the flexible antagonistic spring element (FAS) described by *Friedl* [Friedl et al. 2011a] were designed specifically for the corresponding finger. Moreover, the inertia of the elastic element mechanism is reduced to less than 50% compared to the testbed [Grebenstein et al.

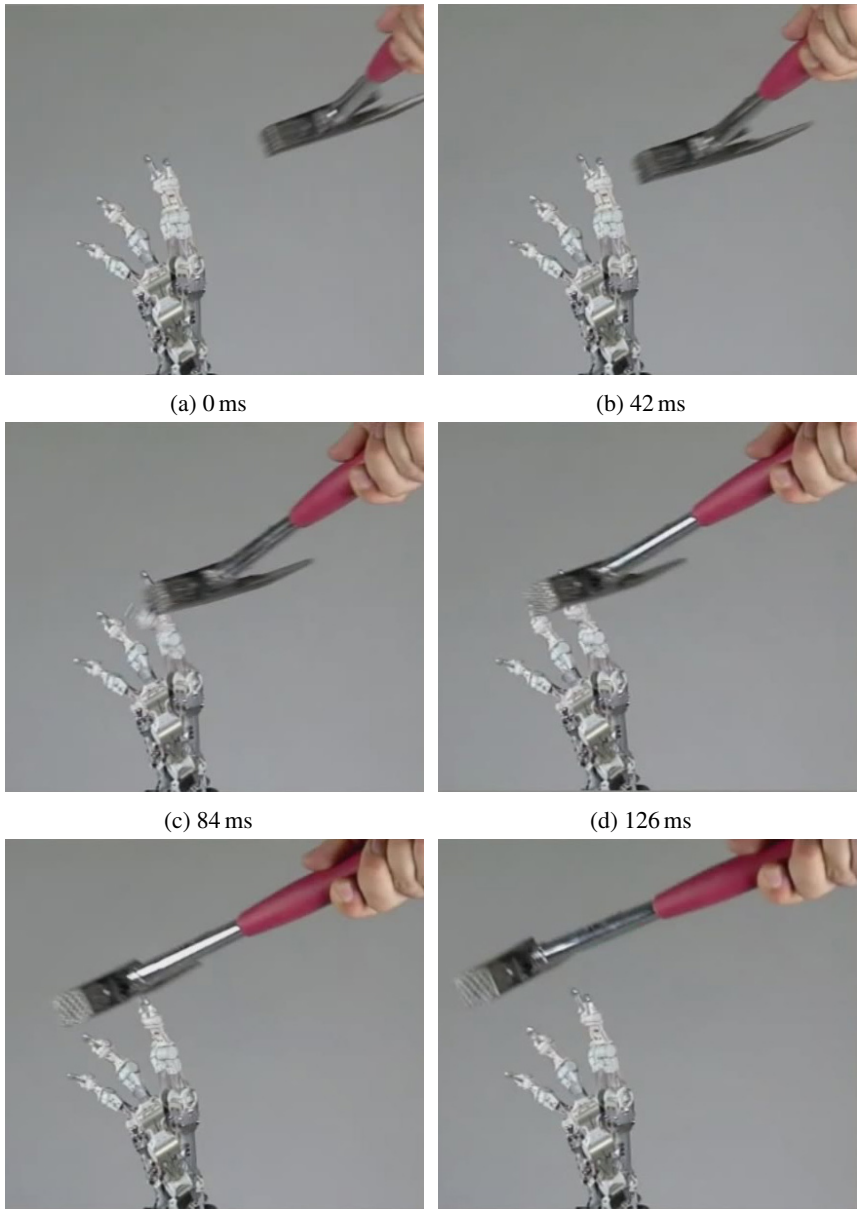

(a) 0 ms (b) 42 ms

(c) 84 ms (d) 126 ms

(e) 168 ms (f) 210 ms

Figure 5.8. High speed images of a hammer hitting the index finger of the hand. The hand is in position control mode and withstands the impact without any damage (even without housings). The fingertip motion in *(c)* is even too fast for the high speed camera (frame rate 600 frames/s).

2011]. The maximum DIP joint speed is reached within less than 2 ms. Due to the larger inertia with respect to the MC joint axis, the MC joint reaches maximum speed after 5 ms. The resulting acceleration reaches from $0.85 * 10^6 °/s^2$ at the MC joint to $1.19 * 10^6 °/s^2$ in generalized joint coordinates.

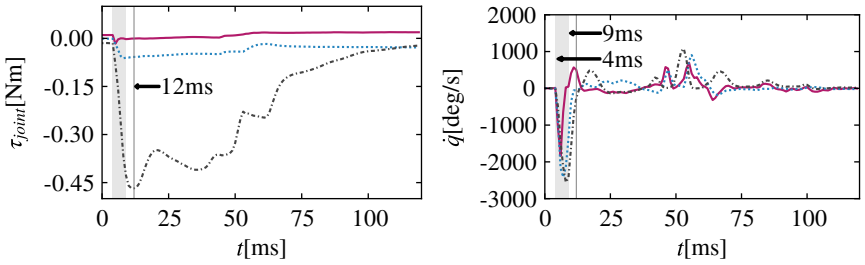

Figure 5.9. Hammer impact: *a*, resulting joint torques and *b*, velocities of MC (·-·-·), PIP (·····) and DIP (——) joint after a hammer hits the distal phalanx of the index finger. The amplitudes after the impact result from the coupling between wrist and fingers. The maximum velocity is more than 4 times the maximum joint speed (MC joint). Consequently, the impact would severely damage the hand without energy storage.

Table 5.1. Key data of the *Awiwi Hand*. The given fingertip forces are the forces used as maximum desired forces to design the elastic element characteristics, not the (partly much higher) maximum values. Since the forearm provides actuators of two sizes for all fingers, all finger joints besides the middle finger PIP and the thumb MP can reach significantly higher forces. (★: coupled DoF; all values rounded down).

Parameter	Finger		
	Index / Middle / Ring	Thumb	Little
Max. joint speed [° / s]			
DIP/IP	1400	1330	1500
PIP/MP	990	780	1170
MC/TMC	640	640	850
Max fingertip force [N]			
	30/30/21	40	15
Range of motion [°]			
DIP/IP	[-30,110]	[-30,80]	[-30,110]
PIP/MP	[-10,135]	[0,80]	[-10,135]
MC/TMC ext/flex	[-30,90]	[-30,30]	[-30,90]
MC/TMC abd/add	[-30,30]	[-46.5,46.5]	[-30,30]
Energy storage capabilities (flexion, extension) [m J]			
DIP/IP	(153,87) / (153,87) /★	(153,87)	★
PIP/MP	(153,87) / (153,153) / (153,87)	(153,87)	(87,48)
MC/TMC	(174,174) / (174,174) / (97,97)	(154,154)	(174,97)
Joint stiffness range [Nm/rad]			
DIP/IP	[1.1,2.5] / [1.3,4.2] /★	[1.5,5.6]	★
PIP/MP	[3.4,12] / [1.2,10.3] / [1.2,15.0]	[2.6,11.0]	[0.8,7.0]
MC/TMC	[3.5,27] / [3.5,21.5] / [2.5,19.9]	[2.9,30.2]	[2.1,11]

5.1.2. Fast Dynamics Using Stored Energy

The energy stored in the elastic elements of the drive train of the *Awiwi Hand* can be converted to kinetic energy and thus enhance the dynamics of the fingers significantly. The following experiments evaluate the the fast dynamics of the hand.

Testbed Results Using the setup from 5.1.1 the dynamic properties of the final design have been evaluated measuring the maximum speed generated by the energy stored within the elastic elements. Starting with a 17° deflection (from zero position) at the MC joint the finger is released while the position controllers keep the MC joint motors at zero position. High speed pictures and measured data are used to evaluate finger joint speed (fig. 5.10). The finger reached a maximum angular speed of 1680 °/s in the MC joint without active joint actuation. The slight change of the motor position is caused by the controller steady-state error under load. The motor velocity does not exceed 64 °/s. Considering that the active maximum speed of the motors is 640 °/s, the joint speed could be increased even further, see figure 5.10 [Grebenstein et al. 2010b].

Results of Hand and Forearm Due to the reduced inertia of the final forearm elastic elements in comparison to the testbed version, the maximum velocity of the finger is approximately doubled with respect to the testbed results during a snapping motion. The experiment consists of deflecting the finger using an external load (similar to how humans snap their fingers, see fig. 5.13), then increasing the pretension forces and finally releasing the finger. The maximum velocity is achieved when the antagonist tendon is allowed to be slack.[4] The maximum link speed was measured to be more than 3500 °/s after releasing the finger (fig. 5.12) [Friedl et al. 2011a].

[4] Since the characteristics of the FAS is highly progressive, the co-contraction / energy transfer effects e.g. described by Hurst and Rizzi [Hurst and Rizzi 2008] do not fall into account for the drives of the hand, even if the tendons are not allowed to run slack.

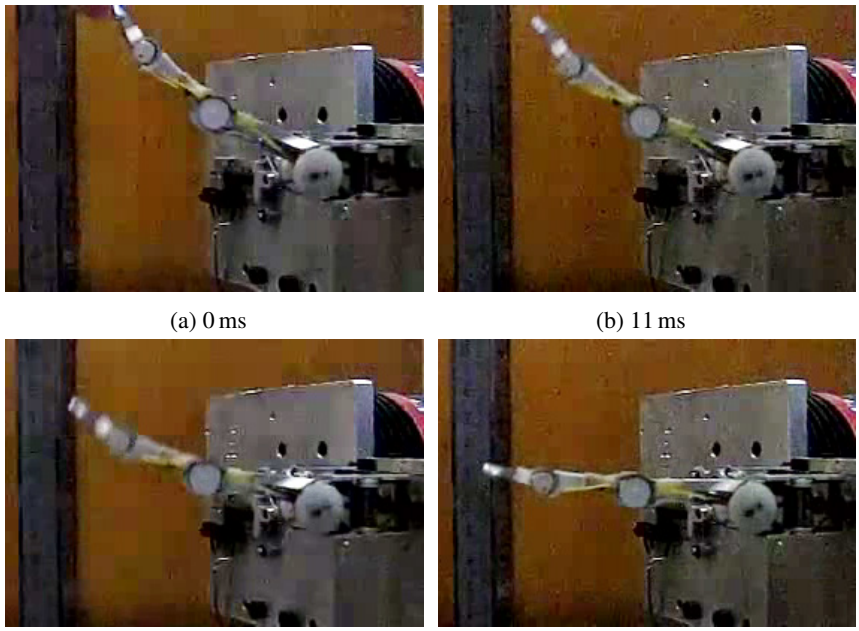

(a) 0 ms (b) 11 ms

(c) 20 ms (d) 31 ms

Figure 5.10. High speed pictures of finger during snapping. The finger is released from a position of 17° deflection within the MC joint. The potential energy stored in the spring is transformed to kinetic energy after release.

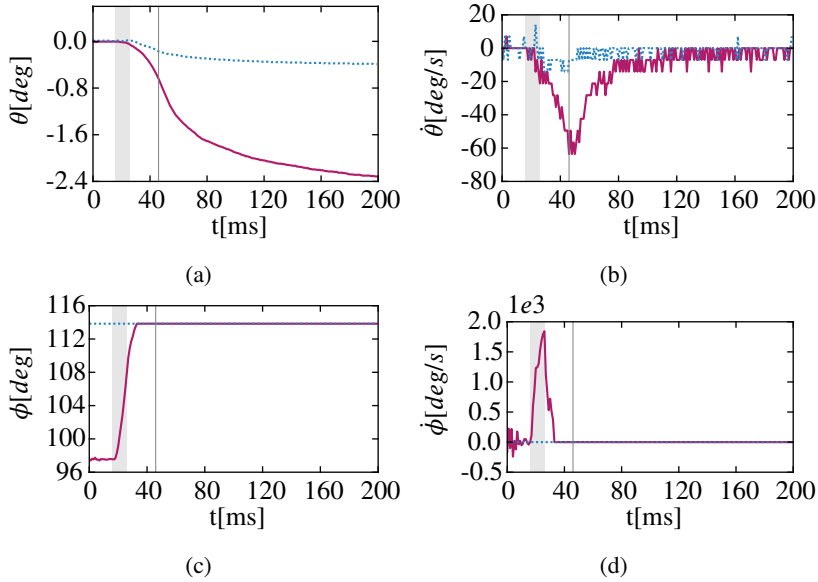

Figure 5.11. Positions and velocities of *motor (top)* and *elastic elements (bottom)* during finger snapping (see fig. 5.10) on the finger testbed. All angles and positions transformed to MC joint coordinates. The extensor (·····) motor moves in order to compensate the regained tendon pretension of the flexor (——) after release. This motion reduces the joint speed.

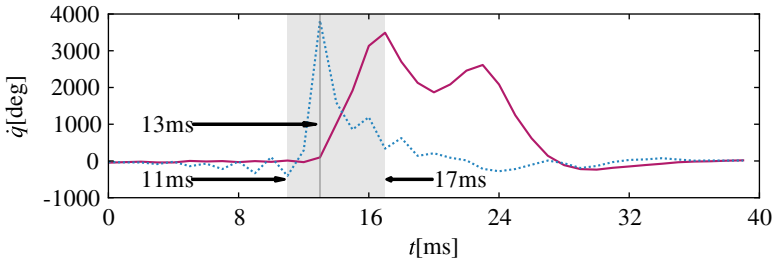

Figure 5.12. Velocity of the index MC (——) and PIP (·····) during the snapping of the finger using the forearm. The maximum speed of the finger joints reaches more than 5 times the maximum speed the drive could generate. The PIP accelerates to maximum speed in 2 ms, whereas the MC joint needs 6 ms to reach its maximum speed due to the higher inertia.

(a) (b)

Figure 5.13. Human snapping fingers: *a*, preloading tendons and muscles; *b*, target position

5.2. Grasping Abilities

Grasping performance is the most important feature of a robot hand. To verify this third goal defined in section 1.4 several tests are performed and reported in the following.

5.2.1. Kinematics Evaluation

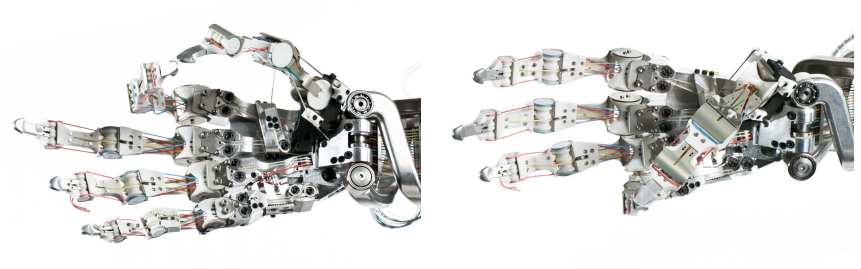

(a) (b)

Figure 5.14. The *Awiwi Hand* performing the Kapandji test; *a*, Kapandji test index finger *b*, Kapandji test little finger

A final verification test for the chosen kinematics was to perform the Kapandji tests (fig. 5.14). The different tests are usually used to evaluate the kinematic capabilities of a human hand before and after surgery or rehabilitation. The kinematics of the hand was designed along those guidelines, and the verification test showed that the hand was able to perform all assigned tests successfully.

5.2.2. Grasping Tests

In order to evaluate the versatility of the hand regarding grasps, the full set of the taxonomy grasps described by *Cutkosky* has been performed [Cutkosky 1989]. This enables comparison with existing hands that performed the taxonomy of grasps, as with NASA's *Robonaut I and II* hands [Diftler et al. 2011]. The exact geometry of the grasped objects is not defined by *Cutkosky*. Consequently, the results achieved by hands have to be interpreted with care. The hand could perform 100% of the taxonomy grasps (see fig. 5.16).

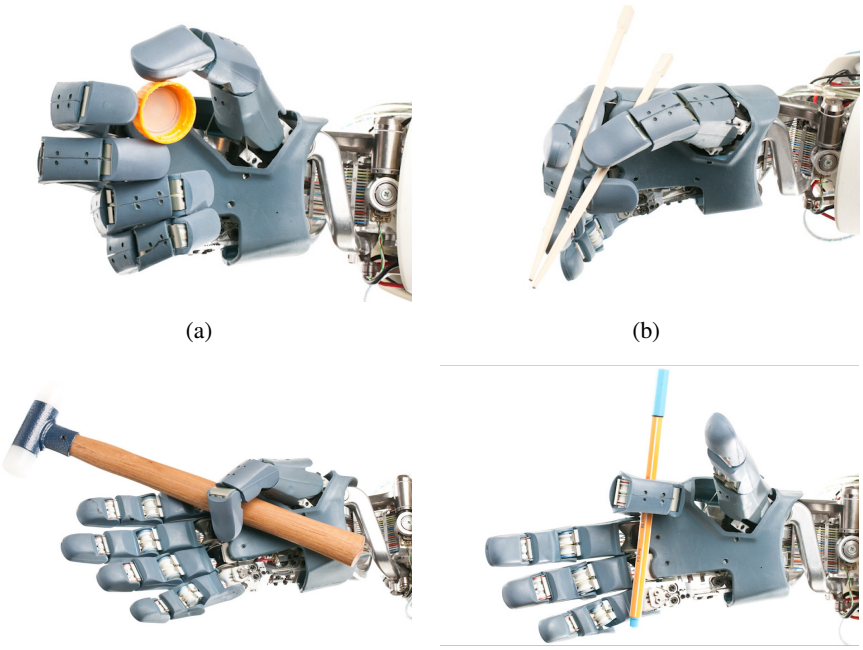

(a) (b)

(c) (d)

Figure 5.15. Grasp of different objects: *(a)* and *(b)* are part of the *Feix* taxonomy, *(c)* and *(d)* are covered by none of the taxonomies but illustrate the range of motion of the *Awiwi Hand*. *a*, grasping a cap; *b*, grasping chopsticks; *c*, fixing an object using only the thumb; *d* fixing an object using only the index finger

Furthermore, grasps of the, more detailed and complete, but less common taxonomy of *T. Feix* [Feix et al. 2009; Feix 2010] have been performed to evaluate the grasping performance of the hand. The *Feix* taxonomy grasps performed by the *Awiwi Hand*, as well as full size pictures of all taxonomy grasps can be found in Appendix A. In figure 5.15 example poses and grasps are given.

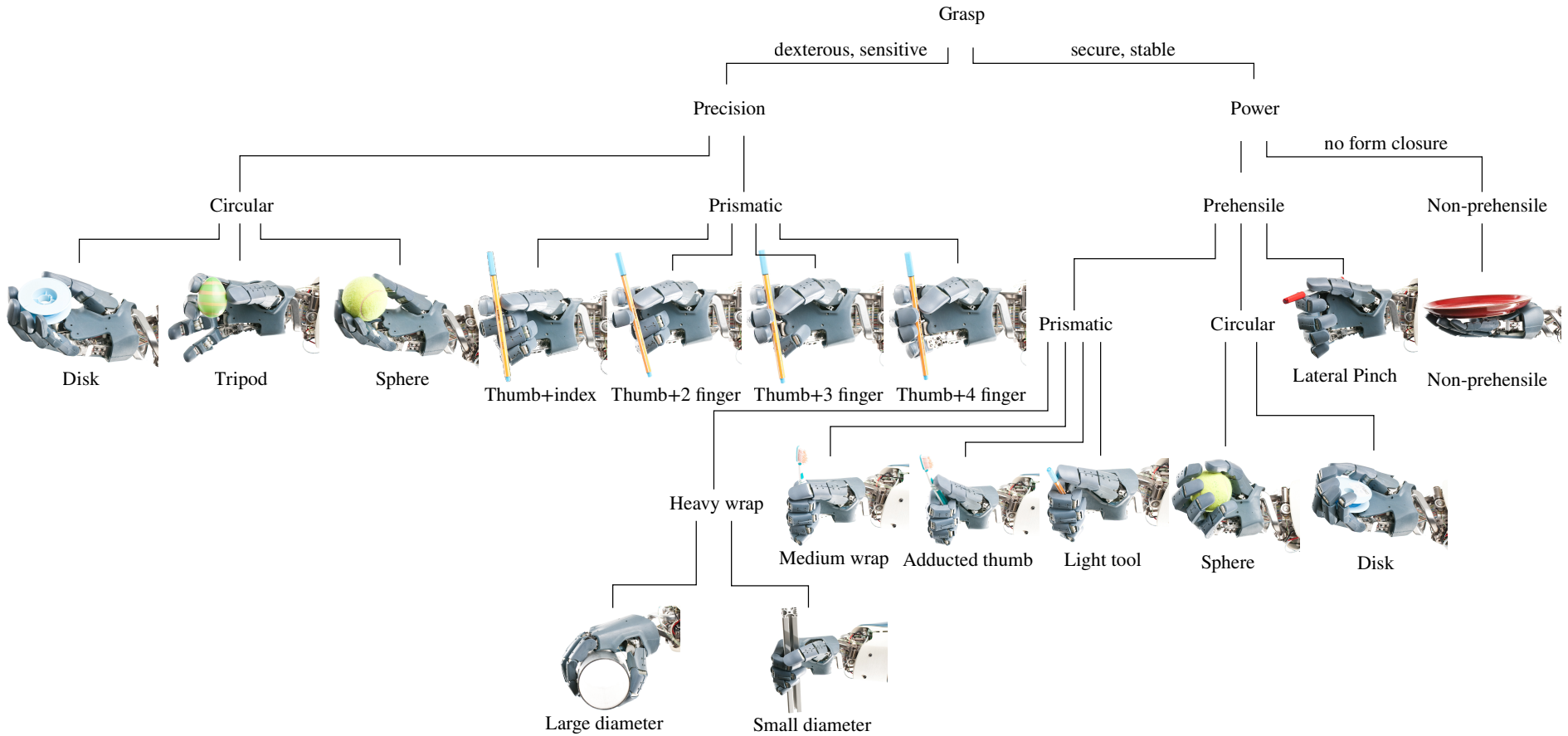
Grasp
dexterous, sensitive
secure, stable
Precision
Power
no form closure
Circular
Prismatic
Prehensile
Non-prehensile
Disk
Tripod
Sphere
Thumb+index
Thumb+2 finger
Thumb+3 finger
Thumb+4 finger
Prismatic
Circular
Lateral Pinch
Non-prehensile
Heavy wrap
Medium wrap
Adducted thumb
Light tool
Sphere
Disk
Large diameter
Small diameter

Figure 5.16. (*Previous page*) *Cutkosky's* taxonomy grasps performed by the *Awiwi Hand* [Cutkosky 1989]. The hand could perform 100% of the taxonomy grasps which, to the authors knowledge, no robot hand reached before. Please find the full size pictures as well as the enhanced taxonomy presented by *Feix* performed by the *Awiwi Hand* in Appendix A [Feix et al. 2009].

5.2.3. Robustness of Power Grasps Against Disturbances

The *DLR Hand Arm System* is intended to interact with or act in unknown and unstructured environments, and therefore has to be able to complete tasks even after collision. This implies that the *Awiwi Hand* has to be able to keep objects grasped firmly, regardless whether the robot or the grasped object collides with the environment.
To evaluate the robustness of grasps against collisions, a rectangular object of 40×40 mm cross section has been grasped with a taught grasp. The grasped object then has been hit such that the impact force is approximately pointing in parallel to the angle bisector of the fingers and the thumb. The impact has been performed from the back of the hand (backhand in the following) as well as from the front (forehand in the following). The impacting object is fixed on a pair of ropes fixed to the ceiling and swings on a circular trajectory. It is released from a height of 82 cm from the lowest point of the trajectory. Using this setup the hand never loses the object. The speed of the hitting alloy impactor of 750 g mass[5] is calculated from the potential energy of the pendulum $E = mgh = \left(0.75\,\mathrm{kg}\,9.81\,\mathrm{m/s^2}\,0.82\,\mathrm{m}\right) \approx 6.03\,\mathrm{J}$ at the release height of 82 cm. This potential energy is completely converted into kinetic energy in the lowest point of the trajectory. Thus, the velocity of the pendulum is

$$v = \sqrt{\frac{2E}{m}} = \sqrt{\frac{2 * 6.03\,\mathrm{J}}{0.75\,\mathrm{kg}}} \approx 4\,\mathrm{m/s}. \tag{5.1}$$

High speed pictures of the impact from the back can be seen in figure 5.17. Within the experiment the tendon forces and the tendon displacements have

[5]The velocity is mass independent

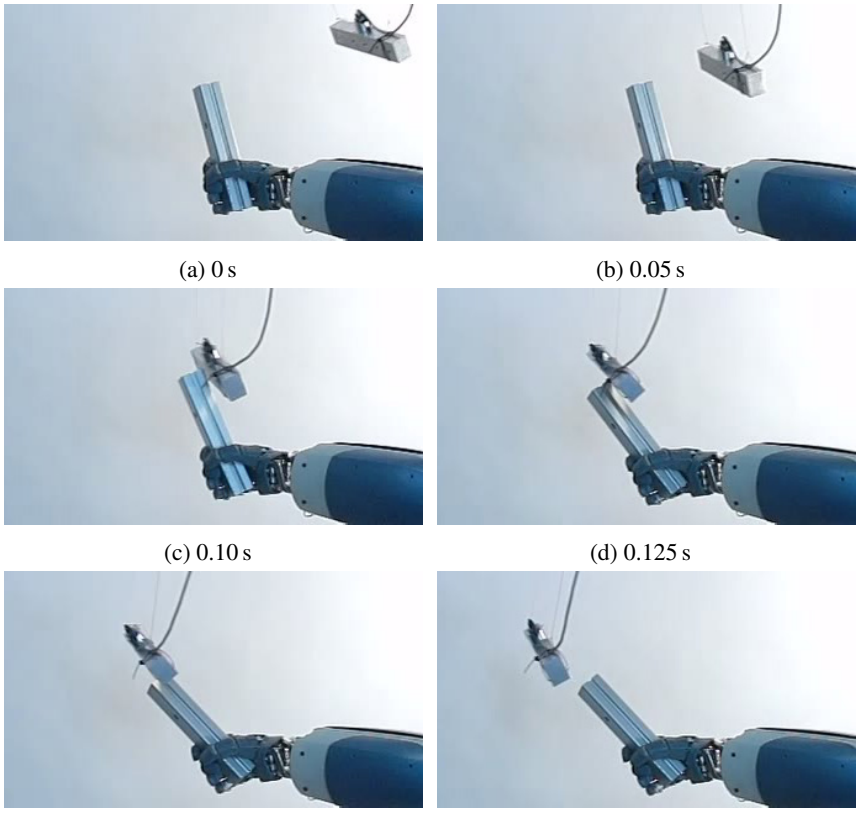

(a) 0 s (b) 0.05 s

(c) 0.10 s (d) 0.125 s

(e) 0.15 s (f) 0.175 s

Figure 5.17. High speed pictures of the object impact. The forces resulting of the impact are mainly carried by the index finger and the thumb.

been measured. Furthermore, the acceleration of the alloy cylinder has been measured by an attached acceleration sensor.
The hand successfully kept the object firmly grasped regardless whether withstanding backhand or forehand impact. The maximum impact forces measured at the tendons as well as the joint velocities are given in table 5.2. Most of the impact is carried by the index finger and the thumb MC flexor tendons. The maximum speed of 1059 °/s is more than 1.5 times the maximum speed of the respective drive (640 °/s). The tendon force, due to the decoupling of link and motor side has a maximum at approximately 70 N (compared to 250 N allowed maximum force),[6] whereas the resulting force in the contact between object and impactor is almost 900 N (see fig. 5.19b). This is 30 times higher than the maximum active fingertip force of the fingers.

Table 5.2. Maximum joint speeds and tendon forces within thumb and index finger during backhand impact (transformed to joint coordinates).

	Joint speed [°/s]		Tendon force [N]	
Joint, tendon	Thumb	Index	Thumb	Index
TMC / MC, flexor/abductor	274.1	156.3	19.9	63.1
TMC / MC, flexor/adductor	**1059.0**	143.6	**24.4**	17.1
TMC / MC, extensor/adductor	513.9	306.9	6.2	25.6
TMC / MC, extensor/abductor	302.4	168.5	22.1	8.4
MCP / PIP, flexor	304.2	287.8	16.4	**69.8**
MCP / PIP, extensor	129.6	136.4	12.7	5.9
IP / DIP, flexor	71.5	147.2	13.4	20.2
IP / DIP, extensor	109.4	110.6	**24.4**	36.1

In hands lacking energy storage, the drive speed is the limiting factor with respect to impacts. Thus, in contrast to the experiments done beforehand the joint speeds resulting from the impact are transformed to drive speeds. The maximum drive velocity required to follow this link motion is larger than 1500 °/s (see fig. 5.17) which far exceeds the maximum speed of the drive of 640 °/s. Consequently, within a hand lacking energy storage the impact energy and in especial the resulting torques would be transferred to the drive train and

[6] 350 N for PIP and MC tendons of the index and middle finger as well as the for all thumb flexor tendons

structure and, most likely, damage the hand.
As a comparison the impact experiment has been repeated with a human hand (without sensor equipment on the hand). The results of this experiment can be seen in figure 5.18. The maximum impact force between object and impactor is notably smaller than with the robot hand, since the inertia of the human arm is smaller than the one of the forearm of the *DLR Hand Arm System*.

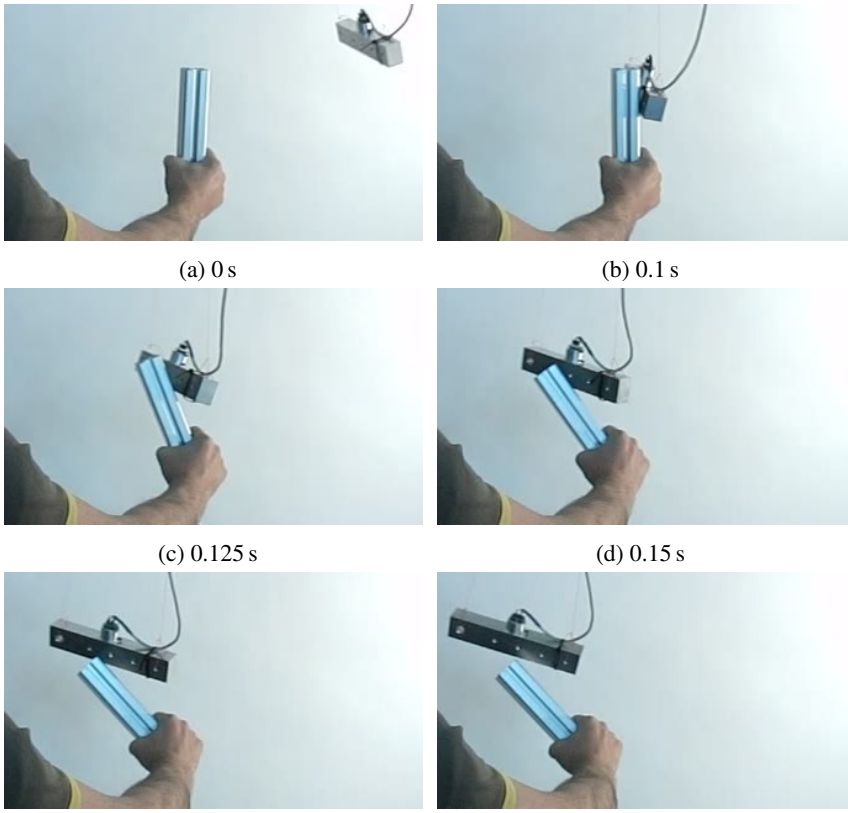

(a) 0 s (b) 0.1 s

(c) 0.125 s (d) 0.15 s

(e) 0.175 s (f) 0.2 s

Figure 5.18. High speed pictures of the object impact grasped by a human. The object is grasped firmly and stiff. In comparison to the *DLR Hand Arm System*, the deflection is of similar range.

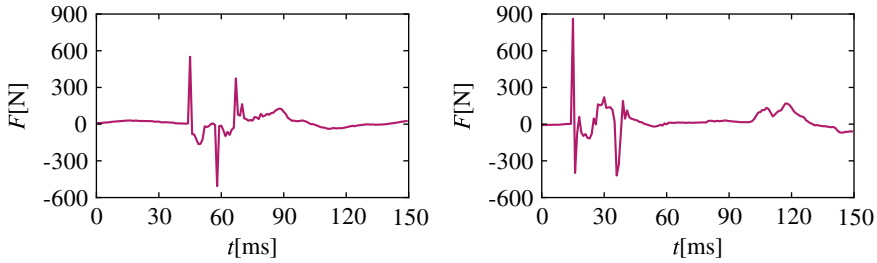

Figure 5.19. Impact force between object and impactor: *a*, human hand; *b*, robot hand. The impact force using the human hand is much lower since the inertia of the human arm (i.e. forearm) is lower than the one of the *DLR Hand Arm System*.

5.3. Summary

In this chapter, experimental results gained with the *Awiwi Hand* described in detail in chapter 4 have been presented. The robustness as well as the fast dynamics of the hand has been proven in experiments performed on the finger testbed as well as the *DLR Hand Arm System*. The *Awiwi Hand* is able to withstand the impact of an hammer without any damage and reaches finger joint speeds of up to 3500 °/s using the energy stored in the elastic elements. The grasping performance has been successfully proven by applying the medical tests described in 4.3.2 as well as by successfully grasping all objects of the *Cutkosky* taxonomy, which has not yet been achieved by any other hand to the authors knowledge. Furthermore, the taxonomy of *Feix* and other difficult to grasp objects, not covered by the taxonomies have been grasped as seen in Appendix A.
Finally, it has been shown that the hand is able to keep objects grasped even after impacts of an object of 750 g at a velocity of 4 m/s. This stability of the grasps against external forces is paramount for the operation of a robot in unstructured and unknown environments.

6
Conclusion

The following chapter summarizes the contribution of this works and the methods that have been used to achieve the goals. Subsequently, the relevance of the achieved results for the future of anthropomorphic robot design and service robotics research will be given. Finally an outlook to future work in the field of the anthropomorphic *Awiwi Hand* and humanoid robotics at DLR will be given.
The *Awiwi Hand*, an anthropomorphic hand for the *DLR Hand Arm System* has been built providing three essential characteristics that make the difference between humanoid and anthropomorphic robots. These are,

- Robustness
- Fast dynamics
- Enhanced grasping performance

Robustness is the key to complete tasks, particularly in unstructured or unknown environments where collisions cannot be avoided. Most robotic applications that include moving obstacles, as the case in physical human robotic interaction scenarios, have to be assumed to take place in (partially) unknown

environments at the current state of robot perception, since the robot only perceives its environment partly or not in realtime.
Moreover, it is of paramount importance to accelerate the pace in the development of autonomous robots and, in particular, task planning to accommodate the demand of the society for fully operational robots, as demonstrated by the Fukushima nuclear power plant accident in Japan in 2011. The achieved robustness enables to speed up the development of task planning algorithms. Iterative methods, which go through repeated failed task attempts to reach the task goal, such as reinforced learning —and human learning—, can now be used freely. Other new methods and concepts can be tested in early development stages without bothering about the potential damage of the costly robots used as development platforms.
Section 5.1.1 clearly shows that the *Awiwi Hand* is significantly more robust than existing state of the art humanoid robot hands. It is able to withstand high speed impacts of a 500 g hammer during operation, which would be painful or even dangerous for human hands. It has been shown in detail, that the drive train is decoupled from the link side by the elastic elements. The energy introduced by an impact is stored in the elastic elements. The maximum load of the drive train is reduced to $1/5^{th}$ of the impact load in the case of the shown experiments.
The ability to store energy not only has been shown to be the key to more robust robots. Section 5.1.2 also illustrates that the potential energy stored in the elastic elements enhances the dynamic capabilities of the hand by a factor of greater than five to a maximum velocity of more than 3500 °/s in the joints.
Grasping performance, for a robot hand, is the most important aspect. To the authors knowledge, the *Awiwi Hand* is the first robot hand that performed the full set of *Cutkosky's* taxonomy grasps. Thus, it is thought to have grasping capabilities superior to state of the art robotic hands, approaching that of the human archetype.[1] This has been demonstrated by grasping objects[2] according to *Cutkosky's* grasp taxonomy as well as the more complete taxonomy presented by *Feix* with the *Awiwi Hand*. Furthermore, the hand has successfully passed the Kapandji test, a medical hand performance tests used by surgeons.

[1] It has to be stated that, at that time, there exist no impartial tests to prove the grasping performance of a robot hand.

[2] Taught grasps, showing the ability of the hand independently of grasp planning and control algorithms from a mechanical perspective

To achieve the demonstrated grasping performance, dynamics, and robustness, a new approach to hand design has been proposed. For the design of the *Awiwi Hand*, the human hand anatomy as well as its movements have been analyzed to deduce the fundamental functionalities a hand should provide. These functionalities are the key for the design of the actuation, the kinematics and the robot hand itself. They have been transferred to the robot hand using the assets and possibilities of robotics technology. For the given requirements, the approach to copy the human hand fails due to the large gap between biology and technology. The material properties of human tissue cannot yet be replicated. On the flip side higher animals, for example, do not posses a free spinning roll joint, as needed for e.g. a wheel. Thus, the author hypothesizes that the anatomy of the human hand in some points might not be the optimal solution to provide the needed functionalities of a hand. Biological limitations should not necessarily be blindly applied to technical systems, or replicated in robot hands. Hence, the author believes that, according to the suggested approach, a proper functional understanding of hands[3] is the key to design "good" robot hands.
Using this design approach, the functionality of the human hand has been analyzed and important functionalities have been derived serving as guideline for the *Awiwi Hand* design, as for example:

- Robustness can be significantly improved using energy storage within the drive train.
- The orientation and placement of the thumb TMC joint is the key to a well functioning hand.
- The hinge joints of the human hand have to provide inclination, and, within the thumb, twist for proper opposition and grasping.
- The hand has to provide dislocatable joints as well as antagonistic actuation to withstand lateral loads.
- The functionality of human MC joints can be achieved using cardan joints if the first axis orientation is chosen correctly.
- The little finger MC joint has to turn frontal and inward to provide the functionalities of opposition and arching of the palm.

[3] Human and robot hands

Following the paradigm that *future robots have to provide energy storage capabilities* the above mentioned methodology of understanding rather than copying the human archetype has been developed in this thesis. This approach is not limited to anthropomorphic hands. It is also applicable to robotic arms as shown for the *DLR Hand Arm System* [Grebenstein et al. 2011], or complete anthropomorphic humanoids and other biologically inspired systems.
Although the hand meets the objectives initially set within this work and, consequently contributes to the development of applications and methods in robotics research, further improvements have to be made. The design of the *Awiwi Hand* and the *DLR Hand Arm System* is intended to provide a maximum of functionality at minimum complexity. Thus, one future key challenge is to reduce the complexity of the system to reduce maintenance time and costs as well as the weight of the hand and the forearm. Introducing couplings /synergies into the hand is one promising, albeit challenging approach to achieve this goal. These couplings/synergies will first be introduced in software using the hand developed in this work and tested in extensive experiments before leading to a hand redesign. Only couplings that can be implemented in hardware with an appropriate hardware effort will be selected. First experiments have been performed by *T. Wimböck* [Wimböck et al. 2012] within the THE project (www.thehandembodied.eu) to evaluate the performance of the *Awiwi Hand* using the synergies suggested by Santello [Santello et al. 1998]. An promising alternative approach to reduce the number of drives is the introduction of underactuation[4] [Birglen et al. 2008] while still keeping the antagonistic variable stiffness approach. As a first step, it is intended to design a coupling for the ring and little finger using underactuation.
On the other hand, the friction introduced by the tendons as well as by the sliding bearings used in the finger joints, is not negligible. In order to further improve its grasping and manipulation performance, concepts such as friction observers have to be developed to deal with the friction of the hand and to compensate the inaccuracies in the finger joint positions. Furthermore, the design has to be optimized in terms of friction, such as using different bearing concepts in the joints, without abandoning the concept of dislocatable joints and antagonistic actuation.
In terms of hand kinematics design and evaluation, the author hypothesizes

[4] Underactuation in tendon actuation is defined by being actuated with less than twice the number of joints tendons.

that the Kapandji test[5] inherently includes most, if not all grasps of the taxonomies presented by *Cutkosky* [Cutkosky 1989] and *Feix* [Feix et al. 2009], and is thus an even better criterion to help optimize and evaluate robot hands. In the first step the Kapandji test, used to design the kinematics of the *Awiwi Hand* in 4.3 is formulated mathematically. This allows the Kapandji test to be used in simulation and optimization in addition to the well known criteria. In the next step the mathematical formulation of the Kapandji test is used to investigate this hypothesis. If the hypothesis can be corroborated, a further step towards fast and effective optimization of robot hands can be made, as the dimension of the cost function can be reduced significantly.
In the future a humanoid torso, with anthropomorphic characteristics, which uses the above mentioned version of the hand with a reduced number of drives will be built. In combination with the intended legs, using variable stiffness, it might one day become a humanoid robot that is able to fall over without any damage or run as fast as a human.
Such humanoid robots, can assist the human in almost all aspects of life. They might assist elderly people, take over unpopular jobs, build habitats on planets (fig. 6.1) or be valuable aides during catastrophes. In particular, operation in environments that are contaminated (e.g. nuclear accidents) or inhospitable (e.g extraterrestrial, submarine, desserts, volcanos, arctic and antarctic zone) is a strong motivation for developing such robots. Consequently, there is a high interest of the society in humanoid robots, for example demonstrated by 515.040 views (as of 4.5.2012) of the *Awiwi Hand* video on youtube.[6] This can be interpreted as the demand for helpful robot assistants and demonstrates the social relevance of robotics.

[5] Eventually supplemented by one or two grasp poses (e.g. large cylinder power grasp) that evaluate full extension and abduction of the thumb

[6] (http://www.youtube.com/watch?v=YqmRKqFqiok). One major aspect of the interest is of course the interest in—and the fear of— resembling the human.

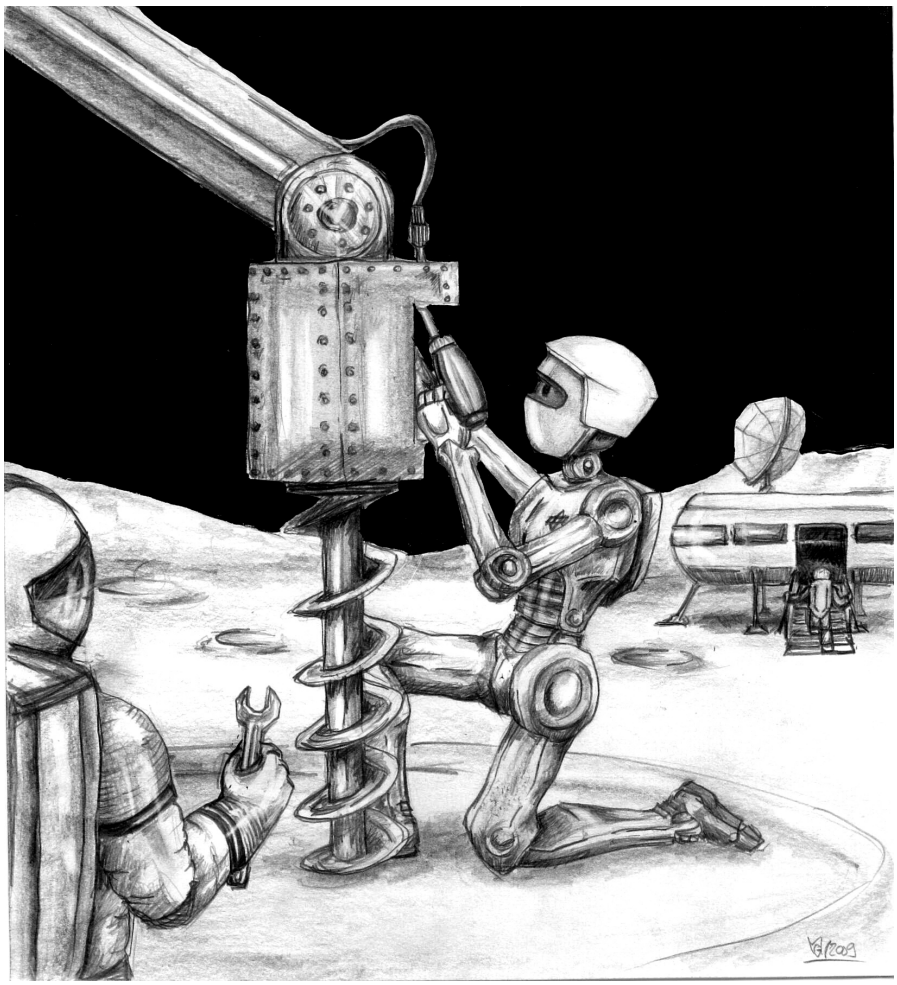

Figure 6.1. The space robot assistant might one day assist astronauts in building extraterrestrial habitats. To achieve this vision, robustness of the robot is crucial, since maintenance, if possible, is of extensive costs in such scenario (courtesy *Martin Görner*).

Appendices

A

Taxonomies and Grasping pictures

In chapter 5 the grasping performance of the *Awiwi Hand* has been evaluated by performing the grasps of the *Cutkosky* taxonomy. In the following larger figures of the performed grasps are shown. In the second part of Appendix A the grasping capabilities of the *Awiwi Hand* are demonstrated by performing the grasps of the more detailed taxonomy suggested by *Feix* [Feix et al. 2009]. The pictures of the performed grasps are shown subsequently. Grasps that are included in the two taxonomies are shown for both for completeness.

A.1. Cutkosky Taxonomy

In the following figures of all *Cutkosky* grasps are shown. The grasps are given following the structure of the taxonomy tree from left to right top to the bottom.

Figure A.1. (*Next page*) *Cutkosky's* [Cutkosky 1989] taxonomy grasps performed by the *Awiwi Hand*. The hand could perform 100% of the taxonomy grasps which is a first in humanoid robotics.

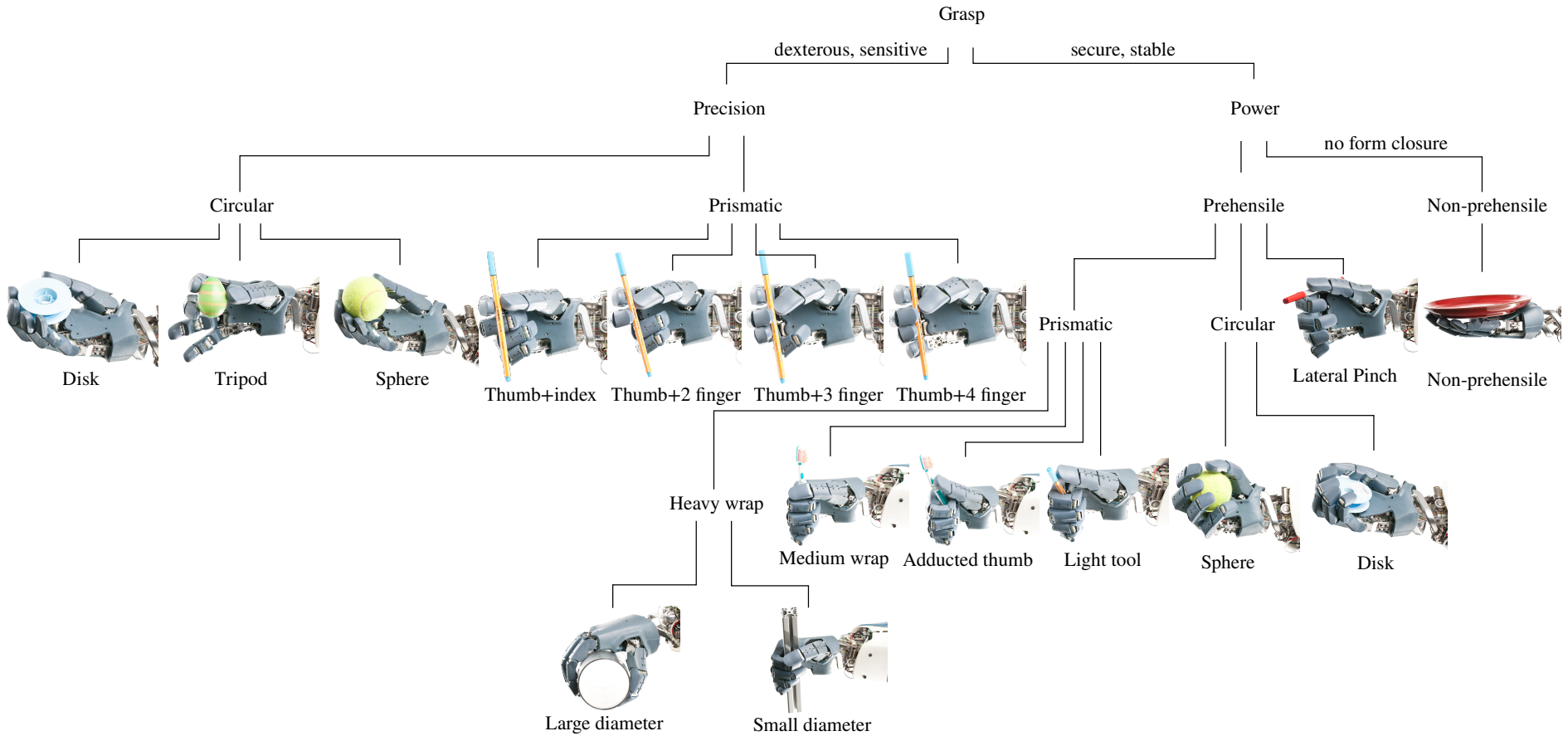
Grasp
dexterous, sensitive
secure, stable
Precision
Power
no form closure
Circular
Prismatic
Prehensile
Non-prehensile
Disk
Tripod
Sphere
Thumb+index
Thumb+2 finger
Thumb+3 finger
Thumb+4 finger
Prismatic
Circular
Lateral Pinch
Non-prehensile
Heavy wrap
Medium wrap
Adducted thumb
Light tool
Sphere
Disk
Large diameter
Small diameter

A.1.1. Precision Grasps

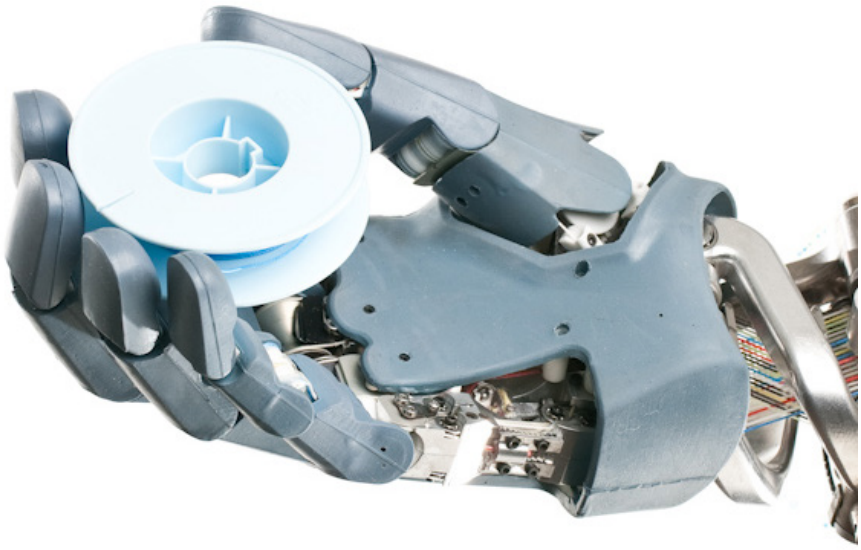

Figure A.2. Cutkosky taxonomy *(1)*: Circular precision grasps of objects *(I)*: disk grasp

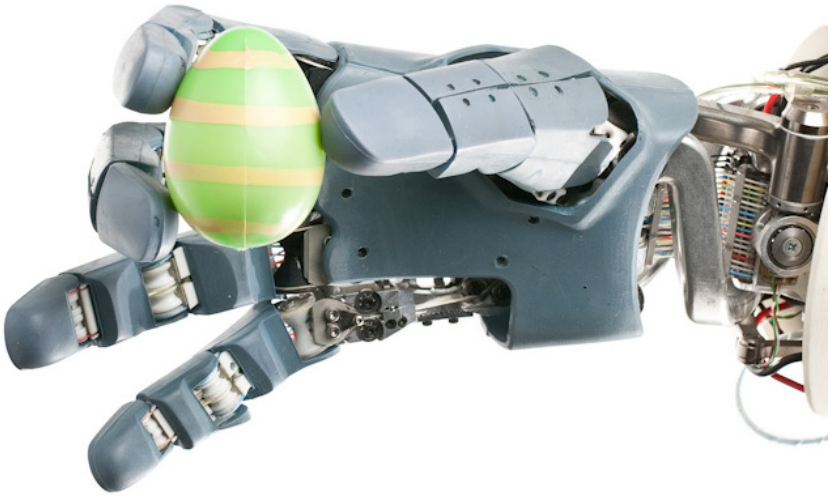

(a)

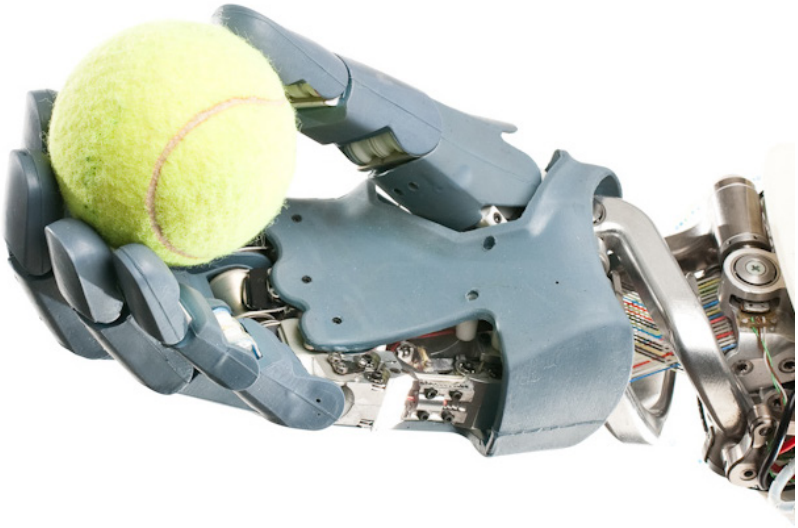

(b)

Figure A.3. Cutkosky taxonomy: circular precision grasps of objects *(II)*: *a*, tripod grasp; *b*, spherical object

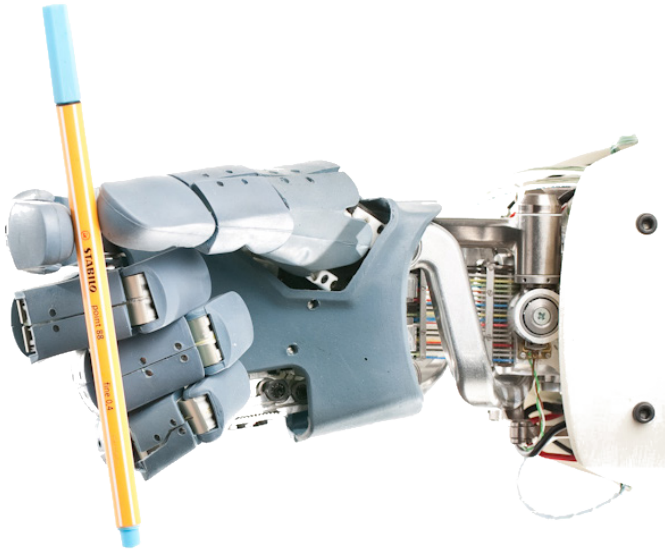

(a)

(b)

Figure A.4. Cutkosky taxonomy: precision grasps of an prismatic object *(I)*; *a*, thumb and index finger; *b*, two fingers and the thumb

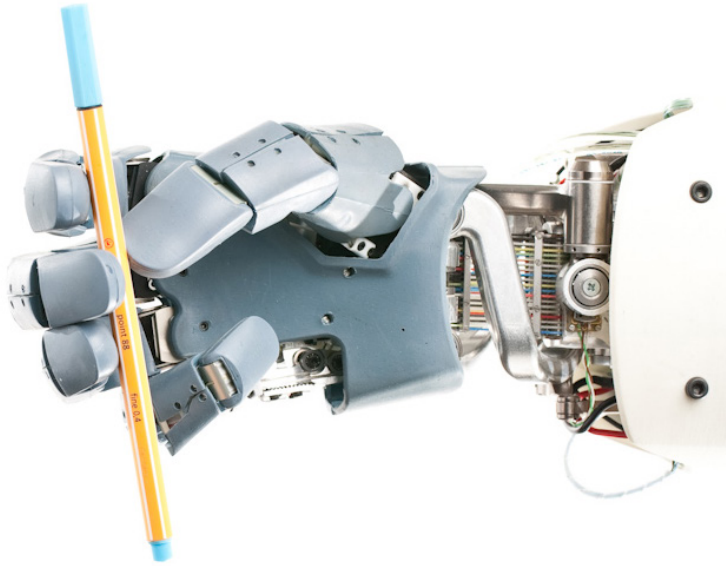

(a)

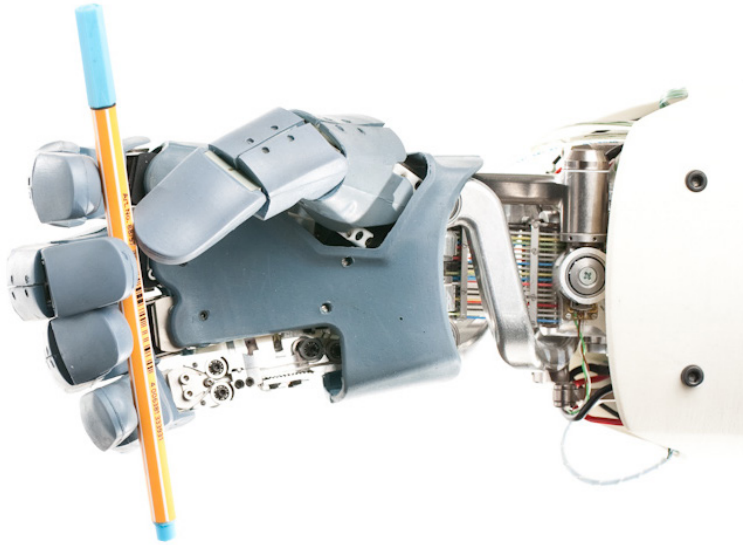

(b)

Figure A.5. Cutkosky taxonomy: precision grasps of an prismatic object *(II)*; *a*, three fingers and the thumb; *b*, four fingers and the thumb

A.1.2. Power Grasps

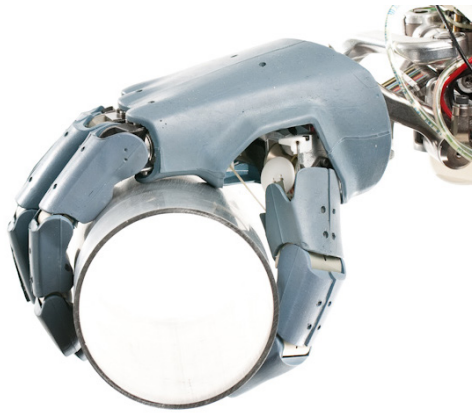

Figure A.6. Cutkosky taxonomy: prismatic, prehensile power grasp, heavy wrap *(I)*: large diameter object

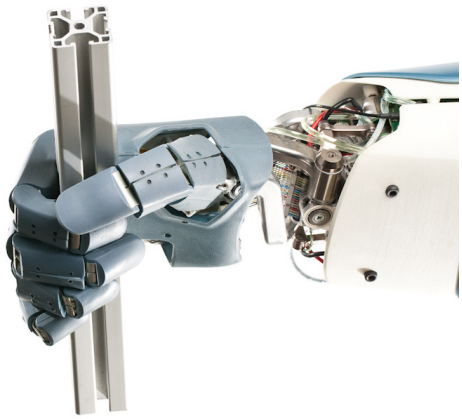

Figure A.7. Cutkosky taxonomy: prismatic, prehensile power grasp, heavy wrap *(II)*: small diameter object

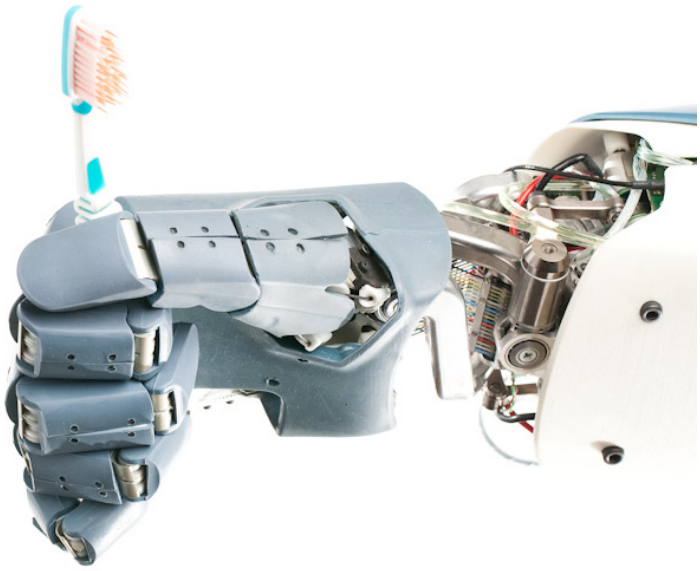

Figure A.8. Cutkosky taxonomy: prismatic, prehensile power grasp *(I)*: medium wrap

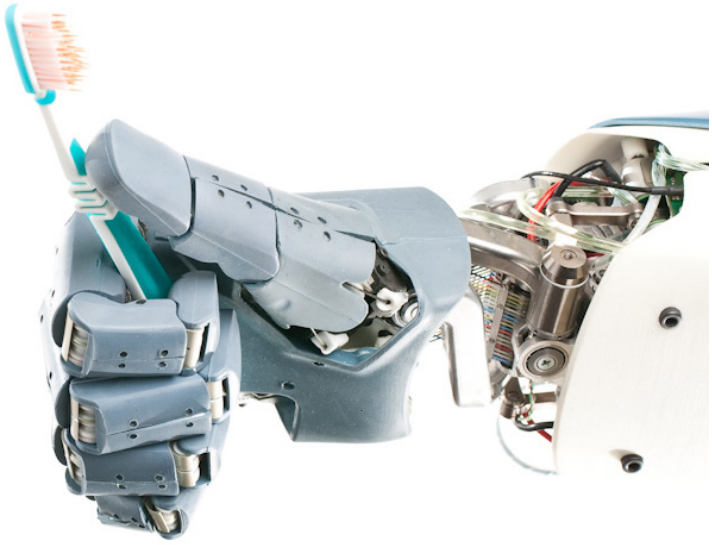

(a)

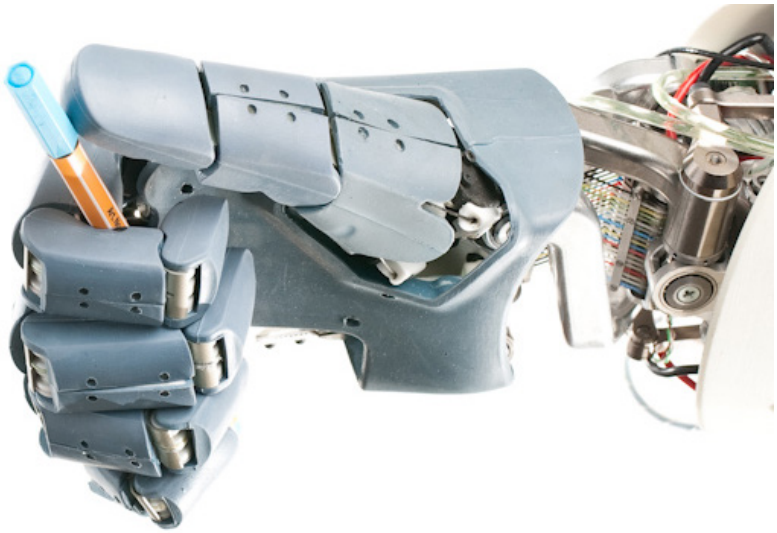

(b)

Figure A.9. Cutkosky taxonomy: prismatic, prehensile power grasp *(II)*: *a*, with adducted thumb; *b*, grasping of light tool

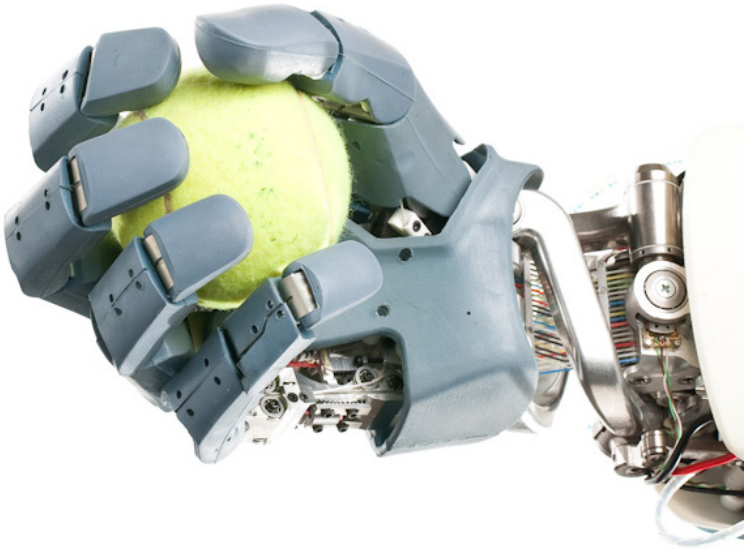

(a)

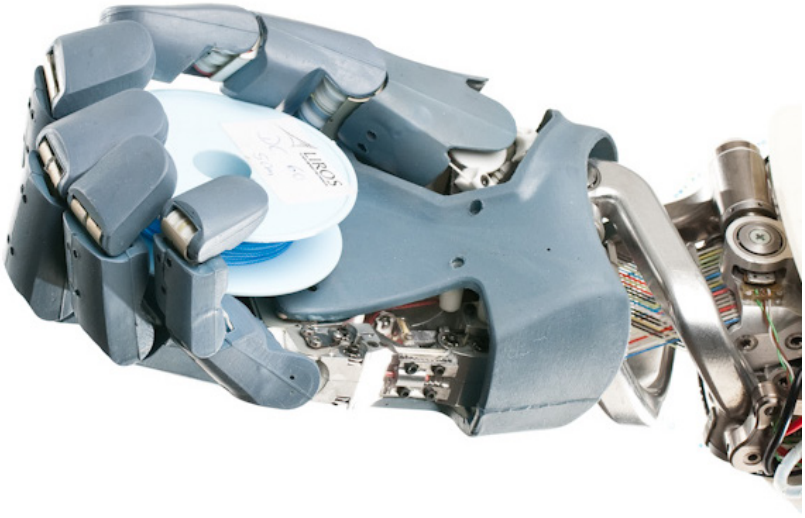

(b)

Figure A.10. Cutkosky taxonomy: circular, prehensile power grasp: wrapping of midsize objects; *a*, spherical object *b*, disk shaped object

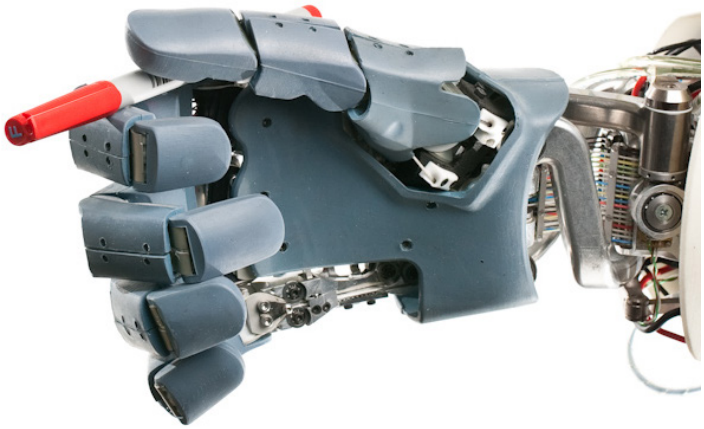

Figure A.11. Cutkosky taxonomy: prehensile lateral pinch power grasp

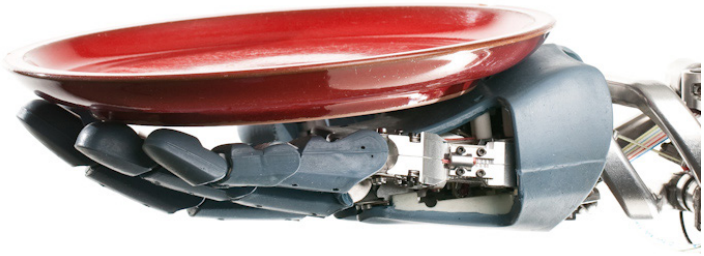

Figure A.12. Cutkosky taxonomy: non-prehensile power grasp without form closure

A.2. Feix Taxonomy

The taxonomy presented by *Feix* [Feix 2010; Feix et al. 2009] gives a more detailed overview of the human grasps than the *Cutkosky* taxonomy. In particular this taxonomy includes several grasps, such as the pinch grasp, and grasping of a scissor, that are not part of the *Cutkosky* taxonomy, but are important to evaluate the performance. This taxonomy is motivated by the development of hand prostheses, and structures the grasps in a matrix as seen in figure A.13. The columns of the matrix distinguish between three types of grasps:

- Power grasp
- Intermediate grasp
- Precision grasp

The three main columns are organized in sub columns that categorize grasps by the type of opposition (*side*, which means lateral contact, and *pad*) and by the number and location of the "virtual 2nd finger".
In the following pictures of grasps from *Feix'* taxonomy are shown. The pictures are placed top to bottom, left to right.

Figure A.13. The taxonomy of *Feix* performed by the *Awiwi Hand* (next page).

		Power					Intermediate			Precision				
	Opposition type	Palm		Pad			Side			Pad				Side
	Virtual 2nd fing.	3-5	2-5	2	2-3	2-4	2	3	3-4	2	2-3	2-4	2-5	3
Thumb Abduction		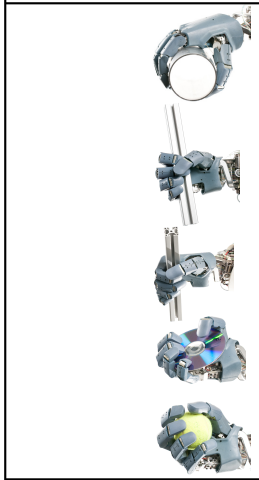								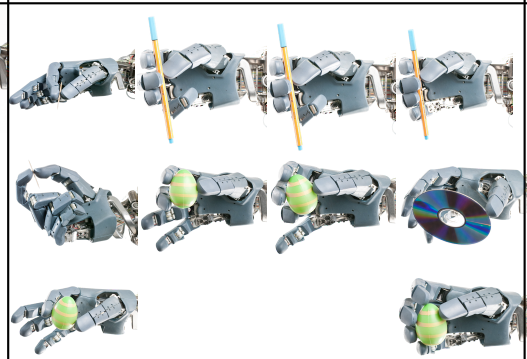				
Thumb Adduction		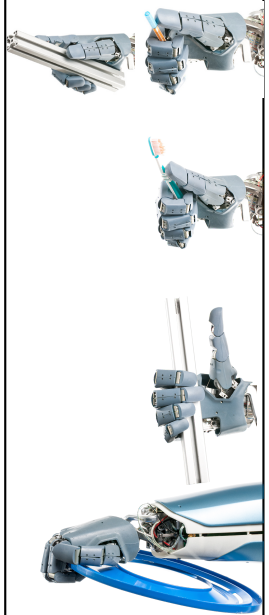					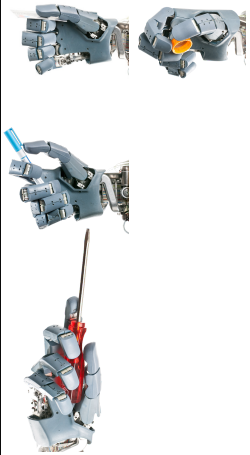							

A.2.1. Power Grasps

Power Grasps with Abducted Thumb and Palm Opposition

Figure A.14. Feix taxonomy: palm power grasps using thumb abduction *(I)*

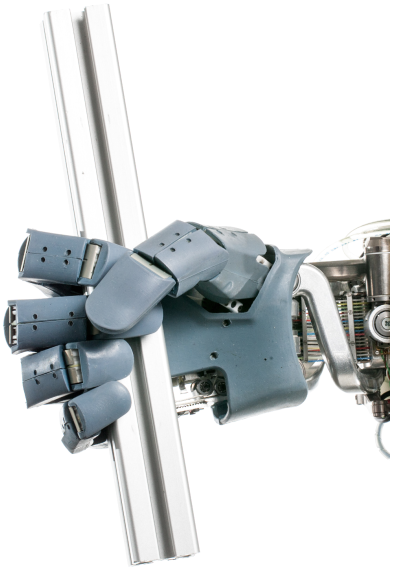

(a)

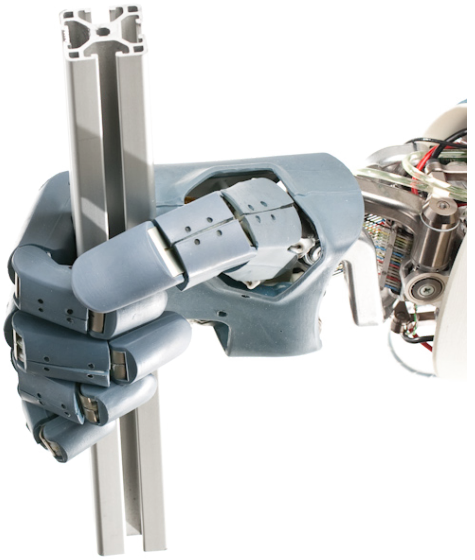

(b)

Figure A.15. Feix taxonomy: palm power grasps using thumb abduction *(II)*

(a)

(b)

Figure A.16. Feix Taxonomy: Palm power grasps using thumb abduction *(III)*

Power Grasps with Adducted Thumb and Palm Opposition

Figure A.17. Feix taxonomy: palm power grasps using thumb adduction *(I)*

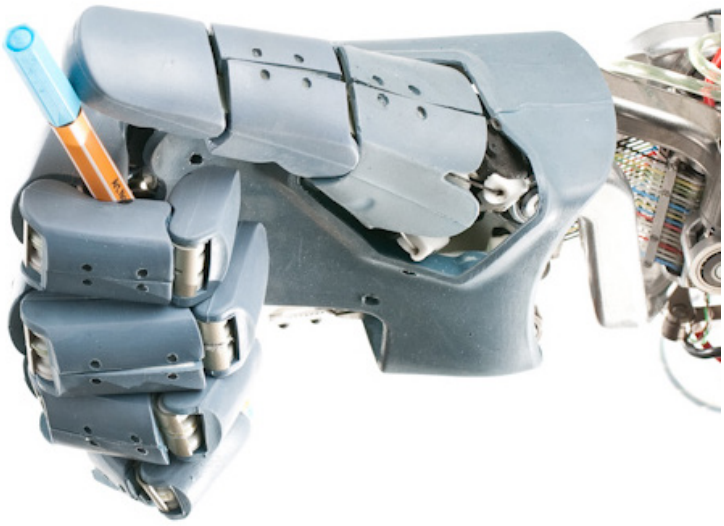

(a)

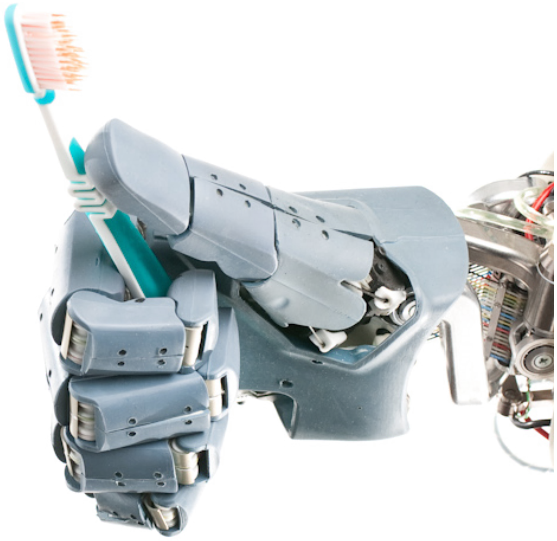

(b)

Figure A.18. Feix taxonomy: palm power grasps using thumb adduction *(II)*

(a)

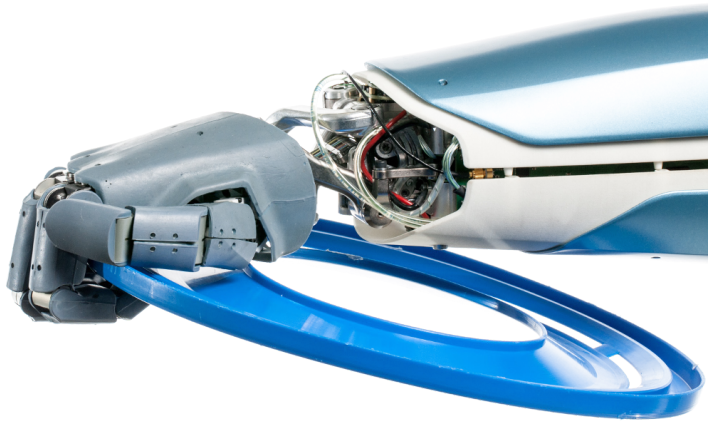

(b)

Figure A.19. Feix taxonomy: pad power grasps using thumb adduction

Power Grasps with Abducted Thumb and Pad Opposition

Figure A.20. Feix taxonomy: pad power grasps using thumb abduction *(I)*

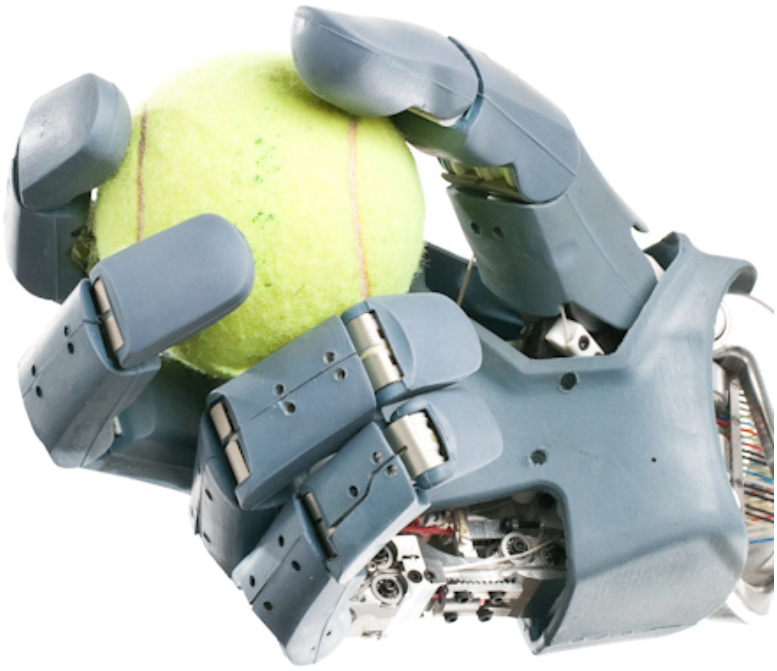

(a)

(b)

Figure A.21. Feix taxonomy: pad power grasps using thumb abduction *(II)*

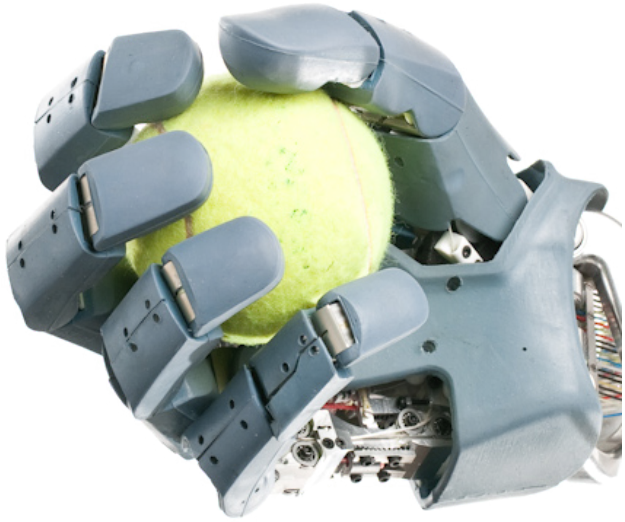

(a)

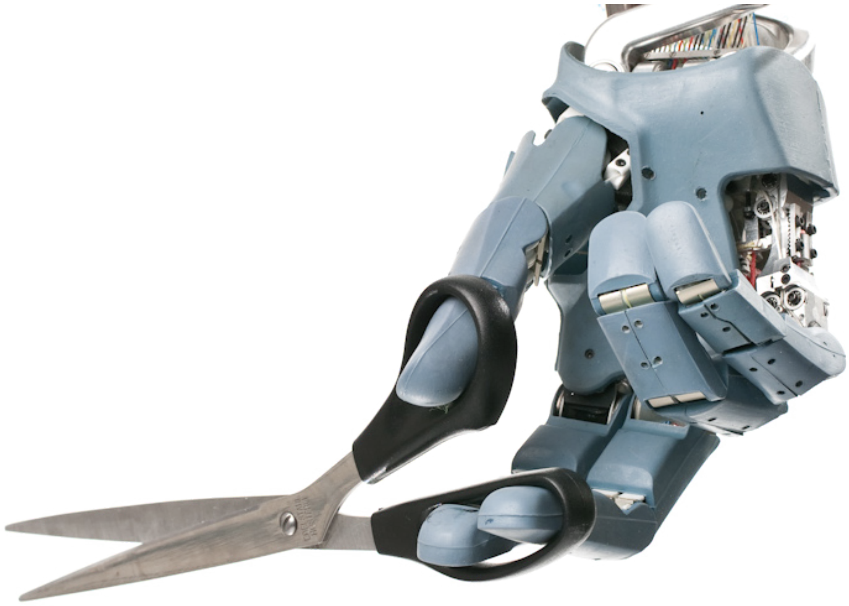

(b)

Figure A.22. Feix taxonomy: pad power grasps using thumb abduction *(III)*

A.2.2. Intermediate Grasps with Lateral Contact (Side Opposition)

Intermediate grasps are neither power grasps nor precision grasps. According to *Feix* all these grasps use lateral contact to the object of at least one finger.

Intermediate Grasps with Abducted Thumb

Figure A.23. Feix taxonomy: intermediate grasps; thumb abduction *(I)*

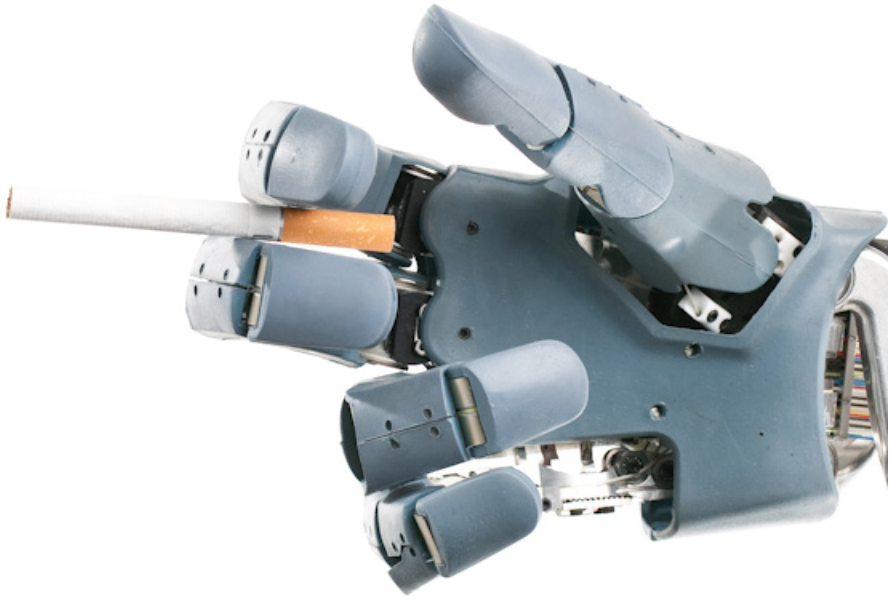

Figure A.24. Feix taxonomy: intermediate grasps using thumb abduction *(II)*

Intermediate Grasps with Adducted Thumb

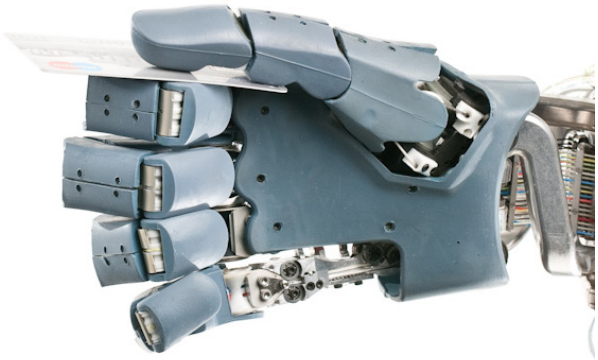

(a)

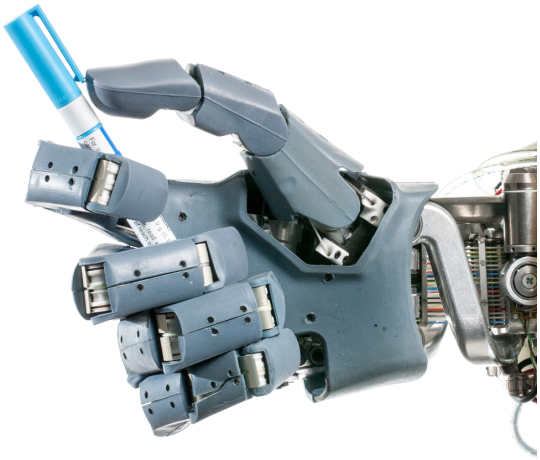

(b)

Figure A.25. Feix taxonomy: intermediate grasps using thumb adduction *(I)*

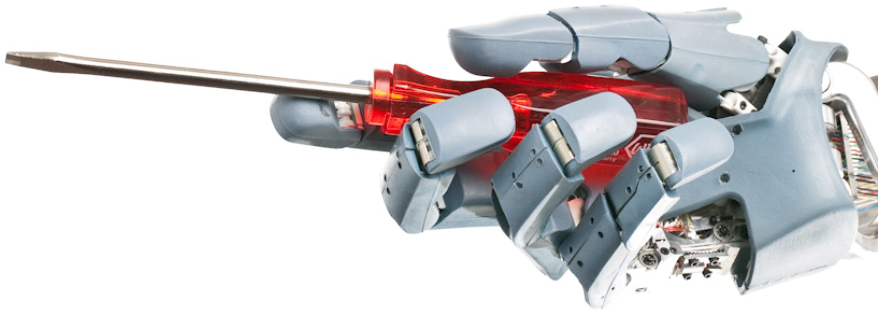

(a)

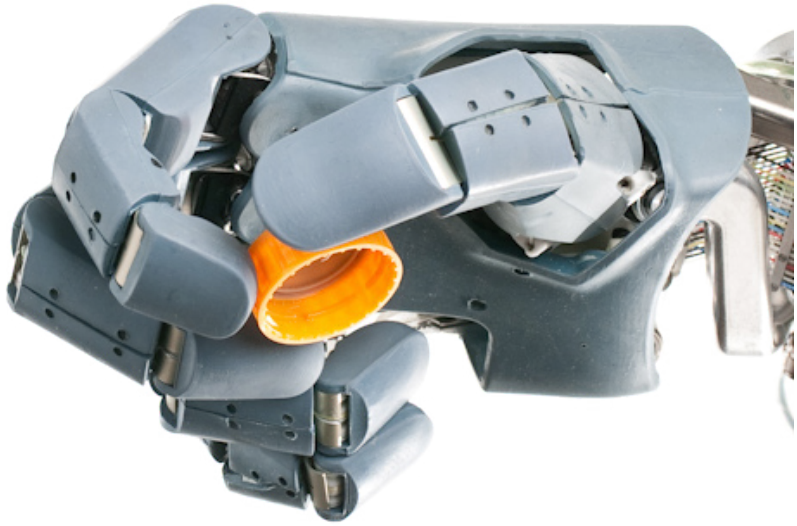

(b)

Figure A.26. Feix taxonomy: intermediate grasps using thumb adduction *(II)*

A.2.3. Precision Grasps

Precision Grasps with Abducted Thumb and Pad Contact

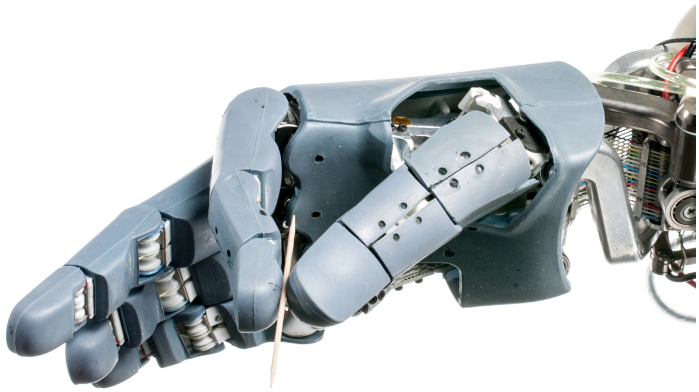

(a)

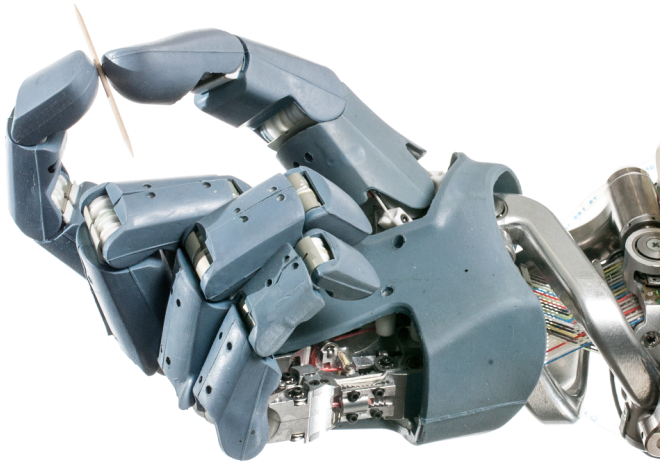

(b)

Figure A.27. Feix taxonomy: palm precision grasps using thumb abduction *(I)*

(a)

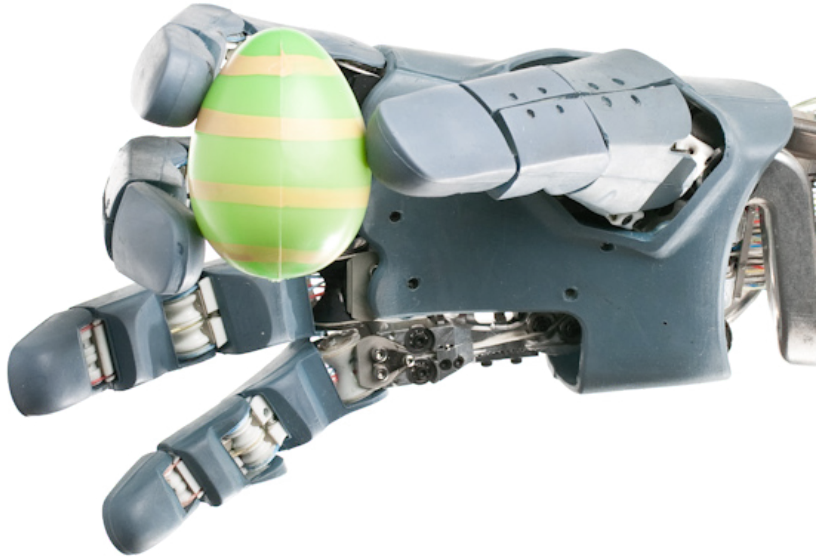

(b)

Figure A.28. Feix taxonomy: palm precision grasps using thumb abduction *(II)*

(a)

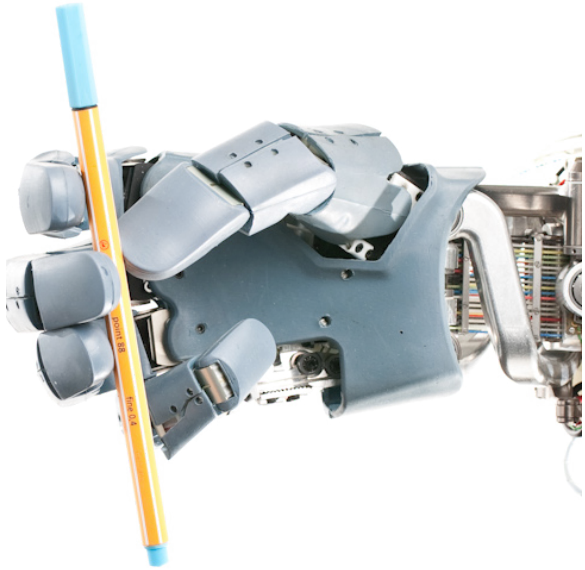

(b)

Figure A.29. Feix taxonomy: palm precision grasps using thumb abduction *(III)*

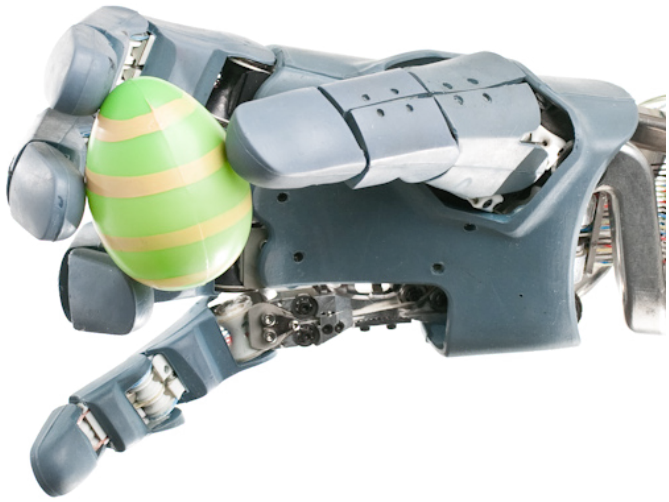

(a)

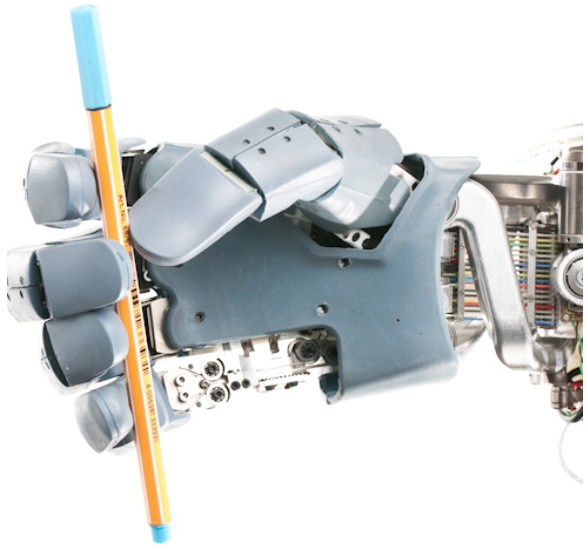

(b)

Figure A.30. Feix taxonomy: palm precision grasps using thumb abduction *(IV)*

(a)

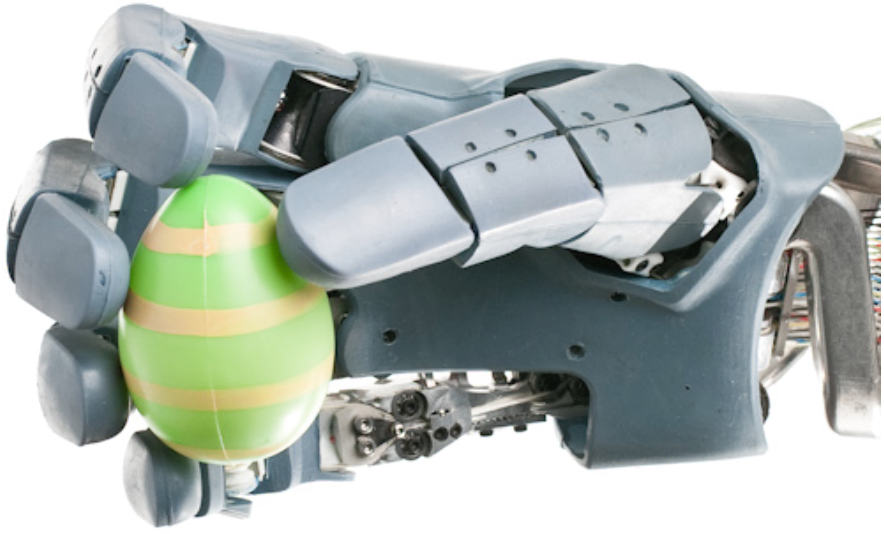

(b)

Figure A.31. Feix taxonomy: palm precision grasps using thumb abduction *(V)*

Precision Grasps with Adducted Thumb and Pad Contact

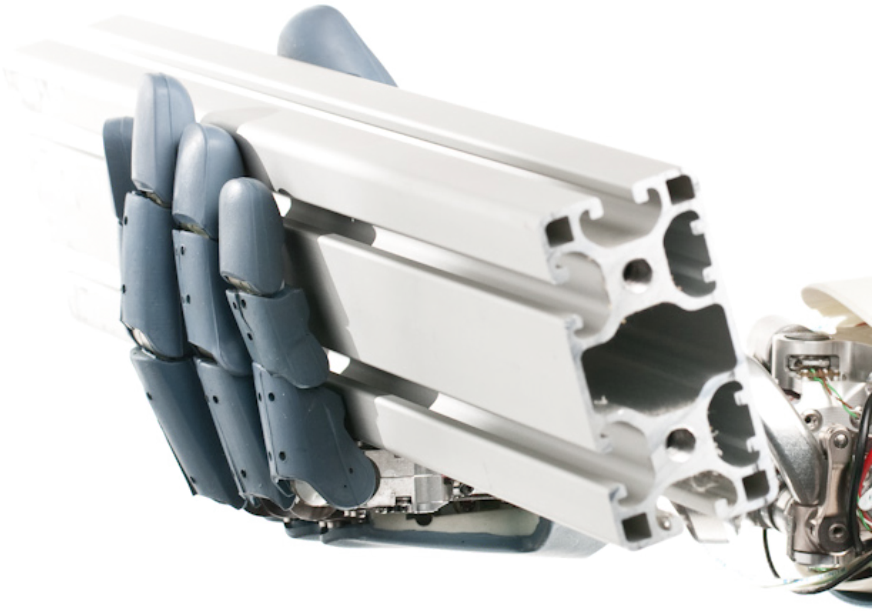

Figure A.32. Feix taxonomy: palm precision grasps using thumb adduction

Precision Grasps with Abducted Thumb and Side Contact

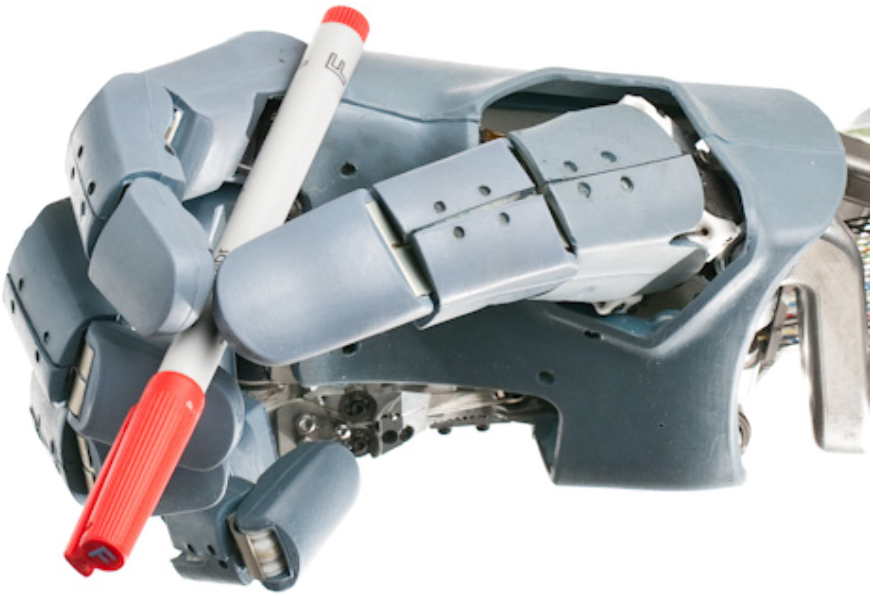

Figure A.33. Feix taxonomy: palm precision grasps using thumb abduction

B
Testbeds and Prototypes

In the following additional information about the finger testbed used for the robustness and dynamics evaluation experiments and earlier finger prototypes are given.

B.1. Finger Testbed

The finger testbed (fig. B.1) consists of eight direct drive motors driving the fingers. The direct drives are chosen to reduce components within the drive train that are difficult to model, so that the characteristics of the fingers can be analyzed more accurately. The tendons of the finger are connected to winders directly attached to the motors. The elastic elements ("tendon side-pull mechanisms", fig. B.3) that produce non-linear spring characteristics are mounted on the backside of the plates carrying the motor (see fig. B.2). Linear potentiometers measure the length of the linear springs (see table B.1) which are directly correlated to the tendon forces. The motor position as well as the elastic element deflection, are measured by absolute sensors.

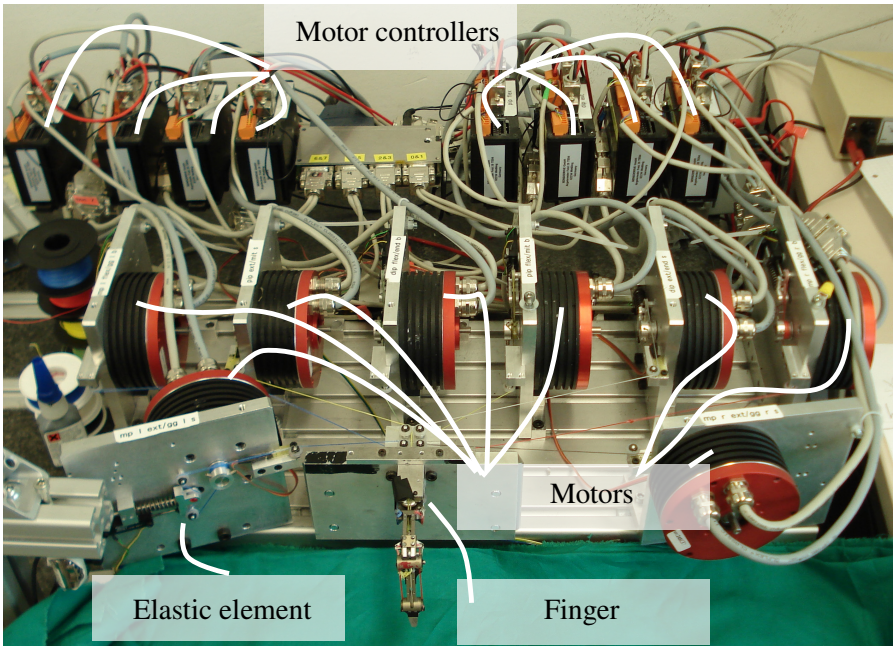

Figure B.1. The antagonistic finger testbed. The finger is driven by eight direct drive motors to reduce the influence of gears in terms of friction, backlash etc. Each drive provides an elastic element of the "tendon side-pull mechanism" type. The finger depicted is the first version as described in B.2

Table B.1. Spring rates used in the finger testbed and maximum travel Δ_{max} of the springs.

Joint	Spring rate [N/mm]	Δ_{max} [mm]
MC	2.127	17
PIP	5.211	19
DIP	1.246	21.9

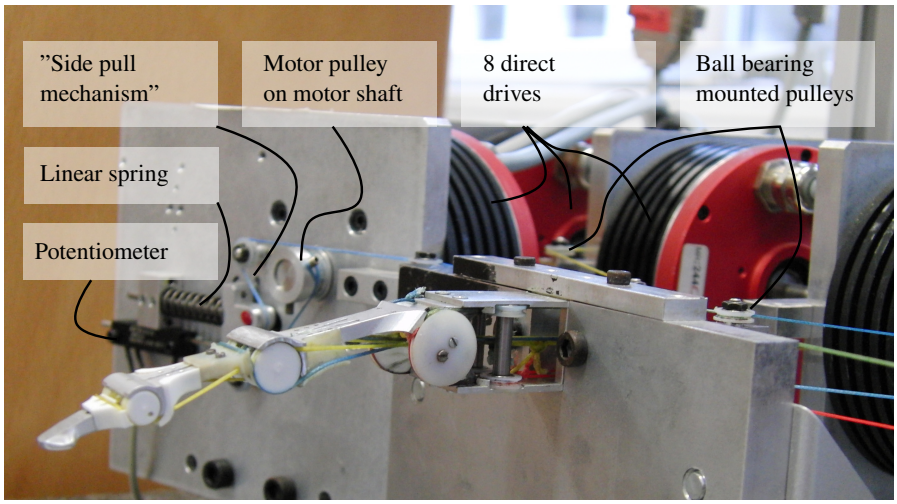

Figure B.2. Setup with the final version of the finger. One of the eight elastic element mechanisms is seen in the background. As in the forearm, they are from the “tendon side-pull mechanism” type.

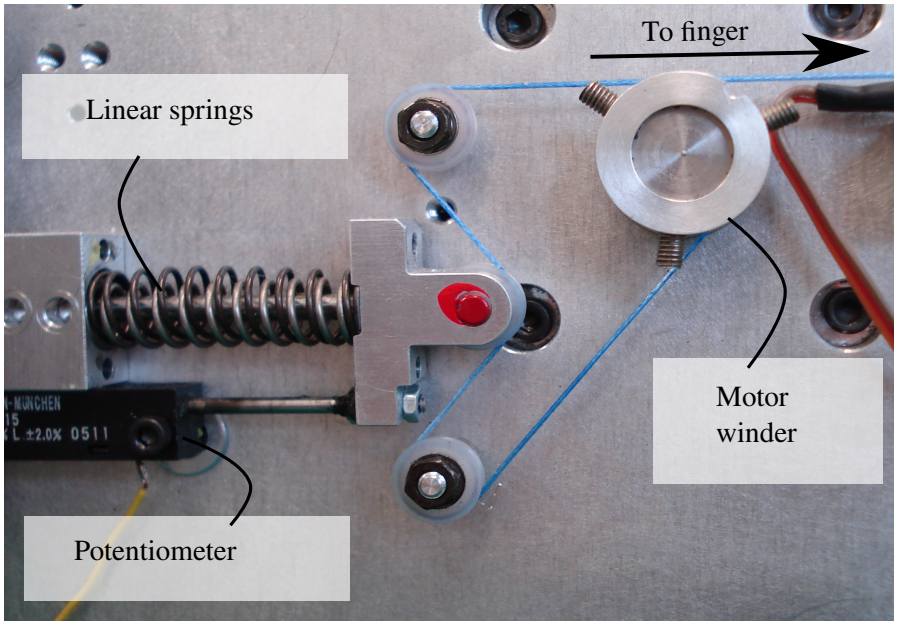

Figure B.3. The "tendon side-pull mechanism" consisting of the winder, which is directly attached to the motor, two fixed pulleys, and the spring loaded pulley. The compression of the spring is measured with a potentiometer. To enable a wider variety of spring rates two linear springs of different spring rates are used in parallel.

B.2. First Version of the Finger

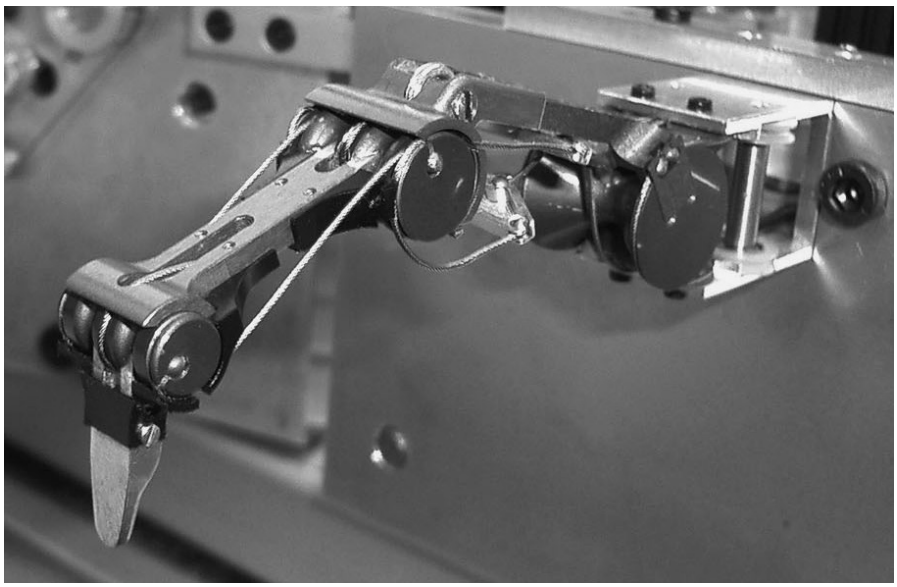

Figure B.4. Side view of the first finger version of the *Awiwi Hand* on the finger testbed. The finger is fully equipped with steel cables attached to the finger by spherical terminals.

The first version of the finger has been in introduced in section 4.5.3. In the following additional information about the first version of the finger is given. In contrast to the final version of the finger, it uses steel cables to achieve higher stiffness and maximum load of the tendons. The terminals of steel cables have to be applied at production time since expensive machines are necessary to guarantee the needed maximum loads. Thus the terminals of the steel cables have to be threaded through all holes along the tendon path. Due to the large diameter of the terminals, it is not possible to route the tendons through the hyperboloid of the MC joint. Consequently, the tendons have been routed using guiding surfaces on the palmar and dorsal side of the finger MC joint as shown in figure B.5. In contrast to the Dyneema tendons, steel cables cannot be spliced. Thus an additional component is needed to achieve the split of the flexors of the PIP and DIP joint. The splitting is provided by two small, highly loaded, alloy triangles which increase the risk of failure of the finger. They

also lower the limits of flexion and extension of the IP joints due to contact with the guide at the MC joint or the PIP joint pan. To reduce abrasive wear by the steel cables[1] all parts have been hard anodized.
As discussed in section 4.5.3 this tendon routing concept has been abandoned, since the steel cables turned out to have significantly more wear than the Dyneema tendons, and they are also prone to folding. The tendon routing limits the finger maximum speed due to coupling of the IP joints and the MC joint.

[1] The steel cables have to be un-coated since sliding guidances are used within the tendon path.

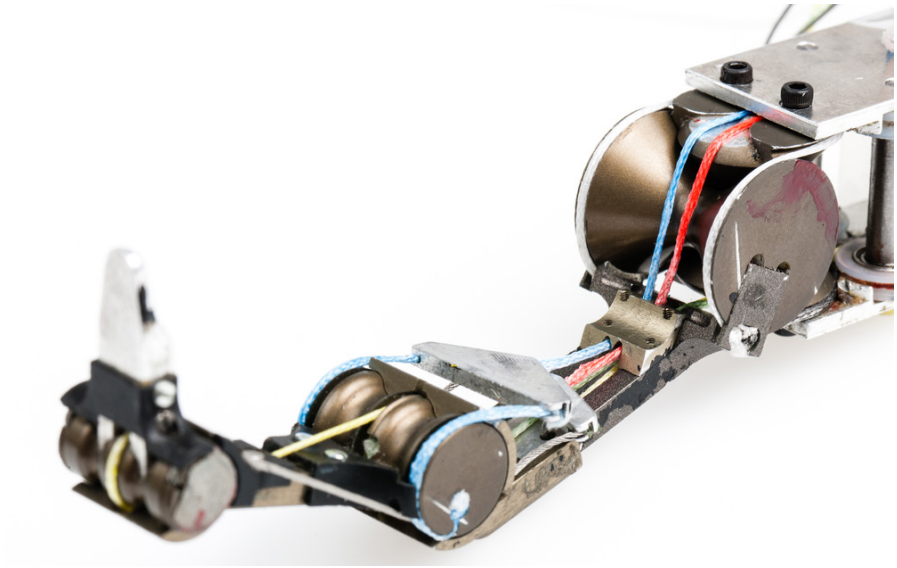

(a)

(b)

Figure B.5. Tendon routing of first finger version equipped with colored Dyneema tendons to illustrate the tendon routing: *a*, routing at the MC joint. The tendons move in a sliding/rolling motion during abduction/adduction of the finger. Notable wear is seen on the guide surface at the MC joint even though the finger has been hard anodized (this finger has been previously used with steel cables over a longer period of time). *b*, the split of the flexors of the PIP and DIP joint is provided by the two small, alloy triangles that limit the flexion and extension of the IP joints.

Bibliography

Adee, S. (2008). *i-LIMB prosthetic hand grabs UK's top engineering award - IEEE Spectrum*. URL: http://spectrum.ieee.org/tech-talk/semiconductors/devices/ilimb_prosthetic_hand_grabs_uk (visited on 04/19/2012).

Albu-Schäffer, A. (2001). "Regelung von Robotern mit elastischen Gelenken am Beispiel der DLR-Leichtbauarme". Dissertation. Technische Universität München.

Arimoto, S., K. Tahara, J. Bae, and M. Yoshida (2003). "A stability theory of a manifold: concurrent realization of grasp and orientation control of an object by a pair of robot fingers". In: *Robotica* 21.02, pp. 163–178. DOI: 10.1017/S026357470200468X.

Balasubramanian, R. and Y. Matsuoka (2008). "Biological stiffness control strategies for the Anatomically Correct Testbed (ACT) Hand". In: *Robotics and Automation, 2008. ICRA 2008. IEEE International Conference on*. (Pasadena, USA, May 19–23, 2008), pp. 737–742.

Bäuml, B., T. Wimböck, and G. Hirzinger (2010). "Kinematically optimal catching a flying ball with a hand-arm-system". In: *Intelligent Robots and Systems (IROS), 2010 IEEE/RSJ International Conference on*. (Taipei, Taiwan, Oct. 18–22, 2010), pp. 2592–2599.

Benninghoff, A. (1994). *Anatomie: makroskopische Anatomie, Embryologie und Histologie des Menschen; Benninghoff*. Ed. by D. Drenckhahn and W. Zenker. 15th ed. Vol. 1. München: Urban & Schwarzenberg. ISBN: 9783541002450.

Biagiotti, L., F. Lotti, C. Melchiorri, and G. Vassura (2002). *How far is the human hand? A review on anthropomorphic end effectors*. URL: `http://www-lar.deis.unibo.it/woda/data/deis-lar-publications/3cbd.Document.pdf` (visited on 05/07/2012).

Bicchi, A. and G. Tonietti (2004). "Fast and soft arm tactics: dealing with the safety-performance trade-off in robot arms design and control". In: *IEEE RAS – Robotics and Automation Magazine* 11, pp. 22–33.

Bicchi, A., G. Tonietti, and R. Schiavi (2004). "Safe and fast actuators for machines interacting with humans". In: *Robotics and Automation, 2004. TExCRA '04. First IEEE Technical Exhibition Based Conference on*. (TEXCRA2004-d, Nov. 18–19, 2004), pp. 17–18. DOI: `10.1109/TEXCRA.2004.1424973`.

Birglen, L., T. Laliberté, and C. Gosselin (2008). *Underactuated robotic hands*. Vol. 40. Springer Tracts in Advanced Robotics. Berlin: Springer. ISBN: 978-3-540-77458-7.

Borst, C., M. Fischer, S. Haidacher, H. Liu, and G. Hirzinger (2003). "DLR Hand II: Experiments and experience with an anthropomorphic hand". In: *Robotics and Automation 2003. Proceedings. ICRA '03 .IEEE International Conference on*. (Taipei, Taiwan, Sept. 14–19, 2003). Vol. 1, pp. 702–707. DOI: `10.1109/ROBOT.2003.1241676`.

Butterfaß, J., M. Fischer, M. Grebenstein, S. Haidacher, and G. Hirzinger (2004). "Design and experiences with DLR Hand II". In: *World Automation Congress: Tenth International Symposium on Robotics with Applications*. (Seville, Spain, June 28–July 1, 2004). Vol. 15, 105—110. DOI: `10.1109/WAC.2004.185205`.

Butterfaß, J., G. Hirzinger, S. Knoch, and H. Liu (1998). "DLR's multisensory articulated hand: I. Hard- and software architecture". In: *Robotics and Automation, 1998. Proceedings. 1998 IEEE International Conference on*. (Leuven, Belgium, May 16–20, 1998), pp. 2081–2086. DOI: `10.1109/ROBOT.1998.680625`.

Carrozza, M. C., G. Cappiello, S. Micera, B. B. Edin, L. Beccai, and C. Cipriani (2006). "Design of a cybernetic hand for perception and action". In: *Biological Cybernetics* 95.6, pp. 629–644. DOI: 10.1007/s00422-006-0124-2.

Chalon, M., W. Friedl, J. Reinecke, T. Wimböck, and A. Albu-Schäffer (2011). "Impedance control of a non-linearly coupled tendon driven thumb". In: *Intelligent Robots and Systems (IROS), 2011 IEEE/RSJ International Conference on*. (S. Francisco, USA, Sept. 25–30, 2011), pp. 4215–4221. DOI: 10.1109/IROS.2011.6094542.

Chalon, M., M. Grebenstein, T. Wimböck, and G. Hirzinger (2010). "The thumb: Guidelines for a robotic design". In: *Intelligent Robots and Systems (IROS), 2010 IEEE/RSJ International Conference on*. (Taipei, Taiwan, Oct. 18–22, 2010), pp. 2153–2858.

Chang, L. Y. and Y. Matsuoka (2006). "A kinematic thumb model for the ACT Hand". In: *Robotics and Automation, 2006. ICRA 2006. Proceedings 2006 IEEE International Conference on*. (Orlando, USA, May 15–19, 2006), pp. 1000–1005. DOI: 10.1109/ROBOT.2006.1641840.

Chou, C.-P. and B. Hannaford (1994). "Static and dynamic characteristics of McKibben pneumatic artificial muscles". In: *Robotics and Automation, 1994. Proceedings. 1994 IEEE International Conference on*. (San Diego, USA, May 8–14, 1994). Vol. 1, pp. 281–286. DOI: 10.1109/ROBOT.1994.350977.

Chou, C. and B. Hannaford (1996). "Measurement and modeling of McKibben pneumatic artificial muscles". In: *IEEE Transactions on Robotics and Automation* 12.1, pp. 90–102. DOI: 10.1109/70.481753.

Clavero, J. A., P. Golanó, O. Fariñas, X. Alomar, J. M. Monill, and M. Esplugas (2003). "Extensor mechanism of the fingers: MR imaging–anatomic correlation". In: *Radiographics* 23.3, pp. 593–611. DOI: 10.1148/rg.233025079.

Cowing, B. *Sore muscles after a car accident | eHow.com*. URL: http://www.ehow.com/facts_6389051_sore-muscles-after-car-accident.html (visited on 05/07/2012).

Craig, J. J. (2004). *Introduction to robotics: Mechanics and control*. 3rd ed. Upper Saddle River: Prentice Hall. ISBN: 0201543613.

Cutkosky, M. R. (1989). "On grasp choice, grasp models, and the design of hands for manufacturing tasks". In: *IEEE Transactions on Robotics and Automation* 5.3, pp. 269–279. DOI: 10.1109/70.34763.

Deshpande, A. D., R. Balasubramanian, R. Lin, B. Dellon, and Y. Matsuoka (2008). "Understanding variable moment arms for the index finger MCP joints through the ACT Hand". In: *Biomedical Robotics and Biomechatronics, 2008. BioRob 2008. 2nd IEEE RAS & EMBS International Conference on*. (Scottsdale, USA, Oct. 19–22, 2008), pp. 776–782.

Deshpande, A. D., J. Ko, D. Fox, and Y. Matsuoka (2009). "Anatomically correct testbed hand control: Muscle and joint control strategies". In: *Robotics and Automation, 2009. ICRA '09 IEEE International Conference on*. (Kobe, Japan, May 12–17, 2009), pp. 4416–4422.

Deshpande, A. D., Z. Xu, M. J. Vande Weghe, B. Brown, J. Ko, L. Chang, D. Wilkinson, S. Bidic, and Y. Matsuoka (2013). "Mechanisms of the Anatomically Correct Testbed (ACT) Hand". In: *IEEE-ASME Transactions on Mechatronics* 18.1, pp. 238–250. In print.

Diftler, M. A., J. S. Mehling, M. E. Abdallah, N. A. Radford, L. B. Bridgwater, A. M. Sanders, R. S. Askew, D. M. Linn, J. D. Yamokoski, F. A. Permenter, B. K. Hargrave, R. Piatt, R. T. Savely, and R. O. Ambrose (2011). "Robonaut 2 - The first humanoid robot in space". In: *Robotics and Automation (ICRA), 2011 IEEE International Conference on*. (Shanghai, China, May 9–13, 2011), pp. 2178–2183. DOI: 10.1109/ICRA.2011.5979830.

Eiberger, O., S. Haddadin, M. Weis, A. Albu-Schäffer, and G. Hirzinger (2010). "On joint design with intrinsic variable compliance: Derivation of the DLR QA-Joint". In: *Robotics and Automation (ICRA), 2010 IEEE International Conference on*. (Anchorage, Alaska, May 3–8, 2010), pp. 1687–1694. DOI: 10.1109/ROBOT.2010.5509662.

Elumotion ltd. (2010). *Elu2-Hand*. URL: http://www.elumotion.com/Pdfs/Elu2-Hand-Data-Sheet-24-2-10-a.pdf (visited on 04/19/2012).

Elumotion ltd. (2012). *Elu-2 Hand*. URL: http://www.elumotion.com/Elu2-hand.htm (visited on 04/19/2012).

English, C. and D. Russell (1999a). "Implementation of variable joint stiffness through antagonistic actuation using rolamite springs". In: *Mechanism and Machine Theory* 34, pp. 27–40. DOI: 10.1016/S0094-114X(97)00103-1.

English, C. and D. Russell (1999b). "Mechanics and stiffness limitations of a variable stiffness actuator for use in prosthetic limbs". In: *Mechanism and Machine Theory* 34.1, pp. 7–25. DOI: 10.1016/S0094-114X(98)00026-3.

Eusebi, A., C. Fantuzzi, C. Melchiorri, M. Sandri, and A. Tonielli (1994). "The UB Hand II control system: Design features and experimental results". In: *Proc. International Conference on Industrial Electronics, Control and Instrumentation (IECON)*. (Bologna, Italy, Sept. 5–9, 1994). Vol. 2, pp. 782–787. DOI: 10.1109/IECON.1994.397885.

Feix, T. (2010). *Human grasping database*. URL: http://grasp.xief.net/documents/taxonomy.pdf (visited on 04/19/2012).

Feix, T., H.-B. Schmiedmayer, J. Romero, and D. Kragić (2009). "A comprehensive grasp taxonomy". In: *Robotics: Science and Systems V; Workshop on Understanding Human Hand for Advancing Robotic Manipulation*. (Seattle, USA, June 28–July 2, 2009).

Ficuciello, F., G. Palli, C. Melchiorri, and B. Siciliano (2011). "Experimental evaluation of postural synergies during reach to grasp with the UB Hand IV". In: *Intelligent Robots and Systems (IROS), 2011 IEEE/RSJ International Conference on*. (S. Francisco, USA, Sept. 25–30, 2011), pp. 1775–1780. DOI: 10.1109/IROS.2011.6094671.

Filippini, R., S. Sen, and A. Bicchi (2007). "Variable impedance actuations for physical human cooperating robots: A comparative analysis of performance, safety and dependability". In: *Proc. IARP-IEEE/RAS-EURON Workshop on Technical Challenges for Dependable Robots in Human Environments.* (Rome, Italy, Apr. 14–15, 2007), pp. 4349–4354.

Flatt, A. E. (2002). "Our thumbs". In: *Proc. (Baylor University. Medical Center)* 15.4, pp. 380–387.

Friedl, W., M. Chalon, J. Reinecke, and M. Grebenstein (2011a). "FAS a flexible antagonistic spring element for a high performance over actuated hand". In: *Intelligent Robots and Systems (IROS), 2011 IEEE/RSJ International Conference on*. (S. Francisco, USA, Sept. 25–30, 2011), pp. 1366–1372. DOI: 10.1109/IROS.2011.6094569.

Friedl, W., H. Höppner, F. Petit, and G. Hirzinger (2011b). "Wrist and Forearm Rotation of the DLR Hand Arm System: Mechanical Design, Shape Analysis and Experimental Validation." In: *Intelligent Robots and Systems (IROS), 2011 IEEE/RSJ International Conference on*. (S. Francisco, USA, Sept. 25–30, 2011), pp. 1836–1842. DOI: 10.1109/IROS.2011.6094616.

Gazeau, J., M. Arsicault, and J. Lallemand (1999). "The L.M.S. Mechanical Hand: Design and control". In: *ROMANSY 12: Theory and practice of robots and manipulators; proceedings of the twelfth CISM-IFToMM Symposium*. Ed. by A. Morecki, G. Bianchi, and M. Wojtyra. Vienna: Springer. ISBN: 3211831436.

Gazeau, J., S. Zehloul, M. Arsicault, and J. Lallemand (2001). "The LMS Hand: Force and position controls in the aim of the fine manipulation of objects". In: *Robotics and Automation, 2001. Proceedings 2001 ICRA. IEEE International Conference on*. (Seoul, Korea, May 21–26, 2001). Vol. 3, pp. 2642–2648.

Geuss, H. (1994). "Development of a anthropometry measurement system for the CAD man model RAMSIS". Dissertation. TU Munich.

Gialias, N. and Y. Matsuoka (2004). "Muscle actuator design for the ACT Hand". In: *Robotics and Automation 2004. Proceedings. ICRA '04. 2004 IEEE International Conference on*. (New Orleans, USA, Apr. 26–May 1, 2004). Vol. 4, pp. 3380–3385. DOI: 10.1109/ROBOT.2004.1308776.

Giurintano, D. J., A. M. Hollister, W. L. Buford, D. E. Thompson, and L. M. Myers (1995). "A virtual five-link model of the thumb." In: *Medical Engineering and Physics* 17.4, pp. 297–303. ISSN: 1350-4533.

Gosling, J., P. Harris, I. Whitmore, and P. L. Willan (2002). *Human anatomy: Color atlas and text*. 4th ed. Philadelphia: Mosby. ISBN: 0 7234 3195 7.

Gray, H. (1999). *Anatomy, descriptive and surgical*. Ed. by T. P. Pick and R. Howden. 1901 Edition. Philadelphia: Courage Books. ISBN: 0 7624 0673 9.

Grebenstein, M. (2006a). "Antagonistic rotating device, especially for moving robot hand elements, has force transmission unit formed in such way that both drive units can act as agonists to apply rotational moment in same direction to joint element". Patent Application DE102006016958A1 (DE). Deutsches Zentrum für Luft- und Raumfahrt e.V.

Grebenstein, M. (2006b). "[DE] Roboterhand [EN] Robotic Hand". Granted Patent DE102006006322B3 (DE). Deutsches Zentrum für Luft- und Raumfahrt e.V.

Grebenstein, M., A. Albu-Schäffer, T. Bahls, M. Chalon, O. Eiberger, W. Friedl, R. Gruber, S. Haddadin, U. Hagn, R. Haslinger, H. Höppner, S. Jörg, M. Nickl, A. Nothhelfer, F. Petit, J. Reill, N. Seitz, T. Wimböck, S. Wolf, T. Wüsthoff, and G. Hirzinger (2011). "The DLR Hand Arm System". In: *Robotics and Automation (ICRA), 2011 IEEE International Conference on*. (Shanghai, China, May 9–13, 2011). DOI: 10.1109/ICRA.2011.5980371.

Grebenstein, M., M. Chalon, W. Friedl, S. Haddadin, T. Wimböck, G. Hirzinger, and R. Siegwart (2012). "The hand of the DLR Hand Arm System: Designed for interaction". In: *International Journal of Robotics Research*: *Towards Autonomous Physical Human-Robot Interaction*. In print.

Grebenstein, M., M. Chalon, G. Hirzinger, and R. Siegwart (2010a). "A method for hand kinematics designers: 7 billion perfect hands". In: *1st International Conference on Applied Bionics and Biomechanics ICABB-2010*. (Venice, Italy, Oct. 14–16, 2010).

Grebenstein, M., M. Chalon, G. Hirzinger, and R. Siegwart (2010b). "Antagonistically driven finger design for the anthropomorphic DLR Hand Arm System". In: *Humanoid Robots (Humanoids), 2010 10th IEEE-RAS International Conference on*. (Nashville, USA, Dec. 6–9, 2010). DOI: 10.1109/ICHR.2010.5686342.

Grebenstein, M. and P. van der Smagt (2008). "Antagonism for a highly anthropomorphic handarmsystem". In: *Advanced Robotics* 22.1: *On Robotic Platforms for Research in Neuroscience, Part 2*, pp. 39–55. DOI: 10.1163/156855308X291836.

Griffin, W. B., R. P. Findley, M. L. Turner, and M. R. Cutkosky (2000). "Calibration and mapping of a human hand for dexterous telemanipulation". In: *ASME IMECE Symposium on Haptic Interfaces for Virtual Environments and Teleoperator Systems*. (Orlando, USA, Nov. 5–10, 2000), pp. 1–8.

Guizzo, E. (2008). *i-LIMB snatches MacRobert award - IEEE Spectrum*. URL: http://spectrum.ieee.org/automaton/robotics/robotics-software/ilimb_snatches_macrobert_award (visited on 04/19/2012).

Haddadin, S., A. Albu-Schäffer, O. Eiberger, and G. Hirzinger (2010). "New insights concerning intrinsic joint elasticity for safety". In: *Intelligent Robots and Systems (IROS), 2010 IEEE/RSJ International Conference on*. (Taipei, Taiwan, Oct. 18–22, 2010), pp. 2181–2187. DOI: 10.1109/IROS.2010.5652037.

Haddadin, S., A. Albu-Schäffer, and G. Hirzinger (2008). "Safety evaluation of physical human-robot interaction via crash-testing". In: *Robotics:Science and Systems III*. Ed. by W. Burgard, O. Brock, and C. Stachniss. Cambridge: The MIT Press, pp. 217–224. ISBN: 978-0-262-52484-1.

Haddadin, S., A. Albu-Schäffer, and G. Hirzinger (2009a). "Requirements for Safe Robots: Measurements, Analysis & New Insights". In: *International Journal of Robotics Research* 28.11-12, pp. 1507–1527. DOI: 10.1177/0278364909343970.

Haddadin, S., T. Laue, U. Frese, S. Wolf, A. Albu-Schäffer, and G. Hirzinger (2009b). "Kick it with elasticity: Safety and performance in human-robot soccer". In: *Robotics and Autonomous Systems* 57.8, pp. 761–775. DOI: 10.1016/j.robot.2009.03.004.

Haidacher, S., J. Butterfaß, M. Fischer, M. Grebenstein, K. Jöhl, K. Kunze, M. Nickl, N. Seitz, and G. Hirzinger (2003). "DLR Hand II: Hard- and software architecture for information processing". In: *Robotics and Automation 2003. Proceedings. ICRA '03 .IEEE International Conference on*. (Taipei, Taiwan, Sept. 14–19, 2003). Vol. 1, pp. 684–689. DOI: 10.1109/ROBOT.2003.1241673.

Ham, R., B. Vanderborght, M. Damme, B. Verrelst, and D. Lefeber (2006). "MACCEPA: the Actuator with Adaptable Compliance for Dynamic Walking Bipeds". In: *Climbing and walking robots*. Ed. by M. Tokhi, G. Virk, and M. Hossain. Berlin: Springer, pp. 759–766. DOI: 10.1007/3-540-26415-9_91.

Hildingsson, C. and G. Toolanen (1990). "Outcome after soft-tissue injury of the cervical spine: A prospective study of 93 car-accident victims, Acta Orthopaedica, Informa Healthcare". In: *Acta Orthopaedica* 61.4, pp. 357–359.

Hirzinger, G., J. Butterfaß, M. Grebenstein, M. Hähnle, I. Schäfer, and N. Sporer (2000). "A mechatronics approach to the design of light-weight arms". In: *Proc. International Workshop on Robotics in Alpe-Adria-Danube Region*. (Maribor, Slovenia, June 1–3, 2000).

Hirzinger, G., J. Butterfaß, S. Knoch, and H. Liu (1998). "DLR's multisensory articulated hand". In: *Experimental Robotics V, The Fith International Symposium Barcelona, Catalonia, June 15–18, 1997*. Ed. by A. Casals and A. T. de Almeida. Lecture Notes in Control and Information Science 232. Berlin: Springer, pp. 47–55. ISBN: 3-540-76218-3.

Hogan, N. (1984). "Impedance control: An approach to manipulation". In: *American Control Conference, 1984*. (San Diego, USA, June 6–8, 1984), pp. 304–313.

Hollister, A., W. L. Buford, L. M. Myers, D. J. Giurintano, and A. Novick (1992). "The axes of rotation of the thumb carpometacarpal joint". In: *Journal of Orthopaedic Research* 10.3, pp. 454–460. DOI: 10.1002/jor.1100100319.

Hollister, A., D. J. Giurintano, W. L. Buford, L. M. Myers, and A. Novick (1995). "The axes of rotation of the thumb interphalangeal and metacarpophalangeal joints". In: *Clinical Orthopaedics and Related Research* 320, pp. 188–193. ISSN: 0009-921X.

Hurst, J. and A. Rizzi (2008). "Series compliance for an efficient running gait". In: *IEEE RAS – Robotics and Automation Magazine* 15.3, pp. 42–51. DOI: 10.1109/MRA.2008.927693.

Iwata, H. and S. Sugano (2009). "Design of human symbiotic robot TWENDY-ONE". In: *Robotics and Automation, 2009. ICRA '09 IEEE International Conference on*. (Kobe, Japan, May 12–17, 2009), pp. 580–586. DOI: 10.1109/ROBOT.2009.5152702.

Jacobsen, S. C., H. Ko, E. Iversen, and C. Davis (1989). "Antagonistic control of a tendon driven manipulator". In: *Robotics and Automation, 1989. Proceedings. 1989 IEEE International Conference on*. (Scottsdale, USA, May 14–20, 1989). Vol. 3, pp. 1334–1339. DOI: 10.1109/ROBOT.1989.100165.

Jacobsen, S. C., J. Wood, D. Knutti, and K. Biggers (1984). "UTAH/MIT dextrous hand - work in progress". In: *International Journal of Robotics Research* 3.4, pp. 21–50. DOI: 10.1177/027836498400300402.

Kaneko, M., M. Higashimori, R. Takenaka, A. Namiki, and M. Ishikawa (2003). "The 100 G capturing robot - too fast to see". In: *IEEE-ASME Transactions on Mechatronics* 8.1, pp. 37–44. DOI: 10.1109/TMECH.2003.809137.

Kapandji, I. A. (1982). *The physiology of the joints: Volume 1 upper limb*. With an intro. by F. Poilleux. 5th ed. Vol. 1. Edinburgh: Churchill Livingstone. ISBN: 0-443-02504-5.

Kapandji, I. A. (1986). "Cotation clinique de l'opposition et de la contre-opposition du pouce". In: *Annales de Chirurgie de la Main* 5.1, pp. 68–73.

Kargov, A., T. Asfour, C. Pylatiuk, R. Oberle, H. Klosek, S. Schulz, K. Regenstein, G. Bretthauer, and R. Dillmann (2005). "Development of an anthropomorphic hand for a mobile assistive robot". In: *Rehabilitation Robotics, 2005. ICORR 2005. 9th International Conference On*. (Chicago, USA, June 28–July 1, 2005), pp. 182–186. DOI: 10.1109/ICORR.2005.1501080.

Kargov, A., C. Pylatiuk, H. Klosek, R. Oberle, S. Schulz, and G. Bretthauer (2006). "Modularly designed lightweight anthropomorphic robot hand". In: *Proc. IEEE International Conference on Multisensor Fusion and Integration for Intelligent Systems*. (Heidelberg, Germany, Sept. 3–6, 2006), pp. 155–159. DOI: 10.1109/MFI.2006.265667.

Kawasaki, H. and T. Komatsu (1998). "Development of an anthropomorphic robot hand driven by built-in servo-motors". In: *Proc. International Conference on Advanced Mechatronics (ICAM)*. (Okayama, Japan, Aug. 3–6, 1998), pp. 215–220.

Kawasaki, H. and T. Komatsu (1999). "Mechanism design of anthropomorphic robot hand: Gifu Hand I". In: *Journal of Robotics and Mechatronics* 11.4, pp. 269–273.

Kawasaki, H., T. Komatsu, and K. Uchiyama (2002). "Dexterous anthropomorphic RobotHand with distributed tactile sensor: Gifu Hand II". In: *IEEE-ASME Transactions on Mechatronics* 7.2, pp. 296–303. DOI: 10.3182/20110828-6-IT-1002.01686.

Khatib, O. (1987). "A unified approach for motion and force control of robot manipulators: The operational space formulation". In: *IEEE Journal of Robotics and Automation* 3.1, pp. 43–53. DOI: 10.1109/JRA.1987.1087068.

Kothera, C. S., M. Jangid, J. Sirohi, and N. M. Wereley (2009). "Experimental characterization and static modeling of McKibben actuators". In: *Journal of Mechanical Design* 131.9, 091010, p. 091010. DOI: 10.1115/1.3158982.

Kuczynski, K. (1975). "The thumb and the saddle." In: *Hand* 7.2, pp. 120–122. DOI: 10.1016/0072-968X(75)90005-4.

Laurin-Kovitz, K., J. E. Colgate, and S. D. R. Carnes (1991). "Design of components for programmable passive impedance". In: *Robotics and Automation, 1991. Proceedings. 1991 IEEE International Conference on*. (Sacramento, USA, Apr. 9–12, 1991), pp. 1476–1481. DOI: 10.1109/ROBOT.1991.131824.

Leijnse, J. (1997). "A generic morphological model of the anatomic variability in the m. flexor digitorum profundus, m. flexor pollicis longus and mm. lumbricales complex". In: *Acta Anatomica* 160, pp. 62–74.

Leijnse, J., J. Bonte, J. Landsmeer, J. Kalker, J. Van der Meulen, and C. Snijders (1992). "Biomechanics of the finger with anatomical restrictions–The significance for the exercising hand of the musician". In: *Journal of Biomechanics* 25.11, pp. 1253–1264.

Leijnse, J. and C. Spoor (2012). "Reverse engineering finger extensor apparatus morphology from measured coupled interphalangeal joint angle trajectories – a generic 2D kinematic model". In: *Journal of Biomechanics* 45.3, pp. 569–578. DOI: 10.1016/j.jbiomech.2011.11.002.

Liu, H., J. Butterfaß, M. Grebenstein, and G. Hirzinger (2001). "DLR multisensory articulated hand I and II". In: *International Workshop on Bio-Robotics and Teleoperation*. (Beijing, China, May 27–30, 2001).

Lotti, F., P. Tiezzi, G. Vassura, L. Biagiotti, and C. Melchiorri (2004a). "UBH 3: An anthropomorphic hand with simplified endo-skeletal structure and soft continuous fingerpads". In: *Robotics and Automation 2004. Proceedings. ICRA '04. 2004 IEEE International Conference on*. (New Orleans, USA, Apr. 26–May 1, 2004). Vol. 5, pp. 4736–4741. DOI: 10.1109/ROBOT.2004.1302466.

Lotti, F., P. Tiezzi, G. Vassura, L. Biagiotti, C. Melchiorri, and G. Palli (2004b). "UBH 3: A Biologically Inspired Robotic Hand". In: *Intelligent Manipulation and Grasping: International Conference*. (Genova, Italy, July 1–2, 2004). Ed. by R. Molfino, pp. 39–45.

Lotti, F., P. Tiezzi, G. Vassura, L. Biagiotti, C. Melchiorri, and G. Palli (2004c). "UBH 3: An anthropomorphic hand with simplified endo-skeletal structure and soft continuous fingerpads". In: *Robotics and Automation 2004. Proceedings. ICRA '04. 2004 IEEE International Conference on*. (New Orleans, USA, Apr. 26–May 1, 2004). Vol. 5, pp. 4736–4741. DOI: 10.1109/ROBOT.2004.1302466.

Lotti, F., P. Tiezzi, G. Vassura, L. Biagiotti, G. Palli, and C. Melchiorri (2005). "Development of UB Hand 3: Early results". In: *Robotics and Automation, 2005. ICRA 2005. Proceedings of the 2005 IEEE International Conference on*. (Barcelona, Spain, Apr. 18–22, 2005), pp. 4488–4493. DOI: 10.1109/ROBOT.2005.1570811.

Lovchik, C. S. and M. A. Diftler (1999). "The Robonaut Hand: A dexterous robot hand for space". In: *Robotics and Automation, 1999. Proceedings. IEEE International Conference on*. (Detroit, USA, May 10–15, 1999). Vol. 2, pp. 907–912. DOI: 10.1109/ROBOT.1999.772420.

Mason, M. T. and K. J. Salisbury (1985). *Robot hands and the mechanics of manipulation*. Cambridge: The MIT Press. ISBN: 0262132052.

Matsuoka, Y., P. Afshar, and M. Oh (2006). "On the design of robotic hands for brain-machine interface". In: *Neurosurgical Focus* 20.5, E3. ISSN: 1092-0684.

McGrouther, D. A., J. C. Colditz, J. M. Harris, and D. W. Stoller (2000). *Interactive hand 2000*. CD-ROM. London: Primal Picture Ltd. ISBN: 978-1902470221.

Meka Robotics LLC (2009). *H2 compliant hand*. URL: http://mekabot.com/product_sheets/meka_H2_hand_product_sheet_10_2009.pdf (visited on 04/19/2012).

Melchiorri, C. and G. Vassura (1992). "Mechanical and control features of the University of Bologna Hand version 2". In: *Intelligent Robots and Systems, 1992., Proceedings of the 1992 1992 IEEE/RSJ International Conference on*. (Raleigh, USA, July 7–10, 1992), pp. 187–193. DOI: 10.1109/IROS.1992.587320.

Meriam, J. L. and L. G. Kraige (2007). *Engineering mechanics: Volume 1; Statics; SI Version*. 6th ed. Vol. 1. Hoboken: Wiley. ISBN: 0471787027.

Miller, A., P. Allen, V. Santos, and F. J. Valero-Cuevas (2005). "From robotic hands to human hands: a visualization and simulation engine for grasping research". In: *Industrial Robot: An International Journal* 32.1, pp. 55–63. DOI: 10.1108/01439910510573309.

Miller, A. and P. K. Allen (2004). "Graspit!: A versatile simulator for robotic grasping". In: *IEEE RAS – Robotics and Automation Magazine* 11.4, pp. 110–122. DOI: 10.1109/MRA.2004.1371616.

Mizuuchi, I., Y. Nakanishi, Y. Sodeyama, Y. Namiki, T. Nishino, N. Muramatsu, J. Urata, K. Hongo, T. Yoshikai, and M. Inaba (2007). "An advanced musculoskeletal humanoid Kojiro". In: *Humanoid Robots, 2007 7th IEEE-RAS International Conference on*. (Pittsburg, USA, Nov. 29–Dec. 1, 2007), pp. 294–299. DOI: 10.1109/ICHR.2007.4813883.

Mizuuchi, I., R. Tajima, T. Yoshikai, D. Sato, K. Nagashima, M. Inaba, Y. Kuniyoshi, and H. Inoue (2002). "The design and control of the flexible spine of a fully tendon-driven humanoid "Kenta"". In: *Intelligent Robots and Systems, 2002. IEEE/RSJ International Conference on*. (Lausanne, Switzerland, Sept. 30–Oct. 4, 2002), pp. 2527–2532. DOI: 10.1109/IRDS.2002.1041649.

Morita, T., H. Iwata, and S. Sugano (1999). "Development of human symbiotic robot: WENDY". In: *Robotics and Automation, 1999. Proceedings. IEEE International Conference on*. (Detroit, USA, May 10–15, 1999). Vol. 4, pp. 3183–3188. DOI: 10.1109/ROBOT.1999.774083.

Mouri, T., H. Kawasaki, K. Yoshikawa, J. Takai, and S. Ito (2002). "Anthropomorphic robot hand: Gifu Hand III". In: *Proc. Control, Automation and Systems (ICCAS),International Conference on,* (Jeonbuk, Korea, Oct. 16–19, 2002), pp. 1288–293.

Napier, J. (1993). *Hands*. Ed. by J. Russel. Princeton: Princeton University Press. ISBN: 0-691-02547-9.

Nierop van, O. A., A. van der Helm, K. J. Overbeeke, and T. J. Djajadiningrat (2008). "A natural human hand model". In: *The Visual Computer* 24.1, pp. 31–44. DOI: 10.1007/s00371-007-0176-x.

Okada, T. (1982). “Computer control of multijointed finger system for precise object-handling”. In: *IEEE Transactions on Systems Man and Cybernetics* 12.3, pp. 289–299. DOI: 10.1109/TSMC.1982.4308818.

Okada, T. and S. Tsuchiya (1977). “On a versatile finger system”. In: *Proc. International Symposium Industrial Robots*. (Tokyo,Japan, Oct. 19–21, 1977), pp. 345–352.

Oxford University Press (2012a). *Definition for anthropomorphism - Oxford Dictionaries Online (World English)*. URL: http://oxforddictionaries.com/definition/anthropomorphism?q=anthropomorphism (visited on 04/19/2012).

Oxford University Press (2012b). *Definition for humanoid - Oxford Dictionaries Online (World English)*. URL: http://oxforddictionaries.com/definition/humanoid?q=humanoid (visited on 04/19/2012).

Oxford University Press (2012c). *Definition for scoliosis - Oxford Dictionaries Online (World English)*. URL: http://oxforddictionaries.com/definition/scoliosis?q=scoliosis (visited on 04/19/2012).

Palli, G., G. Borghesan, and C. Melchiorri (2009). “Tendon-based transmission systems for robotic devices: Models and control algorithms”. In: *Robotics and Automation, 2009. ICRA ’09 IEEE International Conference on*. (Kobe, Japan, May 12–17, 2009), pp. 4063–4068. DOI: 10.1109/ROBOT.2009.5152491.

Palli, G., C. Melchiorri, T. Wimböck, M. Grebenstein, and G. Hirzinger (2007). “Feedback linearization and simultaneous stiffness-position control of robots with antagonistic actuated joints”. In: *Robotics and Automation, 2007 IEEE International Conference on*. (Roma, Italy, Apr. 10–14, 2007), 4367—4372.

Panzer, H., O. Eiberger, M. Grebenstein, P. Schaefer, and P. van der Smagt (2008). “Human motion range data optimizes anthropomorphic robotic hand-arm system design”. In: *Proc. International Conference on Motion and Vibration Control (MOVIC)*. (Munich, Germany, Sept. 15–18, 2008). Technische Universität München, pp. 1–9.

Park, J., B. Kim, J. Song, and H. Kim (2007). "Safe link mechanism based on passive compliance for safe human-robot collision". In: *Robotics and Automation, 2007 IEEE International Conference on*. (Roma, Italy, Apr. 10–14, 2007), pp. 1152–1157. DOI: 10.1109/ROBOT.2007.363140.

Petit, F., M. Chalon, W. Friedl, M. Grebenstein, A. Albu-Schäffer, and G. Hirzinger (2010). "Bidirectional antagonistic variable stiffness actuation: analysis, design and implementation". In: *Robotics and Automation (ICRA), 2010 IEEE International Conference on*. (Anchorage, Alaska, May 3–8, 2010), pp. 4189–4196. DOI: 10.1109/ROBOT.2010.5509267.

Ponting, H. (1907). *Ein Fakir in Benares (Varanasi), Indien*. URL: http://www.geocities.com/blackinkal4/RoyalGeographicalSociety_Asia_2.html (visited on 04/28/2012).

Purschke, F., M. Schulze, and P. Zimmermann (1998). "Virtual reality - New methods for improving and accelerating the development process in vehicle styling and design". In: *Computer Graphics International Conference*, pp. 789–797. DOI: http://doi.ieeecomputersociety.org/10.1109/CGI.1998.694338.

Rosenstein, M. T. and R. A. Grupen (2002). "Velocity-dependent dynamic manipulability". In: *Robotics and Automation, 2002. Proceedings. ICRA '02. IEEE International Conference on*. (Washington D.C., USA, May 11–15, 2002). Vol. 3, pp. 2424–2429. DOI: 10.1109/ROBOT.2002.1013595.

Salisbury, K. J. and B. Roth (1982). "Kinematics and force analysis of articulated mechanical hands". Ph.D. Thesis. Stanford: Stanford University.

Santello, M., M. Flanders, and J. F. Soechting (1998). "Postural hand synergies for tool use". In: *The Journal of Neuroscience* 18.23, pp. 10105–10115.

Santos, V. J. and F. J. Valero-Cuevas (2003). "Anatomical variability naturally leads to multimodal of Denavit-Hartenberg parameters for the human thumb". In: *Engineering in Medicine and Biology Society, 2003. Proceedings of the 25th Annual International Conference of the IEEE*. (Cancun, Mexico, Sept. 17–21, 2003). Vol. 2, pp. 1823–1826. DOI: 10.1109/IEMBS.2003.1279771.

Santos, V. J. and F. J. Valero-Cuevas (2004). "A bayesian approach to biomechanical modeling to optimize over large parameter spaces while considering anatomical variability". In: *Engineering in Medicine and Biology Society, 2004. IEMBS '04. 26th Annual International Conference of the IEEE*. (San Francisco, USA, Sept. 1–5, 2004). Vol. 2, pp. 4626–4629. DOI: 10.1109/IEMBS.2004.1404282.

Schiavi, R., G. Grioli, S. Sen, and A. Bicchi (2008). "VSA-II: A novel prototype of variable stiffness actuator for safe and performing robots interacting with humans". In: *Robotics and Automation, 2008. ICRA 2008. IEEE International Conference on*. (Pasadena, USA, May 19–23, 2008), pp. 2171–2176. DOI: 10.1109/ROBOT.2008.4543528.

Schulz, S., C. Pylatiuk, and G. Bretthauer (2001). "A new ultralight anthropomorphic hand". In: *Robotics and Automation, 2001. Proceedings 2001 ICRA. IEEE International Conference on*. (Seoul, Korea, May 21–26, 2001). Vol. 3, pp. 2437–2441. DOI: 10.1109/ROBOT.2001.932988.

ShadowRobotCompany (2003). *Design of a dextrous hand for advanced CLAWAR applications*. London: Shadow Robot Company.

ShadowRobotCompany (2008). *Shadow dexterous hand C5 technical specification*. URL: http://www.shadowrobot.com/downloads/shadow_dextrous_hand_technical_specification_C6P6.pdf (visited on 04/19/2012).

ShadowRobotCompany (2009). *Shadow dexterous hand C6M technical specification*. URL: http://www.shadowrobot.com/downloads/shadow_dextrous_hand_technical_specification_C6M.pdf (visited on 04/19/2012).

slowmoparkour (2008). *Jan very deep landing side - YouTube*. URL: http://www.youtube.com/watch?v=vOaZHL4Dw5s (visited on 05/07/2012).

Soras, X. de, D. Guinard, F. Moutet, and P. Gerard (1994). "Proposition of a new functional cotation bill for the hand". In: *Annales de Chirurgie de la Main et du Membre Supérieur* 13.5, pp. 297–307. DOI: 10.1016/S0753-9053(05)80065-1.

Stillfried, G. and P. van der Smagt (2008). "Human hand kinematics based on MRI imaging". In: *Robotics:Science and Systems V*. Ed. by J. Trinkle, Y. Matsuoka, and J. A. Castellanos. Vol. 36. 27. Cambridge: The MIT Press, pp. 217–224. ISBN: 978-0-262-51463-7.

Sugaiwa, T., H. Iwata, and S. Sugano (2009). "A motion control for dexterous manipulation with human mimetic hand-arm system". In: *Humanoid Robots, 2009. Humanoids 2009. 9th IEEE-RAS International Conference on*. (Paris, France, Dec. 7–10, 2009), pp. 653–659. DOI: 10.1109/ICHR.2009.5379511.

Sugano, S., S. Tsuto, and I. Kato (1992). "Force control of the robot finger joint equipped with mechanical compliance adjuster". In: *Intelligent Robots and Systems, 1992., Proceedings of the 1992 1992 IEEE/RSJ International Conference on*. (Raleigh, USA, July 7–10, 1992). Vol. 3, pp. 2005–2013. DOI: 10.1109/IROS.1992.601933.

Surentu, J., G. J. M. Tuijthof, and J. L. Herder (2007). "Optimized artificial muscles for an inherently safe robotic arm". In: *Rehabilitation Robotics, 2007. ICORR 2007. IEEE 10th International Conference On*. (Noordwijk aan Zee, Netherlands, June 13–15, 2007), pp. 1070–1076. DOI: 10.1109/ICORR.2007.4428556.

Tonietti, G., R. Schiavi, and A. Bicchi (2005). "Design and control of a variable stiffness actuator for safe and fast physical human/robot interaction". In: *Robotics and Automation, 2005. ICRA 2005. Proceedings of the 2005 IEEE International Conference on*. (Barcelona, Spain, Apr. 18–22, 2005), pp. 526–531. DOI: 10.1109/ROBOT.2005.1570172.

Tonietti, G., R. Schiavi, and A. Bicchi (2006). "Optimal mechanical/control design for safe and fast robotics". In: *Experimental Robotics IX: The 9th Symposium on Experimental Robotics*. Ed. by M. H. A. Jr. and O. Khatib. Springer Tracts in Advanced Robotics 21. Berlin: Springer, pp. 311–320. ISBN: 978-3-540-28816-9.

Touch Bionics Inc. (2012). *i-limb ultra data sheet lo-res.pdf*. URL: http://www.touchbionics.com/media/2210/i-limb%20ultra%20data%20sheet%20lo-res.pdf (visited on 04/19/2012).

Tubiana, R. (1981). *The hand*. Philadelphia: Saunders Press. ISBN: 9780721689074.

Valero-Cuevas, F. J., M. E. Johanson, and J. D. Towles (2003). "Towards a realistic biomechanical model of the thumb: the choice of kinematic description may be more critical than the solution method or the variability/uncertainty of musculoskeletal parameters". In: *Journal of Biomechanics* 36, pp. 1019–1030. DOI: 10.1016/S0021-9290(03)00061-7.

Vande Weghe, M., M. Rogers, M. Weissert, and Y. Matsuoka (2004). "The ACT Hand: Design of the skeletal structure". In: *Robotics and Automation 2004. Proceedings. ICRA '04. 2004 IEEE International Conference on*. (New Orleans, USA, Apr. 26–May 1, 2004). Vol. 4, pp. 3375–3379. DOI: 10.1109/ROBOT.2004.1308775.

Wilkinson, D. D., M. Vande Weghe, and Y. Matsuoka (2003). "An extensor mechanism for an anatomical robotic hand". In: *Robotics and Automation 2003. Proceedings. ICRA '03 .IEEE International Conference on*. (Taipei, Taiwan, Sept. 14–19, 2003). Vol. 1, pp. 238–243. DOI: 10.1109/ROBOT.2003.1241602.

Wimböck, T., B. Jahn, and G. Hirzinger (2011). "Synergy level impedance control for multifingered hands". In: *Intelligent Robots and Systems (IROS), 2011 IEEE/RSJ International Conference on*. (S. Francisco, USA, Sept. 25–30, 2011), pp. 973–979. DOI: 10.1109/IROS.2011.6094555.

Wimböck, T., J. Reinecke, and M. Chalon (2012). "Derivation and verification of synergy coordinates for the DLR Hand Arm System". In: *8th IEEE International Conference on Automation Science and Engineering*. (Seoul, Korea, Aug. 20–24, 2012). In print.

Wolf, S., O. Eiberger, and G. Hirzinger (2011). "The DLR FSJ: Energy based design of a variable stiffness joint". In: *Robotics and Automation (ICRA), 2011 IEEE International Conference on*. (Shanghai, China, May 9–13, 2011), pp. 5082–5089. DOI: 10.1109/ICRA.2011.5980303.

Wolf, S. and G. Hirzinger (2008). "A new variable stiffness design: Matching requirements of the next robot generation". In: *Robotics and Automation, 2008. ICRA 2008. IEEE International Conference on*. (Pasadena, USA, May 19–23, 2008), pp. 1741–1746.

Yoshikawa, T. (2003). *Foundations of robotics: Analysis and control*. Cambridge: MIT Press. ISBN: 978-0262514583.

Zinn, M., O. Khatib, B. Roth, and K. J. Salisbury (2004). "Playing it safe". In: *IEEE RAS – Robotics and Automation Magazine* 11.2, pp. 12–21. DOI: 10.1109/ROBOT.2008.4543528.